Understanding the mechanism and functional effects of caspase-11 regulated nitric oxide production during inflammation and cancer

Thesis submitted to the University of Dublin, Trinity College for the Degree of Doctor of Philosophy

By

Ciara Nulty

Supervised by

Dr Emma Creagh

School of Biochemistry and Immunology

2023

I. Declaration

I, Ciara Nulty, declare that this thesis has not been submitted as an exercise for a degree at this or any other university and it is entirely my own work.

I agree to deposit this thesis in the University's open access institutional repository or allow the library to do so on my behalf, subject to Irish Copyright Legislation and Trinity College Library conditions of use and acknowledgement.

I consent to the examiner retaining a copy of the thesis beyond the examining period, should they so wish.

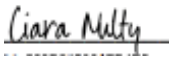

30.12.2022

Ciara Nulty Date submitted

II. Abstract

Inflammatory caspases are a group of cysteine aspartic proteinases essential for the inflammatory process, but when dysregulated are implicated in inflammatory diseases and cancer-associated chronic inflammatory events. Human caspases-4 and -5 (and their murine orthologue caspase-11) induce a form of inflammatory cell death, termed pyroptosis, resulting in the secretion of potent pro-inflammatory cytokines, IL-1β and IL-1α. Caspase-11 has also been reported to regulate STAT1 activation, a key transcriptional activator of inducible nitric oxide synthase (iNOS) which is central to macrophage polarisation. iNOS mediated nitric oxide (NO) production alters macrophage metabolism via modulation of mitochondrial morphology and Kreb's cycle impairment. This study shows that caspase-11 functions to alter mitochondrial metabolism via regulation of NO production.

Understanding the molecular mechanisms underpinning immunometabolism are important for investigating its dysfunction during disease. Investigation of the potential mechanism regulating caspase-11 mediated NO production revealed that caspase-11 inhibits PINK1-induced mitophagy during inflammatory responses, identifying a potential link between caspase-11 mediated suppression of mitophagy and type I IFN driven NO production. The impact of caspase-11 mediated NO production during macrophage metabolic reprogramming in response to M1 stimuli was also examined. A role for caspase-11 during macrophage polarization was identified, regulating iNOS expression and NO production, thereby driving metabolic rewiring towards glycolytic commitment in inflammatory macrophages. Metabolic analysis and measurement of metabolites revealed that caspase-11 driven NO production is required for glycolytic commitment during inflammatory responses, as oxidative phosphorylation (OXPHOS) remains intact in inflammatory M1 polarised *Casp11*$^{-/-}$ BMDM.

Breast cancer is a commonly diagnosed cancer in females and the second leading cause of cancer related death among women. It is a highly heterogeneous disease with distinct molecular patterns and treatment availabilities. Breast cancer development is associated with increased leukocyte infiltration and an inflammatory microenvironment, conducive for tumour development. Breast cancers are classified into 4 molecular subtypes, of which basal-like breast cancer is the most aggressive and difficult to treat, with increased risk of recurrence and metastatic potential. Current investigations of its tumour microenvironment (TME) are underway to uncover targetable features. Immunotherapy is emerging as a viable therapeutic alternative for TNBC patients, with macrophage re-education becoming a targetable component of cancer therapeutics.

Examination of inflammatory caspase expression levels between tumour and normal adjacent breast tissue revealed that inflammatory caspase-5 was more highly expressed in tumours. Further immunohistochemical analysis of a breast cancer tumour microarray revealed significantly higher caspase-5 expression in the stroma of estrogen receptor negative (ER-) tissue. Pyroptosis is closely associated with tumour development and metastasis, however it has both pro-tumour and anti-tumour roles. This study suggests that caspase-5 mediated pyroptosis in tumour associated macrophages (TAMs) is important during breast cancer initiation, which may support immune cell infiltration and activity. Secreted factors from an ER- cell line were shown to induce caspase-11 dependent IL-1α secretion from primary murine macrophages. Dysregulated pyroptosis impairs tumour clearance as disease advances. As CASP5 expression decreases with tumour stage, during advanced disease pyroptosis may become negatively regulated to aid tumour development. COX-2 is associated with poor overall survival in TNBC patients, and increased expression with tumour stage inversely correlates with CASP5. The COX-2 product PGE_2 inhibits caspase-11 mediated pyroptosis, therefore we hypothesise that once caspase-5 contributes to TNBC initiation, PGE2 inhibits caspase-11 mediated pyroptosis to escape immunosurveillance.

III. Acknowledgments

Firstly, I would like to extend my most sincere thanks to my wonderful supervisor Dr Emma Creagh for her endless support and guidance throughout my PhD project. Emma, thank you for always going above and beyond, for your constant guidance, help, support, enthusiasm, and encouragement over the last years. I could not have asked for a better supervisor.

Thank you to all the collaborators who made this project possible. Thank you to Dr. Fred Sheedy, Dr. Emer Hackett and John McGrath for their endless help with mTB infections. Thank you to Dr. Mary Rooney for all the seahorse support and general lab advice over the years. Thank you to Nuno Neto and Dr. Michael Monaghan for their help with FLIM. Joanna Fay and Prof. Elaine Kay for their collaboration with breast patient IHC staining. Thank you to, Dr. John O'Brien, Dr. Manuel Ruether, Eavan McLoughlin and Jerry from the School of Chemistry.
My most special regards to all past and current members of the Creagh lab, Ewelina, Gillian, Sinead, Brian, Ana, Aidan and Aoife. A special thank you to the everyone who has passed through the 6th floor reading room during my time; Callum, Louie, Chloe, Ben, Claire, Rebecca, Stefania, Marilena, Magda, Tania, Vinnie, Megan and Erwina. I would especially like to thank Patricia Hannon Barroeta for being the best friend and support I could ask for.
To my friends, Amy and Meghan thank you for being understanding of last-minute cancelled plans but providing a welcome distraction just when I needed it most.

I would also like to thank all my family. To all my siblings and in-laws, Celina, Philip, Maeve, Edel, Graham, David, Gillian, Kenneth and Marion. Thank you all for being an amazing, supportive, and loving family. I hope I can always be there for you all and as you have for me.

Finally, I would like to say a massive thank you to my extraordinary parents, Christy and Michelle. My entire life you have supported me in whatever I chose to do, and always believed in me and my abilities. I won the lottery by having you as my parents, and I would not have been able to do any of this without you by my side. I will always be grateful!

This PhD was funded by Irish Research Council, Government of Ireland Postgraduate Scholarship 2018 – GOIPG/2018/3407 and The Jane Burrow Research Fund.

IV. PhD Outputs to-date

Publications

Contributing author:

- Caspase-11 regulates the tumour suppressor function of STAT1 in a murine model of colitis-associated carcinogenesis. B. Flood, J. Manils, **C. Nulty**, E. Flis, S. Kenealy, G. Barber, J. Fay, K. H. G. Mills, E. W. Kay & E. M. Creagh. *Oncogene*. (2019) ;38(14):2658-2674. doi: 10.1038/s41388-018-0613-5.
- Caspase-4: A therapeutic target for peptic ulcer disease. Zaslona Z, Flis E, **Nulty C,** Kearney J, Fitzgerald R, Douglas A.R, McNamara D, Smith S, O'Neil L.A.J, Creagh E.M. *Immunohorizons.* (2020) ;12;4(10):627-633. doi: 10.4049/immunohorizons.2000080
- Identification of TLR2 signalling mechanisms which contribute to Barrett's and oesophageal adenocarcinoma disease progression. Flis E, Barber G, **Nulty C**, Keogh B, McGurik P, Anand A, O'Sullivan J, Quante M, Creagh E.M. *Cancers* (2021) ;13, 2065. https:// doi.org/10.3390/cancers13092065
- Regulation, activation and function of caspase-11 during health and disease. Agnew A, **Nulty C**, Creagh E.M. *International Journal of Molecular Science* (2021) ;22, 1506. doi.org/ 10.3390/ijms22041506

First author:

- Evaluating host response to *Helicobacter pylori* using ELISA and Western Blot. **Nulty C,** Barber G, Creagh E.M. *Methods in Molecular Biology, Springer Publisher* (2021) ;2283:175-190. doi: 10.1007/978-1-0716-1302-3_16.
- Caspase-11 regulates Nitric Oxide-mediated Macrophage metabolic reprogramming to alter host responses to *Mycobacterium tuberculosis*. **C. Nulty**, E. Flis, E. Hackett, J. McGrath, N. Neto, J. O'Brien, M. Ruether, M. Monaghan, F. Sheedy, E.M. Creagh. *In preparation.*
- Caspase-11 modulates Tumour Microenvironment of Basal-like Breast Cancer. **Nulty C,** Flood B, Sheehan K, Fay J, Creagh E.M. *In preparation.*

Poster Presentations

- "The influence of hormone receptor status on expression of inflammatory caspases", TBSI Research Symposium, Trinity Biomedical Science Institute, Dublin, September 2019
- "The influence of hormone receptor status on expression of inflammatory caspases", Irish Society for Immunology (ISI), Royal College of Surgeons Ireland (RCSI), Dublin, September 2019

- "The influence of hormone receptor status on expression of inflammatory caspases in the tumour microenvironment", Irish Association of Cancer Research (IACR), Galway, February 2020.
- "Caspase-4 promotes the inflammatory tumour microenvironment of triple negative breast cancer", Irish Association of Cancer Research (IACR), Virtual March 2021.
- "Role for caspase-11 in host defence against *Mycobacterium tuberculosis*", Host-Pathogen Conference (HPC), Dublin 2021.
- "Inflammatory caspase expression in triple negative breast tumour microenvironment promotes disease progression", Irish Association of Cancer Research (IACR) Cork, April 2022.
- "Inflammatory Caspases modulate NO metabolic remodelling: Involvement in ER- Breast Cancer", VIII Workshop on Nitric Oxide and Cancer (ISNOC), Copenhagen, June 2022.

Oral Presentations

- The Role of Caspase-11 during Host Defence against against *Mycobacterium tuberculosis.* Immunology Research Forum (IRF), TBSI Dublin, February 2021.
- Caspase-11 modulates nitric oxide metabolic rewiring in macrophages. Immunometabolism Research Forum (IMF), TBSI Dublin, June 2022.

Course and modules

- LAST-Ireland animal handling training programme (small animals), Ireland, 2018.
- Core Biomedical Research Skills for PhD students, School of Biochemistry and Immunology, September 2018-May 2019, 10 credits.
- Research Integrity and impact in an open scholarship era, Trinity College Dublin, December 2018, 5 credits.

V. Table of Contents

VI. Abbreviations

AD Active domain

AIM2 Absent In Melanoma 2

ALR AIM2-like receptor

ACON2 Aconitase-2

ATP Adenosine triphosphate

ARG Arginase

BMDM Bone marrow-derived macrophages

cIAP Cellular inhibitor of apoptosis protein

CARD Caspase activation and recruitment domain

CAT Cationic transporters

CDL CARD domain linker

cGAMP Cyclin guanosine monophosphate adenosine monophosphate

cGAS Cyclic GMP–AMP synthase

CLR C-type lectin receptors

CM Conditioned media

DAMP Danger associated molecular patterns

DC Dendritic Cells

DNA Deoxyribonucleic acid

DUB Deubiquitinating enzymes

ECAR Extracellular acidification rate

EGF Epidermal growth factor

EMT Epithelial mesenchymal transition

ETC Electron transport chain

ER Estrogen receptor

FDR False discovery rate

FLIM Fluorescent life-time imaging microscope

GSDM Gasdermin

HER2 Human epidermal growth factor receptor 2

HBXIP Hepatitis B virus X-interacting protein

HMGB1 High motility group box-1

HSP Heat shock protein

IBC Inflammatory breast cancer

ICE Interleukin-*1* converting enzyme

IDL Interdomain linker

IFN Interferon

IHC Immunohistochemistry

IL Interleukin

ILC Innate lymphoid cells

iNOS Inducilbe nitric oxide synthase

IRAK IL-1R associated protein kinases

IRF IFN regulator factor

Jak Janus kinase

MaSC Mammary stem cell

MDSC Myeloid derived suppressor cell

MDM Monocyte-derived macrophages

MAPK Mitogen-activated protein kinase

MD2 Myeloid chemoattractant protein

mRNA messenger RNA

Mtb Mycobacterium tuberculosis

MW Molecular weight

MyD88 Myeloid differentiation primary response 88

NCRI National cancer registry Ireland

NFκB Nuclear factor kappa-light-chain-enhancer of B cells

NK Natural killer

NLR NOD-like receptor

NO Nitric oxide

OCR Oxygen consumption rate

OXPHOS Oxidative phosphorylation

LBP LPS binding protein

LDH Lactate dehydrogenase

LPS Lipopolysaccharide

LRR Leucine rich repeat

PAMP Pathogen associated molecular pattern

PBS Phosphate buffered saline

PCR Polymerase chain reaction

PCA Principal component analysis

PINK1 PTEN-induced putative kinase 1

PTM Post-translational modifications

PPP Pentose phosphate pathway

PPR Pattern recognition receptor

PR Progesterone receptor

RIG Retinoic acid inducible gene

RLR RIG-I like receptor

ROS Reactive oxygen species

RT Room temperature

STAT Signal transduction and activator of transcription

STING Stimulator of interferon genes

TACE TNF converting enzyme

TAM Tumour associated macrophage

TCA Tricarboxylate citrate acid

TIRAP TIR domain containing adaptor protein

TLR Toll-like receptor

TNBC Triple negative breast cancer

TNF Tumour necrosis factor

TNFAIP TNFα induced protein

TME Tumour microenvironment

TIME Tumour immune microenvironment

WHO World Health Organisation

1.Chapter 1: Introduction

1.1. Introduction

1.1.1. *Innate Immunity*

Innate immunity is the primary source of defence against invading microbes and was classically considered a non-specific response. Innate immunity senses microbial pathogens which trigger mechanisms to eliminate and resolve threats of infection. The innate immune system is an evolutionary conserved defence system with key features shared across mammals, invertebrates, and plants. Defences of innate immunity include physical barriers such as skin, gastrointestinal and respiratory mucosal tracts, and specialised myeloid, lymphoid and effector cells and non-professional cells such as epithelial cells, fibroblasts, and endothelial cells. Inflammation induced by the presence of pathogens and tissue damage is an essential mechanism of innate immunity and chronic tumour-inducing inflammation is considered a major hallmark of cancer[1]. The other arm of immunity is the adaptive immune response, traditionally defined as the memory response, which arose 500 million years ago and is confined to vertebrates. Innate immune responses are required to activate adaptive immunity, by which B and T cells are activated in response to specific antigens presented by innate immune cells to provide pathogenic clearance[2,3]. Innate immune memory has developed our understanding of innate immunity as a rapid recruitment of phagocytic cells to clear pathogens. Innate immune memory is a non-specific short-lived phenomenon described as the change in reactivity in innate immune cells following previous exposure to stimmuli[4]. Innate memory refers to altered effectiveness of subsequent defensive innate response which may differ to the initial challenges, in either a boosting or dampening manner. Within innate training the phenomenon of memory induction involving innate immune reprogramming by stimuli is referred to as priming[5]. Several studies address the effect of trained memory after the priming of macrophages with bacterial endotoxins for which there is decreased activity of reactivated macrophages with a subsequent challenge[5]. *In vivo* vaccinations for Tuberculosis with gram-negative bacterium *Bacillus Calmette-Guerin* induces a more efficient immune response to a subsequent challenge and additional resistance to unrelated subsequent challenges, mediating a long-term nonspecific effect of the vaccination[6].

Recognition of microbial pathogens by cells of the innate immune system relies upon a family of germ line-encoded pattern recognition receptors (PRRs) which sense pathogen and danger associated molecular patterns (PAMPs/DAMPs). PAMPs are distinct evolutionary conserved structures on pathogens, essential for survival and distinguishable from self. Whereas DAMPs are recognised as host factors in aberrant locations or abnormal molecular complexes resulting

from infection, inflammation, or other cellular stresses. Commonly engaged PAMPs include lipopolysaccharide (LPS), peptidoglycans, flagellin and nucleic acid from bacteria, viruses and fungus, and commonly encountered DAMPs are reactive oxygen species (ROS), deoxyribonucleic acids (DNA) and adenosine triphosphate (ATP)[7]. Upon PAMP or DAMP engagement, PRRs trigger intracellular signalling and activate inflammation and anti-microbial responses. PRR engagement triggers a spectrum of different intracellular signal transduction pathways involving adaptor molecules, kinases, and transcription factors. These ultimately lead to the transcription of genes and synthesis of molecules including cytokines, chemokines and immunoreceptors to aid in innate immune clearance and activation of the adaptive immune response[7,8].

1.1.2. Pattern Recognition Receptors

PRR families are generally divided into either transmembrane, toll-like receptors (TLRs) and C-type lectin receptors (CLRs), or intracellular receptors, nucleotide-binding oligomerisation domain (NOD) like receptors (NLRs), retinoic acid-inducible gene (RIG) I-like receptors (RLRs) and AIM2-like receptors (ALRs)[9]. PRR engagement is dependent on type of PAMP presented by a microorganism or DAMP and the responding cell. However, PRR signal transduction pathways converge at a common set of transcription factors such as nuclear factor- (NF-)κB, mitogen-activated protein kinase (MAPK) and activator protein -1 (AP-1). These transcription factors are drivers of a range of proinflammatory cytokines including IL1, IL6, TNFα[10,11]. Other intramembrane and cytosolic sensors of PAMPs and DAMPs include receptor for advanced glycation end products (RAGE), cyclin guanosine monophosphate adenosine monophosphate (cGAMP) synthase (cGAS), and cysteine aspartic protease (caspase)-11[12].

1.1.3. Toll-like Receptors

TLRs are the most extensively characterised member of the PRR family. Structurally, TLRs are integral glycoproteins consisting of an extracellular or luminal ligand binding domain characterised by N-terminal leucine-rich repeats (LRRs) followed by a transmembrane region and cytoplasmic Toll/IL-1R homology (TIR) domain[13]. Upon PAMP or DAMP engagement with ligand-binding domain of TLR, adaptor molecules myeloid differentiation factor 88 (MyD88) and TIR-domain-containing adaptor protein (TIRAP) are recruited. Oligomerisation of receptors leads to the activation of intracellular signal transduction pathways which culminate at the initiation of transcription factors NF-κB, AP-1 and MAPK. These transcription factors regulate cytokine,

type I interferon (IFN) and chemokine expression[14]. There are 10 known TLRs in humans and 12 in mice. Each TLR recognises different molecular patterns on microorganisms and from self (**Fig.1.1**) [8,11]. TLR4 is the best characterised TLR family member. In addition to its recognition of LPS, several other bacterial components such as mannuronic acid polymers, of gram-negative bacteria, and teichuronic acid from gram-positive bacteria are recognised. Viral components include the F protein of respiratory syncytial virus, endogenous molecules including heat shock proteins, fibronectin III extra domain A and saturated fatty acids are ligands of TLR4. TLR4 signalling requires the formation of a complex for ligand recognition. Signalling of TLR4 initiates with ligand LPS binding to LPS binding protein (LBP) within the serum, which transfer LPS to CD14. CD14 is a glycosylphosphatidylinositol-anchored membrane protein which binds LPS/LBP complex with high affinity. CD14 does not contain an intracellular signalling domain, its role is to function as a LPS receptor complex component. Another protein MD-2, required for TLR4 LPS ligand binding, associates with the extracellular TLR4 domain. TLR4 ligand binds to TLR4/MD-2 complex suggesting a role for MD-2 in determination of binding specificity of the complex for variants of LPS[15]. Once TLR4 ligand binds cell surface receptor, TLR4 homodimerises through interaction between their intracellular TIR domains, leading to conformational changes in the molecule. Following homodimerisation, subsequent recruitment of TIR-domain containing adaptor molecule mediates intracellular signalling. TIR-domain-containing adaptor molecules known to mediate TLR4 signalling include MyD88 and TIRAP, TIR-domain-containing adaptor inducing interferon-β (TRIF), and TRIF-related adaptor molecule (TRAM). Two major pathways induced by TLR4 signalling induced include TIRAP-MyD88 which regulated NF-κB early activation and expression of related inflammatory cytokines, or TRIF-TRAM which regulate interferon regulated factor-3 (IRF3) that leads to the upregulation of type I IFN and co-stimulatory encoding genes. TRIF signalling pathway is also associated with late NF-κB activation via IRF3 induced TNFα expression and secretion which subsequently feeds back binding tumour necrosis factor receptor (TNFR) and NF-κB nuclear translocation[16]. LPS inducing TLR4/MyD88-dependent signalling has the ability to induce transcription of pro-IL-1β via NF-κB transcription factor activation. This potent pro-inflammatory molecule requires a second checkpoint for maturation and secretion as well as the ‘priming` induced by TLR4. This second ‘activation` signal is mediated by caspase-1, whose activation is commonly executed by NLRs and ALRs, major components of inflammasome complexes[17],[18].

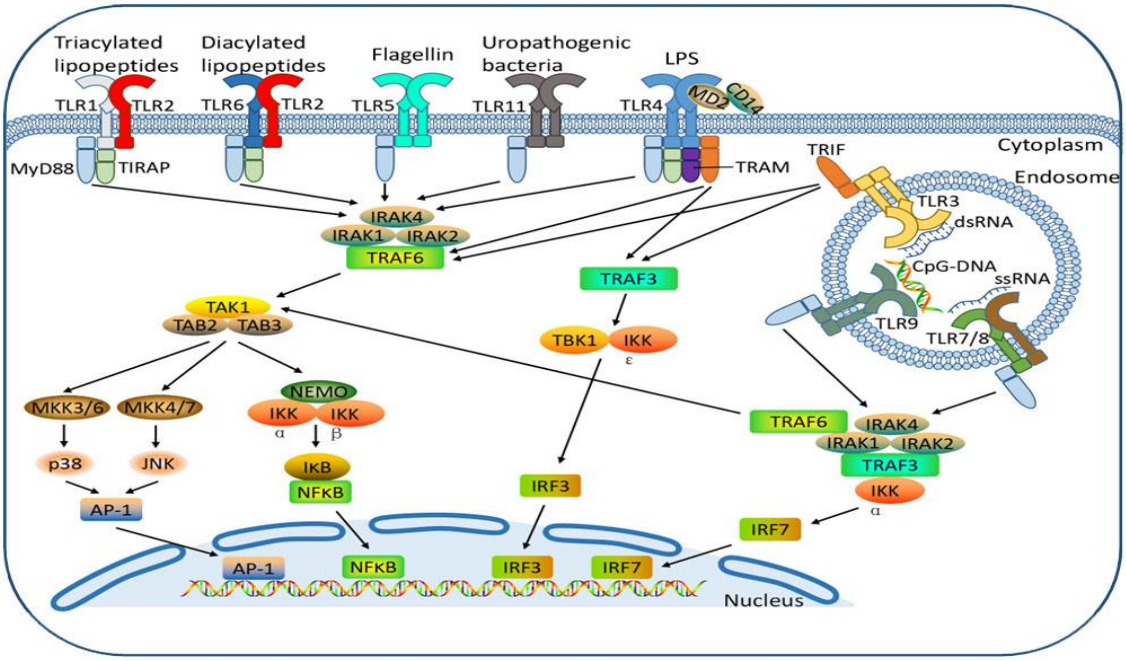

Figure 1.1: TLR localisation, ligands and signalling pathways. TLRs 1, 2, 4, 5, 6, 10, 11 are cell surface transmembrane receptors and TLR 3,7, 8, 9 are intracellular endolysosomal receptors which recognise a variety of specific PAMPs to trigger TLR signalling cascades[19].

1.2. Inflammatory Caspases

1.2.1. Inflammatory Caspases

Caspases are a group of cysteine aspartic proteases involved in apoptosis and cytokine maturation. Caspases can be categorised into 3 families, inflammatory caspases (Group I) or initiator (Group II) or effector (Group III) apoptotic caspases, based on their structure, substrate specificity and function[20]. Inflammatory caspases consist of four members: caspase-1 (previously known as interleukin-1β converting enzyme, ICE), -4, -5 (murine orthologue caspase-11) and -12. The inflammatory caspase genes are located on chromosome 11q22.2-q22.3[21]. The murine genes are located on syntenic region of the mouse chromosome 9A1[22]. Inflammatory caspases were first identified as pre-aspartate-specific proteases involved in the cleavage of the pro-IL-1β (31kDa) precursor to its mature, biologically active form, IL-1β (17kDa)[23]. Interleukin-1β converting enzyme (caspase-1) was identified as a unique cysteine protease composed of two non-identical subunits derived from proenzyme[24],[25]. Caspase enzymatic activity is ruled by dominant specificity for aspartic acid containing proteins and cysteine side chain which act as catalytic nucleophile to employ peptide cleavage[26]. Evolutionarily, caspase zymogens share a conserved N-terminal pro-domain and a C-terminal catalytic domain **(Fig. 1.2)**. Protease domain consists of a large (20kDa) and small (10kDa)

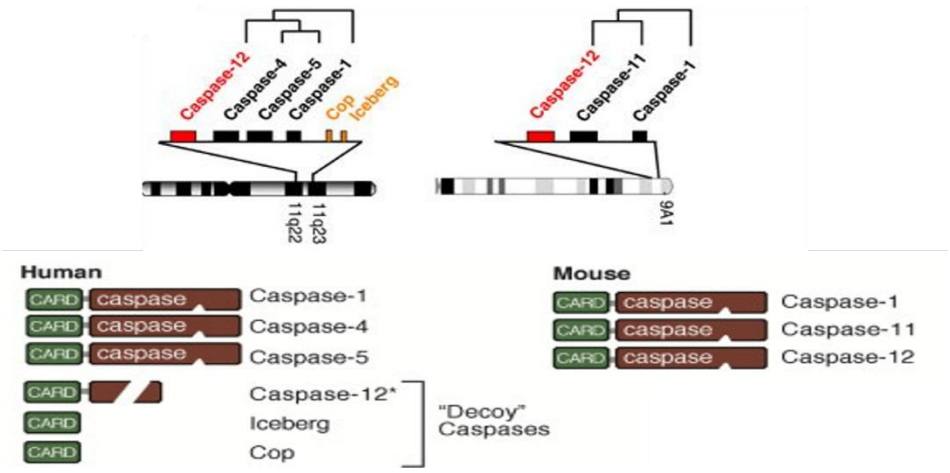

Figure 1.2: Inflammatory caspases chromosomal localisation and structural domains. Chromosome 11q22-23 arranged from telomere to centromere encompasses CASP1, CASP4, CASP5 and CASP12. Murine chromosome 9A1 encompasses CASP1, CASP11 and CASP12. Caspase-4 and -5 in humans has high homology with murine caspase-11 suggesting they may be risen from a duplication event during evolution. Inflammatory caspases consist of a CARD-containing prodomain, and a large and small catalytic subunit. Whereas decoy caspases; Iceberg and CARD-only protein (Cop), a regulator of caspase-1, and caspase-12 a short variant[2128].

subunit that contains the catalytic cysteine residues[27]. Inflammatory caspases are expressed in most cells as inactive monomeric zymogens (pro-caspases) and require processing and heterodimerization to aid it their activation. Casapase-1 is the prototypical member of the inflammatory caspases. During caspase activation, catalytic domains are cleaved into p20 and p10 subunits, which interact with each other immediately to form a heterodimer of p20/p10/p10/p20 construction. This gives rise to an active species, with two catalytic sites per molecule (p46)[27]. Allosteric regulation of caspase-1 active sites such that the occupation of one active site promotes the activity of the second site. Thornberry and colleagues discovery of caspase-1 (ICE), observed that enzymatically active caspase-1 formed a heterodimer (p20/p10) complex in order to mediate pro-IL-1β maturation[24]. Structural studies of caspase-1 suggested that the spatial separation of C-terminus of p20 and N-terminus of p10 would give rise to two alternative assembly pathways and activation *in vivo*[29]. Broz and colleagues observed pyroptosis and cytokine maturation response to pathogens can be mediated by 2 distinct inflammasome complexes. An ASC containing inflammasome platform induces caspase-1 auto-processing and cytokine maturation[30]. Contrastingly, ASC-independent inflammasome activated caspase-1 without induction of auto-processing and do not form large specks visible in the cytoplasm. Instead, ASC-independent caspase-1 activation promotes rapid pyroptosis but inefficiently process IL-1β and IL-18[30]. Schroder and colleagues described the self-cleavage of caspase-1 and

its intrinsic mechanism to terminate inflammasome activity in 2018[31]. Initially, pro-caspase-1 is recruited to the inflammasome platform via N-terminal CARD-CARD domain interactions with ASC of the signalling platform. Engagement with the inflammasome allows caspase-1 activation by increased molecule concentration facilitated dimerization, which enables caspase-1 protease activity[32]. Caspase-1 consists of an N-terminal CARD domain separated by the catalytic domain by CARD domain linker (CDL) and p20 and p10 protease units are separated by an interdomain linker (IDL) (**Fig. 1.3**)[33]. Caspase-1 undergoes proteolytic cleavage at D297 and D316 to remove IDL region, generating p10 and p33 subunits. P33 subunit consisting of p20 and CARD units is further cleaved at D122 and D103 inducing the release of p20 catalytic subunit[30]. Alternative splicing induces the release of alternative products include p24 and p14 subunits. Schroder and colleagues investigated the active species of caspase-1 as it is widely assumed to be p10 and p20 as they are inflammasome activation cleavage products secreted from the cell, and recombinant p20/p10 is catalytically active. Schroder and colleagues described self-processing of p33/p10 subunit by CDL-cleaving to be a regulator mechanism of caspase protease deactivation. Upon CDL cleave p20/p10 subunit is released from the inflammasome. Unbound p20/p10 is unstable and leads to loss of dimeric structure and termination of proteolytic activity[33].

Upon NLRP3 inflammasome activation caspase-1 undergoes post-translational modifications (PTM). K63 polyubiquitination PTM occurring at CARD domain requires cellular inhibitors of apoptosis (cIAP). cIAP1 and cIAP2 deficient mice exhibits attenuated caspase-1 activity[34]. Therefore, cIAPs associated with caspase-1 pro-domain non-degradative ubiquitination is required for caspase-1 proteolytic activity. Accumulation of intracellular superoxide inhibit caspase-1 activity by S-glutathionylation at C362 and C397, which are identically expressed in caspase-4 and caspase-5 sequences, avert proteolysis[35]. S-glutathionylation occurs at cysteine residue to protect against oxidation.

Faucheu and colleagues first identified caspase-4 and caspase-5 as members of the ICE (caspase-1) family in 1996. Caspase-4 and -5 conserved catalytic pentapeptide (Gln-Ala-Cys-Arg-Asp) sites, aspartate-binding pockets are associated with caspase-1 and they are synthesised as inactive precursor zymogens with C-terminal CARD domain[36]. Caspase-4 demonstrated auto-proteolysis and cleavage of p30 caspase-1 precursors[37]. Caspase-5 also demonstrated protease activity of its own precursor dependent on cysteine residue 245 active site[38]. Once proteolytically processed caspase-4 and -5 form heterodimeric active enzymes.

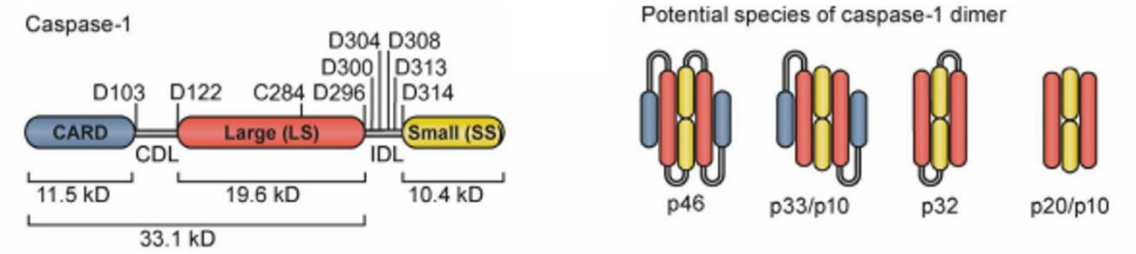

Figure 1.3: Caspase-1 structure and possible species of dimeric caspase-1 generated by self-cleavage. Illustration represents potential self-processing sites within CARD domain linker (CDL) and interdomain linker (IDL) of murine caspase-1, relative to catalytic cysteine (C284)[33].

However, both caspase-4 and –5 failed to cleave pro-IL-1β but when overexpressed induced cell death[35,37,38]. Caspase-4 and -5 are considered human orthologues of murine caspase-11 with 68% and 47% amino acid sequence identity, respectively (**Fig. 1.4**). Early studies of the inflammasome in *Casp1*$^{-/-}$ 129 strain mice obscured the importance of caspase-11. 129 strain has a slice site deletion in *Casp11*, resulting in the premature termination of caspase-11 transcription. Hence *Casp1*$^{-/-}$ mice of 129 strain background are (*Casp1*$^{-/-}$*Casp11*$^{129mt/129mt}$) double knockout of both inflammatory genes.

Caspase-11 overexpression and LPS stimulation has been demonstrated to induce auto-proteolysis at two internal sites resulting in release of processed endogenous fragments. D59 or D80 cleaves CDL to remove N-terminus CARD domain from large subunit and further cleavage at D285 cleaving ILD, separating large and small catalytic domains (**Fig. 1.5**)[39]. Bettina and colleagues demonstrated caspase-11 enzymatic activity and auto-processing using a septic shock model on genetically altered mice[40]. *Casp11*$^{Enz\ C254A/C254A}$ exchanges cysteine for alanine residue at the enzymatic active site 254, mutating activity, and *Casp11*$^{Prc\ D285A/D285A}$ generated by exchanging aspartic acid residues at IDL site for alanine, disrupting the processing between the 2 catalytic subunits. Self-proteolysis of caspase-11 at ILD is essential for the activation of downstream events including GSDMD-N pore formation, and IL-1β and IL-18 secretion[40].

Mounting evidence has suggested an apoptotic role for caspase-4 in endoplasmic reticulum (ER) stress-induced cell death[41,42]. The role of ER involves protein folding, maturation, storage and secretion. ER-stress is triggered when ER capacity is overwhelmed by cellular demand. Accumulation of unfolded protein aggregates proceeds to activate the unfolded protein response (UPR), which in excess irreversibly enables cell death. Caspase-4 is located within the ER and is associated with components of the ER-stress signalling pathway inducing GRP78, an

ER stress marker, CARD-only protein (Cop or pseudoICE), Apf1, and TRAF6[42]. ER-stress induced apoptosis of lung and esophageal cells is regulated by caspase-4[43].

Figure 1.4: Human caspase-4 and -5 and murine caspase-11 sequence alignment. Amino acid sequences of human caspase-4 and-5 and murine caspase-11 were obtained from Uniprot. Accession codes were; caspase-4, P49662; caspase-5, P51878; caspase-11, P70343. Amino acid sequences were aligned using Uniprot BLAST and BOXSHADE. The amino acid homology between caspases is: 63% between human caspase-4 and -5, 68% between human caspase-4 and murine caspase-11, and 47% between human caspase-5 and murine caspase-11. Underlined amino acids of all 3 sequences encode the CARD domain. Amino acids in black indicate lack of similarity, amino acids in red represent identical amino acids, blue indicates 2 amino acids are identical and green indicates conserved amino acids. Identical QACRG sequence identified in all 3 protein sequences, indicted by the black box, is the active site of these zymogens.

Caspase-4 has been reported to interact with TNF receptor-associated factor 6 (TRAF6) and mediates LPS induced-NF-κB dependent production of IL-8 and CC chemokine ligand 4 (CCL4)[44]. LPS induced nuclear translocation of NF-κB is inhibited in caspase-4 deficient clones of monocytic cell line, THP-1. The TRAF6- caspase-4 interaction occurs via a TRAF6-binding motif (PPESGE) identified within caspase-4 and is triggered following LPS stimulation. A TRAF6-binding motif identified within apoptotic caspase-8 is important for mediating NF-κB activation[44]. Caspase-4 mediates IL-1α secretion and cell death, in primary human macrophages, independently of caspase-1 against several pathogens including *Legionella pneumophila*, *Yersinia pseudotuberculosis*, and *Salmonella enterica* serovar *Typhimurium*. These virulent bacterial strains translocate bacterial products to the cytosol for caspase-4 activation through virulence-associated type III and type IV secretion systems (T3SS and T4SS)[45].

Caspase-4/5/11 induce non-canonical inflammasome activation through binding hexa-acylated lipid A, the lipid binding motif of LPS[46]. Under-acylated lipid A expressing pathogens such as *Francisella novicida,* escapes caspase-11 recognition in mice. However, this immune escape is not observed in humans as *F. novicida* is recognised by caspase-4, driving the GSDMD-dependent pyroptosis and non-canonical inflammasome activation in human macrophages[46]. These PAMP recognition differences between caspase-4 and caspase-11 stress the importance of disease models for predicting clinical implications and potential of non-conserved amino acids highlighted in the amino acid sequence cluster alignment of caspase-4/5 and caspase-11.

Similar to caspase-11, caspase-5 expression is upregulated by LPS and IFN-γ[47]. Although caspase-5 and caspase-11 only share 47% identity, data suggests that human caspase-5 is a functional orthologue. Immunoprecipitation experiments demonstrate that the caspase-5 precursor and p20 isoform co-express with caspase-1, as well as other NLRP3 inflammasome components, similar to the caspase-1 and caspase-11 direct physical interaction[48]. A study by Martinon and colleagues demonstrates that caspase-5 participation facilitates more efficient processing of pro-IL-1β[17,49].

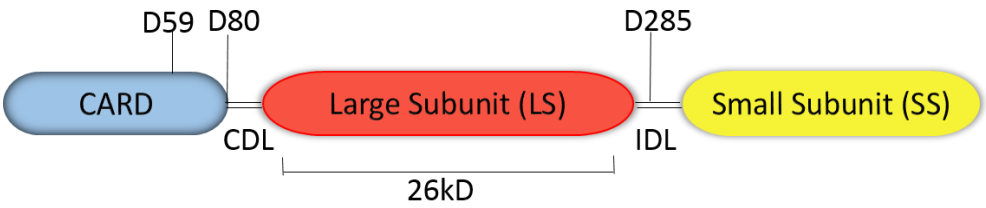

Figure 1.5: Caspase-11 structure and cleavage sites. Illustration of caspase-11 domains, indicating D59 or D80 cleaves CARD domain linker (CDL) to remove N-terminus CARD domain from large subunit and further cleavage at D285 cleaving interdomain linker (ILD), separating large and small catalytic domains.

1.1.1. Caspase-1 Canonical Inflammasome

Caspase-1 is the best characterised inflammatory caspase particularly in terms of its involvement in inflammasome signalling. Inflammasomes are the central signalling hub of innate immunity inflammation and form multiprotein complexes which assembly in response to PAMPs or DAMPs triggering NLRs and ALRs distinct defence signalling assembly. The term inflammasome encompasses a family of multiprotein signalling platforms divided by the NLRs or ALRs involved in assembly[50]. Martinon *et al.,* demonstrated inflammasome assembly comprised of several different NLR protein family members and the adaptor apoptosis-associated speck-like protein (ASC), containing a CARD domain, to provide a platform for pro-caspase-1 cleave and activation which is essential for the maturation of pro-IL-1β and pro-IL-18, and pyroptosis[51]. Upon stimuli sensing of PRRs, inflammasome formation initiates with receptor oligomerisation into a multi-subunit wheel-shaped assembly. This wheel shaped receptor complex nucleates ASC, which aggregates to form macromolecular ASC speck and serve as an activation point for pro-caspase-1[50]. Caspase-1 CARD consists of six anti-parallel α helices with hydrophobic core and charged outer surface. CARD specificity such as length, and charge, dictates CARD-CARD protein interactions. Therefore caspase-1 N-terminal CARD domain is regulated by other CARD containing proteins[51]. It was previously thought that dimeric caspase-1 proximity induced autocatalytic cleavage resulted in release of p20 and p10 subunits[30]. However as previously discussed, Schroder and colleagues suggest a new theory for caspase-1 self-processing activation and as a negative feedback loop to extinguish the inflammasome response.

Although the various inflammasomes respond to specific stimuli two signals are required for the activation of the canonical inflammasome (**Fig. 1.6**)[35]. NLRP3 canonical inflammasome is one of

the most well characterised inflammasome signalling pathways. NLRP3 inflammasome initial signal, signal 1, also known as 'priming` is induced by inflammatory stimuli which triggers NF-κB-dependent gene transcription upregulation of pro-IL-1β and NLRP3. Inflammatory stimuli targeting PRRs including TLR, NOD2 and RAGE, as well as the immune system through anaphylatoxin C3a and C5a receptors and IL-1 and TNF receptors can trigger MyD88 or TRIF signalling pathways leading to NF-κB nuclear translocation[35]. Triggering PRR, cytokine receptors and their subsequent signalling pathways leads to innate priming.

The second signal or 'activation` step is triggered by NLRP3 sensing intracellular PAMPs and DAMPs and involves the subsequent assembly of inflammasome components. Cellular stresses elicited by PAMPs and DAMPs include membrane permeablisation, mitochondrial stress and lysosomal disruption. ATP, nigericin, an ionophore with high affinity for Na+ and K^{+}[52], and complement membrane attack complex are pore-forming agents comprising membrane permeability[35]. Necrotic cell extracellular ATP forms ionic channels on the cell plasma membrane via P2X7R sensing and pannexin-1 channels opening[53]. Complement system MAC assembly forms a pore in membrane enabling the trafficking of small ions triggering osmotic events and Ca^{2+} influx[54]. Mitochondrial stress encompasses metabolic stress, inhibition of respiratory chain complexes, and mitophagy inhibition[55]. Lysosomal rupture due to urea crystal phagocytosis and accumulation subsequently prompts phagolysosome rupture and release of Ca^{2+} and cathepsin B into the cytosol[56]. 'Activation` signalling of NLRP3 inflammasome is likely an indirect response of PAMPs and DAMPs triggering ion fluxes. Ion fluxes are considered to be critical for NLRP3 activation, including K^{+} efflux, Ca^{2+} signalling and Na^{+} influx[57–59]. NIMA-related kinase-7 (NEK7), an additional component of the NLRP3 inflammasome identified in recent years, also requires K^{+} efflux for assembly as part of the NLRP3 inflammasome[60]. Other responses to cellular stress such as reactive oxygen species (ROS) production and lysosomal destabilization can also induce NLRP3 inflammasome assembly independent of K^{+} efflux[61,62,91] (**Fig. 1.6**).

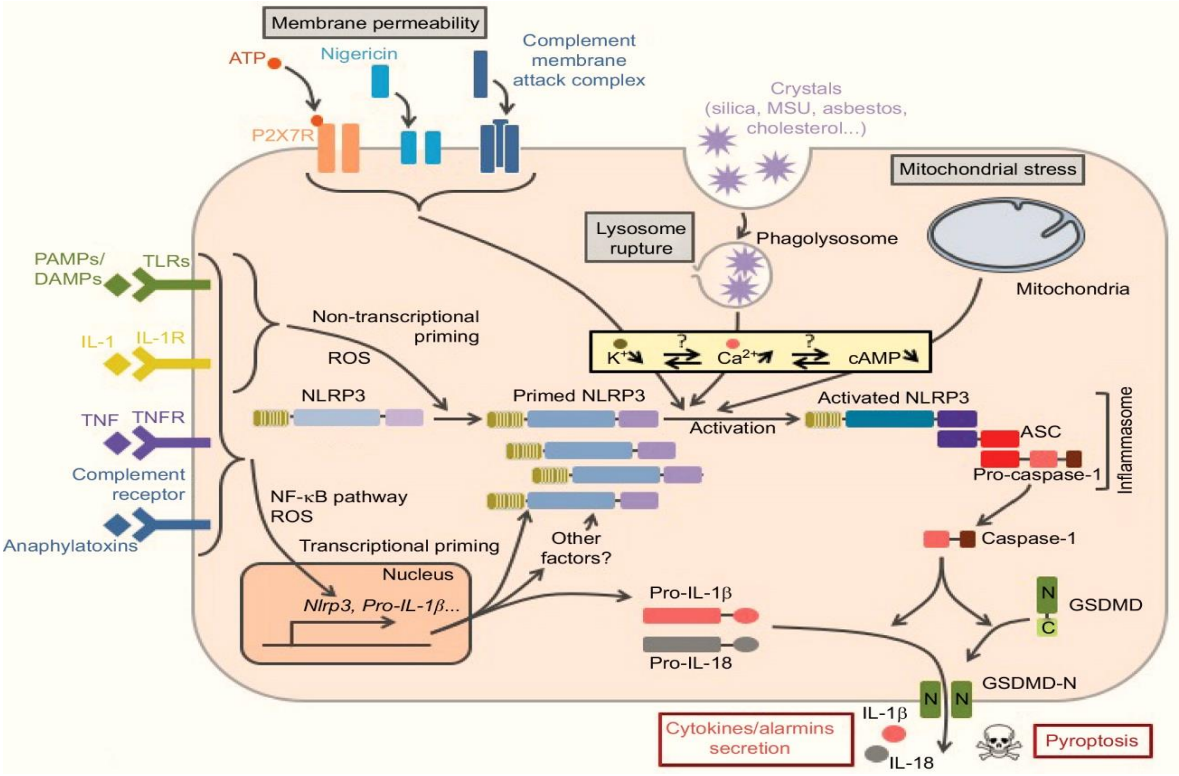

Figure 1.6: NLRP3 inflammasome priming and activation signals. Inflammatory stimuli priming signal including PAMPs/DAMPs, IL-1, TNF and anaphylatoxin induced NF-κB-dependent NLRP3 and pro-IL-1β translation. Non-transcriptional priming involves rapid post-translational modifications of NLRP3 such as phosphorylation and ubiquitination triggered by PAMPs/DAMPs and cytokines. Various cellular stresses induce the activation signal including membrane permeability, lysosomal rupture, and mitochondrial stress. K^+ efflux, Ca^{2+} signalling and decreased cAMP activate the assembly of primed NLRP3. Activated NLRP3/ASC/Pro-caspase-1 inflammasome complex leads to autoproteolysis and activation of caspase-1 which cleaves substrates pro-IL-1β, pro-IL-18 and GSDMD for the maturation and release of potent IL-1β inflammatory cytokine and induce pyroptosis[35].

1.2.2. Caspase-4, -5 and Caspase-11 non-canonical inflammasome

Similar to the canonical inflammasome, the non-canonical inflammasome, which is the most documented role of caspase-11, ultimately leads to pyroptosis and release of mature proinflammatory cytokines, albeit by different mechanism (**Fig. 1.7**)[63]. Caspase-4 and -5 or caspase-11 stimulation ultimately triggers non-canonical inflammasome activation. Reports propose caspase-11 elicits control of NLRP3 assembly, as demonstrated in LPS treatment BMDMs[64]. However, caspase-11 is dispensable for caspase-1 activation in the presence of NLRP3 agonist, ATP. Studies suggest caspase-11 is activated by distinct mechanisms independent on

NLRP3 but acts synergistically to regulate caspase-1 activity[65,66]. Activation requires a transcription-dependent 'priming` signal to upregulate caspase-5 or -11 expression. Caspase-4 is thought to be constitutively expressed within tissue at basal levels, which may increase following stimulation but caspase-5 and caspase-11 expression in macrophages require priming[47,67]. Once expressed within the cell caspase-4, -5 and -11 function as intracellular sensors of LPS[68]. Cytoplasmic translocated penta-acylated and hexa-acylated LPS induce caspase-11 activation, however this is not observed with tetra-acylated LPS[69]. TLR4-mediated caspase-11 priming enhances its activation but is not necessary. TLR4, TRIF and IFNAR-deficient macrophages transfected with LPS produce mature IL-1β and lead to pyroptosis[70]. Caspase-11 can bind cytosolic LPS lipid A moiety directly via its CARD domain which initiates oligomerisation and proximity-induced activation of catalytic subunits[71]. Active caspase-11 proteolytically cleaves Gasdermin D (GSDMD) (30kDa), to release its N-terminal pore-forming fragment (GSDMD-N). Pore formation occurs immediately, with an inner diameter of 10-14 nm, resulting in loss of ionic gradient and cell membrane rupture, pyroptosis[72]. GSDMD-N pore formation triggers K^+ efflux, inflammasome activation and caspase-1 processing, leading to proinflammatory cytokine maturation (**Fig. 1.7**)[25]. Mature IL-1β and other DAMPs are passively released from the cell via GSDMD-N pores. Studies in *Casp1*$^{-/-}$ macrophages reconstituted with mutant auto-cleaved caspase-1 retained the ability to induce pyroptosis but demonstrated a lost capacity for IL-1β maturation and release, demonstrating caspase-11 ability to cleave GSDMD independent of the canonical inflammasome and caspase-1[25].

GSDMD-NT β1–β2 loop pre-pore is critical for insertion into the lipid bilayer, these β loops hydrophobic ends serve as an anchor while surround basic residues interact with acidic lipids. Once the GSDMD-NT fragments are inserted into the lipid bilayer, they oligomerise and form ring-like structures via ragulator-rag-mTORC1-mtROS pathway[73]. Ragulator-Rag is not required for GSDMD cleavage but promotes oligomerisation following insertion into the plasma membrane. Prior biophysical studies could not determine if GSDMD-NT monomers preassembled to form oligomer which insert into plasma membrane, or if monomers inserted into the plasma membrane oligomerised. One hypothesis is that the GSDMD-NT pore enriched negative potential preferentially releases positively charged mature IL-1β, rather than the negatively charged pro-form, via electro-static dependent events[74].

The Tricarboxylate citrate acid (TCA) cycle intermediate, fumarate, and exogenously delivered dimethyl fumarate can convert GSDMD cysteine to S-(2-succinyl)-cysteine, known as succination. This prevents the GSDMD-caspase interaction, thereby inhibiting pyroptosis[75]. Evavold and colleagues suggest a metabolite checkpoint, after itaconate modulated NLRP3

activity or fumarate inhibited GSDMD cleavage, upstream of mTOR to regulate pore formation. Therefore GSDMD-NT cleavage is not equivalent to pyroptosis[76].

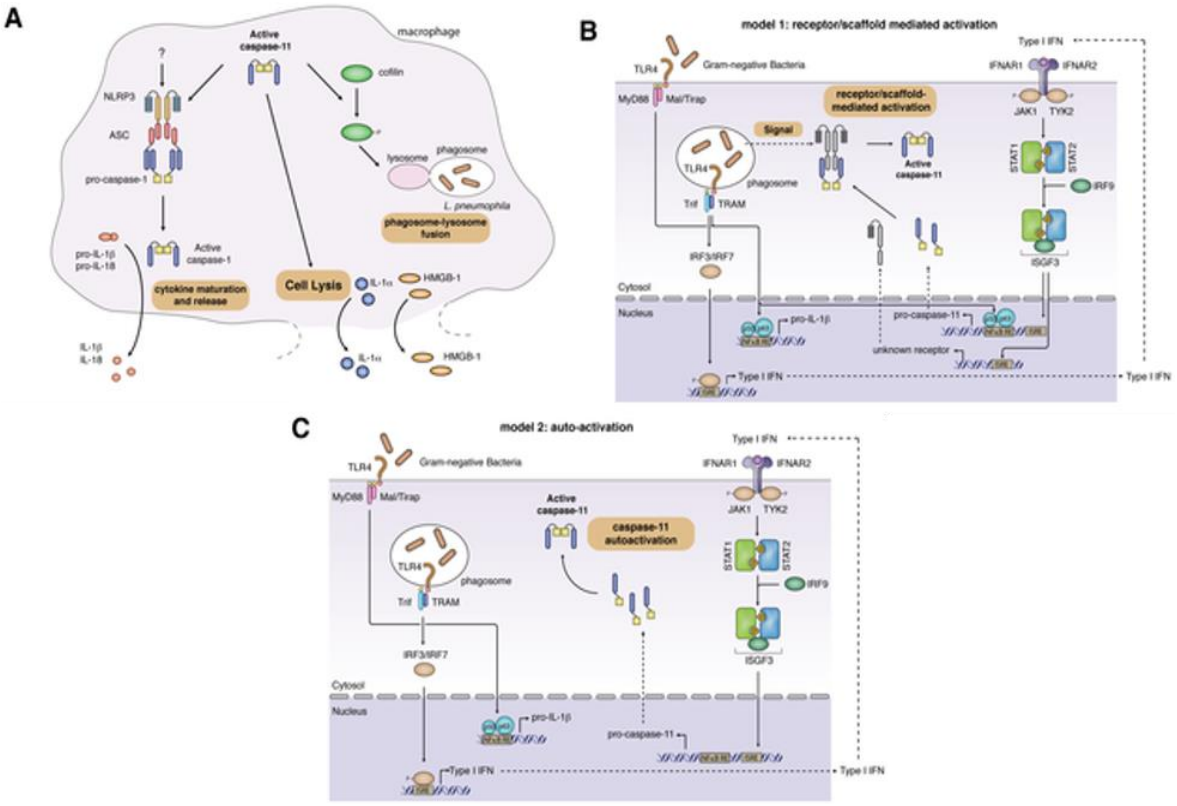

Figure 1.7: Caspase-11 non-canonical inflammasome activation. A. Caspase-11 acts upstream NLRP3/ASC/caspase-1 inflammasome to encourage caspase-1-dependent IL-1β and IL-18 maturation and release. Release of DAMPs; IL-1α and HMGB1 is triggered during caspase-11 induced cell lysis. Active caspase-11 regulates phagosome-lysosome fusion via cofilin phosphorylation. B. TLR4/MyD88 signalling regulates NF-κB activation leading to pro-caspase-11 and pro-IL-1β upregulation. Gram-negative bacteria TLR4/TRIF/IRF3 signalling prompts type I IFN expression. Type I IFN feedback through IFNAR1/IFNAR2 activating Jak/STAT signalling pathway and contribute to pro-caspase-11 expression. Type I IFN signalling is also thought to give rise to the expression of an unknown activator of caspase-11 which may aid its activation during bacterial infection. C. Similarly to the previously mechanism TLR4/MyD88 signalling mediates pro-IL-1β expression and TLR4/TRIF/IRF3 induced type I IFN expression. Type I IFN activates Jak/STAT pathway to upregulate pro-caspase-11 expression. Accumulation of pro-caspase-11 in the cytosol leads to auto-activation of caspase-11[61].

Endogenous type I IFN mediated by TLR4/TRIF signalling is critical for activation of caspase-11 in murine macrophages infected with gram-negative *S.Typhimurium*[66]. Gram negative bacterial TRIF engagement mediates caspase-11 activation via type I IFN, resulting in caspase-11 induction and autoprocessing, identifying TRIF as an important mediator of caspase-11[66]. However, pro-caspase-11 upregulation mediated by type I IFN independent of TLR4 signalling pathway, which is consistent with proposal of existence of IFN-inducible activator of caspase-11 transcription[77]. Caspase-11 induced cell death following infection with *S.Typhimurium* is detrimental to the host in the absence of caspase-1. Caspase-1 deficient mice are more susceptible to infection compared to $Casp1^{-/-}$/$Casp11^{-/-}$ mice as observed by increased bacterial counts and defective neutrophil mediated clearance[78]. $Casp11^{-/-}$ *S.Typhimurium* infected macrophages have decreased lactate dehydrogenase (LDH) release, a measure of cytotoxicity, compared to WT. Therefore caspase-1 and caspase-11 act cohesively during *S.Typhimurium* infection to mediate neutrophil bacterial clearance and macrophage pyroptosis, respectively[78]. Induction of pro-caspase-11 in $TLR4^{-/-}$, $TRIF^{-/-}$ and $MyD88^{-/-}$ macrophages infected with *S.Typhimurium* is significantly delayed, yet not totally abolished, suggesting that caspase-11 transcription may be promoted by several different transcription factors[78].

Schauvilege and colleagues demonstrated that STAT1 as well as NF-κB transcriptional activity induced caspase-11 gene expression in response to treatment with LPS and IFN-γ[77]. Their study concluded that the most important region of the caspase-11 promoter which conferred responsiveness to LPS and IFN-γ stimulation was located within the first 186bp of the transcriptional start site. Mutation of NF-κB caspase-11 transcriptional binding site results in completely loss of LPS inducibility, whereas IFN-γ response is decreased but not completely eliminated. IFN-γ inducibility is completely abrogated when a point mutation is introduced to STAT1 transcriptional binding site of caspase-11 promoter. LPS responsiveness is similarly abolished when mutation of STAT1 binding site is introduced, suggesting that the STAT1 binding region is involved in LPS caspase-11 inducibility, which may be a consequence of a second NF-κB binding site overlapping with STAT1 binding region[77]. Therefore, LPS and IFN-γ regulate caspase-11 transcriptional activation through the activation of NF-κB and STAT1, respectively, with some overlap between the two pathways. Rathinam and colleagues identified TRIF as a regulator of caspase-11 activation. Gram negative bacterial TRIF induction activates caspase-11 via type I IFN, which was found to be necessary for caspase-11 autoactivation. Thereby, demonstrating caspase-11 dependency on type I IFN for caspase-11 activation[66]. A recent study by Zaslona and colleagues examining the role of caspase-11 in allergic airway inflammation further illustrated a relationship between caspase-11 and STAT1. This study supports findings

suggesting that LPS induced type I IFNβ activated by STAT1 mediates caspase-11 transcription. Oligonucleotide pull down of caspase-11 promoter in BMDMs after 2 hours LPS treatment showed co-immunoprecipitation with STAT1, which was inhibited by treatment with prostaglandin E_2 (PGE_2)[79]. TRIF induced signalling pathway promotion of pro-caspase-11 expression through NF-κB or IRF3 may depend on type I IFN production. Macrophages lacking type I IFN components such as IFNAR, IRF3 and STAT1 have delayed pro-caspase-11 upregulation but similar to TLR4 and TRIF, caspase-11 regulation is not completely inhibited[78]. Therefore, LPS recognition or type I IFN signalling alone cannot initiate caspase-11 dependent pyroptosis.

Caspase-11 required pannexin-1 activation to mediate pyroptosis was elucidated by Yang and colleagues[80]. Caspase-11 activation via engagement with cytosolic LPS induces caspase-11-dependent cleavage of pannexin-1, an anion selective channel, leading to release of ATP. Endogenous ATP activates P2X7 receptor inducing transmembrane K^+ and Ca^{2+} flux and consequently mediates cytotoxicity. Cytosolic LPS mediated pyroptotic cell death is abrogated when pannexin-1 and P2X7 are absent. Catalytic activity of caspase-11 is required for pannexin-1 cleavage which is essential for release of ATP, the NLRP3 agonist, and subsequent engagement with P2X7R, to mediate pyroptosis. In an experimental model of endotoxic shock LPS or TLR3 agonist primed caspase-11 followed by secondary LPS challenge demonstrate increased mortality, not observed in either $Casp11^{-/-}$, $Panx1^{-/-}$ or $P2X7^{-/-}$ mice. Therefore pannexin-1 and P2X7 are critical downstream molecules in caspase-11 mediated pyroptosis[80]. In a recent paper by Broz and colleagues pannexin-1 activation was identified to drive NLRP3 inflammasome assembly during intrinsic and extrinsic apoptosis[81]. Additionally, pannexin-1 induced K+ efflux mediated NLRP3 inflammasome activating function drives IL-1β and GSDMD cleavage by caspase-1[82].

Alarmins do not contain signalling peptides to induce their cellular release; instead, their release correlates with loss of membrane integrity during pyroptosis. Caspase-11 mediated pyroptosis is therefore required for the release of alarmins, such as HMGB1 and IL-1α[65]. HMGB1 has been shown to mediate endotoxin delivery to the cytosolic compartments of macrophage and endothelial cells during sepsis, leading to the activation of caspase-11 and induction of pyroptosis[83]. However, caspase-11 was also observed to mediate HMGB1 release from hepatocytes, driving immune cell pyroptosis in the spleen, peritoneum, and gut[84]. LPS stimulated hepatocyte release of HMGB1, while caspase-11 dependent does not lead to the induction of cell death in hepatocytes themselves, but drives immune cell pyroptosis during

sepsis[84]. These studies demonstrate distinct cell-specific roles for HMGB1 in the context of infectious disease.

The processed, 17 kDa form of IL-1α is selectively released from the cell following calcium ionophore stimulation, without any changes in release of the full length 33 kDa form[85]. While calpain has been shown to be responsible for canonical IL-1α cleavage, inflammatory caspases have been implicated in IL-1α secretion from senescent cells that display an altered secretory activity, known as senescence-associated secretory phenotype (SASP)[65]. Murine hepatocytes were shown to require caspase-11 for SASP-driven IL-1α release and immune mediated clearance of senescent cells[86]. Fungal infection studies have provided additional evidence for the importance of caspase-11 mediated pyroptosis for alarmin release. BMDM infected with *Paracoccidioides Brasiliense* were demonstrated to require caspase-11 mediated pyroptosis for the release of IL-1α and the production of nitric oxide, both of which are involved in restriction of fungal replication[87].

1.2.3. Other functions of caspase-11

1.2.3.1. Modulation of Actin Dynamics

During Gram-negative bacterial infection, caspase-11 has been shown to function by promoting phagolysosome fusion, to enable the digestion of phagocytosed bacterium. Amer and colleagues demonstrated that the fusion of *Legionella pneumophila* containing phagosomes with lysosomes is mediated by caspase-11[88]. Interestingly, caspase-11 was dispensable for the delivery of non-pathogenic bacteria to lysosomes, suggesting that caspase-11 regulates an endocytic route that is distinct from other phagocytic pathways, and specific to pathogenic bacteria. Caspase-11 was shown to mediate phagolysosome fusion and clearance of *L. pneumophila* by promoting actin remodelling and the formation of a filamentous actin (F-actin) network around bacteria-containing vacuoles. Caspase-11-deficient BMDM demonstrated an absence of newly formed F-actin networks, which was accompanied by defective *L. pneumophila* clearance and an accumulation of replicative vacuoles. In support of these findings, phagolysosome fusion has also been shown to be prevented by disorganization of the F-actin network during *Mycobacterium avium* infection[89]. Cofilin is a major actin depolymerization factor that regulates cellular polarity during cellular migration, ruffling of the cell membrane, and driving the leading edge forward via depolymerization of F-actin filaments[90,91]. Dynamic phosphorylation of cofilin regulates actin remodelling in cells. Caspase-11 had previously been linked to the regulation of cofilin-mediated actin depolymerization via

its direct interaction with the cofilin activator, actin interacting protein 1 (Aip-1), to promote cell migration during inflammation[91]. The caspase-11 CARD domain was shown to interact with the C-terminal WD40 domain of Aip-1 to influence actin dynamics and cell migration during inflammation, which was independent of the RhoA-Rac-Cdc42 pathway[91]. Amer and colleagues observed that cofilin phosphorylation was impaired in *L. pneumophila* infected caspase-11-deficient BMDM and therefore proposed that caspase-11 functions to activate cofilin-mediated actin remodelling, allowing trafficking of pathogen containing phagosomes to lysosomes, to improve bacterial clearance[88].

A later study from the Amer group suggests that caspase-11 regulates the phosphorylation of cofilin via RhoA GTPase to mediate actin remodelling, phagolysosome fusion, and bacterial clearance during *L. pneumophila* infection[92]. This proposed mechanism is in conflict with the proposal that caspase-11 regulates cofilin activity via its interaction with Aip-1[91]. Activation of RhoA GTPase, mediated by caspase-11, was shown to promote cofilin phosphorylation and actin depolymerization, whereas caspase-1 was shown to promote cofilin dephosphorylation and actin polymerization. The opposing effects of caspase-1 and -11 are proposed to facilitate the dynamic actin remodelling, which is required for the fusion of *Legionella*-containing vacuoles with lysosomes[92]. Similar findings regarding the importance of caspase-11 for phagolysosome fusion have been observed during infection with the Gram-negative bacteria, *Burkholderia cenocepacia*[93]. Caspase-11-deficient macrophages were shown to exhibit defective autophagosome formation and reduced bacterial clearance of *B. cenocepacia*. The authors propose a role for caspase-11 in autophagy through the modulation of actin dynamics during Gram-negative bacterial infection[93].

In addition to caspase-11-deficient cells having altered migration and reduced fusion of lysosomes to pathogen containing vacuoles[88,91], they have also been shown to have enhanced TCR signalling[94]. This study suggests that caspase-11 negatively regulates $CD8^+$ TCR signalling and cytotoxic effector function via reduced T cell expansion/activation, possibly through its ability to regulate actin polymerization[94]. The defective cofilin phosphorylation and actin remodelling observed during caspase-11 deficiency has also been linked to impaired neutrophil migration in an experimental model of gout[95]. *In vitro* experiments demonstrated that, compared to their WT counterparts, caspase-11 deficient neutrophils had decreased cofilin phosphorylation, impaired migration towards the KC chemokine, and were unable to produce neutrophil extracellular traps (NETs) following stimulation with monosodium urate crystals (MSU)[95].

1.2.3.2. Altered Mitochondrial Respiration

A recent study has used a model of ischemia (Femoral artery ligation (FAL)) to examine the importance of caspase-1/11 signalling and autophagosome formation in muscle regeneration[96]. Using caspase-1/11 double knockout mice in the FAL model, they showed that these mice had smaller myofibers in regenerating muscles compared to those of similarly treated WT mice. They also observed an altered metabolic profile in muscle satellite cells from caspase-1/11 knockout mice, which exhibited significantly reduced maximal and spare respiratory potential. Non-mitochondrial oxygen consumption and ATP production was similar between WT and caspase-1/11 groups[96]. However, the mechanism underlying the observed dependence for caspase-1/11 signalling in mitochondrial respiration during ischemia is unknown, and further studies to separate the contribution of caspase-1 and -11 to this process are required.

Caspase-11 has also been recently linked with a role in mitochondrial respiration in the context of Gram-positive infection with Methicillin-resistant *Staphylococcus aureus* (MRSA). Mitochondria from caspase-11 deficient macrophages were shown to produce higher levels of superoxide than WT macrophages in response to MRSA[97]. In the absence of caspase-11, recruitment of mitochondria to MRSA-containing vacuoles was shown to be enhanced, which facilitated enhanced mitochondrial-ROS mediated bacteria killing. The actin depolymerization agent, cytochalasin D, was shown to prevent dissociation of mitochondria from MRSA vacuoles, suggesting that the impaired actin dynamics associated with caspase-11 deficiency is responsible for the enhanced association of MRSA vacuoles with mitochondria[97]. Whether this mechanism also led to the enhanced levels of mitochondrial ROS observed in MRSA-infected caspase-11 deficient macrophages or whether caspase-11 has a specific involvement in regulating mitochondrial respiration has yet to be determined (**Fig. 1.8**).

Investigation of metabolic pathways controlling caspase-11 activation revealed a regulatory role for cyclic adenosine monophosphate (cAMP) in caspase-11 mediated pyroptosis in a model of sepsis[98]. L-adrenaline induced cAMP production promotes protein kinase A (PKA), blocking caspase-11 mediated GSDMD cleavage, pyroptosis, IL-1β and DAMP release. Metabolic regulation of caspase-11 represents an immunometabolic target to control caspase-11 activity[98].

1.2.3.3. Caspase-11 Mediated Coagulation

Recent papers have implicated caspase-11 as an initiator of systemic blood clotting and tissue thrombosis. Li and colleagues demonstrated that in vivo activation of the canonical

inflammasome (via T3SS Gram-negative rod protein) or the non-canonical inflammasome (via LPS) in mice led to GSDMD cleavage and pyroptotic-dependent release of tissue factor (TF), inducing coagulation and lethality[99]. TF positive microvesicles released into circulation can trigger both arterial and venous thrombosis[100]. In a parallel study, Yang and colleagues highlighted a role for caspase-11 mediated GSDMD cleavage and TF release during disseminated intravascular coagulation (DIC) in sepsis[101]. They showed that GSDMD deficiency inhibits endotoxin induced TF activation by reducing phosphatidylserine (PS) exposure on the outer plasma membrane. Once exposed, PS interacts with TF, resulting in its conformational change and activation. TF acts as a high affinity receptor for factor (F)VII and FVIIa, which serves as the initial activator of the coagulation protease cascade. Caspase-11 mediated GSDMD-N pore formation results in Ca^{2+} influx, which activates transmembrane protein 16F (TMEM16F), a calcium dependent phospholipid scramblase, to mediate phosphatidylserine externalization and subsequent activation of the coagulation cascade (**Fig. 1.8**)[100]. The GSDMD-mediated Ca^{2+} influx also triggers repair programs such as endocytosis of damaged membrane or ectosome membrane shedding, which can negatively regulate pyroptosis downstream of GSDMD[102]. Therefore, while GSDMD-mediated Ca^{2+} influx promotes TF activity, it simultaneously inhibits GSDMD-mediated pyroptosis. This identifies a pyroptosis-independent function for caspase-11, and its substrate GSDMD, during intravascular coagulation.

Levels of IL-1α, IL-1β, and GSDMD activation in septic patients correlate with PS exposure on peripheral leukocytes and DIC scores[100] and exposure of vascular endothelial cells to IL-1α and IL-1β increases TF release[103]. However, deletion of the IL-1R does not prevent LPS mediated coagulopathy in sepsis[100]. Furthermore, caspase-11/GSDMD dependent DIC has been shown to be independent of IL-1 signalling[104]. Therefore, the coagulation process also appears to be independent of IL-1 signalling events downstream of caspase-11.

During *Klebsiella pneumoniae* infection, caspase-11 promotes bacterial clearance from the lungs[105]. *K. pneumonia* infection is commonly associated with pneumonia and sepsis. Caspase-11 deficient mice inoculated with low dose *K. pneumoniae* display increased bacterial colonization in the lungs, corresponding with reduced IL-1α and increased TNF levels in bronchoalveolar lavage fluid and reduced neutrophil infiltration[105,106]. The increased *K. pneumoniae* colonization in caspase-$11^{-/-}$ lungs is also linked to significantly less fibrin formation in the lung, observed by reduced cross-linked fibrin and d-dimer, markers of coagulation[105]. This correlates with findings that thrombin-mediated coagulation is protective against *K. pneumoniae* infection of the lung via fibrin polymerization and platelet–neutrophil

interactions[107]. Thus, caspase-11 demonstrates a protective function during *Klebsiella* infection via activation of blood coagulation in the lungs. In summary, these results reveal that caspase-11 and GSDMD are involved in novel mechanisms of coagulation activation and thrombosis as part of the host defence mechanism against bacterial infection.

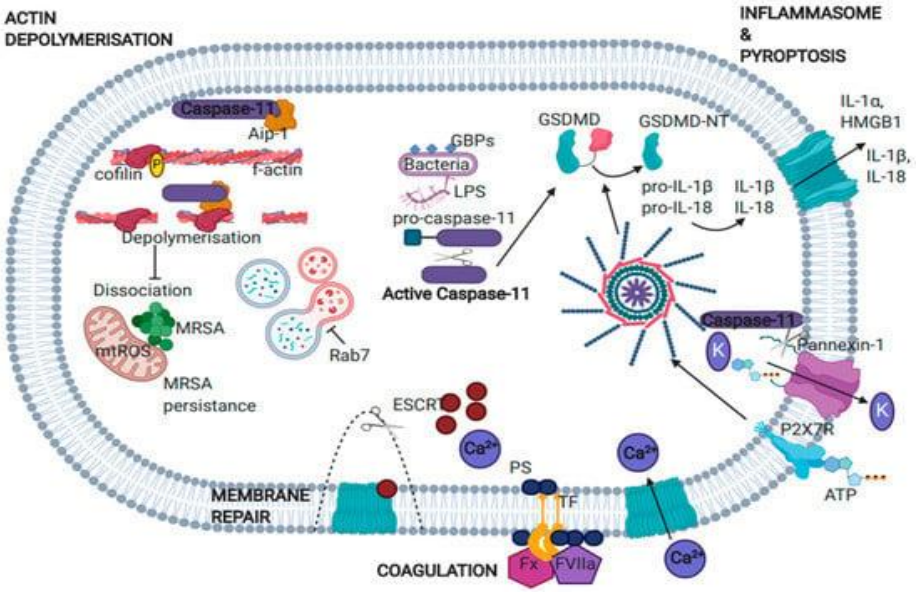

Figure 1.8: Effector functions of caspase-11. Cytosolic LPS binds and activates caspase-11, which leads to non-canonical inflammasome activation and pyroptosis—direct cleavage of GSDMD by caspase-11, generating the pore-forming P30 GSDMD-NT and membrane permeable pores, which passively release alarmins, IL-1α, and HMGB1. Caspase-11 activation triggers NLRP3 inflammasome activation, leading to maturation and release of IL-1β and IL-18. Caspase-11 cleaves Pannexin-1, mediating ATP release and K^+ efflux to trigger activation of the NLRP3 inflammasome. Actin polymerization—Activated caspase-11 directly interacts with Aip-1 leading to cofilin dephosphorylation and activation of cellular migration. During Gram-negative bacterial infection, cofilin drives actin remodelling, leading to phagolysosome fusion and bacterial clearance. However, during MRSA infection, caspase-11 promotion of actin remodelling drives dissociation of mitochondria from MRSA-containing vacuoles, reducing the contribution of mitochondrial ROS to bacterial clearance, enhancing the persistence of MRSA. Coagulation—Caspase-11 and GSDMD-N pore formation mediates Ca^{2+} influx allowing phosphatidylserine (PS) externalization to the outer plasma membrane. Exposed PS interacts with tissue factor (TF), which associates with complement factors to initiate the coagulation cascade. The GSDMD-mediated Ca^{2+} influx also mediates a membrane repair response via ESCRT components, removing GSDMD pores and repairing membrane integrity.

1.3. Macrophage origin, polarisation and activation

Myeloid cells comprise a major population of leukocytes in peripheral blood. All blood derived components originate form bone marrow hematopoietic stem cells which commit to either lymphoid progenitor or myeloid progenitor branches with many subdivisions within each group. Myeloid progenitor is a precursor of granulocytes, monocytes, macrophages, and dendritic cells. Differentiation to various lineages is controlled by transcription factors and terminal differentiation triggered by response to specific colony stimulation factors. Cells of myelomonocytic origin have several options of differentiation critical to innate immunity involvement in disease resolution and bridging the gap to adaptive immunity. Myelomonocytic cells differentiate into mature monocytes, macrophages and dendritic cells[108,109]. Macrophages are professional mononuclear phagocytic cells which ingest and degrade pathogens which penetrate physical barriers of innate immune system. Macrophage ability to differentiate from self is fundamental to their importance in tissue repair under sterile inflammatory conditions. Their phagocytic activity subsequently induces response of adaptive immunity, T cell activation[110]. Macrophage nomenclature is complex due to functional plasticity mediated by the microenvironment.

Macrophage polarization and activation is typically induced by a set of cytokines, growth factors or TLR agonists which induce distinct gene transcription and protein expression. Traditionally the polarisation of macrophages is defined by 2 classes - M1 or classically activated; and M2 or alternatively activated. These terms originated when the polarising effects of IL-4 compared to IFN-γ and LPS mediated gene expression were observed. Mills coined the terminology M1-M2 following observations of distinct arginine metabolism in macrophages of C57BL/6 and Balb/c mice which correlated with varied Th1 and Th2 responses of the same strains. Th1 strain (C57BL/6) stimulated with IFN-γ and LPS more easily induced NO production compared to the Th2 strain (Balb/c). However, LPS treated Th2 strain macrophages were observed to increase arginine metabolism to ornithine[111,112]. However, the concept of classical and alternative activation is highly debated, and this concept has several flaws involving the genetic differences between the 2 species. C57BL/6J bear a deletion in arginine transporter gene promoter region, Slc7a2, hence innate impaired arginine transportation results in the differences metabolism to ornithine between M1 and M2 phenotypes[113,114]. Colony stimulation growth factors are also critical for the induction of M1 and M2 phenotypes. GM-CSF is traditionally considered an M1 polarising factor and M-CSF is defined as an M2 growth factor. Macrophages grown in GM-CSF compared to M-CSF demonstrated differential polarisation dependent on type I IFN signalling.

LPS stimulated macrophages cultured in GM-CSF have impaired secretion of IFN-β, CCL5, CCL12, CXCL10, CCL2 and IL-10 compared to macrophages cultured in M-CSF. The dampened immune response observed in GM-CSF cultured macrophages appears to be depended on enhanced basal secretion of type I IFN genes associated with M-CSF which prime the macrophages for increased activity upon LPS stimulation[115].

Reassessment of macrophage activation has expanded nomenclature ideology to encompass a spectrum of functionally plastic macrophages which cannot be easily defined into subgroups (**Fig. 1.9**)[114,116]. Macrophages are located in virtually all tissues and differentiate from peripheral blood mononuclear cells (PBMCs) circulating the blood stream at a steady state or in response to infection or injury migrate into tissue[117]. Mature monocytes migrate from blood into tissue to replenish long-lived tissue resident macrophages such as alveoli, gastrointestinal, liver (Kupffer cells), central nervous system (microglial cells), bone (osteoblasts) or connective tissue (histiocytes)[118]. The mature monocytes circulating in the blood stream are a heterogeneous therefore the point in which they are recruited from the bloodstream will affect their polarisation and functionality[119,120]. Humans express two populations of monocytes, $CD14^{hi}CD16^{-}$ classical monocytes which account for 90% of the population and $CD14^{+}CD16^{+}$ non-classical monocytes. $CD14^{+}CD16^{+}$ monocytes are smaller than classical monocytes, measuring at 13.8 microns compared to 18.4 microns and expression of class II antigens on cell surface of $CD14^{+}CD16^{+}$ monocytes are 2-fold greater. Another difference appears to be a decreased capability to adhere to plastic, decreased phagocytic ability and reduced expression of CD11b and CD33 cell surface markers. Analysis of tissue resident macrophages revealed a larger population of alveolar macrophages express a $CD14^{+}CD16^{+}$ phenotype in compared to peritoneal macrophages[118,121].

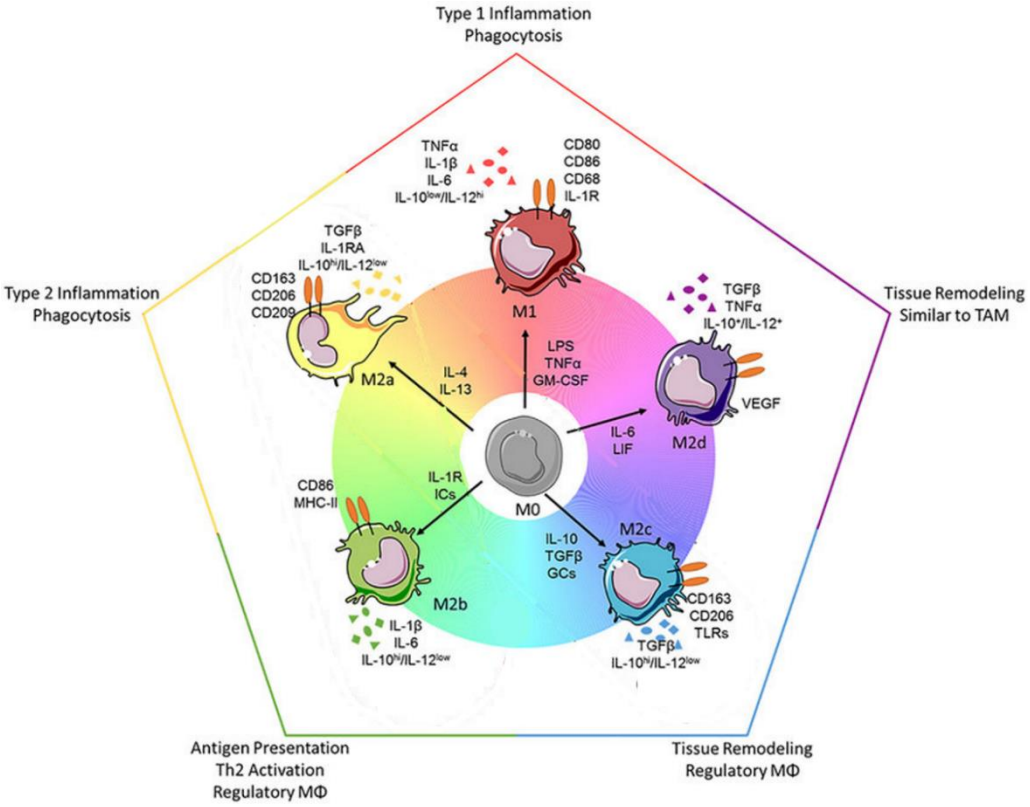

Figure 1.9: Macrophage polarisation spectrum. Macrophage plasticity has led to the subdivision of M2 alternative phenotype to include subsets M2a, M2b, M2c and M2d. M2a and M2b share classical M1 features such as inflammatory and phagocytic functions and release of IL-1β and IL-6 inflammatory cytokines. Each subset is distinguished by factors which induce the specific phenotype, expression of receptors, cytokine release and their functionality[122].

1.3.1. Classically Activated Macrophages

Immune cell mediated secretion of IFN-γ and TNF-α results in effector M1 macrophages which mediate microbicidal and tumouricidal responses and secretion of pro-inflammatory cytokines. An important early source of IFN-γ by the innate immune system is NK cells, which prime macrophages for transcription and secretion of proinflammatory cytokines, as well as increased production of superoxide anions and oxygen or nitrogen radicals for enhanced killing. Early NK cell IFN-γ is a transient response, therefore another source provided by adaptive immune cells such as Th1 cells is required for prolonged classical activation of macrophages[123]. TLR agonist induced MyD88-dependent TNFα secretion in macrophages acts in an autocrine manner in combination with IFN-γ to activate M1 macrophages. Additional TLR signalling TRIF-dependent pathways upregulate IFNβ via IFN regulatory factor 3 (IRF3). Endogenous IFNβ promotes type I IFN signalling inducing an M1 phenotype.

STAT1 and NF-κB or MAPK are important transcription factors associated with M1 polarised macrophages, which mediate the production of IL-1, IL-6, IL-10, IL-23, IFN-β and TNFα cytokines. IL-17-producing Th17 cells are activated by IL-1, IL-6 and IL-23 of classically activated macrophages. M1 macrophages drive antigen specific Th1 and Th17 cell inflammatory responses. Therefore, M1 macrophages express high levels of major histocompatibility complex class II (MHCII), CD68 marker and co-stimulatory molecules CD80 and CD86[196]. CD80/CD86 are stimulated by CD68, T cell receptor, while CTLA-4 serves as an inhibitor of CD68-CD80/CD86 engagement inducing immunosuppression. CD68-CD80/CD86 engagement plays a critical role for regulating inflammation in autoimmune diseases in context of the adaptive immune response. However, its importance in innate immunity has also been demonstrated by neutrophils expressing CD68 binding macrophage CD80/CD86 leading to NF-κB activation and secretion of a range of proinflammatory cytokines, most notably IL-6[124],[125].

M1 macrophage activation is strongly associated with intracellular protein suppressor of cytokine signalling 3 (SOCS3). SOSC3 has been demonstrated to co-localise with inducible nitric oxide synthase (iNOS) in infiltrating macrophages, in a model of acute nephritis. SOCS3 has an important role in driving expression of IL-6 and nitric oxide (NO), while dampening anti-inflammatory molecules IL-10 and SOCS1. SOCS3 mediated IL-6 and NO production is induced by NF-κB and PI3K activity[126]. Arnolds and colleagues also demonstrated SOCS3 to function as a positive regulator for pro-inflammatory cytokine responses and its upregulation is essential for M1 macrophage activation. SOCS3 may prolong M1 phenotype during inflammation, as in the absence of SOCS3 M1 marker NO was impaired while M2 markers, induced by STAT3, CD206 and Arg1 were upregulated. SOCS3 knockdown results in decreased in LPS induced IL-1β, IL-6 and IL-23, Th17 polarising cytokines and IL-12 Th1 polarising cytokine[126]. Therefore, regulating M1 macrophage polarisation and pro-inflammatory cytokine profile.

NO synthesised by nitric oxide synthase (NOS), plays an important role in host defence and immune regulation. There are 3 isoforms of NOS including endothelial NOS (eNOS), inducible NOS (iNOS) and neuronal NOS (nNOS). eNOS and nNOS are located in epithelial cells and neurons and activity is calcium dependent. iNOS however is calcium independent and induction is triggered by a variety of cytokines and factors in a multitude of cells[127]. iNOS most importantly functions as a pro-inflammatory mediator in immune response. The iNOS product, NO, functions as a protective immunoinflammatory molecule to fight and kill microorganisms. However excessive NO production is associated with normal tissue damage, as observed in Borna disease[128]. Contrastingly, $iNOS^{-/-}$ mice are associated with increased development of inflammatory diseases such as experimental autoimmune encephalomyelitis (EAE) and

sepsis[129,130]. iNOS is defined as a hallmark of M1 polarisation, mediated by TLR agonists and cytokines such as IFN-γ. iNOS enzymatic activity functions to generate NO from L-arginine amino acid.

NO inhibits IL-12 p40 protein expression in murine macrophages, independent of its effects on IL-10. NO had also been demonstrated to inhibit TLR and IL-1R dependent signal transduction via its inhibition of IL-1R associated kinase (IRAK) and consequently IRAK and TRAF6 binding. NO donor *S*-nitroso-*N*-acetylpenicillamine (SNAP) treatment attenuated LPS or IL-1β-stimulated NF-κB p40 promoter binding by inhibition of IκB phosphorylation[131]. This suggests that iNOS induced NO production is an important regulator of M1 macrophage activity, highlighting the importance of macrophage derived NO regulation during innate immune inflammation.

1.3.2. Alternatively activated macrophages

Alternatively activated macrophages (M2) otherwise known as wound healing macrophages are induced in response of IL-4 and upregulate mannose receptors such as CD206. Basophils, mast cells and granulocytes are an early source of IL-4 in response to tissue injury and also chitin, a structural protein found in fungi and parasites[132]. M2 macrophages produce chitinase-like molecules such as YM1 and YM2 responsible for the degradation of chitin located on the surface of parasites, fungi and some insects[133]. IL-4 macrophage programming encourages wound healing by promoting arginine metabolism to ornithine, which is a precursor of polyamines and collagen[220]. Therefore IL-4 mediates the production of an extracellular matrix. Th2 cells are another source of IL-4 as well as IL-13, which is commonly used *in vitro* studies to polarise M2 macrophages. These M2 macrophages do not perform antigen presentation to T cells, secretion proinflammatory cytokines or produce radicals similarly to M1 macrophages. M2 macrophages function to regulate wound healing and secrete components of the extracellular matrix. Additionally through the produce of polyamines M2 macrophages indirectly influence cytokine expression and supress lymphocyte clonal expansion[132].

Mannose receptor (cluster of differentiation 206 CD206) is a transmembrane glycoprotein that is a member of the C-type lectin family. CD206 detects pathogens constructed with mannose molecules. CD206 binds sugars like mannose and fructose with high affinity as these sulphated sugars contain 4-sulfated N-acetyl galactosamine terminals with a fibronectin II domain and eight carbohydrate recognition domains[134]. Therefore, CD206 function in immunosurveillance is to scavenger any unwanted mannoglycoproteins. CD206 binding pathogens are intracellular microorganisms, trafficked to TLR9 CpG motif-containing oligodeoxynucleotides by endosomal

delivery observed in murine peritoneal macrophages[135]. Plasticity of macrophages was observed by Porcheray and colleagues investigating alternatively activation of a proinflammatory classically activated macrophage. CD206 expression is strongly induced by anti-inflammatory cytokines including GM-CSF, IL-4 and TGF-β. Mature macrophages stimulated for 5 days with pro- and anti-inflammatory cytokines followed by culture for 5 more days with counter-stimulatory molecules demonstrated a change in morphology characteristic of the counter-stimulation. Reversibility of macrophage phenotype was further demonstrated by measuring CD206 expression after counter-stimulation. GM-CSF, IL-4 and TGF-β, known upregulators of CD206 expression, were counter-stimulated with M-CSF, IL-10 ad TNFα which downregulated CD206 M2 marker expression[136].

YM1 contain carbohydrates and matrix-binding activity consist with M2 wound healing matrix remodelling phenotypes. Ym1 binds to heparin and saccharides with free amino acids such as glucosamine and galactosamine. Ym1 also shares binding specificity with leukocyte homing receptors suggesting Ym1 controls leukocyte recruitment to sites such as the extracellular matrix and lead to dampening of inflammation[137]. Found in the inflammatory zone (FIZZ1) also known as RELMα is a cysteine-rich resistin-like secretory molecule markedly upregulated during allergic lung pulmonary inflammation in hypertrophic, hyperplastic bronchial epithelium and type II alveolar pneumocytes[138]. FIZZ1 and Ym1 expression and arginase activity is induced by IL-4. However IFN-γ antagonises the effect of IL-4 in macrophages, suggesting that type I cytokine microenvironment contributes to maintaining low M2 activity[137].

1.3.3. Arginine metabolism and iNOS signalling

Arginine is considered a conditionally essential amino acid with multiple metabolic fates, as it is endogenously synthesis from citrulline as a precursor of NO or ornithine. Within the body the small intestines are a major source of citrulline for arginine synthesis in the kidney proximal tubules, called the intestinal-renal axis of arginine synthesis. Arginine metabolism is regulated through y+ system of cationic transporters (CAT) and regulated expression of enzymes of the catabolic urea cycle (**Fig. 1.10**). Arginine is metabolised by several enzymes including nitric oxidise synthase (NOS), arginase (Arg), arginine: glycine amidinotransferase (AGAT), and arginine decarboxylase (ADC), which are expressed in an environment and tissue dependent manner[139].

The fate of arginine has emerged as a critical regulator of innate and adaptive immunity. During inflammatory disease the major catabolising enzymes are NOS isoforms (NOS 1-3) and Arg

isoforms (Arg 1-2). NOS1 is also referred to as nNOS due to expression in neurons and brain, NOS2 is additionally known as inducible NOS (iNOS) due to its inducible cellular activation and NOS3 is called eNOS because of its endothelium association. iNOS is a high-output Ca^{2+}-independent synthases with wide range of inducible expression including neutrophils, macrophages, epithelial, and hepatocytes during inflammation and infection[127]. While the two isoforms of Arg are known to catalyse the same biochemical reaction of L-arginine to ornithine, they differ in cellular expression, regulation, and subcellular localisation. As the urea cycle is distributed over two cellular compartments, the cytosol and mitochondria, the different arginase isoforms are important to mediate l-ornithine and polyamine production following electron transport chain (ETC) collapse during inflammatory disease[140]. Therefore, differential expression of NOS and Arg is important in augmenting immune response driven my tissue specific environmental cues. Hence the targeting of arginine metabolism divergence is a potential means of controlling immune response to facilitate disease clearance.

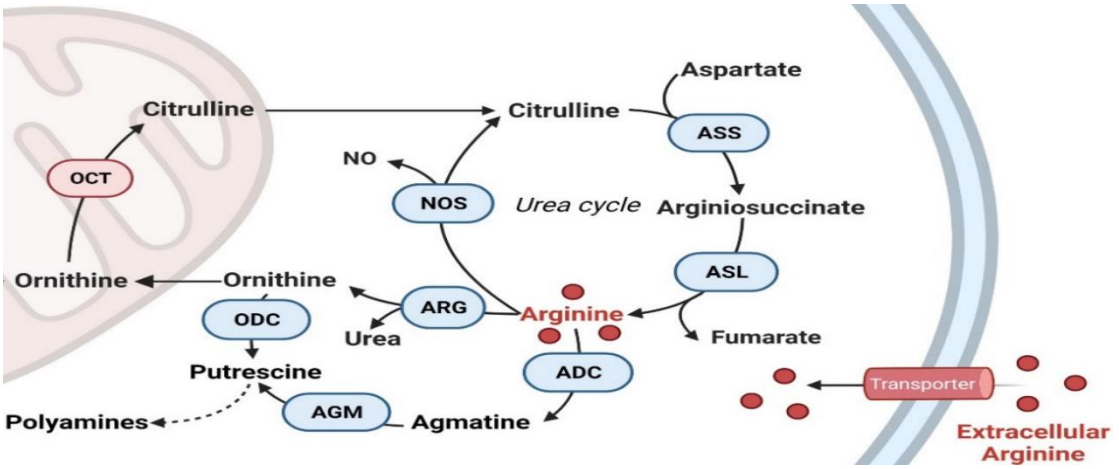

Figure 1.10: Arginine metabolic pathways. Arginine can be directly transported into the cell via cationic amino acid transporters or synthesized from recycled citrulline and aspartate in the urea cycle. Arginine metabolism diverges at the point of L-arginine which can be converted into nitric oxide (NO) or urea and ornithine, important resource for putrescine, which is a key precursor for polyamines. L-arginine deaminated to form citrulline and oxygenated nitrogen derivates from the imino-nitrogen removed from the guanidino group of the L-arginine, catalysed by iNOS to form NO. This reaction requires the co-factor BH4 mediated by NADPH. ASS: argininosuccinate synthetase, ASL: argininosuccinate lyase, ADC: arginine decarboxylase, ODC: ornithine decarboxylase, ARG: arginase, NOS: nitric oxide synthase, OCT: ornithine carbamoyl transferase. Image taken and adapted from Chia-Lin, C. *et al.*, Cancers 2021 , 12(14): 3541[139].

1.3.4. Macrophage Metabolism

Immunometabolism is currently an area of high interest as macrophage plasticity is regulated by mitochondrial metabolism. Under homeostatic conditions oxidative phosphorylation (OXPHOS) is the primary mode of cellular energy production. OXPHOS links the TCA, also known as Kreb's cycle, to the production of adenosine triphosphate (ATP), and requires the orchestration of the ETC and ATP synthase located in the inner mitochondrial membrane. OXPHOS metabolism of glucose to form ATP in the presence of oxygen, is mediated via the transfer of electrons from NADH or $FADH_2$ to O_2 along a series of electron carriers, complexes.

Glycolysis is termed from the breakdown of sugars, observed the consumption of cytosolic glucose to produce two molecules of pyruvate, in a 10-step catalytic reaction process. Therefore, the primary rate limiting step of glycolysis is glucose uptake, via glucose transporter GLUT1[141]. Of the 10 steps of glycolysis, 3 are considered irreversible regulatory steps which are catalysed by hexokinase, phosphofructokinase (PFK-1) and pyruvate kinase.

The 10 steps of glycolysis are divided into two phases (**Fig. 1.11**). Phase one is the preparatory phase in which two ATP moles are consumed per glucose molecule catalysed. During step 1, glucose conversion to glucose 6-phosphate, which at this point can continue down the pathway of glycolysis or alternatively be converted into glycogen or oxidised by the oxidative branch of the pentose phosphate pathway (PPP). PPP is a parallel pathway that occurs alongside glycolysis, converting glucose-6- phosphate into NADPH which can be used in the generation of reactive oxygen and nitrogen species, and ribose-5-phosphate to produce nucleotides. Activated macrophages have been shown to have increased PPP activity and TLR stimulation suppresses carbohydrate-kinase like protein (CARKL), an inhibitor of the PPP pathway. If glucose is to continue down the glycolytic pathway, it must first be converted into fructose-6- phosphate by phosphoglucose isomerase. Therefore, PFK-1 is the first point of commitment to glycolysis and the determinant of the rate of glycolytic flux. PFK-1 activity is tightly regulated for activity only when required, as PFK-1 is inhibited by ATP and TCA metabolites, and activated by AMP and fructose-1, 6-biphosphate, which can boost activity even in the presence of ATP. PFKFB family (6-phosphofructo-2-kinase/fructose2,6-biphosphatase) and TIGAR (Tp53 induced glycolysis and apoptosis regulator) phosphatase ability degrades fructose-1, 6-biphosphate. While during macrophage inflammatory response, PFKFB3 high kinase to phosphatase ratio promotes fructose-1, 6-biphosphate generation by kinase activity to activate PFK-1 and commit to glycolysis.

Phase two, the pay-off phase, involves phosphoglycerate kinase and pyruvate kinase. Phosphoglycerate kinase, the 7th step of glycolysis, catalyses the transfer of high energy phosphoryl group from acyl phosphate of 1,3-biphosphoglycerate and ADP to ATP and 3-phosphoglycerate. This is the first ATP formed from glycolysis to conserve energy supplied from glucose. This step neutralises two ATP consumed by step 1 (hexokinase) and 3 (PFK-1). During phase two, 4 ATP are produced for a net gain of 2 ATP per glucose molecule. Two molecules of NADH are also produced via glyceraldehyde 3-phosphate dehydrogenase oxidation of glyceraldehyde 3-phosphate, associated with NAD+ reduction to NADH.

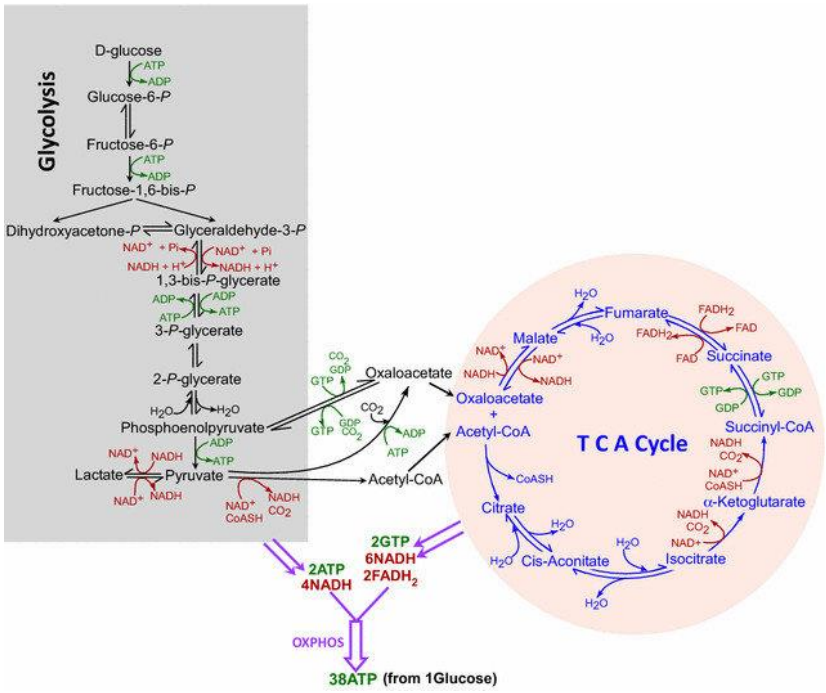

Figure 1.11: Metabolic steps of glycolysis and TCA cycle. ATP/GTP utilization or synthesis is shown in green, while NAD + /NADH and FAD/FADH 2 are shown in red. Also indicated are the numbers of NADH, $FADH_2$, and ATP/GTP generated when one molecule of glucose is consumed following glycolysis, TCA cycle, and oxidative phosphorylation. Abbreviations: Glucose-6-P glucose 6-phosphate, Fructose-6-P fructose 6-phosphate, Fructose -1,6-bis-P fructose 1,6-bisphosphate, Dihydroxyacetone-P dihydroxyacetone phosphate, Glyceraldehyde-3-P glyceraldehyde 3-phosphate, 1,3-Bis-P-glycerate 1,3-bisphosphoglycerate, 3-P-Glycerate 3-phosphoglycerate, 2-P-Glycerate 2-phosphoglycerate, OXPHOS oxidative phosphorylation. Image taken and adapted from Alam, M. *et al*., Clinical and Translational Medicine (2016)[142].

Under aerobic conditions, pyruvate is fated for the TCA cycle. However, under anaerobic conditions pyruvate is reduced to lactate or ethanol, as NADH is reoxidised to NAD+, with no further ATP generated downstream glycolysis. Therefore, the energy potential per glucose

molecule is not fully utilised. Similarly, the Warburg effect, also known as aerobic glycolysis, observes high glucose consumption and lactate production regardless of oxygenated environment. Under aerobic conditions, in cells with intact mitochondria, energy generate from glucose and stored as ATP is higher comparatively to anaerobic glycolysis. Lactate dehydrogenase (LDH) catalyses the interconversion of pyruvate and lactate and accompanying interconversion of NADH and NAD+. LDHA is upregulated in response to metabolic reprogramming in macrophages and dendritic cells[143],[144]. Accumulation of lactate, the final product of glycolysis, is enhanced in response to increased rates of glycolysis and can be used as a surrogate marker of glycolytic activity[145]. The view of lactate as a waste product of metabolism is beginning to be re-examined. Lactate has been shown to inhibit T cell migration[146], polarise tumour-associated macrophages towards an M2-phenotype[147], inhibit pro-inflammatory macrophage responses and glycolytic programming[148] and drive dendritic cells towards a more tolerogenic phenotype[149].

During OXPHOS, majority of glucose is converted to pyruvate for entry into the TCA cycle, with a minority produced lactate (**Fig. 1.11**). Pyruvate is subsequently oxidised to CO_2 and H_2O by mitochondrial enzymes to generate NADH and $FADH^2$, to donor electrons along the ETC. This donation of electrons along the ETC located in the inner mitochondrial membrane allows for OXPHOS to take place and synthesis ATP (**Fig. 1.12**). Complex I and Complex II accept electrons and transfer them via redox reactions. This electron is used to pump protons into the mitochondrial inter-membrane space through complexes I, III and IV, thus generating an electrochemical proton gradient or mitochondrial membrane potential. This proton gradient is used to drive ATP synthase (Complex V) to generate ATP. In the final reaction of the ETC, oxygen acts as the electron acceptor and is reduced to water, thus oxidative phosphorylation requires and consumes oxygen. If oxygen is not present, pyruvate is not processed via the mitochondria and is instead used to produce lactate in the cytoplasm by glycolysis, generating ATP. This method of ATP production is far less efficient, creating 2 molecules of ATP per glucose molecules compared with 36-38 molecules of ATP per glucose molecule generated by OXPHOS..

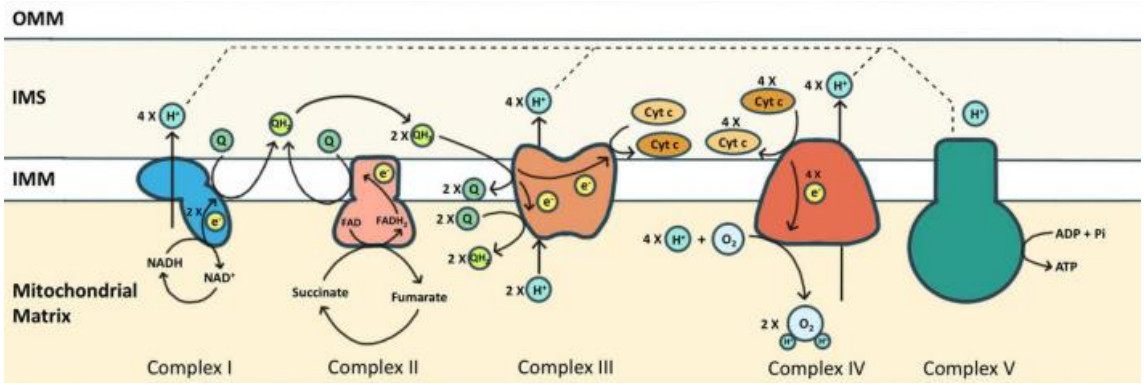

Figure 1.12: The electron transport chain (ETC) consists of complexes I (cI) to V (cV), as well as two free electron carriers, CoQ and cyt *c*. NADH and $FADH_2$ donated electrons to cI and cII, respectively, causing reduction of CoQ into $CoQH_2$. The $CoQH_2$ is in turn oxidized by cIII where the electrons are delivered to cyt *c*. The reduced cyt *c* was then oxidized by cIV where the oxygen molecule was reduced as the terminal electron acceptor. Protons accumulated in the intermembrane space during oxidative phosphorylation via cI, cIII, and cIV, and are essential for cV to drive ATP synthesis. Image taken and adapted from Jeng-Lin, L. *et al.,* Frontiers in Molecular Neuroscience (2021)[150].

Pyruvate decarboxylase complex decarboxylates pyruvate to form acetyl-coA as an intermediate for the entry to the TCA cycle. Acetyl-coA combines with oxaloacetate, losing the CoA group to form a 6-carbon molecule, citrate. Aconitase converts citrate to isocitrate, which is converted to α-ketoglutarate by isocitrate dehydrogenase. In a multistep process, α-ketoglutarate is converted to succinyl-CoA, then succinate, followed by fumarate, malate, and then oxaloacetate. M1 macrophages rely mainly on glycolysis and present two breaks on the TCA cycle that result in accumulation of itaconate (a microbicide compound), citrate and succinate. TCA cycle also undergoes rapid changes during M1 polarization. In the early stage, production of itaconate leads to accumulation of succinate by inhibition of SDH, which stabilizes HIF-1α and augments the inflammatory response. Excess of succinate leads to HIF1α stabilization that, in turn, activates the transcription of glycolytic genes, thus sustaining the glycolytic metabolism of M1 macrophages[144,151]. On the contrary, M2 cells are more dependent on OXPHOS, their TCA cycle is intact and provides the substrates for the complexes of the ETC[152].

Dramatic switches in cell metabolism accompany phenotypic and functional changes of macrophages All these metabolic adaptations are functional to support macrophage activities as well as to sustain their polarization in specific contexts.

1.4. Immunity and Autophagy

Autophagy acts as an immune effector mediating pathogenic clearance and preventing excessive inflammatory response, with autophagy dysfunction often associated with inflammatory disease. There are 3 subtypes of autophagy including macroautophagy, interchangeably referred to as autophagy, microautophagy and chaperone mediated autophagy. Mitophagy, a mitochondrial quality control specialised autophagy, eliminates dysfunctional mitochondria to regulate immune response as mitochondrial stress is a key trigger of innate immune activation, specifically type I IFN production, IL-1β response and apoptosis.

Mitochondrial stress which triggers mitophagy include a variety of insults such as radiation, or chemotherapeutics, genetic mutations, pathogenic infection, or spontaneous dysregulation. These factors lead to an accumulation of damaged mitochondrial proteins, lipids and DNA resulting in loss of mitochondrial membrane integrity and potential, metabolic dysfunction, alterations in energy intermediates or impairment of mitochondrial dynamics. Other mitochondrial quality control process to overcome dysfunctional mitochondrial potentially triggering immune response include mtDNA repair enzymes or mitochondrial morphology transitions to restore proper function. However, mitophagy is induced if mitochondria repair is not sufficient.

The process of mitophagy can be divided into ubiquitin-dependent or -independent pathways. PTEN-induced putative kinase 1 (PINK1) and parkin RBR E3 ubiquitin protein ligase (parkin) mutations are associated with motor disturbance and neurodegenerative disease which genetic analysis later linked mitophagy with a ubiquitin-dependent pathway. PINK1 senses mitochondrial transmembrane potential loss leading to the recruitment of parkin to the damaged mitochondria. In a healthy state, PINK1 N-terminal is targeted for trafficking via translocase of the outer mitochondrial membrane (TOM) and inner mitochondrial membrane (TIM), where it is cleaved by matrix processing peptides. Cleaved PINK1 is then released into the cytosol for proteasomal degradation. In unhealthy cells, where mitochondria are damaged, PINK1 is not cleaved and stabilised by adenine nucleotide translocator, inhibiting TIM23, on the outer mitochondrial membrane to promote the sequence of mitophagy. PINK1 accumulation leads to Ser65 phosphorylation of outer mitochondrial membrane ubiquitin proteins, which recruit cytosolic parkin to trigger activation of its ubiquitin ligase activity. PINK1-dependent phosphorylation of parkin leads to release of RING2 catalytic domain, locking parkin into its functionally active conformation. This activated parkin ubiquitinates outer mitochondrial

membrane proteins such as VDAC triggering the recruitment of autophagy receptors such as optineurin or NDP2. Once recruited, the autophagic machinery is employed (**Fig. 1.13**)[153,154]**.**

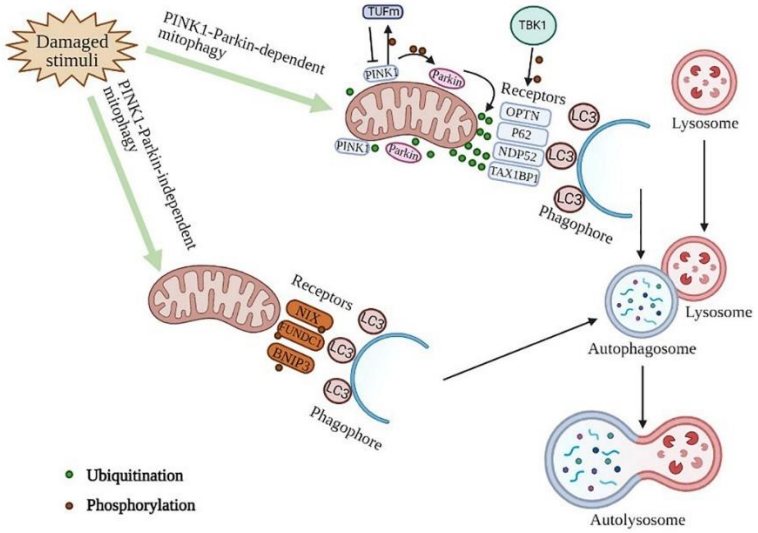

Figure 1.13: Mitophagy ubiquitin-dependent and independent cascade. PINK1 detects disruptions to mitochondrial integrity, signalling the recruitment and activation of parkin, which can then be amplified by ubiquitinating mitochondrial surface proteins. A PINK1-dependent TUFm phosphoswitch determines conversion from activating to suppressing mitophagy. When TUFm is suppressed these ubiquitinated proteins can subsequently be recognized by autophagic receptors that convert mitochondria to autophagosomes for degradation via interacting with LC3 protein directly. TBK1 can phosphorylate autophagic receptors to enhance mitophagy. During ubiquitin independent mitophagy, receptor proteins, such as NIX, FUNDC1, BNIP3, owning the unique ability to interact with processed LC3 independent of ubiquitin, leading to mitochondria conversion to autophagosomes for degradation via interacting with LC3 protein directly. Image taken and adapted from Cheng-Long, Z. *et al.,* Frontiers in Cell and Development Biology (2021)[154].

In macrophages dysfunctional mitochondria are marked by parkin-dependent ubiquitination, followed by recognition by p62, which is transcriptionally upregulated by NF-κB, leading to mitophagy mediated mitochondrial clearance. Therefore, while inflammatory events trigger mitophagy, crosstalk between NF-κB and p62 prevents excessive inflammation and restrains NLRP3 inflammasome overactivity.Ubiquitin chains of Parkin on the OMM are phosphorylated by PINK1, and degrade mitofusions, a GTPase which mediated mitochondrial fusion, and trigger the recruitment of autophagy receptors, committing the damaged mitochondria to mitophagy[155]. Reports suggest mitochondrial fission is a prerequisite for the initiation of

mitophagy as parkin prevents fusion leading to mitophagy. Additionally, inhibition of parkin induced fission prevents mitophagy [156,157]. With increasing evidence demonstrating a significant role of mitophagy in pathologies associated with aging such as cancer, it is suggested that therapeutic intervention to induce mitophagy may have potential to ameliorate these diseases.

1.1. Breast Cancer

1.4.1. Breast Cancer Epidemiology

Breast Cancer is the most commonly diagnosed cancer in females and is the leading cause of cancer related deaths among women globally. Breast cancer impacts approximately 2.3 million women worldwide every year, with 7.3 million women diagnosed in the past 5 years, and it was estimated that 685,000 women died of breast cancer in 2020 alone, which accounts for >15% of all the cancer related deaths in women that year (**Fig. 1.14**). Increasing rates of breast cancer can be seen globally, however with the highest incidence in developed countries[158]. National Cancer Registry Ireland's most recent breast cancer statistics published in May 2020 rates breast cancer as the most common malignant tumour diagnosed in Irish women, with an average of over 3,000 cases of invasive breast cancer diagnosed each year and owing to 30% of all cancer-related incident. Breast cancer diagnosis represents one third of all major malignancies diagnosed. Although there are high five-year survival rates of 88%, it is still the second cause of cancer related deaths in women, after lung cancer. Breast cancer accounted for 17% of all cancer deaths in Irish women[159].

Uncontrollable factors associated with the increased risk of developing breast cancer include; gender, age, family history, race, exposure to radiation, estrogen exposure and pregnancy[160]. Sex is the most significant risk factor for the development of breast cancer because although men can develop breast cancer too, this is a 1:1000 lifetime risk[161]. Epidemiology studies implicate estrogen exposure in the aetiology of breast cancer at all stages. Longer menarche, and longer duration of monthly estrogen exposure increases possibility of breast cancer development. Increased concentrations of endogenous estrogen are strongly associated with increased risk in postmenopausal women[162]. Epidemiology studies uncovered that early menopausal and premenopausal obese women have reduced risk while postmenopausal obesity and menopausal estrogen replacement therapy increased the risk[163]. Hormone replacement therapies (HRT) as well as a treatment to relieve menopausal symptoms can also be administrated to transgender women as a gender alignment therapy. In a Dutch cohort study

it was found that transgender women receiving HRT for a median duration of 18 years, had a 46-fold higher risk of developing breast cancer compared to cisgender men but still lower than cisgender women[164]. Age is the second biggest risk factor for breast cancer. From 30-39 years old the risk of developing breast cancer is 0.44%, whereas over the age of 60 the risk increases to 3.5%. African American women have the highest chance of developing breast cancer with Caucasian women only slightly lower, and women of Asia, Hispanic, and Native American descent the least risk of developing and dying from breast cancer[165]. Environmental risk factors include weight (source of endogenous estrogen), diet, exercise, alcohol consumption, sleeping patterns, and smoking.

Family history is known to be one of the strongest risk factors for this disease, with a lifetime risk ratio of 1.80 in families with one affected first generation relative and 3.90 in families with three affected relatives[166]. Inheritable predisposition indicates an importance of genetic variance in determining disease risk. Identification of BRCA1 and BRCA2 mutations was an important breakthrough in the genetic comprehension of breast cancer[167,168]. BRCA1 and BRCA2 gene mutations increase relative risk of disease development to 30-60% risk by the age of 60, compared to that of 3% from the general population and account for 20% of familial risk[169].

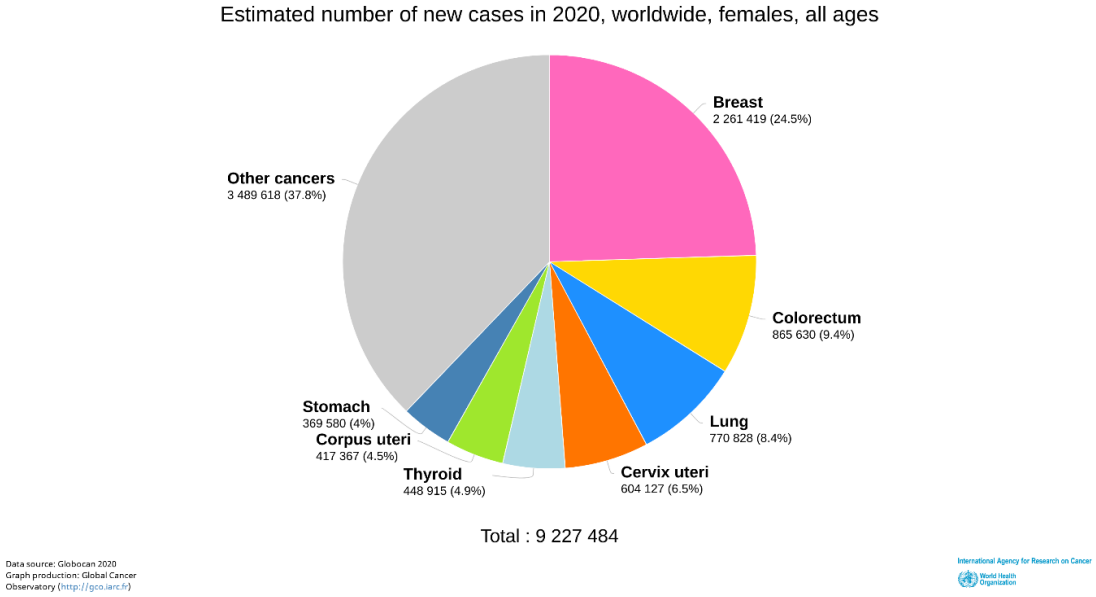

Figure 1.14: Distribution of new female cancer-related incidents across major cancer types in 2020 represented as a percentage of a pie chart[158].

1.4.2. Breast Cancer Subtypes

Invasive breast cancer is a heterogeneous disease with distinct molecular and pathological features, and biological behaviours which can be exploited for diagnosed and treatment. World Health Organisation (WHO) Classification of Tumour of the Breast, has defined 21 morphologically distinct breast cancer subtypes. The most common subtypes defined by their morphology include invasive lobular, tubular, cribriform, metaplastic, apocrine, papillary, and micropapillary[170]. With the era of personalised medicine upon us the progression of molecular classification of breast cancer subtypes has been significant. The four intrinsic subtypes of breast cancer which are classified by their gene expression profile include; luminal A, luminal B, Human epidermal growth factor receptor 2 (Her2) enriched, and basal-like[171,172](**Table 1.1)**. Stratification of breast cancer by subtype has been key for disease characterisation and pivotal for treatment intervention. Perou and colleagues in the early 2000's identified variations in mRNA levels of specific sets of co-expressed genes which would lead to a physiological variation. Gene expression patterns painted from analysis of 8.102 genes identified a distinct molecular portrait[171]. The four intrinsic subtypes of invasive breast cancer arose from gene expression profiling of this study and were unique in their incidence, survival and response to treatment.

Table 1.1: Classification of molecular subtypes

Molecular Class	ER	PR	Her2	Ki67	Percentage incident
Luminal A	+	>20%	_	<14%	67%
Luminal B	+	<20%	+/-	>20%	10%
Her2+	_	_	+		4%
Basal-like	_	_	_		10%

*Estrogen Receptor (ER); Progesterone receptor (PR)[21].

Morphologically, most luminal A tumours are well differentiated non-specific type carcinoma, tubular, lobular, mucinous and neuroendocrine carcinomas[173]. Luminal A are more sensitive to endocrine treatment, indolent, with a low Ki67 score, and prognostically better than luminal B[174]. Gene profiling and immunohistochemistry (IHC)-based classification identified luminal A with the highest expression of ERα gene, GATA-binding protein 3 (GATA-3), X-box-binding protein 1, trefoil factor 3, hepatocyte nuclear factor 3 and estrogen regulated LIV-1. Luminal A subtype does not amplify or expression Her2, 13% demonstrate p53 mutations and 45% display PIK3CA mutation[18]. Prat et al. published, luminal A PR >20% when determined by IHC had improved disease free survival[175], leading St. Gallen expert consensus panel to update the

definition of luminal A in 2013 as, ER+, PR >20%, Her2-, Ki67<14% and classed as “low” recurrence risk based on gene expression assays[176].

Morphologically, most luminal B tumours are less well differentiated with non-specific type carcinoma and micropapillary carcinoma[173]. Luminal B are less sensitive to endocrine therapy, more aggressive, with a higher Ki67 score, and prognostically worse than luminal A[174]. Luminal B subtype demonstrate a lower expression of ERα gene compared to luminal A, and have a higher frequency of p53 mutations (32%) and lower frequency of PIK3CA (32%)[177]. St. Gallen expert consensus panel updated definition of luminal B as, ER+, Her2-, and at least one of the following; PR negative or <20%, Ki67>20% and classed as “high” recurrence risk based on gene expression assays[176].

The Her2+ enriched subtype is associated with a low relapse free survival and overall survival[172]. Amplification of Her2 (ERBB2) oncogene is a well-known indicator of poor prognosis. Her2 is a member of the epidermal growth factor (EGF) receptor family of tyrosine kinase receptors. Her2 does not contain its own ligand-binding domain but rather forms a heterodimer with other members of EGF family, which directly bind ligands, and acts to stabilise binding and enhance tyrosine kinase members of EGF family in downstream signalling pathways including mitogen-activated kinase protein (MAPK) and phosphatidylinositol-3 kinase (PI-3K)[178]. Her2 oncogenic activity is exerted through PI-3K, which inhibits apoptosis, and MAPK, which triggers tumour survival. Although Her2+ enriched subtype has significant advances in treatment with anti-Her2 monoclonal antibody targeted therapies the heterogeneity of the disease still leads to different treatment sensitivities and survival outcomes of patients[179,180]. The St. Gallen expert consensus panel divided Her2-enriched subtype into 2 distinct groups: luminal B-like (ER+, Her2+, any Ki67 and PR value) or non-luminal (ER-, PR-, Her2+), driven by treatment considerations. Hormone receptor positive would be therefore treated with endocrine therapies as well as anti-Her2 therapy and chemotherapy as recommended for all Her2+enriched tumours[176].

Basal-like or triple negative breast cancer (TNBC) is defined by the lack of expression of ER, PR, and Her2 by IHC and is deemed an aggressive cancer. Basal-like subtype presents the worst prognosis with the lowest relapse free survival and overall survival[172]. TNBC has a younger age demographic of women under 40, typically of African American descent, presented at a high tumour grade with a BRCA1 mutation[181]. Due to the lack of receptor expression and the high tumour grade at detection there are no targeted therapies and basal-like breast cancers are hard to treat. Using a transcriptome-based method TNBC is subdivided into different classifications including luminal androgen receptor, immunomodulatory, basal-like immune-suppressed and

mesenchymal-like (**Fig. 1.15)**. Basal-like breast cancer is defined by its epithelial-mesenchymal transition (EMT) phenotype and cancer stem cell (CSC) properties which are driven by inflammatory feedback loops[175].

Additional to Perou's molecular subtyping, Schmidt and colleagues contributed to our knowledge of how gene expression relates to prognosis. Schmidt discovered 3 biological motifs which are important in breast cancer prognosis known as the Schmidt Metagenes. These include proliferation metagenes, B-cell and T-cell associated metagenes, and ER-associated metagenes. Co-regulated genes related to proliferation, B cell and T cell infiltration, and estrogen receptor expression were identified and metagenes were calculated by principal component analysis (PCA) for all genes of a cluster. Data demonstrates that samples characterised by both low ER-metagene expression, and intermediate ER-metagene expression with low proliferation profile were less prone to metastasis. Surprisingly, ER-metagene low and proliferation-metagene high samples were sparsely prone to metastasis, this group was also identified to have high B-cell and T-cell associated metagenes, suggesting lymphoid infiltration as a good prognostic indicator. There is a complete absence of lymphoid infiltration metagenes in the highest ER-metagene cluster. Therefore, subtypes with either high/intermediate ER-metagene expression with low proliferation and no lymphoid infiltration; or low ER-association with high B-cell/T-cell association and high-proliferation, demonstrate low metastasis and have a good prognosis. Intermediate lymphoid infiltration is considered a high risk of recurrence[182]. This is in agreement with the study by Aaltomaa and colleagues which showed that lymphocytic infiltration is associated with a good outcome, particularly in rapidly proliferating tumours[183].

The mammary gland consists of a network of highly branched epithelial tubes embedded in a stromal complex. At birth, mammary tissue is a rudimentary ductal structure of approximately 10 ductal elements which evolve during puberty, pregnancy and lactation in response to steroidal hormone and growth factor exposure. Mammary epithelium is considered highly responsive to local and systemic signalling, resulting in the major changes in morphology of the ductal tree during puberty and pregnancy[184]. A hierarchy of stem cells and progenitor cells of mammary epithelium indicates the existence of bipotent mammary stem cells (MaSCs) *in situ* and long lived unipotent stem cells which drive morphogenesis and homeostasis of the ductal tree. A small proportion of mammary stem cells exist undifferentiated within mammary gland. MaSCs undergo self-renewal to maintain the population and give rise to a variety of differentiated cells[185]. MaSC model has emerged to explain the heterogeneity of breast cancer tumours. Breast cancer molecular subtypes "luminal" A and B, and "basal-like" are named due

to their transcriptome profile similarity to normal mammary luminal and basal epithelial cells. However, the cell of origin from which a tumour arises may not be similar to its namesake. Meyer and colleagues reported PIK3CA mutation, which is present in 30% of all breast cancers including both luminal and basal-like, in luminal mammary progenitor cells gave rise to heterogeneous tumours of luminal and basal differentiation[186,187]. Molecular signalling in normal breast tissue development is dysregulated in breast cancer progression. The major signalling pathways which are hijacked include ER signalling, Her2 signalling and canonical Wnt/ βcatenin signalling[188].

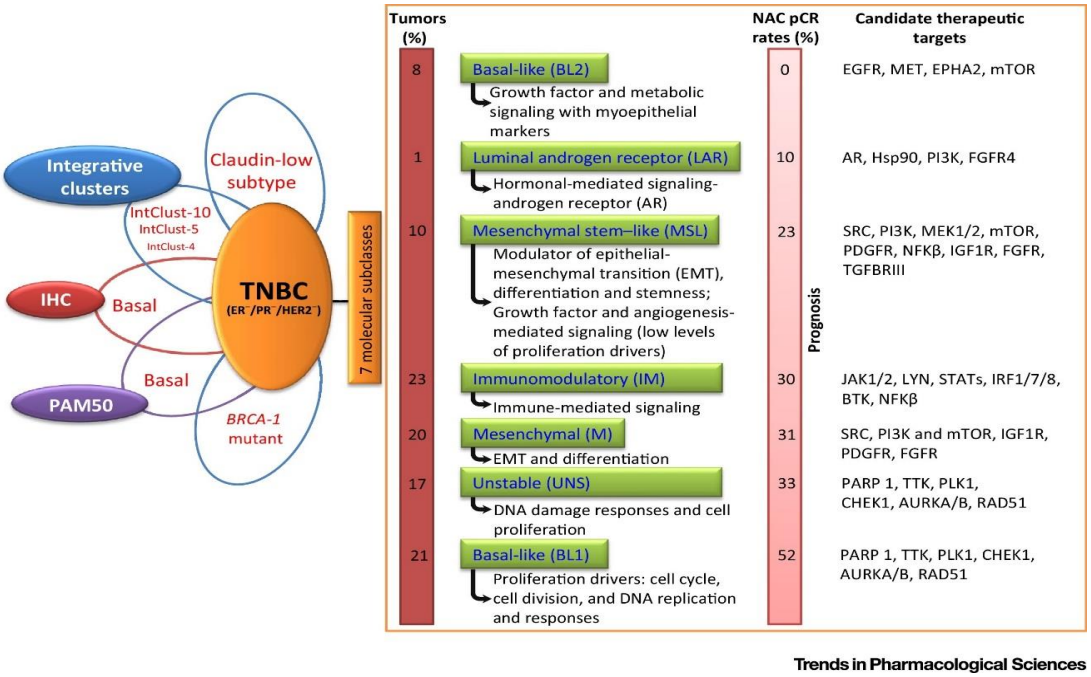

Figure 1.15: Nomenclature and classification of TNBC. TNBC is predominantly basal-like carcinoma (70%). Prediction analysis of microarray-50 (PAM50), integrative gene-expression and copy-number profiling (Integrative clusters: IntClust) have defined the diversity in breast cancers. TNBC subtype itself is molecularly heterogeneous and has been subdivided into six definable molecular subclasses, governed by distinct sets of genes and pathways according to the classification. Each of these subclasses show varying pathological complete response rates following neoadjuvant chemotherapy and may be amenable to targeted therapies using different molecular targets[189].

1.5. Innate Immunity in Breast Cancer

1.5.1. Innate immune response in Breast Cancer

During breast cancer development there is an increased infiltration of leukocytes in parallel with disease progression. Expansion of leukocyte populations and chronic inflammation is associated with neoplastic tissue development and progression of tumourigenesis. However, the promotion of cancer development by the innate immune system is organ specific. Breast cancer is associated with a significant increase of infiltrating immune cells including macrophages, as the most abundant innate immune cells[190,191]. Innate immune cells contributing to the tumour microenvironment include innate immune lymphoid cells and myeloid cells such as granulocytes, macrophages, and dendritic cells.

Innate Lymphoid Cells (ILCs) have a similar morphology as lymphoid cells however they do not possess somatically rearranged antigen receptors or lineage specific markers. There are 3 groups of ILCs divided by their transcription factors and cytokine profile. Group I; natural killer (NK) cells, respond to IL-12, IL-15 and IL-18, trigger T-bet transcription factor and produce type I cytokines, IFN-γ and TNFα. Group II; ILC2, enhance type 2 responses mediated by Gata3 and RORα transcription factors and produce effector cytokines, IL-5, IL-9 and IL-13. Group III; ILC3 express RORγt transcription factor and produce IL-22 and IL-17A. ILCs are involved in intestinal homeostasis and have been implicated in colitis pathogenesis. ILC1, ILC2, ILC3 behave similarly to Th1, Th2 and Th17 cells, respectively[192]. These ILCs have an important role in breast cancer pathogenesis, with a critical immunosurveillance responsibility in early tumour development[126]. IL-15 mediates ILC1 generation, therefore IL-15$^{-/-}$ mice, lacking ILC1 cells, demonstrate accelerated breast cancer tumour growth compared to mice deficient in CD8^{+} T lymphocytes[127]. Whereas ILC2s enhance a type 2 protumourigenic environment. The IL-1 family member, IL-33, stimulates ILC2 type 2 response leading to tumour progression, metastasis, and IL-13 production. IL-13 cytokine is known for its ability to promote macrophage protumourigenic M2 polarization. ILC3s have also been linked to both pro and anti-tumourigenic functions. IL-23 stimulated ILC3s produce IL-17A to promote angiogenesis and MDSC recruitment[193]. However, ILC3s producing IL-22 lead to reduced breast tumour growth[194].

Myeloid cells are the most abundant of all hematopoietic cells and their role in innate immunity is critical for immune maintenance. Myeloid cells are comprised of 3 groups: granulocytes, macrophages, and dendritic cells. Myeloid cells function to eliminate dying cells, protect the

host from harmful pathogens and organise tissue remodelling[108]. Dependent on factors produced by the tumour microenvironment (TME) and as a result of myeloid cell plasticity, myeloid cells cannot only play a pro-inflammatory/anti-tumourigenic role but can also mediate angiogenesis, invasion and metastasis immunosuppressive phenotype. Tumour infiltrating myeloid cells encompass granulocytes, such as neutrophils, basophils and eosinophils, Tie-2 expressing monocytes, dendritic cells, tumour associated macrophages (TAMs), immature myeloid cells and MDSC[195]. Expansion of granulocyte, immature myeloid cell and antigen presenting cell (APC) infiltrating populations was observed in breast cancer tumour compared to non-tumour adjacent tissue[196]. Neutrophils are the most common granulocytes in the breast cancer tumour microenvironment and function to supress the cytotoxic effects of $CD8^+$ T cells[197]. Conversely, neutrophils have also been observed to mediate an anti-tumour function by producing ROS which contribute to inhibition of metastasis[198]. Macrophages are highly plastic myeloid cells influenced by molecules secreted by cancer cells. These secretory factors can polarise macrophages to influence tumour growth and immunosuppression. Murine breast cancer models have been demonstrated to indirectly promote the invasive potential of $CD4^+$ IL-4 producing Th2 cells[199]. IL-4 producing $CD4^+$ T cells regulate TAM polarisation to an M2-like phenotype. M2-like TAM expression of epidermal growth factor mediates mammary malignant epithelial cell growth. Notably EGFR mammary malignant cell expression is associated with low hormone receptor expression[199].

Chronic inflammation mediated by cytokines and hormones is considered an important player in the establishment and progression, angiogenesis, and metastasis of breast cancer. Important cytokines detected locally and systemically in breast cancer patients include IL-1, IL-6, IL-12, IL-33, TNFα, IFN-γ and GMCSF[200].

1.5.2. Inflammasome components and substrates in Breast Cancer

IL-1 represents a family of proinflammatory cytokines; IL-1α, IL-1β and IL-1 receptor antagonist (IL-1ra), IL-18, IL-33, IL-36a, IL-36b, IL-36Ra, IL-36γ, IL-37 and IL-38 of importance to innate and adaptive immunity. IL-1α and IL-1β are encoded on neighbouring genes IL1A and IL1B located on chromosome 2[201]. Both IL-1α and IL-1β bind IL-1R inducing similar physiological effects. IL1 two receptors include IL-1R1 and IL-1R2 which are found expressed on normal epithelial and cancer cells, T-lymphocytes, myeloid cells and fibroblasts[202]. IL-1R1 can initiate signalling transduction pathways whereas IL-1R2 binding soluble ligands and form complexes with type 1 receptors. IL-1 cytokines can function in an autocrine or paracrine manner, to induce the

secretion of other cytokines. IL-1β has an important role in the differentiation and survival of IL-17A producing T helper (Th17) cells[203] IL-1β is expressed by myeloid cells of the tumour microenvironment such as macrophages, dendritic cells and neutrophils as well as epithelial cells, whereas IL-1α is mainly expressed by normal epithelial and tumour cells. Both of which contribute to carcinogenesis, tumour invasiveness, and local immunosuppression. While simultaneously playing an anti-tumour immune role. IL-1β is abundant in the TME, where this cytokine can promote tumour growth, but also antitumor activities[202].

Wu and colleagues demonstrated that IL-1β coordinates tumour promoting inflammation in breast cancer which can be targeted with IL-1 receptor antagonist in patients with metastatic breast cancer providing evidence for IL-1β therapy in treatment resistant breast cancer[204]. IL-1β expression significantly increases with higher histopathologic tumour staging. IL-1β processing was predominantly associated with $CD11c^+$ cells compared to cytokeratin-19 expressing breast tumour cells, with approximately 60% of $CD11c^+$ cells inducing IL-1β expression[204]. CD11c is a type I transmembrane protein located on myeloid cells including dendritic cells, macrophages and neutrophils. IL1B transcripts were associated with $CD45^+$ leukocytes and rarely $CD45^-$ breast cancer and stromal cells[204]. Suggesting monocyte and dendritic cells are the main source of IL-1β in breast cancer tumours. IL-1β secretion positively correlates with T cell cytokines IL-13, IFN-γ, and thymic stromal lympopoietin (TSLP). IL-1β mediates transcription of TSLP in the triple negative breast cancer cell line, MDA-MB-231. Th2 inflammation in breast cancer cells is IL-1β-dependent via TSLP induction[204],[205]. IL-1β produced by myeloid cells of the TME involves NLRP3 and NLRC4 inflammasome activation which is activated by breast cancer derived factors. TCGA gene expression analysis data revealed CASP1, NLRP3, and NLRC4 have high correlation with IL1B transcripts in breast cancer but poor correlation with CASP11 suggesting canonical inflammasome activation[204]. Treatment with a caspase-1 inhibitor decreased the percentage of $HLA\text{-}DR^+$ mature IL-1β. IL-1β production in monocytes and cDCs is triggered by breast cancer cell membrane associated TGFβ. TGFβ neutralising antibody treatment in breast cancer cDCs co-culture reduces the expression of IL-1β and $HLA\text{-}DR^+$ mature IL-1β cell population. A TAK1 inhibitor was used to determine if the inflammasome activation was involved in TGFβ-mediated IL-1β maturation. TAK1 inhibitor treatment resulted in inhibition of caspase-1 activation and IL-1β processing in cDCs and monocytes. Additional TGFβ neutralising antibody treatment in co-cultures inhibitors TAK1 phosphorylation[204] suggesting a role for TGFβ in TAK1 phosphorylation, caspase-1 activation and IL1-β maturation in breast cancer associated myeloid cells. *In vivo* humanised irradiated NOS/SDIC/ $\beta_2m^{-/-}$ mice subcutaneously injected with HS578T breast cancer cells exhibited an inhibition of cancer growth when treated intratumourally with TGFβ

neutralising and/or IL-1R antagonist (anakinra) simultaneously with MDDC and T cells. Anakinra and TGFβ neutralising results in significant decrease in secretion of IL-13, IL-4 and IL-17 whereas IFN-γ and TNF-α upregulate with anakinra treatment[163]. These findings contributing to previous data, implicating breast cancer derived TGF-β with myeloid derived IL-1β and their influence on the population composition of the TME.

A pilot clinical trial of n=11 HER2- metastatic breast cancer patients was conducted (NCT01802970) to determine efficacy of anakinra treatment in combination with chemotherapy. Two patients demonstrated reduction in tumour size when treated with anakinra and chemotherapy combination, 4 patients had disease stabilisation, 2 patients developed anakinra related injection site reactions and stopped treatment and 3 patients had continued disease progression. Examining anakinra's impact on inflammatory markers from blood leukocyte transcriptome demonstrated IL1 related genes (IL1B, IL1R1, IL1R2 and IL1RAP), myeloid cell-related genes (ICAM1, ICAM3, ITGAX, FCGR2a, IL6R, CSFRB and PLAUR) and innate sensing and downstream molecules (TLR1, TLR8, CLEC4A, CLEC7A, SKY and MYD88) which are abundant at baseline are reduced after two weeks of anakinra treatment alone and remained decreased over course of anakinra/chemotherapy regime. In contrast to the suppression of IL1 and TLR related genes by anakinra, increased expression of natural killer cell and cytotoxic T lymphocyte genes essential for immune-mediated tumour destruction was observed[204]. This study Illustrates the treatment potential of anakinra to modulate an anti-tumour microenvironment. $IL1B^{-/-}$ and wildtype (WT) Balb/c and C57BL/6 anti-IL1β treated mice orthotopically implanted with 4T1 breast cancer cells demonstrated tumour regression due to altered immune infiltration and differentiation[206]. Decreased tumour immunosuppression mediated by macrophage was observed and dendritic cell mediated and cytotoxic $CD8^+$ T lymphocytes anti-tumour immunity was also observed to aid tumour regression. Reduced CCL2 and CFS-1 in $IL1B^{-/-}$ and wildtype anti-IL1β treated mice limited the monocyte tumour infiltration and macrophage differentiation and immunosuppressive IL-10 production. Conversely high CD11b+ dendritic cell infiltration producing IL-12 induced anti-tumour response. $CD8^+$ T lymphocytes expression of IFN-γ, TNFα and granzyme B is elevated in IL-1β deficient mice tumour microenvironment inducing tumour suppression[206]. Anti-PD-1 therapy has been demonstrated to reduce tumour burden however in combination with anti-IL-1β there is a complete abolition of breast cancer tumour, supporting anti-IL-1β as a checkpoint inhibitor in cancer treatment[206]. From these studies it is clear that myeloid derived IL-1β influences the cellular composition of the TME and inhibition of IL-1R signalling mediates an anti-tumour cytotoxic environment.

Utilising TCGA and METABRIC dataset it was observed that IL1B transcripts are significantly higher in basal-like breast cancers, which are associated with poor prognosis. Clustering of datasets according to anakinra molecular signature determine from patient blood leukocytes it was revealed that patients who cluster highly with anakinra related IL1 molecular signature are predominantly basal-like breast cancers[204]. This indicates an important association between IL-1 signalling and basal-like breast cancer. IL-1β association contributes to aggressive immunosuppressive environment of basal-like breast cancer.

Inflammasome deficient mice have developed our understanding of the role of the inflammasome in cancer initiation, development, and metastasis. EO771 murine breast cancer cells orthotopically implanted to wildtype and caspase-$1^{-/-}$ C57BL/6 mice demonstrated reduced primary tumour mass in caspase-$1^{-/-}$ mice as well as reduced lung metastasis[207]. Guo and colleagues also investigated upstream of activated caspase-1 and pro-IL-1β to determine the impact of the NLRP3 inflammasome. Similar to caspase-$1^{-/-}$, NLRP3$^{-/-}$ mice display reduced primary tumour mass and number of visible metastases. IL-1β secretion from EO771 mammary tumour and lung metastasis is significantly higher in wildtype compared to both caspase-$1^{-/-}$ and NLRP3$^{-/-}$ mice. Regarding myeloid cell recruitment, caspase-$1^{-/-}$ mice demonstrate a decrease in $CD11b^{+}GR1^{-/low}$ (tumour associated macrophages) and $CD11b^{+}GR1^{+}$ (myeloid-derived suppressor cells) cell populations within the tumour. Whereas $CD11b^{-}GR1^{+}$ neutrophils were comparable between wildtype and caspase-$11^{-/-}$ mice. Investigating myeloid cell inflammasome activity, $CD11b^{+}$ cells were isolated and analysed for IL-1β secretion, which was significantly reduced in caspase-$1^{-/-}$ mice. Reduction in IL-1β expression effects CCL2 expression levels, therefore suggesting caspase-1 induced IL-1β is required for CCL2 macrophage recruitment into the tumour microenvironment. IL-1 receptor antagonist (IL-1Ra) was also utilised to demonstrate reduced tumour mass, visible lung metastases and decreased infiltrating TAMs and MDSCs compared to untreated wildtype controls[207]. Using an orthotopic xenograft mouse model of human breast cancer MDA-MB-231 cells treated with human IL-1Ra it was observed that human breast cancer growth was significantly inhibited and overall improved survival in treated mice[207]. Therefore caspase-1 plays a tumour promoting role in murine mammary carcinoma, promoting macrophage and MDSC infiltration and metastatic potential. Similarly, leptin-induced NLRP3 inflammasome activation leads to the proteolysis of caspase-1 and IL-1β maturation in MCF-7 breast cancer cell lines promoting tumour growth[208]. Exhibiting leptin mediated IL-1β pro-tumourigenic effects in ER+ breast cancer cell line. Inhibition of ER signalling and ROS production markedly decreased leptin-mediated inflammasome activation[208]. Breast cancer tumour homogenates IL-1α expression inversely correlates with ER levels. While IL1ra expression

directly correlates with ER and IL-1β levels. ER- cytokine profiles differ from ER+ patients, suggesting IL-1 family importance in tumourigenesis[194].

IL-6 elevated levels in breast cancer patients serum is associated with poor prognosis[209]. ER+ breast cancer cells EMT phenotype is conferred by IL-6 expression, inducing an aggressive stem-like phenotype[210]. Transglutaminase 2 (TG2) is an inducible transamidating acyltransferase that catalyses Ca^{2+}-dependent protein modifications. TG2 externalisation occurs during inflammation via P2X7 receptor activation[211]. P2X7 is a downstream product of caspase-11 involved in ATP release during pyroptosis[80]. TG2-NFκB-IL6 pathway has been demonstrated to enhance tumour progression and metastasis IL-6 and TG2 expression is correlated and associated with basal-like breast cancer giving a cancer stem-like phenotype of invasiveness and metastatic potential[212]. Overexpression of TG2 in luminal A, MCF-7 breast cancer cell line demonstrated an IL-6 aggressive phenotype triggered by IL-1β in a TG2 dependent manner, similar to basal-like phenotype. TNF-α and TGF-β stimulation potentiated the IL-1β-mediated IL-6 expression. IL-1β treatment of TG2 overexpression MCF-7 breast cancer cells increased stemness, invasion and estrogen-independent tumour growth, and reduced by treatment with anti-IL-1β and anti-IL-6 antibodies. Therefore IL-1β in combination with other inflammatory stimuli such as TNF-α and TGF-β, promote IL-6 expression and tumour aggressiveness in a TG2-dependent manner[212].

In breast cancer, RIG-1 upregulation mediates lymphocyte recruitment and reduces tumour mass. RIG-1 agonist treatment leads to upregulation and mitochondrial localisation of RIG-1 and activation of NF-κB and STAT1 transcription factors[172]. RIG-1 agonist was observed to induce pyroptosis and type I IFN and lymphocyte-recruiting chemokine release triggered by caspase-1 and GSDMD cleavage[213]. Breast cancer is considered a poorly immunogenic disease with low lymphocyte infiltration[214], therefore activation of innate immunity and induction of immunogenic cell death with potent cytokine, interferon and chemokine release could improve tumour microenvironment infiltration and anti-tumour response.

Docosahexaenoic acid (DHA) is an omega-3 fatty acid which exhibits anti-tumour effects including decreased tumour growth and increased apoptosis as well as regulation of inflammation[190]. Clinical trial (NCT03831178) is currently recruiting women with breast cancer to incorporate DHA in combination with chemotherapy. Studies have demonstrated the reduction in breast cancer mass and visible lung metastases by suppressing metalloproteinases when treated with DHA[215]. Pizato and colleagues investigated the potential impact of DHA on

pyroptosis in basal-like breast cancer, MDA-MB-231. DHA induces cytotoxic potential specific for malignant MDA-MB-231 cells but not MCF-10A, normal mammary epithelial cells. Further investigation to deduce how DHA-induced decreased viability demonstrated that DHA treatment leads to increased cell death and induction of pyroptotic markers. DHA stimulates NF-κB translocation, ASC upregulation, caspase-1 and GSDMD cleavage, significantly increases release of IL-1β and triggers HMGB1 translocation from the nucleus to the cytoplasm[190]. DHA induces pore-forming pyroptosis via canonical inflammasome activation leading to HMGB1 translocation. This translocation to the cytoplasm occurs after inflammasome activation and the initiation of pyroptosis to promote inflammatory pathogenesis via DAMP activity on innate immune sensors[190]. Therefore, demonstrating anti-tumourigenic pyroptotic function of the canonical inflammasome during breast cancer in association with DHA.

1.6. Role of Macrophages in the Breast Cancer Tumour Microenvironment

1.6.1. Breast Cancer Tumour Associated Macrophages

Malignant tissue microenvironment influence on tumour associated macrophages (TAMs) can have either a protective or detrimental effect on tumour progression. Within the tumour microenvironment (TME) are a large repertoire of innate and adaptive immune cells, of which macrophages are a largely abundant population. Generally, TAMs are associated with a pro-tumourigenic role in all stages of disease progression, mediating angiogenesis and invasion in primary tumours while establishing tumour niches at metastatic sites. TAMs also promote an immunosuppressive phenotype, preventing activity of innate immune NK cells and adaptive immune T cells. These roles of TAMs make them an attractive avenue for targeted cancer treatment therapies[216].

Breast cancer TAMs are sustained by tissue-resident macrophages and circulating monocytes recruited by the TME[217]. Naïve monocyte-derived macrophages (M0) recruited to the tumour domain are differentiated into M1 or M2-like macrophages dependent on the environmental cues available. As previously described M1 macrophages are induced by type I cytokines such as IFN-γ and TNFα and exhibit anti-tumour activity by releasing pro-inflammatory cytokines including TNF, IL-1 and IL-6 with reactive nitrogen and oxygen intermediates. Whereas M2, pro-tumour, macrophages are activated by type II cytokines including IL-4, IL-10 and IL-13. TAM more closely relate to M2-like macrophages. However as previously stated macrophages cannot be

tightly classified as either M1 or M2 and with the variety of cytokines and growth factors present in the TME attention must be focused on a more spectral plastic polarisation of TAMS.

RNA sequencing of monocytes isolated from women with breast cancer and healthy donors revealed 856 differentially expressed genes in tumour educated monocytes (TEMs) compared to healthy monocytes[218]. Genes associated with migration, angiogenesis, communication and apoptosis were enriched. Further investigation of monocyte subpopulations was performed to develop understanding of TEM transcriptome shift compared to healthy donors. Classical ($CD14^+$, $CD16^-$) and non-classical ($CD14^+$, $CD16^+$) monocyte subpopulations isolated from breast cancer patients and healthy individuals exhibited a significant expansion of non-classical monocytes of cancer patients[218]. Non-classical monocyte expansion correlates with an increase of CX3CL1 and reduction of CCL2 in patient sera. CX3CR1, CX3CL1 receptor, was found to be significantly downregulated in classical monocytes of cancer patients, this downregulation in ligand receptor is consistent with the expansion of non-classical monocytes[218]. This evidence suggests breast cancer patients have an expansive non-classical monocyte population which is recruited to the TME by chemokine CX3CL1. Non-classical monocytes are considered biased progenitors of M2 macrophage polarisation during soft tissue injury and support vascular remodelling as described by Olingy and colleagues. While classical monocytes are recruited from the circulation to inflamed tissue and differentiate to either macrophages or dendritic cells, in soft tissue damage non-classical monocytes extravasate to polymer films and home to perivascular niches where they differentiate to alternatively activated macrophages. Non-classical monocyte molecule FTY720 recruits S1PR3-expressing non-classical monocytes to aid angiogenesis[219].

A meta-analysis study of 2000 breast cancer patients of all stages illustrated higher density of tumour infiltrating TAMs is predictive of a poorer prognosis[220]. Immunohistochemistry analysis of 367 invasive breast cancer microarray demonstrated $CD68^+$ (pan-macrophage marker), $CD11c^+$ (M1 marker), and $CD163^+$ (M2 markers) expression is associated with higher histologically graded, Ki67 higher, hormone receptor negative breast cancer, basal-like breast cancer. High infiltration of $CD11c^+$ and $CD163^+$ in the tumour stroma is also associated with larger tumour mass and $CD163^+$ expressing macrophages located within tumour nests are linked to reduced overall survival (OS) as well as disease free survival (DFS)[221]. In human invasive breast carcinoma tumour stromal associated macrophages (TSMs) and tumour nest macrophages (TNMs) have distinct relationships with clinicopathological parameters and angiogenesis. Cheng and colleagues suggest that TSM and TNM play distinct roles in tumour development as a result of the distinct microenvironments in which they reside[222]. Immunohistochemistry of 97 invasive

breast cancer tissue immunostained with CD68 and CD34 (microvessel stain) demonstrated a close correlation between the presence of TSM and TNM within the TME. However, histologically higher tumour grade and estrogen receptor negative status is associated with higher TSM grade. Increased mitotic count scores correlate with higher TSM grade, whereas TNM significantly correlates with increased microvessel density[222]. TNMs refer to the intra-epithelial tumour infiltrating macrophages while TSMs refer to macrophages infiltrating the fibrous tissue surrounding the tumour nest. This data supports the concept of TAM heterogeneity and functional plasticity within the heterogeneous breast cancer TME.

In vitro studies have also observed breast cancer cells education of macrophages towards an M2-like status. Investigation was performed by culturing M1, M2a and M2c differentiated MDM with conditioned media of MCF-7 (luminal A) and MDA-MB-231 (TNBC) cell lines, demonstrating breast cancer mediated macrophage plasticity. CD14+ monocytes in the presence of MDA-MB-231 CM alone yields an M2 macrophage population, with upregulation of cell surface markers CD14, CD16, CD200R, and CD163. Whereas MCF-7 conditioned media did not have the ability to polarise CD14+ monocytes towards an M2 phenotype[223]. Breast cancer patient data also reveals that M2-like macrophages are associated with hormone receptor negative breast cancers[224]. MDA-MB-231 conditioned media primed macrophages activated by LPS produced higher levels of IL-6, IL-8 and IL-10. CD14+ monocytes differentiated by IFN-γ (M1) in the presence of breast cancer conditioned media had no effect on M1 marker expression or cytokine profile. However, M2 status was influenced by presence of conditioned media. CD14+ monocytes differentiated by IL-10 (M2c) in the presence of breast cancer conditioned media demonstrated decreased CD14 expression in the presence of MDA-MB-231 conditioned media and upregulation of CD163. CD14+ monocytes differentiated by IL-4 (M2a) in the presence of breast cancer conditioned media demonstrated higher $CD14^{hi}CD16^{hi}$ subpopulation in the presence of MDA-MB-231 conditioned media compared to the domain subpopulation $CD14^{lo}CD16^{lo}$ induced by IL-4 alone[223]. MDA-MB-231 conditioned media primed M2a and M2c macrophages activated by LPS produced higher levels of IL-6, IL-8 and IL-10, with the exception of IL-6 secretion by M2c MDA-MB-231 macrophages[223]. Similarly in other studies M1 and M2 polarised macrophages cell surface expression markers are unaffected by MCF-7 conditioned media[225]. Evidence suggests that cues from the tumour microenvironment, particularly of basal-like breast cancer, can overcome typical polarising cytokines mediating macrophage phenotype and adapt macrophage functionality to promote tumour progression. This may also help to develop our understanding of the heterogeneous macrophage population exhibited in breast cancer patient's tumours. M2 –like MDA-MB-231 TAMs contribute to positive feedback of tumour progression as M2

macrophages co-cultured with MDA-MB-231 induces an elongated, spindle morphology associated with mesenchymal transition and tumour migration[225].

1.6.2. Inflammasome components influence on macrophage polarisation

Influence of inflammasome related gene expression and activation on macrophage polarisation is a recent area of study. Liu and colleagues investigated the effect of the NLRP3 inflammasome on macrophage polarisation in a model of allergic inflammation asthma. M2 macrophage polarisation and NLRP3 inflammasome activation are involved in asthma. NLRP3-mediated IL-4 leads downregulation of the M1/M2 ratio. NLRP3 interaction with IRF4 impacts IRF4-dependent IL-4 transcription. Data demonstrates that NLRP3, but not canonical inflammasome platform, promotes M2 macrophage status via IL-4 transcriptional upregulation in murine asthma model[226]. Contrastingly, NLRP3 independent of IL-1 activity facilitates M1 infiltrating renal macrophages during nephrocalcinosis-related chronic kidney disease. 1,3-butanediol treatment inhibition of NLRP3 leads to a shift in towards M2 anti-inflammatory macrophage activation. NLRP3, independent of its role in IL-1β maturation, demonstrates a non-redundant role in TGF-β signalling promoting its involvement in macrophage polarisation[227]. NLRP3 inflammasome activation is implicated in chronic sterile inflammation during obesity correlates with M1 macrophage polarisation in adipose tissue macrophages[228]. Study by Vandanmagsar and colleagues revealed NLRP3-deficient mice adipose tissue macrophages have increased M2-like macrophages associated with increased IL-10 and Arg1 transcripts and reduced M1 macrophage markers TNFα, CCL20 and CXCL11[229]. Evidence is suggestive of a role for NLRP3 in promotion of obesity induced adipose tissue macrophage inflammation. However further investigation discovered NLRP3-deficiency in obese mice does not impact the frequency of M1 and M2 macrophage populations of visceral adipose tissue. Whereas, in subcutaneous adipose tissue NLRP3 autoactivating caspase-1 macrophages correlate with M1 macrophage population. Subcutaneous adipose tissue macrophages from NLRP3$^{-/-}$ mice have increased frequency of M2 macrophage population, without affecting M1 population[229]. Therefore, exhibiting a role for NLRP3 inflammasome activation in promoting M1 macrophage polarising and inflammatory cytokine profile. Awad and colleagues investigated the impact of macrophage polarisation of NLR expression and NLRP3 inflammasome activation. This study revealed the downregulated LPS induced NLRP3 and IL18 transcripts in the presence of M2 polarising cytokines, IL-4 and IL-13. Caspase-1 and caspase-4 mRNA expression was only found to be upregulated in M1, not M2, macrophages. IL-1β and IL-1α secretion is dampened in M2 polarised macrophages treated with activation signal ATP, compared to naïve and M1 macrophages[230]. This study provides an

understanding of inflammasome activity within M1 or M2 polarising environments, clearly demonstrating a dampened inflammasome response in the presence of M2 polarising cytokines and by M2 polarised macrophages.

2.Chapter 2: Materials & Methods

2.1. Materials

Table 2.1 Materials

Material	Source
Agarose (electrophoresis grade)	Invitrogen
Ammonium Sulphate	Sigma Aldrich
Aprotinin	Sigma Aldrich
Bicinchoninic Assay	Thermo Scientific
Bovine Serum Albumin	Sigma Aldrich
Bromophenol Blue	Sigma Aldrich
Cell culture plastics	Cruinn Ltd
Chemiluminscence substrate	Millipore
Dimethyl Sulfoxide (DMSO)	Sigma Aldrich
Dithiothreitol (DTT)	Sigma Aldrich
DNA ladder, Quick-Load Log-2	New England BioLabs
Dulbecco's Modifiied Eagles Medium (DMEM)	Invitrogen
Ethanol	TCD HMF Stores
Ethylenediaminetetracetic acid (EDTA)	Sigma Aldrich
Fluorescent Mounting Media	DAKO
Foetal Bovine Serum	Labtech
Glycine	Sigma Aldrich
Glycerol	Sigma Aldrich
GoTaq Hot Start Master Mix	Promega
Griess Reagent	Enzo Life Sciences
High Binding Affinity 96 well plate	Cruinn Diagnostics
Hydrochloric acid	Sigma Aldrich
IFNy recombinant protein	Invivogen
IL-4 recombinant protein	Invivogen
GMCSF recombinant protein	Invivogen
Human recombinant Insulin	Sigma Aldrich
Isopropanol	TCD HMF Stores
Lipofectamine 2000	Invitrogen
Leupeptin	Sigma Aldrich
Lipopolysaccharide (LPS)	Sigma Aldrich

Methanol	TCD HMF Stores
0.45µM Nitrolcellulose Membrane	Sigma Aldrich
NP-40	Sigma Aldrich
Nuclease-free water	Biosciences
Opti-MEM	Biosciences
Penicillin Streptomycin	Invitrogen
Phenylmethylsulphonyl fluoride (PMSF)	Sigma Aldrich
Potassium chloride	Sigma Aldrich
Potassium hydroxide	Sigma Aldrich
Phosphate buffered Saline (1X)	Biosciences
Protein ladder (SeeBlue Plus2)	Biosciences
Proteinase K	Sigma Aldrich
Protogel (Acrylamide)	Analab
RPMI 1640 Glutamax	Biosciences
Sodium azide	Sigma Aldrich
Sodium chloride	Sigma Aldrich
Sodium deoxycholate	Sigma Aldrich
Sodium phosphate monobasic	Sigma Aldrich
Sodium phosphate dibasic	Sigma Aldrich
Sodium Dodecyl Sulphate (SDS)	Sigma Aldrich
SYBR Safe DNA stain	Biosciences
SYBR Green	Biosciences
Tetramethylethlenediamine (TEMED)	MWG
Trisma-Base	Sigma Aldrich
TrypLE Express	Biosciences
Virkon Tablets	VWR

Table 2.2 Buffers

Name	Receipe
DNA extraction buffer	100mM Tris 5mM EDTA 02% SDS 200mM NaCl 500µg/mL Proteinase K
2X Lammeli Buffer	11% (v/v) Glycerol 10% (w/v) SDS 0.1% (w/v) Bromophenol blue 2.5mM Tris-HCl 100mM DTT pH6.8
10X Phosphate buffered Saline (PBS)	1.45M NaCl 227mM $NaHPO_4$ 39nM NaH_2PO_4 pH 7.2
10X Tris-Buffered Saline (TBS)	10mM Trizma Base 150mM NaCl pH8.0
10X Transfer Buffer	0.25M Trizma Base 1.9M Glycine
10X Running Buffer	0.25M Trizma Base 1.9M Glycine 35mM SDS
2x Lamemli	20% (v/v) Glycerol 20% (w/v) SDS 0.2% (w/v) Bromophenol blue 125mM Tris-HCl 300mM DTT pH 6.8
Immunoprecipiation (IP) lysis buffer	150mM NaCl 50mM Tris-HCl pH 8.0 1% (v/v) NP-40

	Supplemented with: 1mM PMSF 1µg/µL Leupeptin 1µg/µL Aprotinin
Radioimmunoprecipitation Assay (RIPA) lysis buffer	150mM NaCl 50mM Tris-HCl pH 8.0 1% (v/v) NP-40 0.1% (w/v) SDS 0.5% (w/v) sodium deoxycholate Supplemented with: 1mM PMSF 1µg/µL Leupeptin 1µg/µL Aprotinin

2.2. Cell Culture

Table 2.3: Immortalised Cell lines

Name	Description	Growth Media	Subculture
MCF-7	Human estrogen receptor positive invasive breast ductal carcinoma. Differentiated mammary epithelium derived from metastatic site; pleural effusion. Process estradiol via cytoplasmic estrogen receptors. WNT7B oncogene.	DMEM GlutaMAX	1:3 to 1:6
T47D	Human estrogen positive invasive breast ductal carcinoma. Differentiated mammary epithelium derived from metastatic site; pleural effusion. WNT7B oncogene.	RPMI-1640 GlutaMAX	1:3 to 1:5
CAMA-1	Human estrogen receptor positive breast adenocarcinoma. Differentiated mammary epithelium derived from metastatic site; pleural effusion. Poorly differentiated stage III tumour.	DMEM GlutaMAX	1:3 to 1:4
ZR-75-1	Human estrogen receptor positive invasive breast ductal carcinoma. Differentiated mammary epithelium derived from metastatic site; ascites.	DMEM GlutaMAX	1:4 to 1:6
BT549	Human invasive breast ductal carcinoma. Polymorphic with epithelial like components.	DMEM GlutaMAX	1:2 to 1:6
HS578T	Human invasive breast carcinoma. Polygonal morphology. Does not express estrogen receptor.	DMEM GlutaMAX	1:3 to 1:8

MDA-MB-231	Human breast adenocarcinoma. Differentiated mammary epithelium derived from metastatic site; pleural effusion. WNT7B oncogene.	DMEM GlutaMAX	1:2 to 1:4
RAW264.7	Mouse macrophage derived from Abelson murine leukemia virus-induced tumour; ascites. Established from adult male BALB/c strain.	DMEM GlutaMAX	1:3 to 1:6
L929	Mouse subcutaneous connective tissue fibroblasts derived from C3H/An strain.	DMEM GlutaMAX	1:2 to 1:8

Cell culture procedures were carried out in a laminar II grade biosafety cabinet using aseptic technique. All equipment and reagents were thoroughly sprayed with 70% ethanol before and after each use, UV-C germicidal lamp installed within the biosafety cabinet was turned on for 15 minutes daily, and cabinets were cleaned weekly with virkon followed by 70% ethanol.

Cell lines were cultured in appropriate growth media as specified in **Table 2.3**. Growth media was supplemented with 10% heat inactivated foetal bovine serum (FBS) endotoxins <0.2EU/mL (100U/mL) and 1% penicillin-streptomycin (Pen-Strep) (100µg/ml). MCF-7 was additionally supplemented with 0.01mg/mL human recombinant insulin. Cells were cultured in T75cm^3 and T175cm^3 flasks in log growth phase and subcultured at approximately 80% confluency before cells reached stationary phase. Cells were subcultured 2-3 times per week but not beyond the passage number 40. Cells were growth in a humidified incubator at 37°C 5% CO_2. Cells morphology and visible signs of infection were monitored daily using a light microscope (Lecia, DMIL).

Immortalised adherent cell lines were subcultured 2-3 times a week once they have reached approximately 80% confluency. This was achieved by first removing all media from the flask and washing with 5mL PBS. Adherent cells were detached from the base of the flask by enzymatic cell dissociation using TrypLE, approximately 2mL incubated for 3 minutes at 37°C 5% CO_2. Detachment of cells was confirmed under light microscope as small round cells floating. Gentle tapping of the flask against a solid work surface helps provide full detachment of cells. Once detached TrypLE was neutralised using 3 times the volume of media before being transferred to a 50mL falcon tube and centrifuged (5 mins at 400 x g). Supernatants were discards and cell

pellet was resuspended in 1mL of media. Following **Table 2.3** subculture ratio cells were seeded in a new flask with fresh media.

2.2.1. Monocyte Derived Macrophages (MDM)

To generate human MDM, peripheral blood mononuclear cells (PBMCs) were isolated from human buffy coat packs obtained from the Irish Blood Transfusion Service. PBMCs were isolated by members of Prof. Aisling Dunnes Lab using density gradient centrifugation with Lymphoprep. PBMCs were seeded $2x10^6$cell/mL on Corning Costar Non-treated 12 well plate (Merck) in RPMI-1640 supplemented with 10% human A/B serum (Sigma Aldrich)[231]. Non-adherent cells were washed away after 3 days every 2 days, with a total culture period of 7-9 days to allow macrophage differentiation prior to experimentation.

2.2.2. Bone Marrow Derived Macrophages (BMDM) Isolation

BMDM were isolated from the femur and tibiae of C57BL/6J WT and Caspase-11 knockout (*Casp11*$^{-/-}$) mice. Mice were housed in Trinity Biomedical Sciences Institute's sterile pathogen free facility and were humanely sacrificed by inhalation of CO_2 gas. Following euthanasia, mice were sprayed with 70% ethanol and leg bones were dissected and removed from the carcass. The remainder of the procedure was carried out in a grade II laminar biosafety cabinet. Femur and tibiae, cleaned of fat and muscle, were flushed with media using a 25-gauge sterile syringe to remove all bone marrow cells and filtered through a 0.4µM mesh filter. Bone marrow cells were centrifuged at 400 x g for 5 mins. Supernatants were discarded and cell pellet was resuspended in 3mL of red blood cell lysis buffer for exactly 2 mins. Immediately after 2 mins, 7 mL complete DMEM was added to neutralise the action of red blood cell lysis buffer and centrifuged at 400 x g for 5 mins. If the pellet still appeared red this step was repeated. Isolated bone marrow cells were seeded in T175cm^3 flask in DMEM supplemented with 20% (v/v) L929 conditioned media (CM), 10% (v/v) FBs and 1% (v/v) PenStrep. L929 constitutively express Macrophage Colony Stimulating Factor (M-CSF) and to a lesser extent Granulocyte Macrophage Colony Stimulating Factor (GM-CSF) for macrophage differentiation. BMDM were cultured for 8 days with a change of media every 3 days.

2.2.3. Cell Counting

A haemocytometer under a light microscope was used to calculate the concentration of cells per millilitre in a sample. Haemocytometer and specialised slip were cleaned using 70% ethanol before the slip was fixed into place on the haemocytometer creating a counting chamber with a known volume of $1x10^4$mL. $1x10^4$mL diluted cell suspension was pipetted under the coverslip mounted on the haemocytometer into the chamber, allowing suspension to be drawn out by

capillary action. Under the light microscope at a magnification of 10X cells within 1 set of 16 squares were counted. Only cells within the squares or on the right or bottom boundary line were included in the count. This was repeated for 4 sets of 16 squares. The average was found and multiplied by the dilution factor of the cell suspension and multiplied by $1x10^4$ to give the concentration of cells per millilitre.

2.2.4. 2.1.5. Cryopreservation

Stocks of all cell lines were cryopreserved in liquid nitrogen. Cell pellets were obtained after centrifugation at 400 x g for 5 mins. Supernatants were discarded and cells were resuspended at a concentration of $1x10^7$cell/mL in freezing media (10% (v/v) dimethylsulfoxide (DMSO), 50% (v/v) FBS, and 40% (v/v) growth medium). 1mL cell suspension was aliquoted in 1.5mL cryopreservation vials and place into Mr. Frosty and stored in a -80°C freezer for a minimum of 24 hours. Mr.Frosty container ensures cells are slowly frozen at a rate of -1°C/min to minimize risk of hypothermal shock. After 24 hours cells can be transferred to a liquid nitrogen container for long term storage.

2.2.5. . Thawing cells

Cell stocks frozen in liquid nitrogen were removed and defrosted immediately in 37°C water bath. Before completely thawed cell were transfer into 10mL of pre-warmed medium and centrifuge at 400 x g for 5 mins. Discard supernatant and resuspend in fresh 10mL of media and transfer to a T25cm^3 flask. Incubate at 37°C 5% CO_2 until approximately 80% confluent. Cells were passaged twice before used in any experiments.

2.2.6. Mycoplasma Testing

Mycoplasma infections are a major problem in continuous culture of cell lines. Mycoplasma lacks a cell well and adherence to cell surfaces make these infections invisible to identify by light microscope. Cell culture supernatants and cell membranes are suitable for growth of mycoplasma and they are also resistant to most antibiotics which target cell wall synthesis. Mycoplasma infections can lead to erroneous results and even the loss of a unique cell line. Mycoplasma testing was performed by PCR as described by Young *et al.* **(Table 2.4)**[232]**.**

Table 2.4: Mycoplasma PCR primers

Primer	**Sequence**
Forward	TGCACCATCTGTCACTCTGTTAACCTC
Reverse	GGGAGCAAACAGGATTAGATACCCT

1mL of cultured media was taken from confluent flask of cell line to be tested and transferred into a 1.5mL eppendorf tube. Supernatant was centrifuged at 400 x g for 5 mins, to pellet any cellular debris. GoTaq Hot Start Green Master Mix (GoTaq Hot Start Polymerase, dNTPs, $MgCl_2$ and reaction buffer) was used to set up the reaction following **Table 2.5**. Nuclease-free water was used as a negative control and media from a previously positive cell line was used as mycoplasma positive control. PCR reaction was performed using a PTC-200 Peltier Thermal Cycle (Bio-Rad, Dublin, Ireland) (**Table 2.6**). Amplified DNA products were run on 2% agarose DNA gel by DNA electrophoresis and visualised under UV light by GelDoc-it Systems (UVP, LLC, CA, USA).

Table 2.5: PCR Reaction Mix

Reagent	**Volume (µL)**
Template DNA (100ng)	2
GoTaq Hot Start Master Mix	10
Forward Primer	0.4
Reverse Primer	0.4
Nuclease-free water	7.2

Table 2.6: PCR Thermal Cycle Program

Event	**Denaturing**	**Annealing**			**Extension**	
Temperature (°C)	94	94	55	72	72	4
Time (Cycles)	3 mins (1)	1 min (35)	1 min (35)	1 min (35)	10 mins (1)	∞

2.2.7. DNA Agarose Gel

1X TAE buffer was used to prepare 2% agarose (w/v) gel and heated until fully dissolved. 1:10,000 SYBR Safe DNA stain was added to 2% Agarose TAE mix and stirred. Mixture was poured into DNA gel cast, ensuring no air bubbles were formed and comb was inserted. Gel was allowed to set for approximately 1.5 hours in the dark. Once the gel was set, Horizon 11.14 Gel Electrophoresis Apparatus rig (Life Sciences) was set up with gel and immersed in 1X TAE Buffer. 7µL Quick Load 2-Log DNA ladder (0.1kB-10kB) and 20µL PCR products were loaded into wells. Electrophoresis was ran at 120V for 40 mins. DNA bands were visualised under a UV light using GelDoc-it Systems (UVP, LLC, CA, USA).

2.2.8. L929 Cell Line and Conditioned Media (CM)

L929 is an immortalised mouse fibroblast cell line derived from subcutaneous connective areolar and adipose tissues of a 100 day old male C3H/An mouse. L929 CM is commonly used as a source of M-CSF and GM-CSF when differentiating BMDM. L929 are cultured in DMEM supplement in 10% FBS and 1% PenStrep. L929 are seeded at a density of $20x10^6$ cells in a T175cm^3 flask in 40mL complete DMEM. Cells were growth in humidified incubator at 37°C 5% CO_2 for 10 days. Subsequent CM was collected and filtered through 0.2µM filter and stored at -20°C.

2.3. Animal Studies

Caspase-11 knockout mice were generated from C57BL/6J background and acquired from Prof. Junying Yuan's laboratory (Harvard Medicial School, MA, USA). *CASP11* active site, QACRG, which is located in exon 5 was disrupted by homologous recombination of a replacement vector. Neogene encoding neomycin phosphotransferase was inserted in place of a 1.5kb *CASP11* fragment. The insertion of this neogene resulted in the deletion of 16 amino acids at exon 5 within caspase-11 active site encoding region, subsequently preventing caspase-11 forming a functionally active protein. This constructed vector was transfected into J1 embryonic stem (ES) cells and clonally expanded. C57BL/6J blastocytes were microinjected with Mutant *CASP11* ES cell clones and implanted into falsely pregnant females. Chimeric male progeny were then mated with female C57BL/6J to obtain a germline transmission of the mutant allele.

Mice were transported to Trinity College Dublin where they were recrossed with C57BL/6J (Harlan Laboratories, UK). Heterozygous and homozygous breeding pairs were maintained to established homozygous *Casp11*$^{-/-}$ and wild type (WT) littermates. Mice are maintained in Trinity Biomedical Sciences Institute's pathogen free facility.

Nos2-/- mice were generated from C57BL/6J background originally produced by Drs. Carl Nathan and John MacMicking at Cornell University Medical College and Dr. John Mudgett at Merck Research Laboratories. The line was generated by deleting the first 4 exons and part of the promoter region of the Nos2 gene through gene targeting in 129S7-derived AB2.1 ES cells. Mice maintained in Department of Genetics (Trinity College Dublin) comparative medicine unit were gifted by Prof. Sarah Doyle. All animal procedures are reviewed and approved by Trinity College Dublin Animal Ethics Committee and Health Products Regulator Authority (HPRA).

2.3.1. DNA Extraction from Ear Punch

Genomic DNA was extracted by digesting ear punches of mice using 500µL DNA extraction buffer and incubated overnight at 55°C. Digested ear punches were centrifuged at 20,000 x g for 10 mins at 4°C. 450µL of sample supernatants was added to 950µL ice cold ethanol, to precipitate DNA. Supernatant ethanol mixture was vortexed and centrifuged at 20,000 x g for 10 mins at 4°C. Pellet DNA was allowed to air dry before being resuspended in 35µL nuclease-free water. DNA isolation was stored at -20°C.

2.3.2. DNA Quantification

Once genomic DNA was isolated, NanoDrop ND-1000 spectrophometer (Thermo Fisher Scientific Inc., Waltham MA, USA) was used to determine the DNA concentration. Quality and purity of RNA isolate are also assessed as ratios of absorbance, 260/280 and 260/230. `Pure' DNA isolates typically yield a 260/280 ratio of approximately 2.0, which is dependent on pH and ionic strength of the blank and sample buffers. Significantly skewed purity ratios may be due to the presence of contaminants such as phenol and protein which have absorb stronger at 280nm. 260/230 ratio typically yields value from 1.8-2.2. Low yields indicate presence of contaminants such as phenol, EDTA and carbohydrates.

2µL nuclease-free water was pipetted onto the lower optical surface and the pedestal was lowered to perform a blank nucleic acid measurement. 2µL genomic DNA was added to the lower optical surface and the pedestal was lowered and measurements were recorded. DNA concentration and purity recorded are independent on the volume of sample, volume is only necessary to bridge the gap between the 2 optical surfaces.

2.3.3. PCR amplification of genomic DNA for genotyping

Following isolating and quantification of genomic DNA, PCR was performed to amplify DNA. WT and KO *CASP11* primers (**Table 2.7**) were designed to amplify particular regions of the WT and *CASP11* KO genes. GoTaq Hot Start Green Master Mix was used to set up the reaction, as previously describe Section 2.2, following **Table 2.5**. PCR thermal cycle (**Table 2.6**) was performed using a PTC-200 Peltier Thermal Cycle.

Table 2.7: *CASP11* Primers

Name	Primer
SY21 (WT forward)	GGCATGGAGTCAGAGATGAAAGAC
SY22 (WT reverse)	GCCCATGTGGCATTACCTGCCAGC
SYKO (Mutant forward)	AGATCTACACCTCTGCACAACTGG
PJK (Mutant reverse)	TGGCGCTACCGGTGGATGTGGAATTGT

2.3.4. AOM/DSS model; Colon homogenates

Chemically induced azoxymethane (AOM)/ dextran sodium sulfate (DSS) model for colitis associated colorectal cancer (CAC) was performed by Dr. Brian Flood (TBSI CMU). The AOM/DSS model involves initial administration of the DNA methylating agent AOM followed by repeated cycles of DSS which is an inflammatory agent that disrupts the epithelial lining of the colon. AOM activation requires several activation steps including hydroxylation which results in the formation of methylazoxymethanol (MAM). MAM can alkylate macromolecules in the colon and regulates the methylation at the O6 or N7 positions of guanine (O6-methyl-deoxyguanosine and N7-methyl-deoxyguanosine) within the DNA molecule. Methylation at the O6-position of guanine appears to be the predominant mutagenic lesion that occurs as a result of AOM administration.

C57BL/6J *Casp11*$^{-/-}$ and WT littermates were divided into treatment groups containing 3 mice and control groups contained 2 mice for each genotype. Mice were injected intraperitoneally on day 0 and 21 of AOM-DSS experimental CAC protocol with 12.5mg/kg AOM. After 14 days, 2.5% (w/v) DSS was administered in drinking water over 7 days followed by regular drinking water for 2 weeks. 3 cycles of 2% (w/v) DSS administered to drinking water was followed for 4, 5, 4 days respectively interspaced by normal drinking water. Throughout protocol animals were scored daily for clinical features of disease progression by their weight loss, stool consistency and rectal bleeding. At day 17, week6 and week 15; AOM/DSS trial endpoint, mice were humanely sacrificed exposure to carbon dioxide followed by cervical dislocation. Colons were removed from cecocolonic junction to rectum. Colons were examined for presence of macroscopic tumours. Sections of distal to middle colon were collected in 500 µl of RIPA buffer (50 mM TRIS; 150 mM NaCl; 0.02% (w/v) NaN_3; 0.1% (w/v) SDS; 1% (v/v) NP-40; 0.5% (w/v) sodium deoxycholate) containing 5 mM EDTA, 1 µg/ml leupeptin, 1.7 µg/ml aprotinin and 0.1 mM PMSF and stored at -20°C for Western Blot analysis.

2.4. Western Blot

2.4.1. Sample preparation

Cells for lysis were taken from incubator and viewed under light microscope before placing on ice. Supernatants were collected and stored at -20°C for later analysis by ELISA. Cells were washed with ice cold PBS and lysed with lysis buffer for approximately 10 mins. Radioimmunoprecipitation Assay (RIPA) buffer is high stringency ionic denaturing buffer used to generate whole cell protein extracts. It can disrupt protein-protein interactions and therefore can be problematic in pull down assays. Immunoprecipitation (IP) buffer is a low stringency lysis buffer, a modified RIPA formulation without the ionic SDS. This allows the solubilisation of cytoplasmic proteins without the dispensation of genomic DNA. Lysis buffers were supplemented with protease and phosphatase inhibitors, leupeptin (lysosomal), phenylmethylsulfonyl fluoride (PMSF) (serine and cysteine proteases) and aprotinin (trypsin, chymotryosin, and plasmin). Cell lysates were transferred to 1.5mL eppendorf tubes and centrifuged at 20,000 x g at 4°C for 10 mins (Eppendorf 5417R refrigerated centrifuge). Cellular debris was pelleted, and soluble protein lysates were transferred to fresh 1.5mL eppendorf tube and stored at -20°C for short term storage or -80°C for long term storage.

2.4.2. Determining Protein Concentration

Bicinchoninic acid (BCA) assay is a colourimetric assay used for the quantification of total protein in a sample lysate from which protein concentration can be normalised. BCA assay is dependent on two reactions. Firstly on the reduction of Cu^{2+} to Cu^{+} by peptide bonds under alkaline conditions. The amount of Cu^{2+} which is produced is directly proportional to the amount of protein present. Secondly, the reduced Cu^{+} ion chelates with two bicinchoninic acid molecules to produce a purple colour which absorbs light at a wavelength of 562nm. Cu^{+} bicinchoninic acid complex absorbance is near liner with increasing protein concentration over a working range of 20-2000µg/mL.

Bovine serum albumin (BSA) serial dilution of 2.5-300µg/mL was generated by a two-fold dilution with PBS to produce a standard curve. 50µL of diluted sample (1:25-1:100) was added in duplicate to F-bottomed 96 well plate. 50µL of MicroBCA Working Reagent was added to each well. Working reagent is composed of 25 parts Reagent MA, 24 parts Reagents MB and one-part Reagent MC. The plate was then incubated in the dark at 37°C for 30mins. Absorbance was read at a wavelength of 562nm using SpectraMax PLUS Microplate Reader (Molecular Devices). Unknown protein concentration of sample lysates was determined relevant to BSA standard

curve. Once calculated protein concentration was normalised using PBS. Samples were prepared in laemmli buffer containing 1:10 dithiothreitol (DTT) and boiled at 70°C for mins to reduce intra and inter-molecular disulphide bonds, denature proteins and give an overall negative charge.

2.4.3. Sodium Dodecyl Sulphate Polyacrylamide Gel Electrophoresis

Sodium Dodecyl Sulphate Polyacrylamide Gel (SDS-PAGE) electrophoresis is a method to separate proteins based solely upon the molecular weight of the polypeptide chains. Use of SDS-PAGE and sample preparation in 2X laemmli buffer removes the influence of structure and charge on the rate of protein migration. Polyacrylamide gel forms a mesh-like matrix suitable for the separation of polypeptide chains based on molecular weight. SDS is an anionic detergent which provides net negative charge which attracted to an anode when an electrical charge is applied across the gel. As a result, smaller polypeptide chains move faster through the mesh-like matrix of the gel towards the anode leading a spread of proteins based on molecular weight. SDS-PAGE was made using the recipe in **Table 2.8**. Glass plates were cleaned with ethanol, assembled and clamped, ensuring there were no leaks. Resolving gel was prepared in a laminar fume hood adding 10% APS and TEMED last. APS provides free radicals which drive acrylamide/bisacrylamide polymerisation while TEMED accelerates the polymerisation process by catalysing the formation of free radicals generated by APS. Resolving gel solution was mixed and immediately poured into glass cast leaving approximately 1.5cm of stacking gel and comb. Isopropanol was carefully laid over resolving gel to remove air bubbles and set gel in a level line. Once set after approximately 20mins all remanence of isopropanol was washed with dH_2O before stacking gel was prepared and poured. Combs were immediately inserted before gel could begin to set.

Glass casts were place in an electrode assemble (Biorad gel electrophoresis rig) ensuring all seals were tight. Once secure electrode assemble was place in a buffer tank and filled with 1 X Running buffer. Combs were removed slowly to form straight uniformed wells. 5µL SeeBlue Plus2 pre-stained protein ladder was loaded in the first well as a reference guide of known molecular weights and protein lysates loaded (>7µg protein/well, <40µg protein/well). An electrical charge of 90 V was applied until samples migrated through the stacking gel. Once samples entered resolving gel electrical charge was increased to 120 V. Electrophoresis was continued until dyed front reached the bottom of the cast.

2.4.4. Nitrocellulose Wet Transfer

Directly following electrophoresis SDS-PAGE was removed from glass cast and stacking gel was discarded. A transfer sandwich was assembled to transfer proteins from SDS-PAGE to nitrocellulose membrane. 10 mins prior to transfer nitrocellulose membrane was activated with dH_2O. The transfer sandwich was set up as follows; clear side on the gel holder cassette, a foam pad, two sheets of 7.5x9cm^2 filter paper, nitrocellulose membrane 6.5x8cm^2, SDS-PAGE, three sheets of 7.5x9cm^2 filter paper, a foam pad, and the black side of the gel cassette holder. Take care to avoid and remove all air bubbles before sealing cassette closed. Fit gel holder cassette in transfer rig and submerge in buffer tank containing 1 X Transfer buffer and an ice pack. Proteins were transferred at 200mA from 40-90 mins dependent on protein size. Higher molecular weight proteins require longer transfer periods compared to small proteins.

Table 2.8: Solutions for preparing 15ml Resolving Gel and 5ml Stacking Gel for 2 gel moulds.

Reagents	**10% Resolving**	**12% Resolving**	**15% Resolving**	**5% Stacking**
dH_2O	5.9mL	4.9mL	3.4mL	3.4mL
1.5M Tris-HCl (pH8.8)	3.8mL	3.8mL	3.8mL	-
1M Tris-HCl (pH6.8)	-	-	-	630µL
Protogel (30% acrylamide, 0.8% bisacrylamide)	5.0mL	6mL	7.5mL	830µL
10% SDS	150µL	150µL	150µL	50µL
10% APS	150µL	150µL	150µL	50µL
TEMED	6µL	6µL	6µL	5µL

2.4.5. Blocking, Immunoblotting and Protein Visualisation

Once transfer was complete the nitrocellulose membrane was removed from transfer sandwich and block in 5% NFDM (non-fat dried milk 5% (w/v) 1 X TBST). 5% NFDM blocked non-specific binding sites on the nitrocellulose membrane. Membrane was incubated for 1 hour at RT in 5% NFDM on rocker. Following blocking, membrane was probed for protein of interest using relevant primary antibody diluted in 5% NFDM or 5% BSA overnight at 4°C (**Table 2.9**). Next day the membrane was washed using 1 X TBST 3 x 10 mins, before incubating with relevant

secondary antibody conjugated with horse-radish peroxidase (HRP) for 1 hour at RT on rocker (**Table 2.10**). Following incubation in secondary antibody, membrane was washed using 1 X TBST 3 x 10 mins. Proteins were detected using enhanced chemiluminescent (ECL) HRP substrate. Immobilon ECL HRP substrate (Millipore) 500uL part A and 500uL part B was mixed and washed over nitrocellulose membrane for 30 secs. The ECL substrate consists of luminol, an enhancer such as modified phenol, and oxidising reagent hydrogen peroxide. When applied to the HRP labelled secondary antibody excited intermediates are generated and release blue emission at 450nm wavelength upon their decay to ground state. Addition of enhancers allows the reaction to proceed for prolonged duration without a significance reduction in light signal output. The signal appears as a chemiluminescent band on the membrane which was visualised on BioRad Gel Doc XR+System using Bio-Rad ChemiDocTM MP Imaging system for analysis.

Table 2.9: Primary Antibodies for Immunoblot

Name	Features	Dilution	Source
mCaspase-1 (sc-514)	Rabbit polyclonal Clone M-20	1:500	Santa Cruz
hCaspase-1 (sc-622)	Rabbit polyclonal Clone A-19	1:500	Santa Cruz
Caspase-4 (M029-3)	Mouse monoclonal Clone 4BD	1:1000	MBL
Caspase-5	Rabbit monoclonal Clone D3G4W	1:1000	Cell Signalling
mCaspase-11 (C1354)	Rat monoclonal Clonal 17D9	1:1000	Cell Signalling
IL-1beta	Goat polyclonal Clone AF-401	1:1000	R&D systems
GSDMD	Rabbit monoclonal	1:1000	Sigma
STAT1	Rabbit monoclonal Clone 9172	1:1000	Cell Signalling
pSTAT1 (Try701)	Rabbit monoclonal Clone 58D6	1:1000	Cell Signalling
pSTAT1 (Ser727)	Rabbit monoclonal Clone D3D7	1:1000	Cell Signalling
STAT2	Rabbit Clone D9J7L	1:1000	Cell Signalling

pSTAT2 Y690	Rabbit monoclonal Clone D3P2P	1:1000	Cell Signalling
Jak1	Rabbit monoclonal Clone Ab-1022	1:1000	Sigma
pJak1 (Tyr1022)	Rabbit monoclonal	1:1000	Sigma
Jak2	Rabbit monoclonal Clone D2E12B XP(R)	1:1000	Cell Signalling
pJak2 (Tyr1007)	Rabbit monoclonal Clone D15E2	1:1000	Cell Signalling
iNOS	Rabbit polyclonal Clone D6B6S	1:1000	Cell Signalling
PINK1	Rabbit polyclonal (PA5-85930)	1:500	Invitrogen
Parkin	Rabbit monoclonal Clone (PRK8)	1:500	Santa Cruz
p62	Rabbit monoclonal (EPR4844)	1:500	Abcam
LC3B	Rabbit monoclonal Clone (D11) XP	1:1000	Cell Signalling
Arginase-1	Rabbit monoclonal PA5-85267 RRID:AB_2792410	1:1000	Invitrogen
Arginase-2	Rabbit monoclonal Cat# MA527815 RRID:AB_2735112	1:1000	Invitrogen
STING	Rabbit polyclonal LS-C108557	1:1000	LSBio
pTBK1 (Ser172)	Rabbit polyclonal Clone D52C2	1:1000	Cell Signalling
pIRF3 (Ser396)	Rabbit monoclonal Clone 3D4G	1:1000	Cell Signalling
Aconitase-2	Rabbit monoclonal Clone 6922	1:1000	Cell Signalling

B-Actin (A3854)	Mouse monoclonal Peroxidase conjugated Clone AC-15	1:10,000	Sigma Aldrich
GAPDHB-Actin (A3854)	Mouse monoclonal Clone 6C5Mouse	1:10,000	Sigma Aldrich

* 5% NFDM interacts with phosphor-proteins. Therefore use 5% BSA or goat serum.

Table 2.10: Secondary Antibodies for Immunoblot

Name	Dilution	Source
HRP conjugated goat anti-rabbit IgG	1:2500	Jackson Immunolabs
HRP conjugated goat anti-mouse IgG	1:2500	Jackson Immunolabs
HRP conjugated goat anti-rat IgG	1:2500	Jackson Immunolabs
HRP conjugated donkey anti-goat IgG	1:2500	Jackson Immunolabs

2.4.6. Densitometry

Western blots were analysed by densitometry using ImageLab 6.0 program. Densitometry is a quantitative measure of optical density (pixels) generated when ECL emits photons during energy decay when exposed to HRP conjugated secondary antibodies. Densitometry identifies the pixels of a band and measures the density for direct comparison to another band. Lanes were assigned for each well in which samples were loaded and bands were assigned a box of equal area. ImageLab removed all background noise and calculated a density for each band selected. Values were normalised against loading control. Relative density of each band was calculated against reference band, untreated control, to calculate the fold change.

2.5. Caspase-11/TSTAT1 Co-Immunoprecipiation

Co-IP is a molecular biology technique used to identify protein-protein interactions. This technique isolates individual proteins using an antibody specific to the particular protein. Consequently, proteins which directly bind and form a complex with the specific protein are also isolated.

Raw264.7 cells were seeded $1x10^5$cell/mL in $100mm^3$ cell culture dish and stimulated with LPS (1µg/mL) for 8 hours. Cells were lysed using low stringency IP buffer, not containing non-ionic detergents NP-40 or triton x-100, on ice for 10 mins. Cell lysates were centrifuged at 20,000 x g for 10 mins at 4°C. Protein lysates were transferred to new eppendorf and cellular debris discarded. 20uL of protein lysate was labelled as input and stored in -20°C. 1ug anti-caspase-11

primary antibody was added to the lysate and incubated for 1 hour RT on roller. Followed by the addition of 20uL IgG-binding Protein A/G heavy and light chain beads. Lysates were incubated overnight with caspase-11/Protein A/G beads at 4°C on roller. Following day, protein lysates were centrifuged at 150 x g for 5 mins at 4°C. Supernatants were labelled as output and stored in -20°C. Pellet containing IgG bead and caspase-11 complex was washed and centrifuged 150 x g for 5 mins at 4°C, 3 times with ice cold IP buffer. IgG bead and protein complex was resuspended in 20µL IP buffer and labelled Caspase-11 Co-IP. Sample lysates were prepared in lamelli buffer and DTT as previously described and were loaded on SDS-PAGE and Immunoblotted against primary antibodies caspase-11 and STAT1.

2.6. Reverse Transcription Quantitative Polymerase Chain Reaction

Quantitative polymerase chain reaction (qPCR) is used to detect and quantify nucleic acids. Reverse transcription (RT) is first performed to convert RNA transcripts to complementary DNA (cDNA) followed by qPCR. qPCR involves fluorescent labelling of cDNA which can be measured in real time proportionally to the amount of DNA being replicated. SYBR green is a dsDNA binding dye that intercalates non-specifically into dsDNA, when bound to DNA becomes immobilised and energy released as fluorescence. PCR amplifies DNA in 3 repeating steps; denaturing, annealing and elongation, and fluorescent labelling allows quantitative measurement of DNA amplified at the end of each cycle.

2.6.1. RNA Isolation

RNA was isolated from BMDM using Isolate II RNA Mini kit (Bioline) following the manufacturer's instructions. Supernatants were removed and stored for ELISA analysis in -20°C. Cells were washed with PBS and lysed with Lysis buffer RLY and 2% (v/v) DTT for 10 mins on ice. Once cells are lysed, lysates were filtered by loading onto Isolate II violet Filter in a 2mL collection tube and centrifuged for 1 min at 11,000 x g. Equal amounts 70% ethanol to Lysis buffer RLY was added to homogenised lysate to precipitate nucleic acids. Isolate II blue mini column was placed in a 2mL collection tube and loaded with lysate and centrifuged for 30 sec at 11,000 x g. Equal parts membrane desalting buffer to Lysis buffer RLY was added to column and centrifuged for 1 min at 11,000 x g to dry. Next, DNA was digested using 95µL DNase I reaction buffer (1:10 DNase I to DNase Reaction Buffer). DNase I reaction buffer was incubated for 15 mins at RT. Column was then washed 3 times, once with RW1 to deactivate DNase I activity and twice with RW2 and centrifuged between each wash for 3 secs at 11,000 x g with the final centrifuge for 2 mins.

Column was then placed in a new 1.5mL collection tube and 60uL of nuclease-free water was used to elute RNA from silica membrane. Column was centrifuged at 11,000 x g for 1 min to collect the eluted RNA.

2.6.2. RNA Quantification and Normalisation

Once RNA was isolated, NanoDrop ND-1000 spectrophometer was used to determine the RNA concentration. Quality and purity of RNA isolate are also assessed as ratios of absorbance, 260/280 and 260/230, as previously describe in section 2.3. All samples were then normalised to the same RNA concentration (80ng/µL) using nuclease-free water.

2.6.3. Reverse Transcription

High Capacity cDNA Reverse transcription kit (Applied Biosystems) was used to perform reverse transcription of RNA to cDNA, following the manufacturer's guidelines.

RT kit was thawed, and master mix was prepared (**Table 2.11**). 5.8µL master mix was added to PCR tubes with 1.4µL sample RNA (approximately 1µg RNA). PCR tube lids were securely sealed, and PCR thermal cycle (**Table 2.12**) was performed using a PTC-200 Peltier Thermal Cycle. Following reverse transcription cDNA products were diluted in 1:8 with nuclease-free water and stored and -20°C.

Table 2.11: Reverse Transcription Master Mix

Reagent	**Volume (µL)**
10X Reverse Transcription (RT) buffer	2
25X deoxyribose nucleoside triphosphate (dNTP) mix	0.8
10X RT random primers	2
Reverse Transcriptase (RT)	1
RNA/nuclease-free water	14.2 (1µg)

Table 2.12: RT Thermal Cycle programme

Steps	**1**	**2**	**3**	**4**
Time (mins)	25	37	85	4
Temperature (°C)	10	120	5	∞

2.6.4. Quantitative Real Time PCR

cDNA reverse transcriptase products were quantified by real time quantitative PCR using ABI 7500 Fast Real PCR system and SYBR Green PCR Core Reagents (Invitrogen). PCR reaction mix with primers for genes of interest were prepared on ice (**Table 2.13 and 2.14**). 4.7µL cDNA

product was added in duplicate to 96 well PCR MicroAmp Plate (Biosciences). 5.3µL of relevant primer mix was added to appropriate wells. Reaction was carried out on ABI 7500 Fast Real PCR system and gene expression was normalised to GAPDH. $2^{-\Delta\Delta CT}$ method was used to calculate the mRNA expression fold change relative to control samples and control gene (GAPDH).

Table 2.13: qPCR Reaction Mixture

Reagent	Volume (µL)
SYBR Green PCR Core Reagents (2X)	5
Primers (Forward + Reverse)	0.3

Table 2.14: PCR Primers

Gene Name	Forward Primer	Reverse Primer
iNOS	CCAAGCCCTCACCTACTTCC	CTCTGAGGGCTGACACAAGG
Arg1	CTCCAAGCCAAAGTCCTTAGAG	AGGAGCTGTCATTAGGGACAT
Arg2	GGATCCAGAAGGTGATGGAA	AGAGCTGACAGCAACCCTGT
Slc7a1	TTCGGTTATGGGATCTGGCACAG T	TTTGCACTGGTCCAAGTTGCTGT C
Slc7a2	CCCGAGTATCGTGGTGTCTT	CTCTTGCGACACTGGACGTA

2.7. Assays

2.7.1. Enzyme-linked Immunosorbent Assay (ELISA)

ELISA is a colourimetric detection method to quantify a specific protein in a complex mixture. Sandwich ELISA quantifies target protein (antigen) between two layers of antibodies; capture and detection. Capture antibody immobilises the target antibody to the plate and indirectly presence the target protein. Detection antibody binds the presented analyte at a different epitope. Therefore, target antigen must contain two antigenic sites capable of binding two antibodies. HRP conjugated antibody in combination with colourimetric substrate TMB, produce a coloured signal which accumulates over time relative to the amount of HRP conjugated antibody bound to the detection antibody. Once desired colour intensity is achieved the product absorbance is measured after a stop solution is added to provide a fixed endpoint for the assay. Commercially available ELISA kits were used to detect and quantify levels of cytokines secreted into supernatants. Cytokine concentrations were determined according to manufacturer guidelines (**Table 2.15**). High binding affinity 96 well plate (Greiner, Cruinn) were coated with 50µL working concentration capture antibody per well and incubated overnight at 4°C. Following

day, ELISA plate was washed with ELISA wash buffer (PBS + 0.05% (v/v) Tween20) 4 times. 100µL assay diluent (PBS + 1% (w/v) BSA) was added to each well to reduce non-specific binding, for 2hours at RT on orbital rocker. ELISA washes were repeated before 50µL standards/samples were added in duplicate to appropriate wells. Standard serial dilution was generated by a 2-fold dilution using assay diluent, over a range of 7 concentrations. ELISA plate with samples was incubate for 2 hours at RT or overnight at 4°C on an orbital rocker. ELISA washes were repeated before 50µL of biotinylated detection antibody was added to each well for 1 hour at RT. Washing step was repeated and 50µL HRP-conjugated Streptavidin was applied across wells and incubated for 30mins at RT. The final wash step was performed 5 times followed by addition of 50µL of tetramethylbenzidine (TMB) substrate which was incubated at RT for 15-30mins in the dark. Once detection was visualised, 50µL 1M H_2SO_4 was added to each well to stop the colour development. OD values were determined by measuring absorbance at a wavelength of 450nm and 570nm using SpectraMax PLUS Microplate Reader (Molecular Devices). Cytokine concentrations secreted into supernatants were calculated using the known concentrations of recombinant cytokines generated standard curve.

In the case for IFN-β non-kit reagents were used to determine concentration.

Table 2.15: Mouse ELISA kit

Cytokine	**Supplier**	**Top Working Standard**
IL-1α	Biolegend/MSC	125pg/mL
IL-10	Biolegend/MSC	2000pg/mL

Table 2.16: Non-kit reagents

Step	**Reagent**	**Suppplie**
Capture	Monoclonal rat anti-mouse IFN-β	Santa Cruz
Detection	Polyclonal rabbit anti-mouse IFN-β	PBL Assay Science
HRP	Streptavidin HRP	R&D
Standard	Recombinant mouse IFN-β	PBL Interferon Source

2.7.2. Griess Assay

Griess assay is a colourimetric assay used to determine the amount of nitrite ions presence in a solution for quantitative analysis. Nitric oxide within an oxygenated aqueous solution is known to rapidly oxidate into both NO_2^- (nitrite) and NO_3^- (nitrate). NO has a short half-life in which NO oxidises to NO_2 followed by the dimerization to N_2O_4. In water N_2O_4 reacts to form NO_2^- and NO_3^- In an oxygen containing aqueous solution NO primarily oxidises into nitrite with little no or nitrate, unless in the presence of oxyhemoglobulin or oxymyoglobulin in which both NO and NO_2^- are completely oxidised to NO_3^-.

Griess assay is based on a two-step diazotization acid-catalysed reaction, which uses sulphanilamide and *N*-1-napthyethylenediamine dihydrochloride (NED) under acidic conditions (phosphoric acid), to detects NO_2^- present in solution. Acidified nitrite produces a nitrosating agent which reacts sulphanilamide, an aromatic amine, to undergo diazotisation reaction resulting in the formation of diazonium ion intermediate. Once diazonium salt is formed reaction with electron rich coupling agent NED leads to highly coloured diazo dye which is measurable by spectrophotometry.

Step 1: Nitrite in solution reacts with sulphanilamide under acid conditions to produce diazonium ion intermediate.

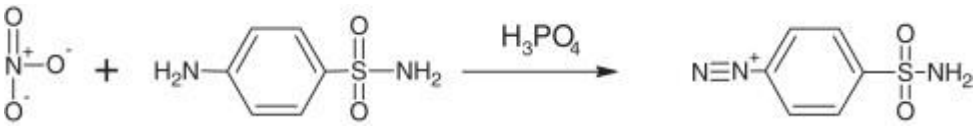

Step 2: Diazo intermediate reacts with NED to form final coloured product, azo dye

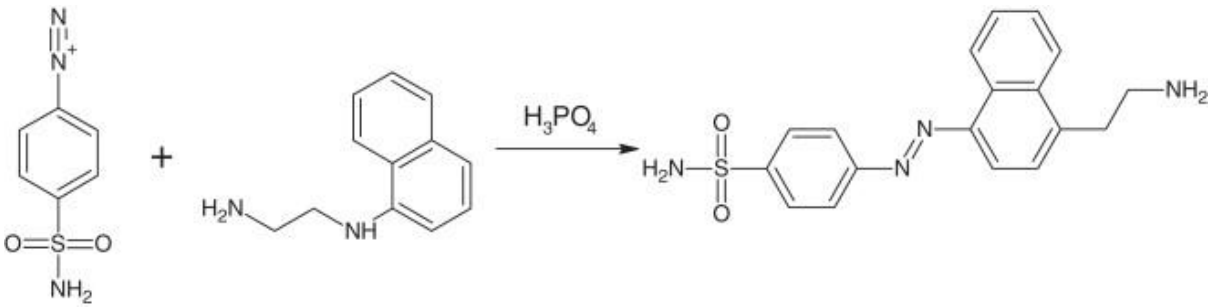

Standard serial dilution of nitric acid was generated by a 2-fold serial dilution over a range of 7 concentrations, with a top standard of 100µM and a detection limit of 2.5µM. 50µL of standard and samples were added in duplication to a 96 well plate and 50µL of Griess Reagent (Enzo Life Sciences) was added to each well. Sample and griess reagent were incubated at RT for 15-30mins

and absorbance values were read at 540nm using SpectraMax PLUS Microplate Reader (Molecular Devices).

2.7.3. MitoSOX; Mitochondrial Superoxide Indictor Assay

MitoSOX Red superoxide indicator is novel fluorogenic dyes specifically targeted to mitochondria in live cells. Oxidation of the MitoSOX reagent by mitochondrial superoxide produces bright red fluorescence. Dihydroethidium, also referred to as hydroethidine (HE), can be oxidised to ethidium that binds to DNA to emit fluorescence. MitoSOX is a synthetic derivative of dihydroethidium containing a cationic triphenylphosphonium moiety. It can accumulate in the mitochondria and can thus detect mitochondrial ROS which can be detected by flow cytometry, fluorometry or microscopy.

WT and *Casp11-/-* BMDM cells were seeded in 12 well plates at a density of 1×10^6 cells/mL in complete media and the following day were treated with LPS. 1 hour prior to harvest cells were treated with antimycin A as a positive control. After incubation, cells were harvested, washed with PBS then stained with MitoSOX™ Red (2.5 µM) for 20 min at 37°C in the dark, and then washed with warm PBS and analysed by flow cytometry. The mean fluorescence intensity (MFI) values of Mitosox (510/580 nm) were obtained with the FL-2 channel using the bandpass filter of 585/340nm on a BD Accuri C6 flow cytometer.

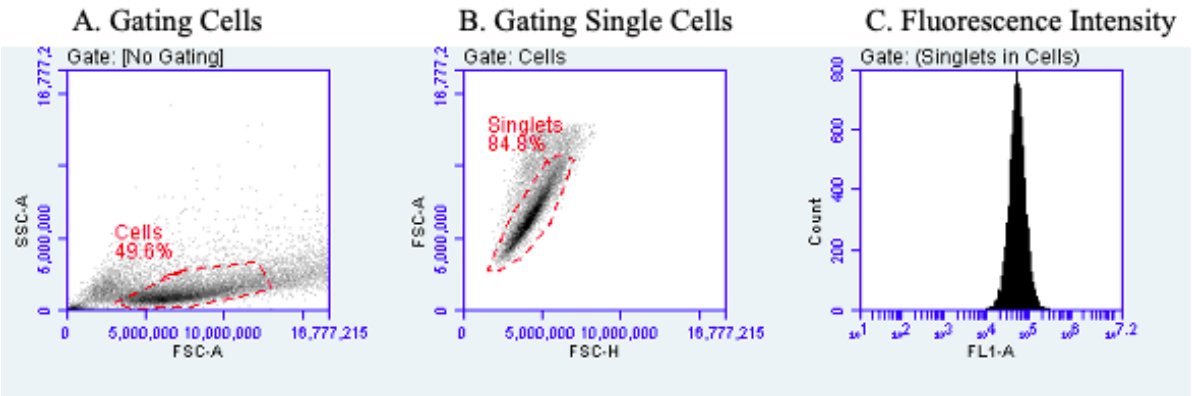

Figure 2.1: Gating Strategy: MitoSOX staining was analysed using the BD Accuri flow cytometer. Forward scatter area (FSC-A) was plotted against side scatter area (SSC-A) on a dot plot and gated to exclude any debris from the cell population **(A)**. This was further analysed on another dot plot where forward side scatter area (FSC-A) was plotted against forward scatter height (FSC-H), and this was gated to include singlets and exclude doublets as well as clumped cells **(B)**. This was then analysed on an FL1-A histogram to obtain MFI values **(C)**.

2.8. Microscopy

2.8.1. Immunofluorescence in RAW264.7 Cells

RAW264.7 cells were seeded on coverslips in 24 well plate at a density of $1x10^5$cell/mL and cultured overnight. The following day, cells were stimulated with LPS (1µg/mL) for 0, 0.5, 2, 4, 8 and 16 hours. Once stimulations were complete, supernatants were removed, and cells were gently washed with 500µL PBS. Cells were fixed with 500µL 3% paraformaldehyde for 15 mins at RT. Once fixed, cells were washed with PBS 3 x 5mins. Cells were permeabilised with 200µL PBS + 0.2% triton x-100 (v/v) for 10 mins. Following permeabilisation, cells were washed again with PBS and blocked with 200µL 2% BSA (w/v) in PBS and incubated for 1 hour at RT. Permeabilised fixed cells were incubated in primary antibody (**Table 2.17**) diluted in blocking buffer overnight in a humidified chamber. The next day cells were washed 3 x 5 mins in PBS. Cells were incubated in secondary antibody (**Table 2.17**) for 30min at RT in humidified chamber. Cells were washed a final time 3 x 5 mins in PBS and mounted to glass slides with DAKO mounting media and DAPI (1:100 dilution). Slides were viewed using Olympus BX51 research microscope (Olympus Inc., Tokyo, Japan) and images were taken at 20X magnification.

Table 2.17 Primary and Secondary Antibodies used for Immunofluorescence

Primary Antibody	Dilution	Alexa Fluor-conjugated Secondary Antibody	Dilution
Caspase-11	1:100	Goat anti-Rat Fluro Plus 647	1:500
STAT1	1:150	Goat anti-Rabbit Fluro Plus 488	1:500

2.8.2. Immunohistochemistry (IHC) of Breast Cancer Patient Resections

Immunohistochemical staining of breast cancer patient resection was approved by the Medical Research Ethic Committee, Beamount hospital. Tumour (n=9) and adjacent normal (n=9) from invasive breast carcinoma tissue were immunohistochemistry stained and score for caspase-4 and -5 expression levels in epithelial cells and stromal compartment. Similarly, tumour microarray (TMA) containing 26 invasive breast carcinoma patient tumour cores of mixed molecular subtype were analysis by IHC staining of caspase-4 and -5.

Bond III immunostainer from Lecia Biosystems (Newcastle upon Tune, UK) was performed by Joanna Fay, a member of Prof. Elaine Kay's group at the Royal College Society of Ireland (RCSI), Beamount hospital, Dublin. BOND dewax solution was used for deparaffinisation of slides before treated with BOND Epitope Retrieval Solution I. BOND epitope retrieval solution I, is a citrate

base ph6 epitope retrieval solution used for formalin-fixed paraffin embedded tissues. Primary antibodies, anti-caspase-4 (MBL, 1:200) and anti-caspase-5 (MBL, 1:100), were diluted in Bond Primary Antibody Diluent. Primary antibody was visualised using BOND polymer Refine Detection Kit. This biotin-free, multifunctional linker systems has increased tissue penetration, enhancing tissue sensitivity and blocks peroxide. In the presence of secondary-HRP antibody peroxidase enzyme the chromogen, 3,3'-Diaminobenzidine (DAB), develops a brown precipitate. Tissue sections are counterstained using haematoxylin and a coverslip is mounted. IHC staining was assessed as a measure of percentage positivity, intensity, or combined score. Percentage positivity is graded on a scale of 0-4 with 0 = no staining, 1= 1-25% staining, 2= 26-50% staining, 3= 51-75% staining and 4= 76-100% staining. Intensity was also measured on a scale from 0-3 where 0= no staining, 1= weak staining, 2= moderate staining and 4= strong staining. Addition of these 2 scores gives rise to combined score.

2.9. Mycobacterium tuberculosis infection

Mycobacterium tuberculosis (Mtb) infection was carried out by Emer E. Hackett and John McGrath from Frederick J. Sheedy's Lab, Trinity College Dublin. *Mtb* strain H37Ra was obtained from ATCC and prepared according to the manufacturer's instruction and stored in -80°C. To prepare for Mtb infection, aliquots were thawed and reconstituted in 5mL sterile PBS and sonicated for 16 minutes, followed by centrifuging at 3800 x G for 10 mins. Sonification and centrifugation is repeated 15 times. During the last centrifugation, supernatants were discarded and the cell pellete was resuspended in 2mL DMEM and sonicated for a further 15 minutes. Mtb cell suspension was then passed through a series of decreasing needles gauge size down to 25G and the cell suspension passes through without any resistance. Mtb cells were grown in Middelbrook 7H9 broth (Difco) supplemented with enrichment medium and 0.05% Tween 80 (Difco) in sterile water. Once in log phase, Mtb was sub-cultured weekly for 4-5 weeks. On the day of Mtb infection, log-phase bacteria was collected and centrifuged at 1600 x G for 10 mins, pellet was resuspended in DMEM. Cell suspension was passed through 25G needle several times, until no resistance, to remove clumps. Bacteria was centrifuged again at 70 x G for 3 minutes to obtain a single cell suspension. Supernatants optical density was measured at (OD_{600nm}) to quantify Mtb. Macrophages were infected at a MOI of 5 bacilli per cell (MOI 5) for 3 h. After 3h media with bacteria were collected and bacteria were removed by centrifugation at 18,000 g for 10 min. Macrophages were washed with DMEM to remove remaining bacteria and bacteria-free media was returned to the wells. Macrophages and supernatants were collected after 3 h, 24 h and 72 h for analysis. Baseline growth was assessed by lysing 3 h time-

point in 0.1% Triton-X for 10 min. Serial dilutions were plated on 7H10 Middlebrook Agar plates in triplicate and colony-forming units enumerated after incubation at 37°C for 14 – 21 days after plating. For later growth measurements this lysate was combined with pelleted extracellular bacteria, obtained by centrifugation of supernatant.

2.10. Agilent Seahorse XF analyser; oxygen consumption rate (OCR) and extracellular acidification rate (ECAR)

Agilent Seahorse XF analyser measures the two major metabolic pathways of the mitochondria, respiration, and glycolysis in live, real time respiring cells. Agilent seahorse XF analyser measures oxygen consumption rate (OCR) as a measure of mitochondrial respiration and extracellular acidification rate (ECAR) to determine glycolytic capacity. This platform automatic measurement of energy metabolism in real-time is performed a by a series of inhibitor injections which are key regulators of mitochondrial metabolism. Initial OCR measured by the seahorse analyser is mitochondrial basal respiration, once determined sequential compound injection of oligomycin; to measure ATP-linked respiration, (Carbonyl cyanide-p-trifluoromethoxy phenylhydrazone) FCCP; to measure maximal respiration and Antimycin A (AMA) /Rotenone; to determine reserve capacity, as illustrated in **Fig. 2.2**. Non-mitochondrial respiration and proton leak can also be indirectly measured by OCR.

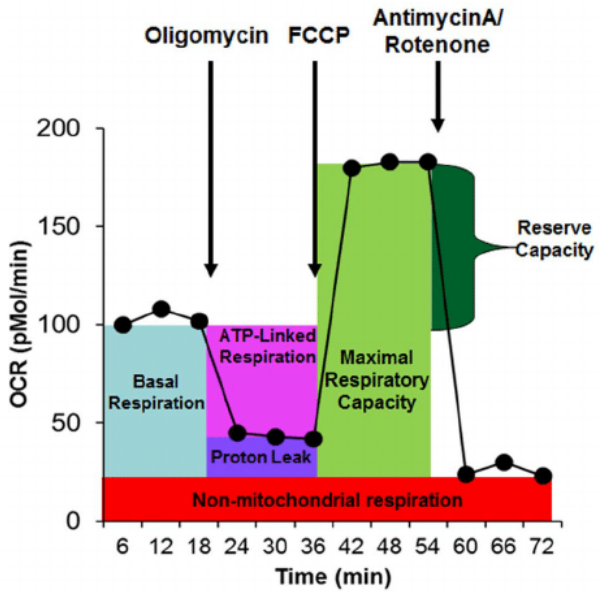

Figure2.2: Seahorse assay; OCR measurement in response to metabolic inhibitors; Oligomycin, FCCP, Antimycin A and Rotenone.

Oligomycin is an inhibitor of ATP synthase (complex V). Oligomycin directly blocks F_1F_0-ATPase subunit proton channel which is required for the oxidative phosphorylation of ADP to ATP. Oligomycin injection impacts the ETC leading to a reduction in electron flow. This results in a decreased in OCR which is linked to ATP production. FCCP is a protonophore, uncoupling agent which mediates a collapse of the proton gradient across the mitochondrial inner membrane. FCCP disrupts ATP synthesis by promoting H^+ ion movement through the mitochondrial membrane before the H^+ ion have been purposely used in oxidative phosphorylation energy requirements. Injection of FCCP leads to free flow of electrons through the ETC as proton gradient is collapsed, and complex IV oxygen consumption is at a maximal rate. Thirdly is a mixture being antimycin/rotenone. Antimycin A, which inhibit complex I and III, respectively, to completely shut down the ETC driven mitochondrial respiration. Rotenone is a lipophilic inhibitor which inhibits electron transfer from the iron-sulphur centre of complex I to electron carrier, ubiquinone (coenzyme Q10). Antimycin A binds the Qi site of cytochrome c reductase, inhibiting the oxidation of ubiquinol in the ETC which blocks the mitochondrial electron transfer between cytochrome b and c (**Fig. 2.3**). Complete inhibition of the ETC enables the calculation of reserve capacity, non-mitochondrial respiration, and proton leakage.

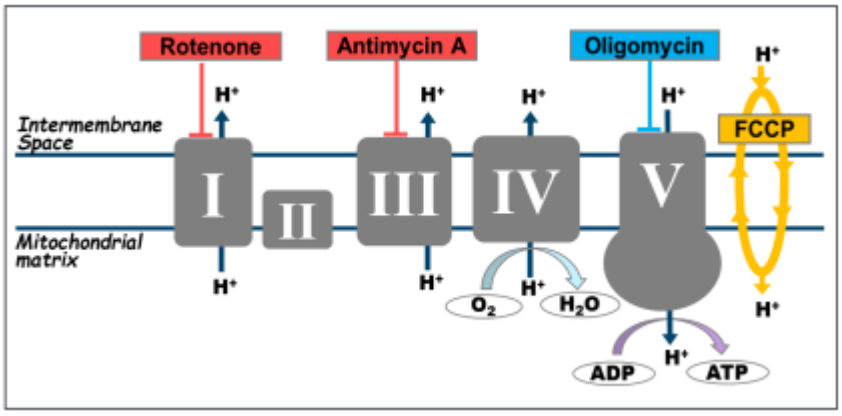

Figure 2.3: Inhibitors of the ETC

The other major metabolic pathway is glycolysis, which referred to the consumption of glucose converted into pyruvate, and subsequently conversion to lactate in the mitochondria and water and CO_2 in the cytoplasm. Glucose consumption results in proton release into extracellular conditions and acidification of medium, measured by ECAR. Saturation of glucose allows the cells catabolise it through the glycolytic pathway to pyruvate, leading to ATP, NADH, proton and water production. Glucose to pyruvate conversion leads to proton release and rapid acidification referred to as basal glycolysis. Oligomycin, the inhibitor of ATP synthase, is utilised to inhibit ATP

mitochondrial respiration and shifts energy production to glycolysis. Subsequently ECAR increases revealing cellular maximal glycolysis.

Seahorse XF HS Mini Analyser was used to measure OCR and ECAR in an 8 well miniplate format. BMDM were seeded in 6 of the 8 wells of the seahorse miniplate, as two wells (A and H) are background controls, at a density of 80,000 cells per well in a volume of 80µl in DMEM + 10% FBS. Once seeded cells were incubated at 5% CO_2, 37°C overnight. The next day, media was exchanged, and cells were either unstimulated or stimulated with LPS (100ng/mL) and IFNγ (50ng/mL) and incubated for 48h at 5% CO_2, 37°C. 1 hour prior to seahorse analysis completely DMEM was exchanged for 180uL XF DMEM media supplemented with glucose and L-glutamine. XF media contains no phenol red, is free of bicarbonate and has a low buffering capacity. Miniplate was incubated in non- CO_2, 37°C for 1 hour.
24 hours prior to seahorse analysis, XFp Sensor Cartridge was hydrated with 200uL XF calibrant in each well and incubated in non- CO_2, 37°C. Before loading cartridge into seahorse XF analyser each injection port was prepared with metabolic inhibitors. Port A was filled with 10uM Oligomycin at a volume 20uL (final concentration 1uM injected), port B was filled with 10uM FCCP at a volume 22uL (final concentration 1uM injected) and port C was filled with 5uM AMA/rotenone at a volume 25uL (final concentration 0.5uM injected). Once compounds were loaded into injection ports XFp Sensors Cartridge was placed in Seahorse XF HS Mini Analyser instrument tray for instrument calibration.

2.11. 2P-Fluorescence lifetime imaging microscope (FLIM) of NAD(P)H

WT and *Casp11*$^{-/-}$ BMDM were seeded 10^6cell/mL in 35 mm^3 petri dishes and incubated overnight at 5% CO_2, 37°C. The next day media was exchange for phenol free DMEM +10%FBS and unstimulated or stimulated with LPS (100ng/mL) and IFNγ (50ng/mL) for 6 hours. Each stimulation condition was staggered by 15 minutes to account for acquisition of data. After 6 hours fluorescence lifetime imaging microscopy (FLIM) of NAD(P)H was performed on a custom upright (Olympus BX61WI) laser multiphoton microscope system performed by Nuno Neto (School of Bioengineering, TCD). An 80MHz titanium:sapphire laser (Chameleon, Coherent) was used for multiphoton excitation and upright scanning microscope was used coupled with a water-immersion 25x objective (Olympus, 1.05NA) and temperature-controlled stage at 37 °C. Two-photon excitation of NAD(P)H and FAD^+ was performed using 760 nm and 800 nm, respectively, as excitation wavelength. A 455/90 nm and 502/547 nm bandpass filter was used

to isolate NAD(P)H and FAD^+ fluorescence emission signals. Acquisition of images (512x512 pixel) spanned over 30 sec collection time with a pixel dwell time of 3.81 µs. A PicoHarp 300 TCSPC system operating in the time-tagged mode coupled with a PMA hybrid detector (PicoQuanT GmbH, Germany) was used for fluorescence decay measurements yielding 256-time bins per pixel. Culture dishes were placed on an incubating microscope stage at 37°C and for each individual sample, at least three separate images from different areas of the dish were acquired. The fluorescence images and decay curves for NAD(P)H were obtained and the overall decay curve was generated by the contribution of all pixels and was fitted with a double exponential decay curve, for GFP and NAD(P)H, respectively.

(Eq. 1) $\mathbf{I(t) = \alpha 1 e^{-t/\tau 1} + \alpha 2 e^{-t/\tau 2} + c}$

I(t) corresponds to the fluorescence intensity measured at time t after laser excitation; α1 and α2 represents the fraction of the overall signal comprise of a short – free NADH and long lifetime – protein bound NADH component, respectively. τ1 and τ2 are the short and long lifetime components, respectively; c corresponds to background light. X 2 value is calculated to evaluate the goodness of multiexponential fit to the raw fluorescence decay data. In this study all the values with X 2 < 1.3 were considered good fits. The average lifetime (τavg) of NAD(P)H for each pixel is calculated by a weighted average of both free and bound lifetime contributions

(Eq. 2). $\boldsymbol{\tau avg = (\tau 1 \times \alpha 1 + \tau 2 \times \alpha 2)\ (\alpha 1 + \alpha 2)}$

The optical redox ratio (ORR) was calculated using equation 2:

ORR = FAD+ NAD(P)H

With NAD(P)H being the total fluorescence intensity acquired at the 455-490nm and FAD + the total fluorescence intensity acquired at 502-547nm. The intensity of both images at different channels was obtained by conserving the same region of interest (ROI) in the Symphotime® software.

2.12. TMRM Staining and Mitochondrial Morphology

Mitochondria are dynamic organelle which in response to environment and cellular cues undergo fission or fusion. Mitochondrial dynamism is thought as mitochondrial quality control to maintain healthy mitochondrial network, with optimal function, number, and shape. During cellular stress mitochondria fuse, mixing organelle content, followed by fission to produce two

health daughter mitochondria, known as functional complementation. When mitochondria have sustained damage, repair is achieved my fission, segregating the damaged component, which is further eliminated by autophagy or mitophagy. This interplay of mitochondria fission and fusion also supports metabolic shifts.

Tetramethylrhodamine, methyl ester (TMRM) is a cell permeant, lipophilic cationic, red-orange, fluorescent dye which is readily sequestered by active healthy mitochondria with intact membrane potential. Mitochondria electrical gradient along the inner and outer mitochondrial membrane is known as mitochondrial membrane potential ($\Delta\psi_m$). $\Delta\psi_m$ drives the generation of ATP by mitochondria and is measured by the accumulation of TMRM. TMRM staining enables monitoring of mitochondria morphology. Measuring mitochondrial length, width and area and thereby calculating mitochondrial aspect ratio and eccentricity provides inside into the dynamic metabolic related dynamism of mitochondrial fission and fusion.

Mitochondrial aspect ratio, which is defined as the ratio between the centreline length and average width, is calculated relative to a circle to be 1.

Aspect Ratio = (Mitochondrial width/ L) x π/4

Elongation of mitochondria is related to eccentricity, defined as a measure of deviation from a circle. Eccentricity of 0 is a circle.

Eccentricity = 1- (A / (0.25 π L^2))

A is the area, L is the centreline length.

WT and *Caspase-11*$^{-/-}$ BMDM were seeded 10^6cell/mL in 35 mm^3 petri dishes and incubated overnight at 5% CO_2, 37°C. The next day media was exchange for phenol free DMEM +10%FBS and unstimulated or stimulated with LPS (100ng/mL) and IFNγ (50ng/mL) for 6 hours. Each stimulation condition was staggered by 15 minutes to account for acquisition of data. After 6 hours cell growth medium was removed from the cells and cell staining solution was added to the cells and incubated for 30 mins at 37°C. Cell staining solution was prepared fresh adding 10µL of 100µM TMRM (1000X) stock solution to 10mL of cell growth media to make 100nM TMRM staining solution. TMRM staining is detectable in TRITC filter setting (UV red) with an absorbance peak at 548 nm and emission peak at 574 nm.

2.13. ^{1}H Nuclear Magnetic Resonance (NMR) spectroscopy

Bruker Avance II 600 NMR performed by Dr. John O'Brien (Tcd, School of Chemistry) was employed to examine intracellular and extracellular metabolites in resting (M0) and M1 inflammatory polarised WT and *Caspase-11*$^{-/-}$ BMDM. This spectrometer has a crypoprobe triple resonance probe with z-gradients for Proton (^{1}H) 2D and 3D structural NMR at very high signal to noise ratio and is designed for protein NMR. NMR spectra were acquired at Bruker Avance II 600 NMR (600 MHz) *DD2 Premium Compact spectrometer with a tripleresonance, 5 mm enhanced room temperature probe and Agilent VNMRj software.* 1D 1 H NMR spectra were recorded using the NOESY-Presat pulse sequence. Optimal 90 degree pulse width and solvent presaturation frequency were determined (16,000 number of scans, 12 ppm window width, 15 seconds relaxation delay). Each sample was equilibrated at room temperature and shimmed prior to data acquisition. Data analysis performed by Dr. Manuel Ruether (TCD, School of Chemistry) was carried out using the software TopSpin, AssureNMR Bruker and SIMBA. AssureNMR can efficiently evaluate complex biological mixtures such as cell culture supernatants. Targeted fingerprinting enables identification and quantification of metabolites, enhanced by public datasets.

2.13.1. Extracellular and Intracellular metabolite Extraction

WT and *Casp11*$^{-/-}$ BMDMs were seeded at 10^{7} cells in $10\mathrm{cm}^{3}$ dish O/N prior treatment. Cells were stimulated with LPS (100 ng/ml) and IFNγ (50 ng/mL) for 48h. For extracellular metabolite extraction culture supernatants and complete culture media were collected and filtered using 10kDa molecular weight cut-off (MWCO) centrifugal filter. 10kDa MWCO concentrators were washes 3-4 times with PBS prior to use. 2mL collected supernatants and complete DMEM media were added to centrifugal concentration and centrifuged at 4000 x g for 10 minutes. 10kDa filtrate was collected and transfers to a fresh 3.5mL Eppendorf. Supernatants are diluted 1:3 in NMR solvent (25mM Na_2HPO_4/Na_2HPO_4, 0.4mM imidazole, 0.005% TSP in 5% D_2O and 95% H_2O at pH7). Intracellular metabolites were extracted from whole cell lysates using 9:1 methanol: chloroform precipitation. Once culture media was aspirated, culture dishes were rinses with 5mL warmed PBS for <5secs. Culture dishes were either placed in -80°C or short-term store or freeze snapped with 10mL LN_2. Culture dishes was kept on dry ice as LN_2 evaporated within 10 secs for the subsequent quenching procedure. 1mL ice-cold 90% methanol / 10% chloroform was added to each dish. Rubber policeman was used to scrape adherent cells in organic solvent and transferred to 1.5mL eppendorfs. Cell extracts were centrifuged at 16000 x g for 10 minutes at

4°C. Supernatants were transferred to round bottom flasks where organic solvent was removed using rotor vacuum and dried product was resuspended in 600µL NMR solvent and transferred to 5mm NMR tubes for subsequent NMR analysis of intracellular metabolites. Metabolite's spectra were measured by 600Hz H^1 NMR. AssureNMR (Bruker) software analysis of metabolites.

2.13.2. Determination of protein content

1uL of intracellular metabolite extracts were used to measure protein concentration by BCA protein assay kit as previously described in section 2.4.2 for the normalisation of intracellular and extracellular metabolites.

3.Chapter 3: Caspase-11 regulation of PINK1-mitophagy mediates type I IFN dependent iNOS expression in murine macrophages

3.1. Introduction

Interferon-induced and STAT1-mediated transcriptional regulation of caspase-11 expression has been well documented[233]. As previously introduced, TLR4-TRIF dependent type I IFN production is crucial for caspase-11 expression and sufficiently triggers auto processing[66]. While type II IFN mediated STAT1 directly binds the caspase-11 gene promoter region to regulate gene expression[77]. However, the role caspase-11 contributes during STAT1 activation observed in innate immune defence has been under reported. The Creagh lab has previously shown that LPS stimulated STAT1 phosphorylation in BMDM is regulated by caspase-11 expression, as *Casp11*$^{-/-}$ BMDM demonstrated impaired pSTAT1 expression during an LPS timecourse[234]. This impairment does not appear to be type II IFN dependent, as LPS stimulated *IFNγ*$^{-/-}$ BMDM STAT1 phosphorylation levels were equivalent to that of WT. However, in the absence of the type I IFN receptor - IFNAR1 - LPS mediated STAT1 phosphorylation is impaired, suggesting that LPS mediated caspase-11 activity regulates STAT1 phosphorylation by autocrine type I IFN signalling[234]. These results suggest that LPS-mediated upregulation of caspase-11 regulates STAT1 activation, via type I IFN signalling.

3.1.1. Canonical STAT1 activation

IFN signalling involves four families of proteins including type I and II IFN receptors, receptor associated Janus Protein tyrosine kinases (Jaks), STATs, and interferon regulator factor (IRF) family of transcription factors. Type II IFN dependent signalling involves extracellular polypeptide ligand, IFNγ, binding receptor, IFNGR, catalysing the activation of Jak1 and Jak2 via auto- and trans-phosphorylation. IFNGR consists of an α-subunit (IFNGR1), required for extracellular ligand binding, and a β-subunit (IFNGR2) containing intracellular domain which are necessary for constitutive and specific association with Jaks[235]. Notably, IFNGR1 and IFNGR2 are not pre-associated on the surface of unstimulated cells but rather their complex association is mediated in an IFN-dependent manner[236], forming a heterodimer complex (**Fig. 3.1**). Jak1 preferentially associates with the IFNGR alpha chain, whereas Jak2 associates with the beta chain. Prior to IFNγ ligand binding IFNGR, Jak1 is associated with the alpha subunit, while stimulation is required for Jak2 to form complex at subunit beta[237]. IFNγ signalling results in Jak tyrosine phosphorylation, kinase activity and recruitment of STAT1α. Activated Jak phosphorylates IFNGR on tyrosine residues such as Y440, forming a docking site for STAT1 via Src-homology 2 (SH2) domain[238]. Biochemical structural studies of STATs identified several domains, including N-terminal domain (NTD), coiled-coil domain (CCD), DNA binding domain

(DBD), linker (LK) domain, SH2, tyrosine activation domain, and transcriptional activation domain (TAD). STAT1 CCD hydrophilic protrusion is important in receptor binding, tyrosine phosphorylation and nuclear translocation. Once docked STAT1 is phosphorylated at tyrosine residue 701 leading to homodimer formation via reciprocal phosphotyrosine 701 – SH2 domain interactions[239].

A STAT1 conformational shift is important in target gene activation and mediating termination of signal transmission. IFN exposure mediated STAT1 homodimerisation, leading to parallel configuration via interaction of SH2 domain of one monomer with phosphotyrosine-701 of the paired monomer. Spatial reorientation of parallel to anti-parallel dimer complex involved DBD of one monomer and CCD phenylalanine 172 residue of the other monomer, promoting conformational change[239]. Dephosphorylation is required for shuttling back to the cytoplasm for continuous nucleo-cytoplasmic cycling. Once phosphorylated and trafficked into the nucleus, STAT1 binds palindromic motifs in the promoter region of γ-activated sequences (GAS). LK domain connects the DBD with SH2 domain to mediate DNA binding capacity to promoter region[240].

Type I IFN, IFNα and IFNβ, similarly signal via lFNAR1 and IFNAR2. Following association, Jak1 and tyrosine kinase 2 (Tyk2) dimerise leading to Jak1 autophosphorylation. STAT1/STAT2 recruitment and heterodimerisation leads to immunomodulatory gene expression via binding IFN-stimulated response element (ISRE). Type I IFN can activate all seven members of STAT family in different cell types, leading to different homodimer, STAT1 or STAT2, and heterodimer formation, STAT1/STAT2.

All IFNs can mediate STAT1 homodimerization via phosphorylation of a tyrosine residue leading to modulated gene expression, via the activity of GAS. However, the type of IFN inducing signalling is important to the nature of STAT1 protein-protein interaction and specific gene transcriptional targeting. IRFs modulate STAT dimer activity regulating their binding of various genes. IRF N-terminal contains a DNA-binding domain, and C-terminal region contains a phosphorylation dependent regulation site. IRF9 interaction with the STAT1-STAT2 heterodimer forms ISGF3, or with STAT2 homodimers, STAT2/IRF9 complex, activated in response to type I IFN, targeting genes harbouring interferon-stimulated response elements (ISRE) (**Fig 3.1**).

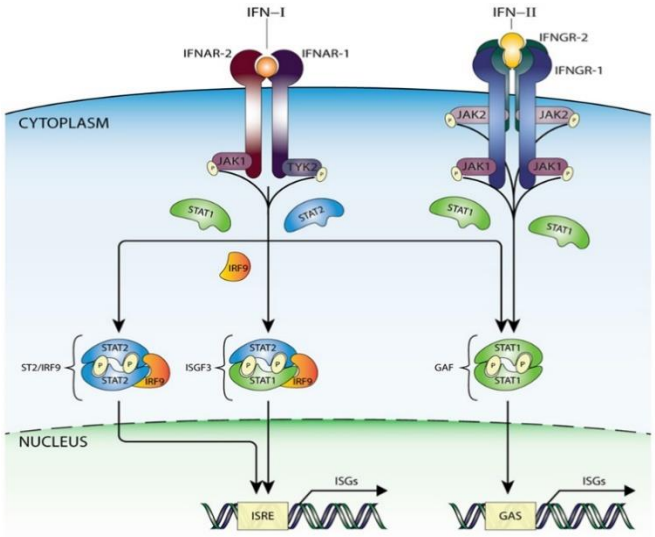

Figure 3.1: IFN activated ISGs transcription via ISRE or GAS induced activity. Type I IFN recognition by IFNAR1 and IFNAR2 subunits promotes Jak1/Tyk2 dimerisation and kinase mediated transphosphorylation, leading to STAT recruitment. Type I IFN activation is involved in three complex formations; STAT2 homodimerisation associated with IRF9 (ST2/IRF9), STAT1/STAT2 heterodimerisation associated with IRF9 (ISGF3) or STAT1 homodimerisation (GAF). Both ST2/IRF9 and ISGF3 bind ISRE motifs present in more than 300 ISGs. GAF which specifically recognises GAS motifs is also inducible via type II IFNs. Type II IFN interacts with IFNGR1 and IFNGR2 resulting in Jak1 and Jak2 phosphorylation and recruitment of STAT1. Jak1 and Jak2 kinases mediate STAT1 phosphorylation, resulting in GAF formation. GAF nuclear translocation mediates GAS containing genes transcriptional regulation. Image taken from Michalska *et al., Frontiers in Immunology* 2018 [9:1135][240].

3.1.2. Non-canonical TLR mediated STAT activation

Several TLR ligands have been illustrated to mediate STAT1 phosphorylation at two different positions, Y701 and S727. Activation of TLR2 and TLR4 rapidly lead to phosphorylated STAT1 at S727, comparable to IFNα induction. Whereas, TLR4 and TLR3, albeit delayed, mediate Y701 phosphorylation during an early window[241],[242]. Mechanistic investigation of the TLR induced STAT activation pathway revealed that TLR mediated S727 phosphorylation is independent of autocrine IFN signalling, as its activation is unaffected in *Irf3*$^{-/-}$ or *Irf7*$^{-/-}$ BMDM stimulated with TLR ligands[243]. As previously mentioned, TLR4-mediated Y701 activation is type I IFN autocrine signalling dependent, as in the absence of IFNAR1, LPS stimulated BMDM have impaired Y701 phosphorylation[234,244]. Luu and colleagues have reported an IFN-independent TLR induced pathway which mediates S727 phosphorylation via a MyD88-TRIF signalling cascade[243]. This TLR signalling pathway interacts with TRAF6, directly recruiting STAT1 to lead to S727

phosphorylation[241,243]. However, the S-cytosolic kinase inducing phosphorylation has yet to be uncovered.

TLR3-induced STAT1 phosphorylation is mediated by transactivation of type I IFN signalling. Dempoya and colleagues reported that initial STAT1 Y701 phosphorylation by TLR3 involves signalling via RIG-I-MAVs in a type I IFN dependent and independent manner[241], as in the absence of RIG-I, type I or II IFN does not completely rescue early STAT1 Y701 phosphorylation. However, in the absence of RIG-I and type I IFN signalling TLR3 activation still leads to STAT1 phosphorylation with delayed kinetics, suggesting that this late phosphorylation is a result of an unidentified innate immune regulator uninvolved in initial antiviral activity.

3.1.3. Signalling involved in iNOS expression

The type of IFN inducing signalling is important to the nature of STAT1 protein-protein interaction and specific gene transcriptional targeting. A major transcriptional target of STAT1 is iNOS. iNOS is a member of nitric oxide synthases (NOS) family, which produces nitric oxide (NO) from available intracellular L-arginine by its NADPH-dependent catalytic activity[127]. iNOS expression is regulated by two major signalling pathways, MAPK and Jak/STAT, in response to PAMPs or cytokines. Activation of MAPK by LPS or TNFα subsequently leads to NF-κB and AP-1 activation. Additionally, iNOS expression is also induced by IFN activation of Jak/STAT1, most commonly IFNγ, which translocates to the nucleus, inducing IRF-1 transcription. IRF-1 can directly bind NF-κB p50 subunit, resulting in simultaneous IRF-1 and NF-κB colocalization at the iNOS promoter region, greatly amplifying iNOS gene expression, although both factors individually induce iNOS gene expression. The iNOS promoter contains GAS site specific for STAT1α, where IFN co-stimulation with LPS is required for optimal iNOS gene expression[245].

LPS priming induces NFκB-STAT1 association responsible for iNOS expression. As multiple studies have illustrated, TLR4 signalling leads to secretion of IFNβ which is kinetically timed to be consistent with STAT1 phosphorylation and IRF-1 expression[244,234,243,246]. Inhibition of IFNβ signalling following LPS stimulation attenuates iNOS expression[247,248], confirming that LPS regulation of both NF-κB and indirect STAT1 signalling pathways amplifies iNOS expression and NO production.

3.1.4. Autophagy and Innate immunity

Autophagy is an evolutionary conserved catabolic process by which cells degrade and recycle their own components for energy metabolism. There are 3 subtypes of autophagy including macroautophagy, interchangeably referred to as autophagy, microautophagy and chaperone

mediated autophagy. Autophagy is known to play a critical role in inflammation and is essential for cellular differentiation, homeostasis and survival[249].

The autophagy cascade begins with nucleation of the phagophore following ULK1/2 complex induction. ATG12–ATG5-ATG16L1 complex, the class III PtdIns3K complex, LC3-II, and ATG9 aid phagophore elongation. Once the outer membrane expands sufficiently to encapsulate the cargo, the autophagosome is formed and LC3-II is cleaved. Next, autophagosome- lysosome fusion occurs to form an autolysosome, the contents of which are degraded following exposure to the lysosome's acidic lumen and resident hydrolases. The degradation products are transported to the cytosol for reuse in biosynthetic processes or cellular energy via lysosomal permeases[250].

Autophagy is an important component of innate immunity utilised by macrophages, with increasing evidence supporting a role for autophagy in modulating macrophage response and activity[251–253]. TLR4 dependent TRIF-TICAM1 dependent signalling regulates autophagosome formation. Mechanistic studies utilising TLR2 signals mediate MAPK1/3 phosphorylation and stimulate autophagy dependent NF-κB. Inhibition of autophagy in M2-like macrophages has been shown to rescue NF-κB activity, shifting activity towards a more M1-like proinflammatory producing macrophage[251]. Thereby suggesting a role for autophagy during NF-κB macrophage polarisation.

3.1.5. Caspase-11 and autophagy

Several reports have demonstrated crosstalk between autophagy and inflammasomes, with the majority identifying a negative regulatory function of autophagy on inflammasome signalling[252,253]. However, inflammasome signalling has been reported to promote autophagy[254], suggesting that a negative regulatory feedback loop may exist to resolve excessive inflammation. Recent studies have proposed an additional role for caspase-11 in the regulation of autophagy. Caspase-11-mediated modulation of actin polymerisation promotes the maturation of phagosomes harbouring intracellular pathogens and autophagosome formation[91]. Infection with *B. cenocepacia* in the absence of caspase-11 results in defective autophagosome formation, as demonstrated by an accumulation of small GTPase RAB7, reduced pathogen co-localisation with LC3 and acidic lysosomal compartment[95]. This study indicates a non-pyroptotic role for caspase-11 during pathogen clearance by facilitation of autophagosome biogenesis and trafficking.

Mitophagy, a mitochondrial quality control specialised autophagy, has similarly been illustrated to be regulated by caspase-1 and caspase-11 activity[255,256]. Classical macrophage activation is

associated with early inhibition of mitophagy, aiding cellular metabolism towards glycolysis. Investigation of the mechanism underlying LPS-mediated inhibition of autophagy during macrophage M1 polarisation revealed that STAT1 driven caspase-11 inhibited mitophagy via direct PINK1 degradation and Parkin inactivation[256].

3.1.6. Autophagy and iNOS

Multiple studies suggest that autophagy may play a role in the regulation of NO bioavailability. Chloroquine, an aminoquinoline drug, accumulates within the lysosome inhibiting the final step of autophagy, autolysosome formation. Chloroquine-mediated inhibition of serum deprivation-induced autophagy results in increased NO production[257]. Additionally, shear stress induced eNOS phosphorylation and NO production is severely impacted in autophagy deficient cells. This reduction in autophagy induced NO production coincides with increased ROS and proinflammatory cytokine production[258]. Similarly, iNOS negatively regulates NF-κB signalling pathways to dampen proinflammatory cytokine production, as in the absence of NOS2, the inflammatory secretome is reduced[259]. In contrast, induction of autophagy with rapamycin mediates NO production[260]. However, the mechanism underlying autophagy regulated NO production has yet to be identified.

3.2. Hypothesis and aims of Chapter 3

Hypothesis: Caspase-11 inhibition of autophagy mediates type I IFN autocrine signalling inducing STAT1 activation, iNOS induction and NO production.

Specific Aims:

1. Investigate the impact of caspase-11 expression on STAT1 and STAT2 activation in murine BMDM following LPS stimulation.
2. Determine whether inflammasome activation and GSDMD processing are involved in LPS-mediated iNOS expression and NO production.
3. Investigate whether LPS-mediated caspase-11, once expressed, directly interacts with STAT1 to mediate activation.
4. Determine the ability of caspase-11 to regulate IFN and Jak signalling upstream of STAT1 activation.
5. Examine the role of caspase-11 during mitophagy in response to LPS in murine BMDM.

3.3. Results

3.3.1. Caspase-11 regulates STAT1 phosphorylation (at Tyrosine 701) and subsequent NO production in murine macrophages

Previous findings from the Creagh Lab have identified a role for caspase-11 during STAT1 phosphorylation in a murine inflammatory model of colorectal adenocarcinoma, AOM/DSS[234]. This study demonstrated that caspase-11 regulates LPS and IL-1β mediated STAT1 phosphorylation and nuclear translocation in murine macrophages and intestinal epithelial cells. LPS mediates STAT1 activation via either type I IFN autocrine signalling dependent activity or directly activated via TRAF6 mediated TLR-STAT crosstalk[243,261]. Previous studies have shown, utilising *Ifnar1*$^{-/-}$ BMDM, that LPS mediated STAT1 Y701 phosphorylation is type I IFN dependent[234]. Whereas Luu and colleagues described rapid phosphorylation of STAT1 S727 as a direct result of TLR activation but not Y701. STAT1 S727 occurs independently of TLR-induced type I IFN expression and is regulated by MyD88 dependent TRIF mediated TRAF6[243]. Although TRAF6 recruits STAT1 to the TLR signalosome, the cytosolic S-kinase mediating STAT1 S727 phosphorylation is unknown. TLR4 signalling has been shown to lead to caspase-4 and TRAF6 interaction via a TRAF6 binding motif within caspase-4 amino acid sequence (PPESGE)[44]. This sequence is homologous between species with caspase-11 containing a similar sequence (PEESLN). Therefore, we hypothesised a role for caspase-11 and TRAF6 during LPS-mediated TLR4 signalling induction of S727 phosphorylation. Type I and II IFN induced S727 phosphorylation is also dependent upon Y701 phosphorylation, this was found to be independent of cellular stress mediated p38-MAPK signalling such as LPS[262].

During canonical pathway activation, receptor tyrosine kinase activation results in STAT1 docking to the transmembrane complex, mediating Y701 phosphorylation. Type I IFN signalling leads to STAT1 dimerisation via SH2 domains, to form STAT1 homodimers or recruit STAT2 to regulate STAT1/STAT2 heterodimer formation. Our understanding of LPS-mediated STAT dimerization in the presence of caspase-11 had not been addressed and is of importance for understanding specific gene transcription targets. Here, we investigate STAT1 and STAT2 phosphorylation in response to LPS stimulation, to determine whether caspase-11 regulation of STAT activity is specific to STAT1.

Firstly, we wished to confirm our previous findings that STAT1 Y701 phosphorylation is impaired in caspase-11 deficient macrophages in response to LPS. To investigate the role of caspase-11 in STAT activation, WT and *Casp11*$^{-/-}$ BMDM were stimulated with LPS (1µg/mL) over a 24 hour timecourse. We observed that LPS potently stimulated STAT1 Y701 phosphorylation within 2-4h, which resolved by 8-24h in WT BMDM (**Fig. 3.1 A**), whereas induction of STAT1 Y701

phosphorylation was impaired in *Casp11*$^{-/-}$ BMDM. Quantitative analysis by densitometry revealed this LPS-mediated STAT1 Y701 activation is severely impaired in the absence of caspase-11 (**Fig. 3.1 B**), confirming previous observations. In contrast, LPS-TLR4 induced STAT2 S689 phosphorylation similarly occurs in both WT and *Casp11*$^{-/-}$ BMDM at 2h post LPS stimulation and begins to resolve by 8h post stimulation (**Fig. 3.1 A**). Densitometric analysis confirmed that LPS-mediated STAT2 phosphorylation is independent of caspase-11 expression (**Fig. 3.1 C**). STAT1 S727 phosphorylation was also measured in this context, as this modification increases transcription factor affinity to chromatin during gene expression. As previously mentioned, S727 phosphorylation is independent of Y701 phosphorylation during LPS stimulation. However, we hypothesised that caspase-11 may participate in TRAF6 mediated TLR-STAT crosstalk. As expected S727 is rapidly phosphorylated after 30mins but our results found that this non-canonical activation does not appear to be significantly impacted by caspase-11 (**Fig. 3.1 A, D**). These data suggest that LPS-induced caspase-11 mediates STAT1 homodimer activation indirectly, via autocrine IFN signalling.

3.3.2. Caspase-11 regulation of STAT1 Y701 phosphorylation and NO production is independent of noncanonical inflammasome - GSDMD mediated pyroptosis

The most documented caspase-11 function involves the activation of the non-canonical inflammasome, which drives the lytic form of cell death, pyroptosis, via cleavage of pore-forming GSDMD, leading to processing and release of inflammatory cytokines IL-1β and IL-18. To determine whether GSDMD processing is required for caspase-11's role in iNOS induction and NO production, we examined GSDMD during NO production in response to TLR4 signalling.

This was carried out utilising GFP and GSDMD knockdown immortalised BMDM, stimulated with LPS over a 24 hour timecourse. LPS mediated STAT1 activation occurred in GFP and *Gsdmd*$^{-/-}$ iBMDM with similar kinetics to those previously observed, with STAT1 Y701 phosphorylation induced at 2-4 h and resolution occurring by 8h post stimulation, with no observable difference in STAT1 Y701 phosphorylation in the absence of GSDMD (**Fig. 3.2 A**). Therefore, as expected iNOS expression and NO production was not impaired. Data revealed similar iNOS expression following 24h LPS in GFP and *Gsdmd*$^{-/-}$ iBMDM and similar NO production, measured indirectly as nitrite by griess assay (**Fig. 3.2 A, B**). These findings are not unexpected, as we suggest the mechanism by which caspase-11 regulates TLR4-induced STAT1 phosphorylation is type I IFN dependent and release of these cytokines does not involve pyroptotic cell death.

We wanted to confirm findings that NO production induced by LPS stimulation is independent of GSDMD-mediated pyroptosis using the pharmacological inhibitor, disulfiram. Hu and colleagues illustrated that disulfiram functions to inhibit pyroptosis by blocking gasdermin D pore formation, improving survival in mice with LPS-induced sepsis[263]. Pore formation inhibition by disulfiram is specific to GSDMD at nanomolar concentrations via modification of Cys191/192. Thus, while disulfiram allows processing of IL-1β and GSDMD to occur, GSDMD oligomerisation is inhibited, thereby preventing IL-1β release and pyroptosis[263].

The non-toxic concentration of disulfiram which would inhibit LPS mediated LDH release in BMDM was initially determined by pre-treating WT BMDM with a range of concentrations (10-0.1μM) 1 hour prior to stimulation with LPS (1μg/mL) for 24 hours. We observed that 10-1μM disulfiram pre-treatment induced LDH release without LPS stimulation, suggesting cytotoxicity at this concentration range. (**Fig. 3.3 A**). Previous studies observed disulfiram IC50 = 10.3 ± 0.5 μM in iBMDM treated 1 hour prior to electroporation with LPS[263]. We observed 0.1μM disulfiram pre-treatment was sufficient to decrease LPS mediated LDH release without any drug induced cytotoxic effects (**Fig. 3.3 A**). Continuing with this range of concentrations, we pre-treated BMDM for 1 hour prior to LPS stimulation for 24 hours. Measuring NO production in the supernatants from these experiments revealed that LPS-mediated NO production was abrogated at highly cytotoxic concentrations of disulfiram (10-5μM), as cell viability is dramatically impacted (Fig 3.3 A-B). However, at the non-cytotoxic concentration (0.1μM), we observed that disulfiram pre-treatment did not reduce NO production compared to the vehicle control. Similar to findings with *Gsdmd*$^{-/-}$ iBMDM, disulfiram had no observed effects on NO production (**Fig. 3.3 B**). NO is a small electro-negative free radical molecule which rapidly diffuses the phospholipid plasma membrane once generated, without the requirement for physical pore formation to enhance NO extracellular release.

Next, we sought to determine whether caspase-11 protease activity mediated NO production. Typically, caspase-11 proteolytic activation, leading to noncanonical inflammasome activation and GSDMD mediated pyroptosis, requires priming followed by intracellular detection of LPS lipid A motif by the pro-caspase-11 CARD domain. Cytosolic LPS induces caspase-11 dimerisation and auto-cleavage, necessary for acquisition of basal proteolytic activity[264]. To investigate whether caspase-11 protease activity is required to mediate NO production, we used a tetrapeptide inhibitor of inflammatory caspases-1, -4 and -5, Ac-WEHD-CHO (Trp-Glu-His-Asp-aldehyde). To determine the Ac-WEHD-CHO concentration which sufficiently inhibited caspase activity, IL-1β secretion from LPS (1μg/mL, 24 h) treated PMA-differentiated THP-1 macrophages

was measured in the presence/absence of Ac-WEHD-CHO (10-5μM) pre-treatment. We observed that pre-treatment with both 10μM and 5μM Ac-WEHD-CHO reduced LPS induced IL-1β secretion in macrophages, with 10μM having the most robust reduction (**Fig. 3.4 A**). Therefore, we continued with this concentration in consequent examination of caspase-11 enzymatic activity.

To determine whether caspase-11 enzymatic activity is required during LPS mediated NO production, we pre-treated WT BMDM with 10μM Ac-WEHD-CHO followed by 24h LPS stimulation and measured nitrite levels of the supernatants. From these data we observed decreased production of NO following pre-treatment with Ac-WEHD-CHO in response to LPS (**Fig 3.4 B**). Therefore, rendering the protease pocket inactive does appear to alter macrophage NO production in response to extracellular LPS signalling (**Fig. 3.4 B**). Altogether these data indicate an enzymatic role for caspase-11 in the regulation of iNOS expression and NO production via STAT1 activation, which is independent of caspase-11's role in GSDMD-mediated pyroptosis.

3.3.3. Caspase-11 does not directly interact with STAT1 in cytosol

Next, we sought to determine whether caspase-11 regulation of STAT1 phosphorylation may be induced due to a direct interaction or a result of autocrine type I IFN signalling. First, we aimed to determine the kinetics of a direct interaction between caspase-11 and STAT1. As previously mentioned, Dempoya and colleagues described dsRNA induced activation of STAT1 phosphorylation as biphasic, with early and late stage activation mechanisms[241]. Early regulation of STAT1 activation is RIG-I-MAVS and type I IFN driven, whereas the second phase is reported to be independent of RIG-I-MAVS and type I IFN independent. Dempoya suggest that an unknown sensor of dsRNA, in this model, drives STAT1 activation. Therefore, we sought to determine whether caspase-11 maybe be the unknown molecule involved in driving this late phase STAT1 activation. TLR-STAT1 crosstalk mediated by TRAF6 has been described in detail by Luu and colleagues. However, the cytosolic kinase which mediates TRAF6 phosphate transfer to STAT1 is also unidentified[243]. Caspase-4, human orthologue of caspase-11, can interact directly with TRAF6 binding motif[44]. Thereby suggesting a possible role for caspase-11 in crosstalk between TLR signalling and late stage STAT1 phosphorylation.

Firstly, we aimed to determine the correlation of kinetics for STAT1 phosphorylation and caspase-11 upregulation. To do this, we stimulated immortalised murine macrophage cell line RAW264.7 with LPS (1μg/mL) over a 24 hour time course. Following TLR4 activation both STAT1 S727 and Y701 were rapidly phosphorylated after 2 hours, the earliest time point measured, and

resolved by 24 hours (**Fig, 3.5**). Analysis by western blot also revealed detectable caspase-11 expression within 4 hours, increasing at 8 and 24 hours (**Fig.3.5**). Utilising this information, we next investigated whether caspase-11 and STAT1 interacted directly following 8 hours stimulation with LPS, when caspase-11 expression has peaked and STAT1 late phosphorylation is still detectable.

Immunoprecipitation (IP) of caspase-11 was performed 8 hours post LPS stimulation in RAW264.7 cells. To confirm total caspase-11 pull-down from whole cell lysates, caspase-11 immunoblotting was performed. Before pull-down was performed 10% of whole cell lysate was separated as input fraction, to confirm that stimulation induced caspase-11 expression. Lysate left over after bead-caspase-11 antibody complex pull-down was also used as residue fraction, to determine the efficiency of the caspase-11 pull down. Caspase-11 immunoblot reveals a successful caspase-11 pull-down, marked by the blue arrow in the IP lane following 8 h LPS stimulation (**Fig. 3.6**). There was no detectable caspase-11 in the residue lane with LPS stimulation (**Fig. 3.6**), confirming that caspase-11 expressed following 8 hours LPS stimulation was successfully immunoprecipitated. Next to determine co-IP of STAT1 with caspase-11, we immunoblotted for tSTAT1. Protein A/G beads have a detectable band near the molecular weight of STAT1 denoted by the blue arrow. However, we can see at low exposure tSTAT1 is detectable in input and residue indicated by the green arrow but not in the IP lane stimulated with LPS, where every protein which directly interacts with caspase-11 after 8 hours should be co-expressed (**Fig. 3.6**). Results suggest that caspase-11 does not directly interact with tSTAT1 to facilitate its phosphorylation at 8 hours LPS stimulation.

Next, we wanted to determine whether any caspase-11 and tSTAT1 co-localisation occurred following LPS stimulation, to indicate whether they may participate in a direct signalling cascade. Immunofluorescent staining of caspase-11 and tSTAT1 was performed over an 8 h LPS timecourse in RAW264.7 cell line revealed caspase-11 speck formation within 8 h LPS stimulation (Fig. 3.7), while tSTAT1 nuclear translocation peaked at 4h (**Fig. 3.7**). From this timecourse analysis there was no co-localisation of caspase-11 and tSTAT1 to suggest that an interaction is involved for caspase-11 mediated STAT1 Y701 phosphorylation. These findings are not unexpected as TRAF6 mediated phosphorylation of STAT1 is at the S727 residue. These data suggest that caspase-11 regulation of STAT1 Y701 is type I IFN autocrine signalling dependent, confirming previous findings utilising *Ifnar1*$^{-/-}$ BMDM.

3.3.4. Type I IFN and Jak activation is impaired in absence of caspase-11

To further investigate the mechanism of caspase-11 mediated STAT1 activation we analysed the phosphorylation of upstream tyrosine kinases, Jak1 and Jak2. Jak serves as the cytoplasmic transphosphorylation signalling platform, which mediates receptor phosphorylation, and recruitment and phosphorylation of STATs. Classically, it is suggested that type I IFN signalling is associated with TYK2 and Jak1, while type II IFN I associated with Jak1 and Jak2. However, in the absence of Jak1, cells still partially respond to IFNy, whereas it is completely abrogated in the absence of Jak2[265]. Therefore, we aimed to investigate whether Jak tyrosine kinase activity is involved in LPS mediated STAT1 Y701 phosphorylation.

To determine the role of caspase-11 in TLR4 signalling mediated Jak phosphorylation we stimulated WT and *Casp11*$^{-/-}$ BMDM with LPS over a 24 h timecourse. Western blot analysis revealed that Jak1 phosphorylation at Y1022 was detectable in WT BMDM at 4 h following LPS stimulation with sustained phosphorylation up to 24 h. However, impaired induction of Jak1 phosphorylation was observed in the absence of caspase-11 (**Fig. 3.8 A**), with pJak1 Y1022 only detectable at 24 h in LPS-stimulated *Casp11*$^{-/-}$ BMDM (**Fig. 3.8 A-B**). In contrast, no significant differences in the kinetics of Jak2 phosphorylation (Y1007) were observed between WT and *Casp11*$^{-/-}$ BMDM (**Fig. 3.8**). Previous studies have reported that LPS is involved in Jak2 activation in macrophages, inhibition of which reduces STAT1 activity and STAT1 mediated cytokine production[265–267]. Similarly, previous data unpublished from the Creagh Lab illustrate the reduced STAT1 Y701 phosphorylation following LPS stimulation in BMDM pre-treated with Jak1/2 inhibitor ruxolitinib. These data develop our hypothesis that LPS mediated caspase-11 regulates type I IFN responses.

Next, we investigated the secretion of IFNβ from WT and *Casp11*$^{-/-}$ BMDM stimulated with LPS over a 24h timecourse, by ELISA. We observed similar initial levels of IFN-β secretion at 2-8 h in both WT and *Casp11*$^{-/-}$ BMDM (**Fig. 3.9**). However, in WT BMDM IFN-β secretion continued to increase to the 24h timepoint, while less sustained secretion levels were observed in *Casp11*$^{-/-}$ BMDM by 24h (**Fig. 3.9**). Secretion of IFNβ at 2 h is consistent with the timing of STAT1 Y701 phosphorylation in response to LPS. To determine whether exogenous recombinant IFN-β stimulation of STAT1 activation (Y701 phosphorylation) rescues the impaired STAT1 activation kinetics observed in the absence of caspase-11, we performed an IFN-β (2000U/mL) time course across 24h. Data showed that IFN-β rapidly induced Y701 phosphorylation after 0.5-2 h and

resolution after 4 h, in both WT and Casp11-/- BMDM (**Fig. 3.10**), confirming that IFNβ-mediated STAT1 activation is independent of caspase-11.

To date we have observed impaired STAT1 Y701 phosphorylation at 2-4 h following LPS stimulation in the absence of caspase-11 as well as impaired IFNβ secretion, iNOS expression and NO production at 24h following LPS stimulation in *Casp11*$^{-/-}$ BMDM. However, our findings show that LPS induced type I IFN-β production is dependent on caspase-11 expression at 24h only. While treatment with exogenous IFN-β rescued the ability to induce NO production, these kinetics suggest that STAT1 activation upstream of IFN-β production boosts LPS mediated NO production.

To establish whether caspase-11 mediated IFN-β production mediates iNOS induction and NO production, WT and *Casp11*$^{-/-}$ BMDM were co-stimulated with LPS (24 h) and recombinant IFN-β (30 min), to compensate for the IFN-β secretion differences observed in *Casp11*$^{-/-}$ BMDM at later time points and to mimic the kinetics observed in WT BMDM. Nitrite levels measured by Griess assay showed that LPS priming in combination with recombinant IFN-β stimulation induced NO production in *Casp11*$^{-/-}$ BMDM to similar levels observed in WT stimulated with LPS alone or LPS in combination with IFN-β (**Fig. 3.11**). Additionally, we observed that exogenous IFNβ alone did not induce NO production in BMDM, suggesting that LPS-induced MAPK and STAT1 activity are required for potent NO production via autocrine type I IFN signalling. This data suggests that at late IFNβ signalling in LPS primed macrophages is required to promote NO production. This rapid induction and resolution of IFN-β mediated STAT1 activation as well as the increased secretion of IFN-β at 24h in WT BMDM stimulated with LPS suggests that late prolonged type I IFN activity is important for iNOS expression and NO production.

Previous literature has shown TLR3/4 activation in macrophages is capable of inducing type I IFN autocrine classical STAT1 activation (Y701 phosphorylation), although with delayed kinetics[241,242]. We have revealed caspase-11 involvement in the regulation of type I IFN mediated STAT1 activation. However, we have not yet shown how caspase-11 is driving a type I IFN response.

3.3.5. Caspase-11, mitochondrial morphology and mtROS

Previous reports in the literature have demonstrated that mitochondrial fragmentation/fission is associated with damaged mitochondria and can instigate innate immune responses such as

inflammasome activity, apoptotic caspases, and type I IFN[155,268]. Mitochondrial cycling through fission and fusion aids damaged mitochondrial repair by segregation or exchange of material to maintain a healthy network, mitochondrial content, and metabolism. Fission is key for maintenance of mitochondrial quality and integrity, as during fission defective mitochondria are selected for fragmentation, and turned over for mitophagy. Classically defective mitochondria have decreased membrane potential (ΔΨM) and enhanced fission. Increased mitochondrial biogenesis is likely beneficial to restore partially defective mitochondria by mixing the organelle content. As mitochondria lose their membrane potential, fission is drastically increased while fusion is inhibited. Elimination of unsalvageable mitochondria involves mitophagy and elimination of defective mitochondria by Pink1 and Parkin-mediated degradation. Loss or mutations in either of these mitophagy proteins is linked to accumulation of damaged mitochondria, as observed in Parkinson's disease. As previously mentioned, caspase-11 has been reported to be involved in inhibition of Pink-1 mediated mitophagy and accumulation of damaged mitochondria[256]. Therefore, we hypothesise that caspase-11 is involved in the accumulation of damaged mitochondria during macrophage inflammation, inducing type I IFN responses and leading to NO production, central to M1 polarisation.

We investigated mitochondrial morphology in response to M1 stimulation in WT and *Casp11*$^{-/-}$ murine macrophages, to provide evidence for caspase-11 involvement in mitochondrial dynamics and network health. Mitochondrial morphology assessment was carried out microscopically, by measuring two parameters - aspect ratio and eccentricity. These parameter measurements were performed using automated script generated in CellProfiler, an image analysis software pipeline to quantify intracellular mitochondrial morphology and fluorescence intensity. Aspect ratio measures the ratio of height to width, a high aspect ratio measurement is associated with an elongated mitochondrial morphology (fusion), while a lower aspect ratio is associated with a more circular morphology (fission). Eccentricity is the ratio of length of the short axis to the length of the long axis, where 0 is a perfect circle and 1 is a line. High eccentricity is a measure of elongation (fusion) and closer to 0 is representative of a circular morphology (fisson). To assess mitochondrial morphology, WT and *Casp11*$^{-/-}$ BMDM were left untreated (M0) or stimulated for 6 hours with M1 cytokines (100ng/mL LPS and 50ng/mL IFNγ). While there are no significant differences in mitochondrial morphology between resting (M0) or M1 WT compared to *Casp11*$^{-/-}$ BMDM, there is a trend that M0 and M1 *Casp11*$^{-/-}$ have a more elongated morphology (fusion), while WT have a more spheroid morphology (fisson) (**Fig. 3.12 A-B**). While elongated mitochondria are observed in both WT and *Casp11*$^{-/-}$ M1 BMDM, it is unsurprising that the shortened fragmented mitochondria appear more frequently in WT M1 BMDM.

Dependent upon mitochondrial damage, fragmented mitochondria either fuse to mix mtDNA content and generate a health network or undergo mitophagy[269]. Therefore, it is unsurprising that, in the absence of caspase-11, there is an increase in fused elongated mitochondria as mitophagy can proceed. Further analysis, measuring the fold changes in aspect ratio and eccentricity in M1 macrophages compared to resting M0 macrophages showed significant differences in circular (WT) vs elongated (*Casp11*$^{-/-}$) mitochondrial morphologies (**Fig. 3.12 C-D**). Therefore, in this snapshot of treatment with M1 polarising cytokines for 6 hours, we observe higher induction of fission in WT mitochondria, suggesting mitochondrial damage and an increased requirement for mitochondrial maintenance and mitophagy in M1 polarised WT BMDM, compared to *Casp11*$^{-/-}$ BMDM.

Mitochondrial membrane potential is closely linked with integrity and mitophagy. Therefore, we wanted to determine whether caspase-11 is involved regulation of mitochondrial membrane potential (ΔΨM). WT and *Casp11*$^{-/-}$ BMDM were stimulated with M1 polarising cytokines for 6 hours, followed by TMRM intensity staining as a measure of ΔΨM. TMRM accumulates in active mitochondria with intact ΔΨM, where healthy functioning mitochondria have a bright signal, but loss of membrane potential will dim the signal. Lower TMRM staining is indicative of membrane depolarization. Data reveals significantly higher TMRM staining intensity in resting M0 *Casp11*$^{-/-}$ BMDM, compared to WT (**Fig. 3.13 A-B**), suggesting that basal mitochondrial network health is greater in the absence of caspase-11. However, following 6 hour M1 stimulation, TMRM intensity significantly increases in WT BMDM, to levels more similar to that observed in *Casp11*$^{-/-}$ BMDM (**Fig. 3.13 A-B).** This result was contrary to the result that we predicted, we expected that M1 polarised WT mitochondria would have decreased ΔΨM, indictive of impaired function and a prerequisite for mitophagy, as depolarization although not alone precedes the translocation of PINK1 at the OMM[153]. However, previous reports have demonstrated increased ΔΨM during proinflammatory responses in BMDM[270]. Mills and colleagues suggest that LPS activated cells, which generate ATP by glycolysis, have a higher ΔΨM, as protons pumped through ETC complexes across the inner mitochondrial membrane are no longer being used by ATP synthase to generate ATP[270]. This study suggests that the M1-mediated shift from oxidative phosphorylation to glycolysis and consequent increased ΔΨM provides a pro-inflammatory signal, increasing mitochondrial ROS to contribute further to inflammation[153].

Previous reports in the literature have shown that caspase-11 plays a role in PINK1 degradation, inhibiting mitophagy[256]. As previously discussed, mitochondrial dynamics and induction of mitophagy will eliminate accumulated mtDNA from the cytosol which would otherwise trigger STING activity and a type I IFN innate immune response[156,157]. We therefore hypothesised that caspase-11-mediated PINK1 degradation and mitophagy inhibition instigates the type I IFN-STAT1-iNOS response that we have previously shown to be driven by caspase-11 in response to LPS stimulation.

To investigate the role of mitophagy in LPS induced iNOS expression, WT BMDM were treated with ivermectin (0.1-1μM), an antiviral drug with multiple mechanisms of action including the induction of acute mitochondrial damage, as observed by decreased OCR and fragmentation of the mitochondrial network, leading to the induction of PINK1-Parkin-dependent mitophagy[271,272,273]. Pretreatment with ivermectin before LPS stimulation was performed to determine whether induction of mitophagy would impair iNOS expression and NO production, similar to observations in *Casp11*$^{-/-}$ BMDM. We found that BMDM pretreated with ivermectin had decreased expression of iNOS (**Fig. 3.14 A**) and significantly reduced NO production (**Fig. 3.14 B**) following LPS stimulation. This is consistent with previous reports in the literature in which ivermectin has been shown to inhibit LPS-induced production of inflammatory cytokines by blocking NF-κB, NO and PGE2 production, as well as NOS2 and COX2 upregulation, by inhibiting phosphorylation of MAPK, p38, ERK1/2, and JNK in macrophages[272,274]. These data confirm the ability of a pharmacological inducer of mitophagy to suppress LPS-mediated NO production, supporting the hypothesis that LPS-mediated inhibition of mitophagy drives macrophage iNOS expression and NO production.

As previously mentioned, Patoli and colleagues reported a novel role for inflammatory caspases in the inhibition of PINK1-Parkin dependent mitophagy[255,256]. The study by Patoli and colleagues reported that caspase-1 and caspase-11 enzymatic activity mediated PINK1 degradation in a STAT1 dependent manner. Reduced PINK1 expression, observed during an LPS timecourse in BMDM, is associated with defective mitochondria[256]. STAT1-deficient macrophages basally have higher PINK1 expression and LPS-mediated inhibition is less pronounced compared to WT. It is noteworthy that the STAT1 deficient mice used in this study are of the 129SV genetic strain, which do not express caspase-11. Patoli and colleagues also observe increased PINK1 expression in Casp11 siRNA Raw264.7 immortalised macrophage cell line stimulated with M1 polarising cytokines compared to scrambled control[9]. Therefore, our next aim was to investigate the role of caspase-11 during mitophagy in macrophages in response to inflammatory stimuli.

The role of caspase-11 in PINK1-Parkin dependent mitophagy was investigated by LPS-stimulating WT and *Casp11*$^{-/-}$ BMDM over a 24 h timecourse. A modest increase in PINK1 expression was observed in response to LPS stimulation in WT BMDM (**Fig. 3.15**). In contrast, and similar to STAT1-deficient 129SV BMDM, *Casp11*$^{-/-}$ BMDM showed rapidly increased PINK1 expression within 30 mins LPS stimulation, which was sustained until 24 h (**Fig. 3.15**). This suggests that in the absence of caspase-11, PINK1 degradation is impaired and mitophagy can proceed. As mitophagy is a specialized form of autophagy which functions to scavenge impaired mitochondria, we also investigated the expression of the classical autophagy markers, p62 and LC3, expressed downstream of PINK1-Parkin mediated mitophagy[275]. Through assistance and connection with Parkin, p62 is essential for the regulation of mitophagy, therefore aberrant p62 can disturb mitophagy and mitochondrial quality. Typically, during autophagy LC3-I, microtubular and cytoplasmic, is lapidated to LC3-II, associated with autophagosome membranes. P62 then localizes at the autophagosome with LC3-II. P62 acts as a recognition receptor for dysfunctional mitochondrial ubiquitination. Parkin directly interacts with and ubiquitinates p62 at K13 to promote proteasomal degradation[276]. However, Lazarou found that PINK1 recruited autophagy receptors NDP52 and optineurin, but not p62, independent of parkin[277]. Therefore, although the role of p62 during mitophagy is controversial, it is considered that parkin recruits p62 to mediate mitophagy and manage mitochondrial quality control. Therefore, we also measured p62 and LC3 expression in WT and *Casp11*$^{-/-}$ BMDM following a 24 hour LPS timecourse.

Increased expression of LC3-II in WT BMDM was observed following 8 and 24 h exposure to LPS, however increased LC3-II expression was not evident in *Casp11*$^{-/-}$ BMDM (**Fig. 3.15**). Lapidation of LC3-I to LC3-II is important for the recruitment of p62, for consequential degradation during autophagy. However, accumulation of LC3-II without degradation of p62 is indicative of stalled autophagy. We observed p62 accumulation after 2 h following LPS stimulation in both WT and *Casp11*$^{-/-}$ BMDM with increased accumulation over a 24 h timecourse (**Fig. 3.15**). In WT BMDM, LPS stimulated the conversion of LC3-II at 8-24h and p62 accumulation, suggesting impaired autophagy, while in *Casp11*$^{-/-}$ BMDM p62 is upregulated but LC3-II does not accumulate (**Fig. 3.15**). Several studies have reported a role for TLR4 signalling in autophagy. Similar to our findings, LPS stimulation was shown to mediate LC3-II conversion and p62 accumulation in a time dependent manner[278]. In the absence of caspase-11, we observe increased p62 accumulation with a lack of corresponding LC3-II accumulation (**Fig. 3.15**). To further investigate autophagic flux we next aimed to use autophagy inhibitor, bafilomycin-A1 (BAF-A1).

The role of caspase-11 during autophagic flux (the balance between autophagosome generation and clearance) in TLR4-stimulated BMDM was assessed utilizing bafilomycin-A1, a late-stage autophagy inhibitor which functions to prevent autophagosome and lysosome fusion. WT and *Casp11*$^{-/-}$ BMDM were stimulated with LPS over an 8-hour timecourse, before treatment with bafilomycin-A1 for 2 hour prior to harvesting. Western blot analysis revealed that treatment of WT BMDM with BAF-A1increased caspase-11 expression following 8 hour LPS stimulation (**Fig. 3.16**). Therefore, inhibition of autophagy appears to stimulate caspase-11 expression during this proinflammatory response. Analysis for expression of the autophagy markers p62 and LC3-II revealed that treatment with BAF-A1 increased p62 and LC3B accumulation in LPS-stimulated WT BMDM, suggesting that BAF-A1 treatment stalled the autophagic flux in these cells. While LC3-II expression similarly increased following BAF-1A treatment in *Casp11-/-* BMDM. Difference in p62 expression were not observed in *Casp11*$^{-/-}$ BMDM (**Fig. 3.16**). These data suggest that autophagic flux is already stalled or is absent in LPS-stimulated *Casp11*$^{-/-}$ BMDM, as treatment with an autophagy inhibitor does not alter the expression of p62 or LC3-II. Data generated to date suggests that caspase-11 inhibits mitophagy following LPS stimulation, supported by results which show that *Casp11*$^{-/-}$ macrophages have higher levels of PINK1 and p62 upregulation, but lower levels of Parkin and LC3-II accumulation, compared to WT. Inhibition of autophagic flux, using BAF-A1, revealed that autophagy markers LC3-II and p62 accumulated in WT but not *Casp11*$^{-/-}$ BMDM, suggesting that caspase-11 is involved in mediating basal autophagy.

Disturbance in mitochondrial dynamics mediated by mitophagy regulates type I IFN response and later mitochondrial ROS production. Increased mtROS levels inhibit TLR9 induced type I IFN production via blocking IRF7 phosphorylation[279]. Jezek and colleagues proposed a model in which a mitochondrial fragmented phenotype and ROS production are interconnected[280]. ROS are a byproduct of OXPHOS, generated due to incomplete oxygen reduction. Chronic or excessive exposure to ROS can induce cellular stress and activate pro-survival pathways including mitophagy. A previous report by Hegazi revealed that caspase-11 involvement during MRSA infection impaired mtROS production[97], suggesting that in the absence of caspase-11 increased mtROS may activate mitophagy. As previous reports show that mtROS inhibits IFNβ production, this suggests that caspase-11 may affect mtROS production to mediate IFNβ production in our system. Therefore, we aimed to investigate the role of caspase-11 in mtROS production in response to proinflammatory stimuli.

WT and *Casp11*$^{-/-}$ BMDM were LPS stimulated for 24h and mitochondrial superoxide production was measured using Mitosox red reagent. Antimycin A, an inhibitor of ETC complex II, served as a positive control for superoxide production. In response to LPS stimulation WT BMDM had suppressed mtROS levels relative to non-treated control (**Fig. 3.17**). In contrast, LPS stimulated *Casp11*$^{-/-}$ BMDM had elevated mtROS production relative to untreated control (**Fig. 3.17**). LPS induced mtROS production from *Casp11*$^{-/-}$ BMDM was of similar median fluorescent intensity as antimycin A (positive control), whereas addition of antimycin A markedly increased mtROS production in WT BMDM. In response to LPS, *Casp11*$^{-/-}$ BMDM had significantly elevated levels of mtROS compared to WT (**Fig 3.17 C**). These data suggest that caspase-11 limits mtROS production in response to proinflammatory stimuli. Previous reports have shown that inhibition of mitophagy causes increased mtROS[268,281]. Therefore, as we observe increased PINK1 mitophagy accompanied by elevated mtROS production in the absence of caspase-11, we hypothesise that, mitophagy induced mtROS limits NO production in the absence of caspase-11.

Lastly, we proposed that inhibition of mitophagy and accumulation of fragmented damaged mitochondria following LPS stimulation mediates cytoplasmic mtDNA induction of IFNβ and NO production. LPS induces mtDNA synthesis and release into the cytosol, contributing to STING and NF-κB activation, promoting type I IFN responses and proinflammatory cytokine release[282]. Defective mitophagy is a source of mtDNA cytosolic leakage leading to STING activation in macrophages[156]. Therefore, we hypothesized that LPS-mediated inhibition of mitophagy may cause release of mtDNA into the cytosol, leading to IFNβ activation and NO production. We proposed that treatment of *Casp11*$^{-/-}$ BMDM with the synthetic dsDNA mimic and TLR9 ligand, poly(dA:dT), would rescue their ability to induce NO production. As we previously observed that exogenous IFNβ induction of NO production required LPS co-stimulation, WT and *Casp11*$^{-/-}$ BMDM were primed with LPS overnight followed by poly(dA:dT) transfection for 4 h. Results show that LPS primed BMDM transfected with endosomal membrane TLR9 ligand poly(dA:dT) have elevated expression of NO production in WT and *Casp11*$^{-/-}$ BMDM (**Fig. 3.18 A**). As previously illustrated *Casp11*$^{-/-}$ BMDM have impaired NO production at 24h after LPS stimulation. However, these results show that an exogenous source of dsDNA can rescue NO production, as observed by no difference in nitrite production between WT and *Casp11-/-* after LPS prime followed by poly(dA:dT) transfection.

Therefore, our proposed mechanism for caspase-11 regulation of NO production involves inhibition of mitophagy and consequent mtDNA cytosolic leakage, to promote type I IFN responses to regulate autocrine signalling of STAT1 transcription and iNOS expression, thereby inducing NO production.

3.4. Summary of main findings of Chapter 3

- Caspase-11-mediated regulation of iNOS following LPS stimulation is dependent on type I IFN-STAT1 signalling and is not due to direct interaction of caspase-11 and STAT1.
- Exogenous IFNβ stimulation after LPS priming rescues the ability of caspase-11 deficient macrophages to induce NO production.
- The enzymatic activity of caspase-11 is required for its role in NO production, however gasdermin D cleavage and pyroptosis are not involved.
- During mitochondrial fusion-fission cycling, caspase-11 contributes to the accumulation of fragmented small, damaged mitochondria following proinflammatory stimuli.
- Caspase-11 regulates expression levels of the mitophagy marker, PINK1, thereby leading to the inhibition of mitophagy and these fragmented damaged mitochondria.
- The TLR9 ligand, poly(dA:dT), as a mimic of mtDNA cytosolic leakage, rescues NO production in caspase-11 deficient macrophages.

3.5. Discussion

In this study, we illustrate that STAT1-IFNβ autocrine signalling mediated iNOS expression and NO production is dependent upon caspase-11, independent of the non-canonical inflammasome and pyroptosis. Type I IFN supports iNOS expression synergistically with proinflammatory stimuli, coinciding with enhanced STAT1 binding to iNOS promoter region[283]. NO is a key regulator of the M1 macrophage immunometabolic shift towards glycolysis and mediator of proinflammatory activation. Therefore, a concise understanding of NO regulation in response to proinflammatory events is of importance. While the crucial role of type II IFN during iNOS expression is well-known, research on the role of type I IFN during iNOS transcription is lacking, although previous research reports IFNα/β driving human and murine macrophage iNOS expression.

3.5.1. TLR dependent type I IFN STAT1 activation kinetics

STAT1 and NF-κB are of particular importance during regulation of iNOS gene transcription. STAT1 mediated iNOS expression is biochemical pathway and cell-dependent, as the STAT1 homodimer or the STAT2-IRF9 complex (ISF-3) can support iNOS expression[283]. Data reveals that LPS regulated STAT1 phosphorylation induced iNOS expression, as in the absence of caspase-11 early STAT1 phosphorylation at 2-4h is impaired and NO production is reduced compared to WT BMDM. However, we observe no caspase-11 regulated difference in STAT2 phosphorylation in response to LPS, suggesting that LPS induced iNOS expression in BMDM is STAT1 homodimer activated and regulated by caspase-11. Additionally, we found no altered phosphorylation of STAT1 at S727, which is rapidly induced by TLR ligands and is independent of IFN autocrine signalling.

The Creagh Lab previous study revealed that LPS mediated STAT1 activation occurs via type I IFN autocrine signalling, utilising IFNAR$^{-/-}$ BMDM[284]. In our current study we show that LPS-mediated caspase-11 expression regulates IFNβ secretion. Additionally, we showed the downstream impact of caspase-11 mediated IFNβ secretion on iNOS expression and subsequently NO production. Previous reports have implicated IFNα/β autocrine signalling to be critical for induction of murine STAT1 activation and iNOS expression induced by TLR ligands[246],[248]. However, we observed IFN-β alone could not induce NO production, yet in combination with LPS stimulation IFN-β rescued NO production in the absence of caspase-11. Previous studies have similarly shown IFN-β (100-500U/mL) could not induce NO production, but in combination

with IL-1β and TNF-α, enhanced NO production was shown at 24 hours continuing for 48 hours[283]. In this study Bachmann and colleagues found that IFN-β mediated STAT1 phosphorylation enhanced binding to GAS/ISRE-promoter region, required for elevated iNOS expression. Additionally, in response to *Listeria Monocytogenes* in macrophages, Wienerroither and colleagues describe IFN-I/ISGF3 and NF-κB synergism to promote the production of iNOS. NF-κB promoter priming via transcriptional elongation and type I IFN induced ISGF3 association with core mediator at transcriptional start site for polymerase II binding[285]. Initially, NF-κB binds *Nos2 promoter,* coined transcriptional memory effect, leading to subsequent IFN-I-dependent ISGF3 transcriptional activity. NF-κB is necessary for the recruitment of TFIIH and pTEFb, the complexes containing the RNA polymerase II (Pol II) kinases CDK7 and CDK9, whereas ISGF3 is essential for binding of the general transcription factor TFIID and Pol II[286].

Within the murine iNOS promoter, a specific region (−912 to −1,029 bp relative to the transcription start site) was found to mediate STAT1-induced iNOS transcriptional activation which may be achieved by STAT1-homodimers (in response to IFNγ or type I IFN) or by the type I IFN/ISGF3 axis. STAT1 binding elements, GAS/ISRE sequence (−951 to −935 bp) bind STAT1 homodimers or ISGF3, and an additional ISRE site (−924 to −912 bp) also binding ISGF3, adjacent to iNOS promoter. Therefore, for future work we proposed investigating STAT1 binding to this region in the absence or presence of caspase-11, and potential role of IFN-β supporting enhanced STAT1-dependent transcriptional activity of iNOS promoter, utilising ChIP analysis. Additionally, to illustrate LPS mediated NF-κB activity is required to induced iNOS expression, besides regulating IFN-β production. We propose inhibiting LPS mediated NF-κB, using IκB inhibitors, in combination with exogenous IFN-β stimulation.

Cruz and colleagues reported that Jak/STAT signalling pathway in combination with IκB-α degradation in response to LPS is important for iNOS expression[32]. Investigation of IFNα/β autocrine signalling induction of murine STAT1 activation and iNOS expression induced by TLR ligands found that endogenous IFNβ detection correlates with STAT1 phosphorylation and IRF-1 kinetics. IFNβ neutralising antibody attenuates LPS-induced iNOS expression[246,248]. Mechanistically, Jacobs and colleagues describe a model for LPS induced iNOS expression suggesting LPS mediated NF-κB activation transcribed and translated IFNβ 2-4 hours post TLR4 ligand binding. IFNβ autocrine signalling via IFNAR results in rapid STAT1 phosphorylation within 30 minutes of secretion. pSTAT1 mediated IRF1 expression which acts in concert with NF-κB and STAT1 to promote iNOS expression[248]. These data support our findings which show that LPS induced caspase-11 expression regulates IFNβ-mediated STAT1 activation and iNOS expression.

The kinetics of our findings similarly reveal that LPS mediated IFNβ secretion is first detectable 2 h post-stimulation and that exogenous IFNβ induces rapid induction (30 mins) of STAT1 Y701 phosphorylation. In response to TLR4 signalling, STAT1 Y701 phosphorylation is evident at 2 h post stimulation and resolves by 8 h, correlating with IFNβ release and activity timeframe. However, the impact of caspase-11 during LPS induced STAT1 activation, which we propose to be type I IFN dependent, has altered kinetics. Firstly, in response to LPS, *Casp11*$^{-/-}$ BMDM have a similar IFNβ secretory profile as WT BMDM at early timepoints. It is not until 24h time point that we see significant differences in IFNβ secretion in WT compared to *Casp11*$^{-/-}$ BMDM. However, we observe impaired STAT1 Y701 phosphorylation at 2-4 h in response to LPS stimulation in *Casp11*$^{-/-}$ BMDM, which is resolved by 8 h. During this timeframe we have found IFNβ levels to be similar between WT and *Casp11*$^{-/-}$, although a non-significant reduction in IFNβ secretion was observed in *Casp11*$^{-/-}$ at 2 h compared to WT, which only becomes significant by 24h. These kinetics suggest there is a late-stage type I IFN response which is enhancing iNOS expression.

STAT1 activation by TLR ligands has been reported to be a biphasic event, with early activation (<3h) predominantly type I IFN dependent. Dempoya and colleagues found in response to poly(I:C) initial pSTAT1 activation is RIG-I- IFNβ dependent as targeting IFNAR suppressed initial poly(I:C) induced STAT1 phosphorylation. However, late STAT1 phosphorylation (>8h) is neither type I IFN or RIG-I dependent[241], demonstrating TLR ligand-mediated STAT1 phosphorylation kinetics is autocrine type I IFN-dependent. Due to the heterogeneity of type I IFN response to viral infections, molecular studies have further illustrated the bimodal nature of IFN-β expression. Hwang and colleagues observed, using Cy5-labelled poly(I:C) and IFNβ-GFP reporter cells, two distinct IFNβ expressing populations. While 95% poly(I:C) was transfected after 8 hours, only 37% of cells were GFP-positive[287]. To examine if this effect was due to delayed production, a further 14-hour time course was examined to determine whether GFP-positive cells express higher GFP at later stage than GFP-negative cells. This single cell approach illustrated that type I IFN is expressed in a minority of cells although dsRNA has successfully been transfected, and without early stage IFNβ production, late stage IFNβ production is impaired.

In addition to autocrine IFNβ signalling, there are several routes to restrain STAT1 phosphorylation, including; 1. cytoplasmic phosphatase, dephosphorylating receptor activity; 2. SOCs, induced by STATs, binding the receptor to stall signalling; and 3. PIAS blocking STAT1 binding chromatin[288]. IFN signalling activation is transient, requiring kinase mediated phosphorylation to activate the signalling cascade, with the duration of phosphorylation

controlling the duration of ISG induction. Phosphatase mediated dephosphorylation events are crucial in restricting IFN responses.

However, LPS mediated pSTAT1 is not type II IFN dependent as *ifnγ*-/- LPS stimulated BMDM do not have impaired STAT1 phosphorylation. While we previously observed that LPS mediated STAT1 activation is type I IFN dependent, as *ifnar-/- LPS stimulated BMDM have impaired STAT1 phosphoylation*[284]. Although we had not identified the type I IFN signalling cascade regulated by caspase-11. In the absence of caspase-11, early Jak1 phosphorylation and STAT1 phosphorylation (<4h) in response to LPS is impaired. We observed a trend of reduced IFN-β at 2h in *Casp11-/-* BMDM, however differences between genotypes do not become significant until 24h, when STAT1 activation is already resolved. We suggest that the prolonged type I IFN secretion illustrated in WT BMDM after 24h LPS may elevate iNOS expression, in addition to the enhance iNOS expression. As we observed type I IFN secretion is only dependent on caspase-11 at later timepoint of 24h, future studies could treat LPS stimulated BMDM after 8 hour with anti-IFNβ antibody to determine the impact of late stage IFNβ secretion on iNOS expression and NO production, while retaining potential early (2-4h) type I IFN mediated autocrine STAT1 phosphorylation and IRF1 activity. Additionally, pretreatment with anti-IFNβ neutralising antibody would also validate previous IFNAR-/- results and demonstrate the importance of early IFNβ signalling.

3.5.2. Mitophagy in M1 macrophage polarisation – influence on type I IFN response

Type I IFNs are most commonly known as anti-viral cytokines rapidly induced by a plethora of PAMPS including viral- or bacterial-derived dsRNA, ssRNA, glycoproteins, or LPS recognised by PRRs. Additionally, host DNA and RNA is also capable of inducing type I IFN via cytosolic DNA sensors which recognise self-PAMPs in damaged cells. The mechanism for LPS induced type I IFN expression is well described as being mediated through TRIF and TRAF3, involving TBK-1 and IKKε activation, leading to IRF-3/7 phosphorylation which induces type I IFN production. However, identifying the mechanisms governing the recognition of self-PAMPs to generate type I IFN responses is also important for understanding sterile inflammation and anti-tumour effects. We propose that cytosolic DNA sensing may account for the late stage (24 h) differences in LPS mediated type I IFN secretion observed in the absence of caspase-11. Huang and colleagues reported LPS enhanced DNA-induced IFN-β production via cGAS activity. LPS inhibition of

autophagy, indicated by high LC3I:LC3II expression and p62 accumulation, is proposed to activate cGAS activity. While combined LPS stimulation and DNA transfection induced autophagy, these stimuli enhanced IFN-β production 24h post transfection[289].

Patoli and colleagues investigation of mitophagy driven macrophage anti-bacterial defence during sepsis, showed the inhibitory role of caspase-11 on mitophagy during M1 polarisation[256]. Our findings support this study, as we found in the absence of caspase-11, PINK1 expression is upregulated in response to LPS, compared to WT BMDM. Reports have found this autophagy dysfunction in response to LPS leads to the release of mtDNA into the cytosol, contributing to NLRP3 activation and IL-1β and IL-18 secretion[290]. Therefore, while Patoli illustrated caspase-11 inhibited PINK-1 mediated M1 induced mitophagy in murine macrophages, we speculate that impaired mitophagy during inflammation results in cytosolic DNA sensing induces IFN-β secretion, which enhances iNOS expression and NO production.

The mitochondrial healthy network is maintained by a dynamic process of fusion and fission, which is intimately associated with mitophagy. Stress induced fragmentation of mitochondria leads to mitophagy as damaged mitochondria accumulate. Fusion is associated with the compensation of missing components, leading to the mixing of two mitochondria to rescue the impaired organelle. Hence, fusion mitigates PINK-1 mediated mitophagy[291]. However, mutation of the fission associated protein, Drp1, inhibits mitophagy, suggesting that fission is required for the induction of mitophagy[292]. While the mitochondrial morphology of *Casp11*$^{-/-}$ BMDM is found to be elongated and in a state of fusion, we also found that PINK1 expression was elevated across a 24h timecourse, compared to their WT counterparts, suggesting that LPS induces mitophagy in the absence of caspase-11. We observed higher numbers of WT BMDM undergoing fission, as observed by less elongated morphology, which had been reported to be an indicator of mitophagy [269]. However, we suggest that the absence of mitophagy in WT LPS BMDM, consequent with the lack of PINK-1, results in an accumulation of damaged mitochondria under fission which cannot be cleared. Therefore, while initially these findings in the absence of the caspase-11 appear to contrast with fission induced mitophagy, we suggest the higher volume of mitochondrial fusion in *Casp11*$^{-/-}$ BMDM is due to mitophagy clearance of damaged mitochondria associated with fission. These data reveal an inhibitory role for caspase-11 during mitophagy, leading to type I IFN-mediated iNOS expression.

Emerging research is implicating mitophagy in the role of type I IFN production, IL-1β secretion and apoptosis. While mechanistic understanding is unclear, mtDNA accumulation in cytosol or

the extracellular space triggers type I IFN and ISGs. Cytosolic mtDNA binds cGAS, which catalyses ATP and GTP to synthesis cGAMP, which acts as a messenger to activate STING, which further activates TANK-binding kinase 1 (TBK1) via its C terminal PLPLRT/SD motif. TBK1 promotes IRF3 dimerization and translocation into the nucleus, where it triggers the expression of type I IFN and various ISGs[155]. Additionally, mtDNA is a potential ligand for TLR9 as extracellular oxidized mtDNA has been shown to induce the TLR9- and IRF7-dependent production of IFN-α to augment type I IFN responses[293]. We also observe increased mtROS in the absence of caspase-11, which has previously been implicated to inhibit TLR9 induced type I IFN production via blocking IRF7 phosphorylation[31], suggesting mtROS detected in the absence of caspase-11 may negatively impact cytosolic mtDNA mediated type I IFN response.

Mitochondrial dysfunction is associated with increased iNOS expression and NO production, while excessive NO production is known to feedback on damaged mitochondrial proteins and autophagy repair pathways to enhance bioenergetic dysfunction[294]. Similar to these reports, we have shown that pretreatment with the mitophagy inducer, ivermectin, in LPS stimulated BMDM leads to impaired NO production. Ivermectin has been demonstrated to limit expression of type I and type II IFN and ISGs, promoting an M2-like macrophage phenotype[295]. Previous reports have linked poly(I:C) with enhanced NO production, in combination with a priming stimuli mediating NF-κB activity. These studies support our findings which indicate that poly(dA:dT) alone cannot induce NO production. However, in combination with LPS priming poly(dA:dT) induces NO in *Casp11*$^{-/-}$ BMDM to similar levels as those observed in WT BMDM. Herein data presented suggests that mitophagy released mtDNA induced NO production is regulated by caspase-11. However, we have yet to confirm that the accumulation of cytosolic mtDNA in WT BMDM compared to *Casp11-/-* leads to IFNβ-mediated NO production.

As we observe caspase-11 mediated late IFN-β secretion, we hypothesise that this is a consequence of mitophagy inhibition and damaged mitochondria, leading to activation of the DNA sensing STING pathway. To determine whether the role of caspase-11 in mitophagy influences late stage type I IFN production, we hypothesise that mitophagy induced in LPS stimulated WT BMDM will impair late stage IFNβ expression. As we have yet to show that accumulation of cytosolic mtDNA differs in WT BMDM compared to *Casp11-/-* , leading to STING or TLR9 mediated IFNβ-mediated NO production, a future experiment measuring cytosolic accumulation of mtDNA compared to mitochondrial residing mtDNA could be performed. We hypothesise that clearance of cytosolic mtDNA by treatment with ethidium bromide would reduce type I IFN production and NO production. In parallel, we suggest that, in the absence of

caspase-11, treatment with mitophagy inhibitors, such as chloroquine/ liensinine, would enhance mtDNA release and mediate type I IFN induced NO production.

Wang and colleagues reported LPS induced inflammation in macrophages is alleviated by damaged mitochondria clearance by PINK1 mediated mitophagy[14]. PINK1 siRNA led to increased ROS, IL-1β and TNF-α following LPS stimulation, revealing that PINK1 mediated mitophagy dampens inflammatory responses. Similar reports further support the role of mitophagy during innate immune responses[256]. While programmed mitophagy has been previously shown to reprogram metabolism towards OXPHOS[296]. Miyazaki and colleagues found PINK1 regulates mitochondrial activation through mitophagy by glycolytic suppression[297], as following glycolytic suppression mitophagy is dependent on PINK1. Therefore, autophagy is not only a driving force of OXPHOS but is also enhanced by suppression of glycolysis.

Therefore caspase-11 role during mitophagy may be linked to macrophage metabolism and functionality. Additionally, NO mediated by caspase-11 is central to M1 macrophage polarisation and immunometabolism. In the next chapter, we aim to investigate the potential role of caspase-11 in mediating NO production during macrophage 'classical' activation.

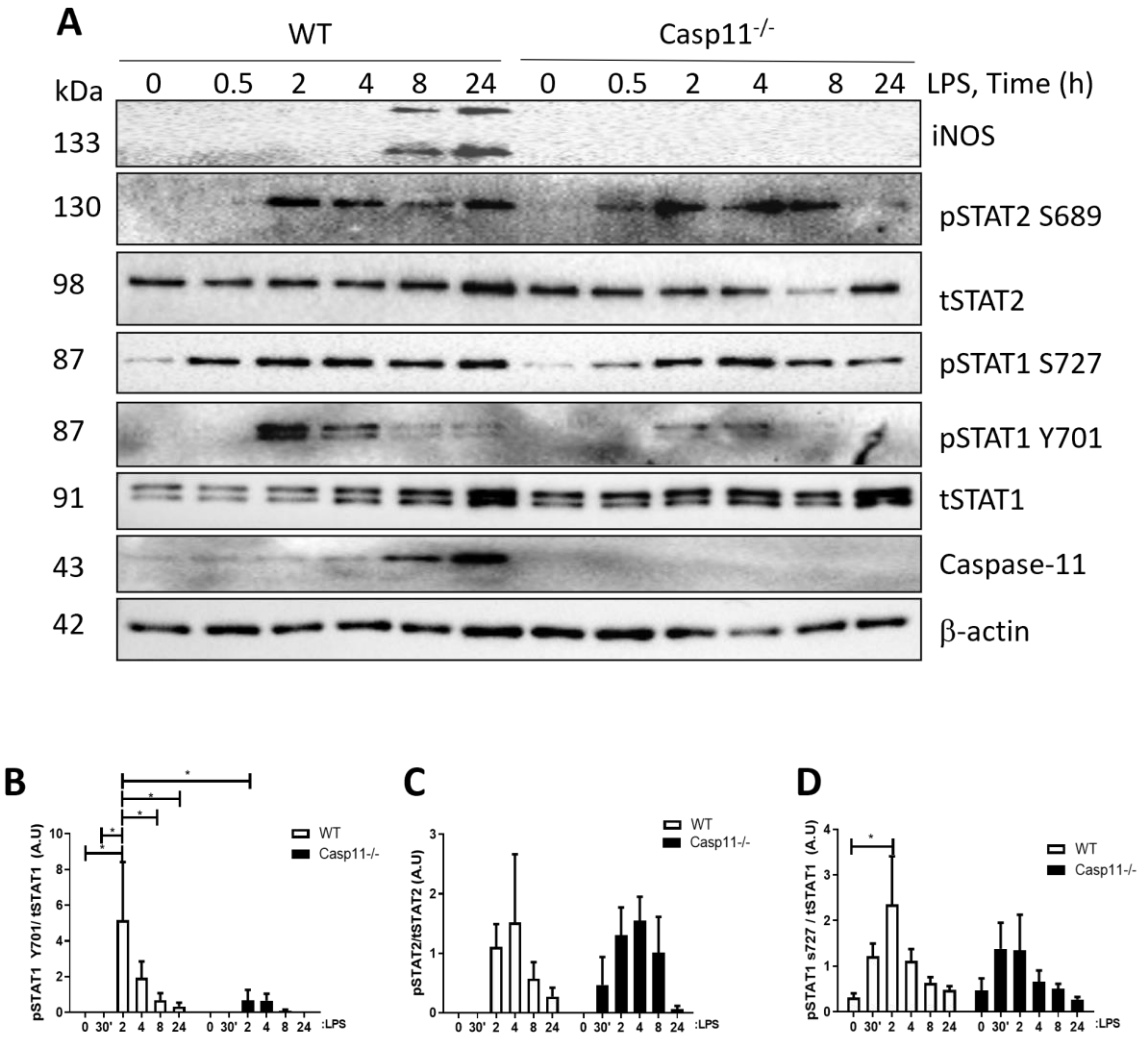

Figure 3.1: Caspase-11 regulates STAT1 phosphorylation on Tyrosine 701 in murine macrophages, following LPS stimulation

WT and *Casp11*$^{-/-}$ BMDM were seeded at 10^6 cells/ ml in 24 well plate 24 h prior to treatment. Cells were stimulated with LPS (1 mg/mL) over a 24 h timecourse, as indicated. Whole cell lysates of WT and *Casp11*$^{-/-}$ BMDM (20 µg) were analysed for expression of (A) pSTAT2 Y689, total STAT2 (tSTAT2), pSTAT1 S727, pSTAT1 Y701, total STAT1, caspase-11 and β-actin, as loading control. Blots are representative of three independent experiments. Densitometry analysis was performed of (B) pSTAT1 Y701 (relative to tSTAT1), (C) pSTAT2 Y689 (relative to tSTAT2), (D) pSTAT1 Y727 (relative to tSTAT1) and) (n=3) and were analysed by two-way ANOVA; *p<0.05, **p <0.01 (Tukey post-test).

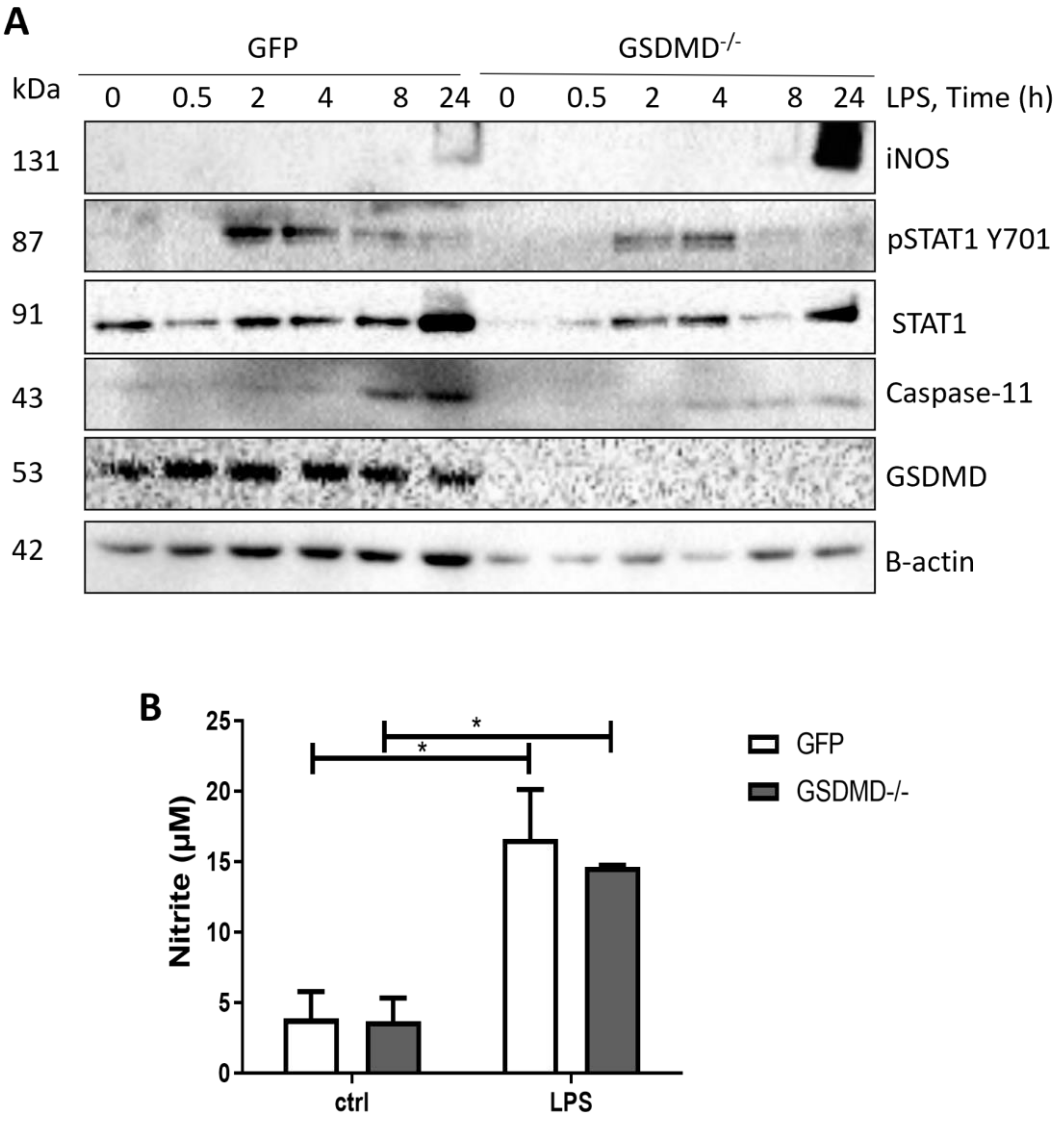

Figure 3.2: Caspase-11 regulation of STAT1 tyrosine 701 phosphorylation, iNOS induction and NO production is independent of GSDMD

GFP and *Gsdmd*$^{-/-}$ iBMDM were seeded at 10^6 cells/ ml in 24 well plate. 24 h later, cells were stimulated with LPS (1 μg/mL) over a 24 h time-course, as indicated. Whole cell lysates of GFP and *Gsdmd*$^{-/-}$ iBMDM $^{-/-}$ (20 μg) were analysed by western blot for expression of (A) iNOS, pSTAT1 Y701, total STAT1, caspase-11, GSDMD and β-actin, as loading control. Blots are representative of three independent experiments. Supernatants were analysed for (B) nitrite production by Griess assay (n=3) and analysed by two-way ANOVA; *p <0.05 (Sidak post-test).

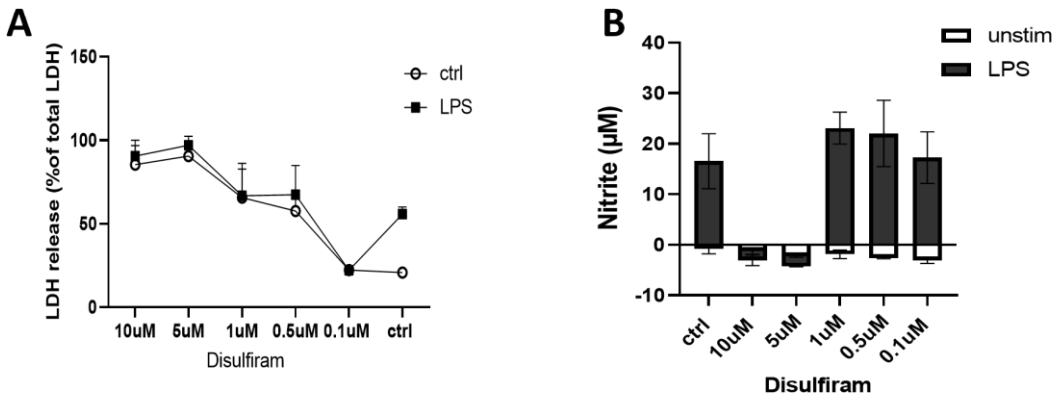

Figure 3.3: Non-toxic doses (<0.1µM) of the GSDMD inhibitor, disulfiram, inhibit LPS mediated pyroptosis but do not affect NO production

BMDM were seeded at 10^6 cells/ ml in 96 well plate. 24 h later, cells were pre-treated with disulfiram for 1 h at the indicated concentration range. BMDM were subsequently stimulated with LPS (1 ug/ml) for 24 h. Supernatants were analysed for: (A) Cell death, determined by CytoTox96 cytotoxicity assay which measures LDH release (analysed as % LDH released relative to maximal LDH); and (B) Nitrite production, using Griess assay. Statistical analysis was performed using two-tailed *ANOVA* test to compare disulfiram treated and untreated BMDM mean ± SEM values from 3 independent experiments.

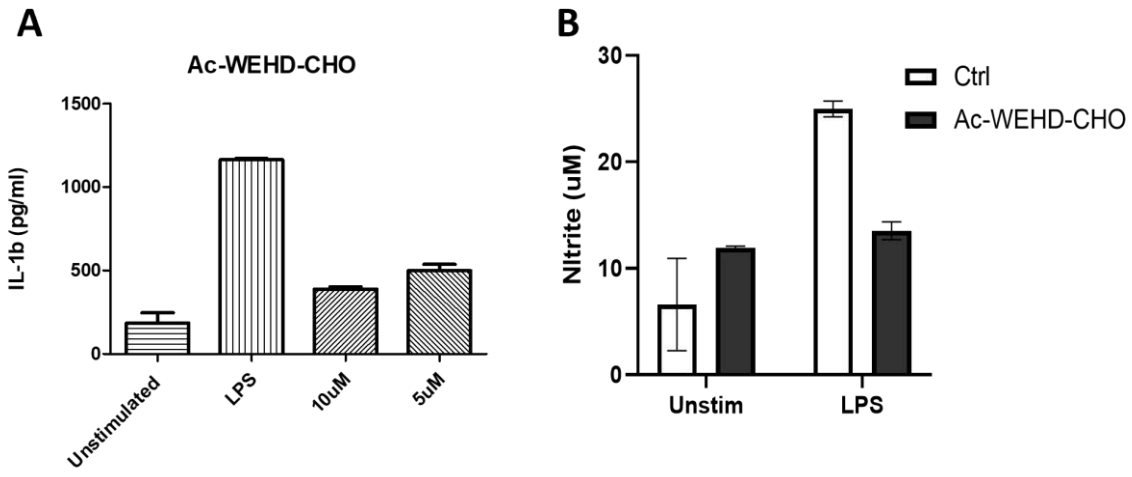

Figure 3.4: Caspase inhibitor Ac-WEHD-CHO impairs LPS induced NO production

(A) PMA differentiated (10ng/mL for 48h) THP-1 cells were pre-treated with Ac-WEHD-CHO (at indicated concentration range) followed by LPS (1µg/mL, 24 h) stimulation. Supernatants were analysed for IL-1β secretion by ELISA. (B) WT BMDM (seeded at 10^6 cells/ ml, 24 well plate for 24 h) were pre-treated (1 h) with Ac-WEHD-CHO (10µM) followed by LPS (1µg/mL, 24 h) stimulation. Supernatants were analysed for Nitrite production by Griess assay. Statistical analysis was performed using (A) paired student's t-test or (B) two-tailed *ANOVA* test to compare Ac-WEHD-CHO treated and untreated BMDM mean ± SEM values from 3 independent experiments.

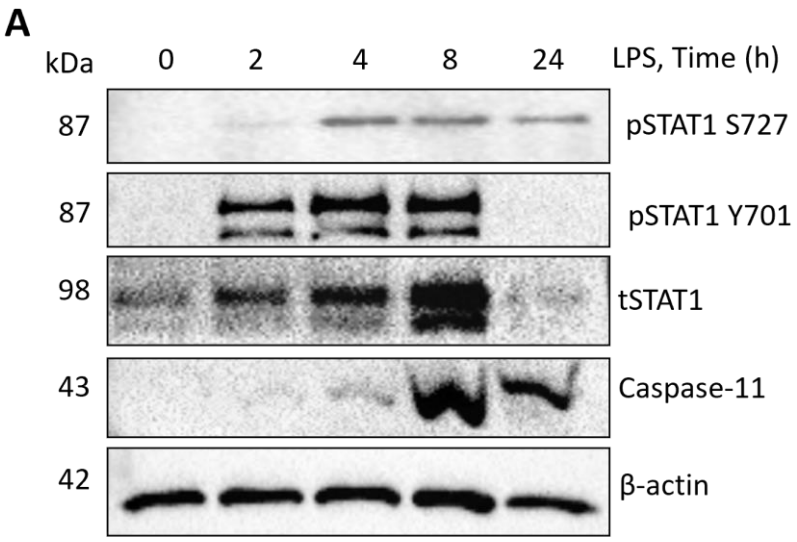

Figure 3.5: Kinetics of LPS-induced pSTAT1 activation and caspase-11 expression

RAW264.7 immortalised murine macrophage cell line were stimulated with LPS (1 ug/ml) over a 24 h timecourse, as indicated. Whole cell lysates (20 µg) were analysed by western blot for expression of (A) pSTAT1 S727, pSTAT1 Y701, total STAT1, caspase-11 and β-actin, as loading control. Blots are representative of three independent experiments.

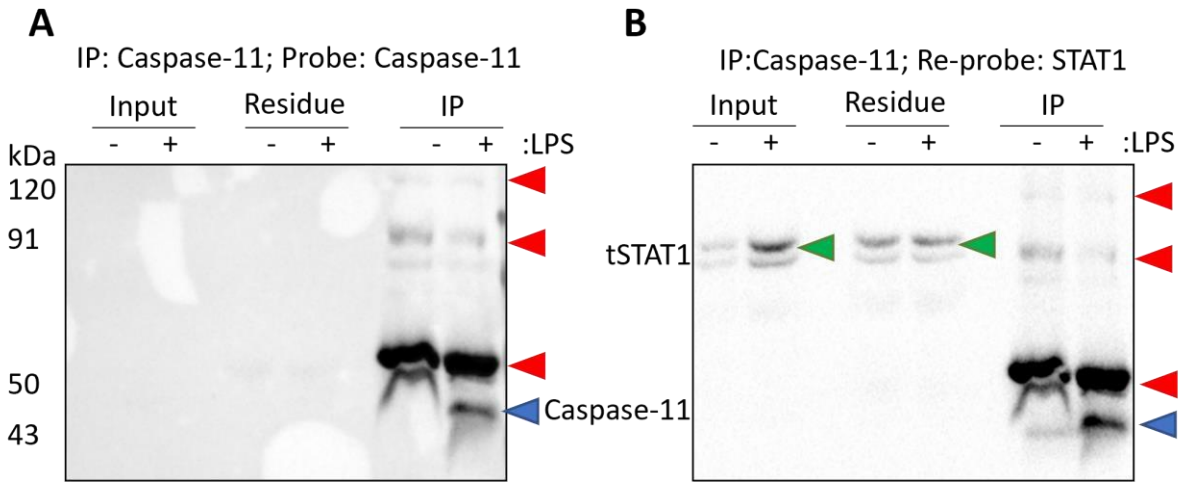

Figure 3.6: Caspase-11 and STAT1 do not directly interact

RAW264.7 immortalised murine macrophage cell line was seeded at $5x10^5$ cells/ mL in $10cm^3$ dish and were stimulated with LPS (1 ug/mL) for 8 hours. Following stimulation caspase-11 was immunoprecipitated from the cytoplasmic lysate (1µg/µL anti-caspase-11 antibody). Input (10%), residue (lysate after IP) and IP lysates were analysed for (A) caspase-11 and (B) total STAT1. Blots are representative of three independent experiments. Blue arrows indicate protein probed for caspase-11, green arrows indicated tSTAT1 and red arrows indicate non-specific binding

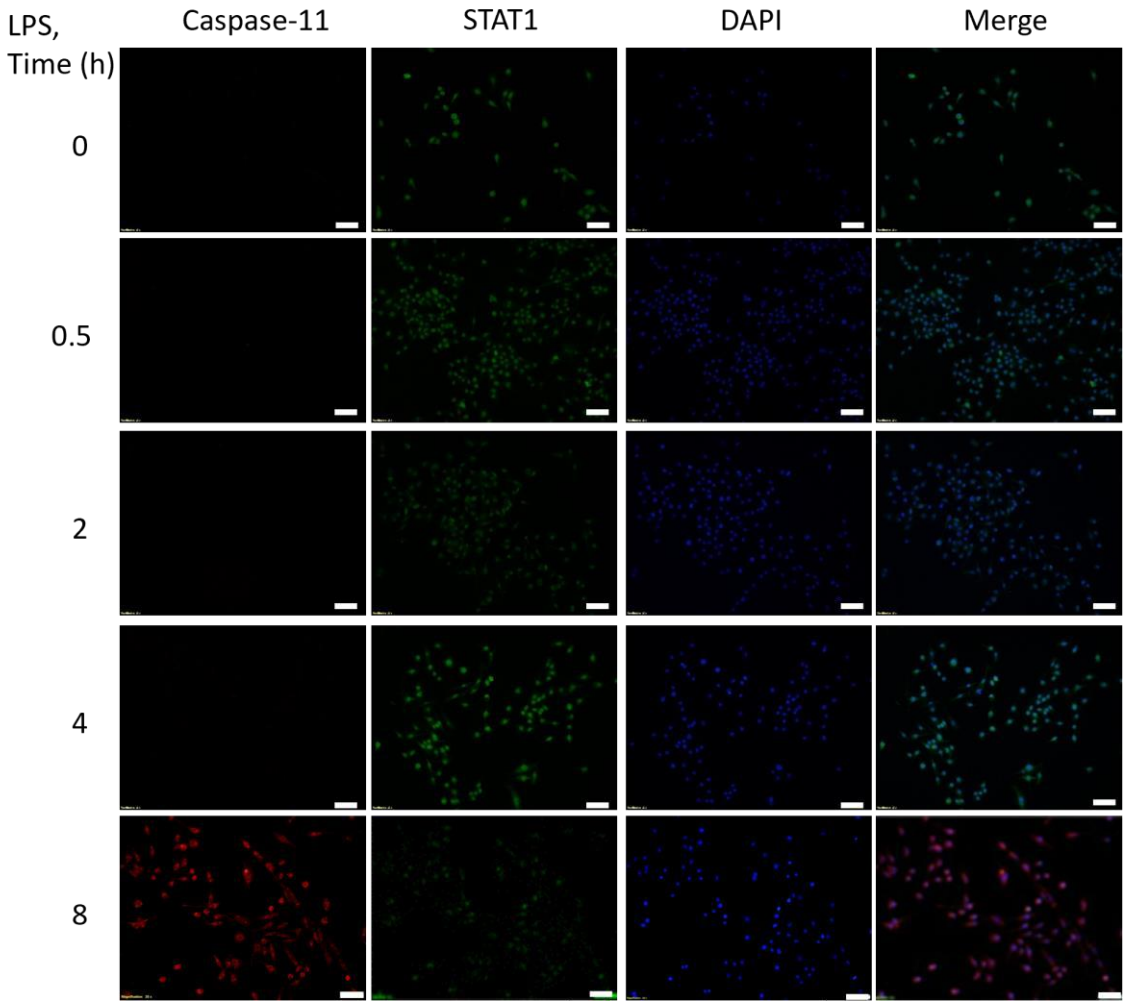

Figure 3.7: Caspase-11 forms specks after 8 hours LPS stimulation and STAT1 begins nuclear translocation at 4 hours

RAW264.7 immortalised murine macrophage cell line was seeded at $1.5x10^5$ cells on coverslips in a 24 well plate. Cells were stimulated with LPS (1 ug/ml) over an 8 hour timecourse, as indicated. Following stimulation, cells were fixed with 4% paraformaldehyde, permeabilised with 0.2% Triton X-100 and co-stained for caspase11 (red), total STAT1 (green) and DAPI (blue). Immunofluorescence was viewed on Olympus BX51 and images were taken at 20X magnification. Scale bar 50µm. Immunofluorescence images were merged to visualise co-localisation of proteins.

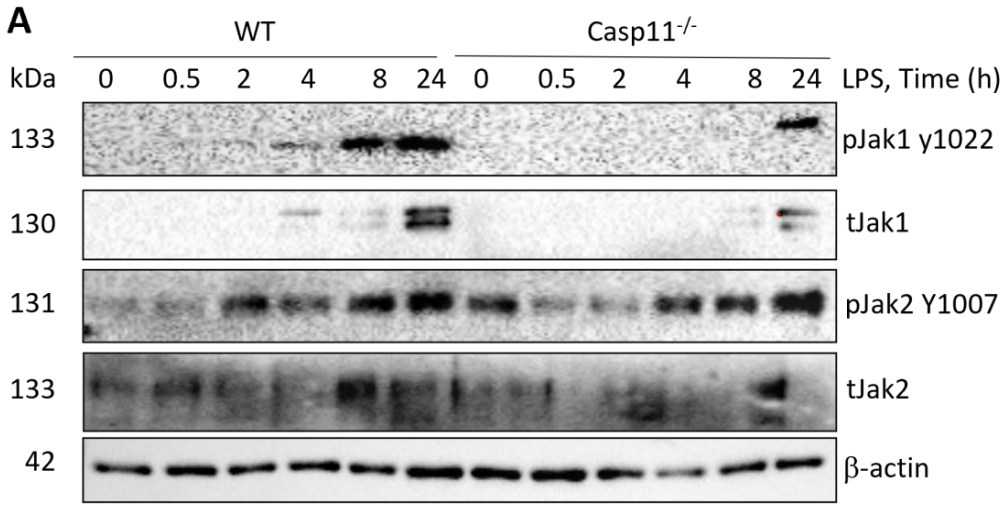

Figure 3.8: Caspase-11 regulates Jak1 phosphorylation following LPS stimulation

WT and *Casp11*$^{-/-}$ BMDMs (seeded at 10^6 cells/ mL, 24 well plate for 24 h prior to treatment) were stimulated with LPS (1 ug/mL) over a 24 h timecourse, as indicated. Whole cell lysates (20 µg) were for analysed by western blot for expression of (A) pJAK1, total JAK1 , pJAK2, total JAK2, and β-actin, as loading control. Blots are representative of three independent experiments.

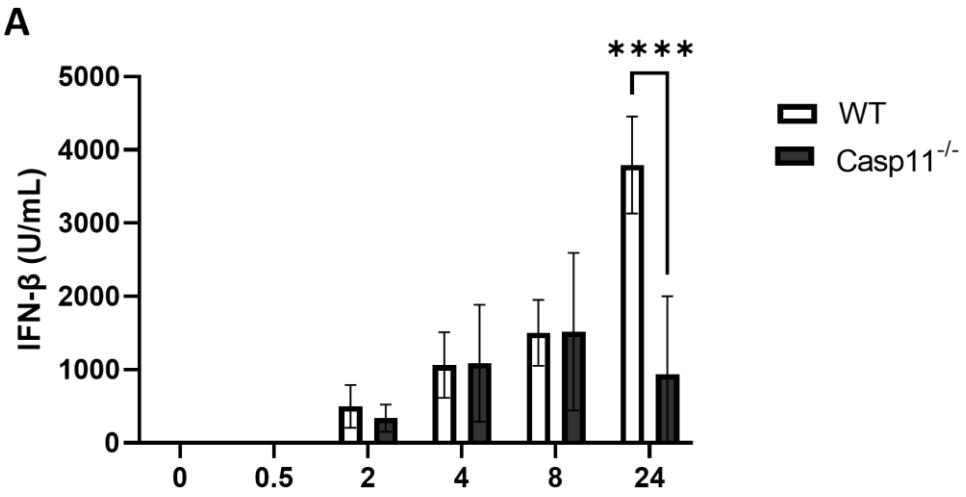

Figure 3.9: Caspase-11 regulates IFNβ secretion in response to LPS stimulation.

WT and *Casp11*$^{-/-}$ BMDM were seeded at 10^6 cells/ mL in 24 well plate 24 h prior to treatment. Cells were stimulated with LPS (1 ug/mL) over a 24 h timecourse, as indicated. Supernatants of WT and *Casp11*$^{-/-}$ BMDM were analysed for (A) IFNβ secretion by ELISA. Values represent the mean ± S.E.M of n=3. Statistical analysis was performed using two-way ANOVA ****p<0.0001 (Tukey post-test).

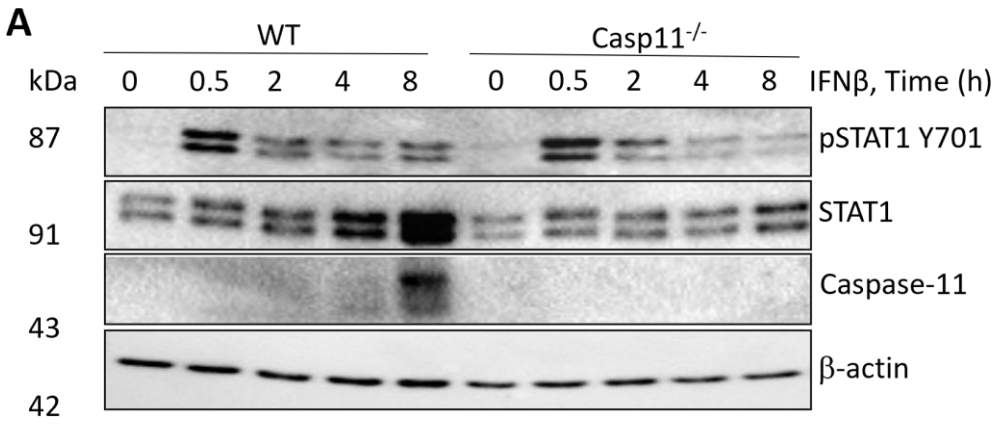

Figure 3.10: Exogenous IFNβ rescues STAT1 phosphorylation in the absence of caspase-11

WT and *Casp11*$^{-/-}$ BMDMs were seeded at 10^6 cells/ ml in 24 well plate 8 h prior treatment. Cells were stimulated with IFNβ (100U/ml) over a 24 h timecourse, as indicated. Whole cell lysates (20 µg) were analysed by western blot for expression of (A) pSTAT1 Y701, total STAT1, caspase-11 and β-actin, as loading control. Blots are representative of three independent experiments.

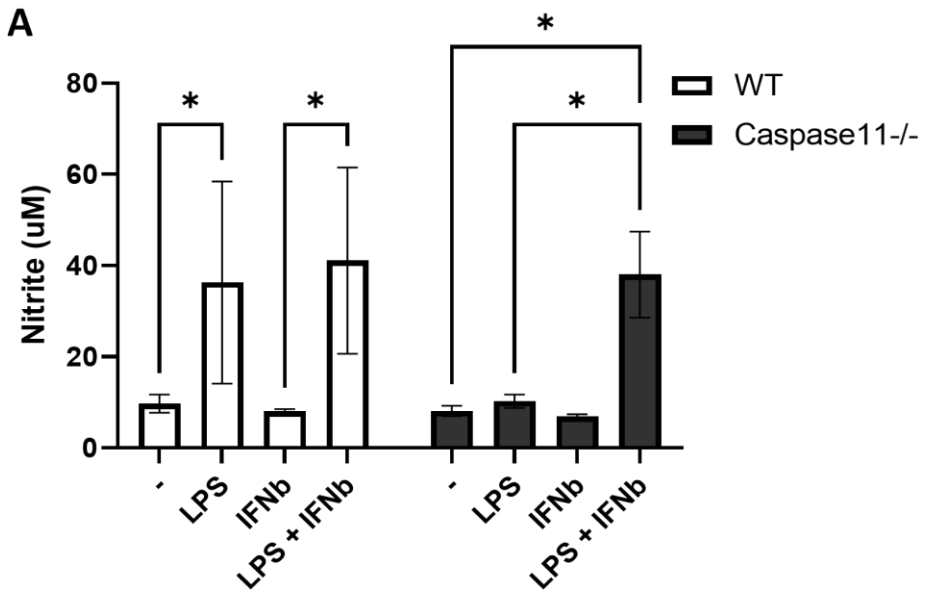

Figure 3.11. Exogenous type I recues NO production in the absence of caspase-11

WT and *Casp11*$^{-/-}$ BMDM were seeded at 10^6 cells/ mL in 96 well plate 24 h prior treatment. Cells were primed with LPS for 18 hours followed by stimulation with IFNβ (2000U/ml) for 30 mins. Supernatants of WT and *Casp11*$^{-/-}$ BMDM were analysed for the production of (A) Nitrite by Griess assay. Values represent the mean ± S.E.M of n=3. Statistical analysis was performed using two-way ANOVA *p<0.05 (Tukey post test).

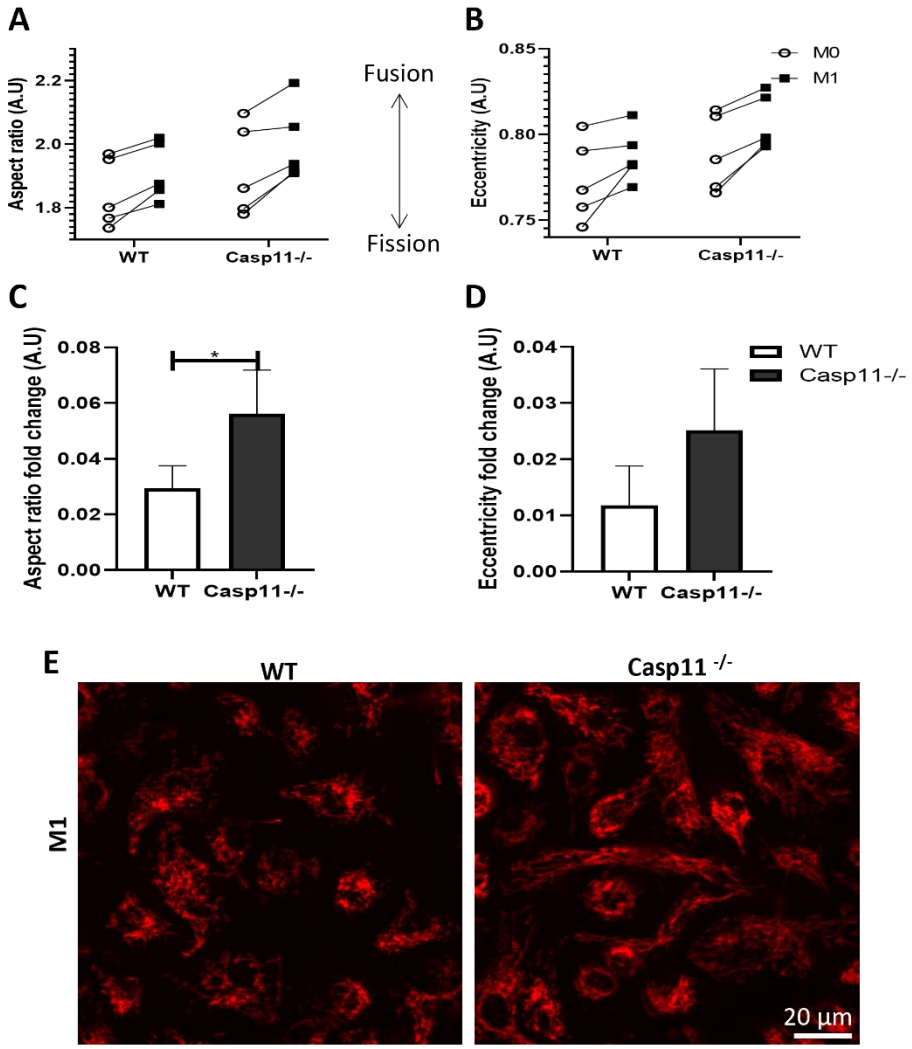

Figure 3.12: Absence of caspase-11 during M1 polarisation alters mitochondrial morphology

WT and *Casp11*$^{-/-}$ BMDM were seeded at 10^6 cells/mL in $3cm^3$ dish O/N prior treatment. Cells were unstimulated (M0) or stimulated with LPS (100 ng/ml) and IFNγ (50 ng/mL) (M1) for 6 h. Cells were stained with TMRM and mitochondrial morphology was non-invasively determine by upright (Olympus BX61WI) microscope as a measure of (A) aspect ratio and (B) eccentricity. (C) Aspect ratio and (D) eccentricity as a measure of fold change relative to M0 BMDM. (E) Representative immunofluorescence images (20µM) of TMRM staining in M1 stimulated (6 h) WT and *Casp11*$^{-/-}$ BMDM. Values represent the mean ± S.E.M of n=3. Statistical analysis was performed using two-way ANOVA ; *p<0.05 (Sidak post-test).

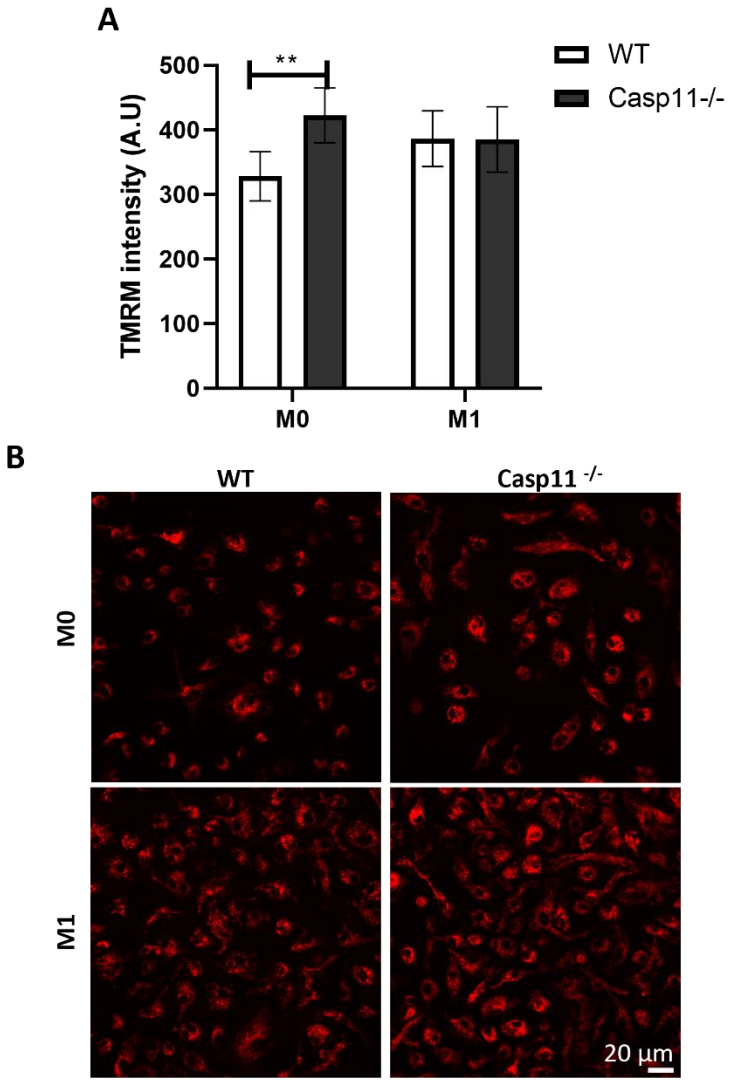

Figure 3.13: Resting macrophage mitochondria have increased membrane potential in the absence of caspase-11

WT and *Casp11*$^{-/-}$ BMDMs were seeded at 10^6 cells/mL in $3cm^3$ dish O/N prior treatment. Cells were unstimulated (M0) or M1 stimulated (LPS (100 ng/ml), IFNγ (50 ng/mL)) for 6 h. (A) Cells were stained with TMRM and fluorescence was measured by upright (Olympus BX61WI) microscope as a measure of mitochondrial membrane potential. Values represent the mean ± S.E.M of n=3. Statistical analysis was performed using two-way ANOVA ; *p<0.05 (Sidak post test). (B) Representative immunofluorescence images (20µM) of TMRM staining in unstimulated (M0) and M1 stimulated (6 h) WT and *Casp11*$^{-/-}$ BMDM.

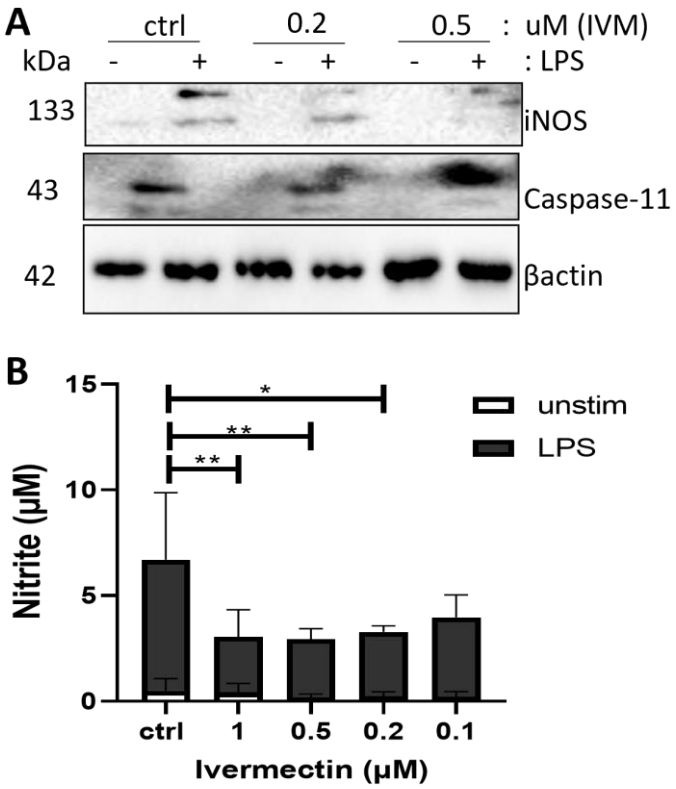

Figure 3.14: Mitophagy inducer ivermectin impairs iNOS expression and NO production in WT BMDM

WT and *Casp11*$^{-/-}$ BMDM were seeded at 10^6 cells/ mL in 24 well plate 24 h prior treatment. Cells were pretreated for 1 h with (0.1-1μM) ivermectin (IVM) before stimulation with LPS (1 ug/mL) for 24 h. Whole cell lysates (20 μg) were analysed by western blot for expression of (A) iNOS, caspase-11 and β-actin, as loading control. Blots are representative of three independent experiments. (B) Supernatants were analysed for the production of Nitrite by Griess assay. Statistical analysis was performed using two-tailed *ANOVA* test to compare ivermectin treated and untreated BMDM mean ± SEM values from 3 independent experiments. *p<0.05, **p<0.01 (Tukey post test).

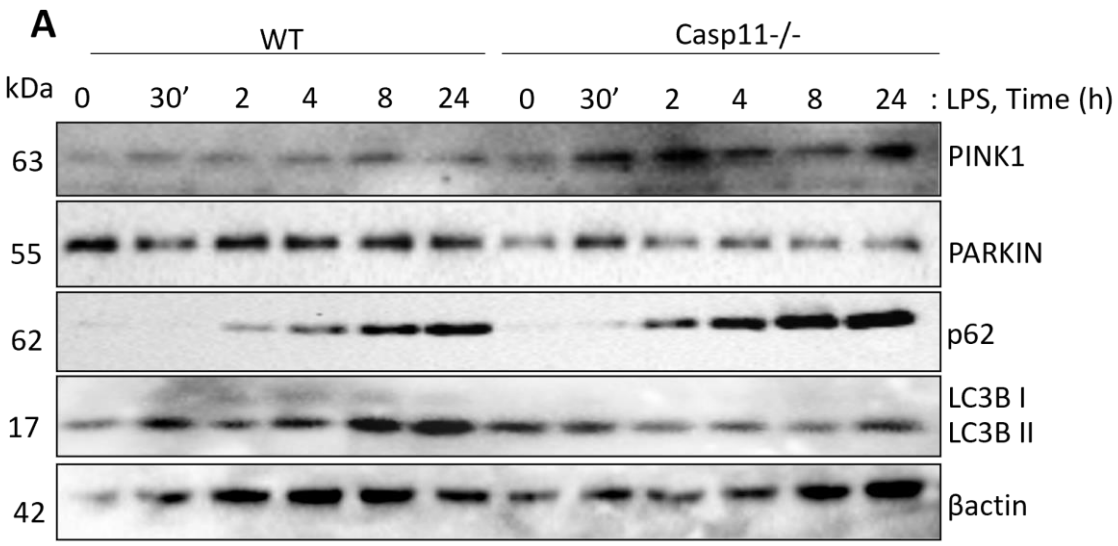

Figure 3.15: Caspase-11 regulates PINK1/PARKIN induced mitophagy in LPS stimulated BMDM

WT and *Casp11*$^{-/-}$ BMDM were seeded at 10^6 cells/ mL in 24 well plate 24 h prior treatment. Cells were stimulated with LPS (1 ug/ml) over a 24 h timecourse, as indicated. Whole cell lysates of WT and *Casp11*$^{-/-}$ BMDM (20 µg) were analysed by western blot for expression of (A) PINK1, PARKIN, p62, LC3B-II and β-actin, as loading control. Blots are representative of three independent experiments.

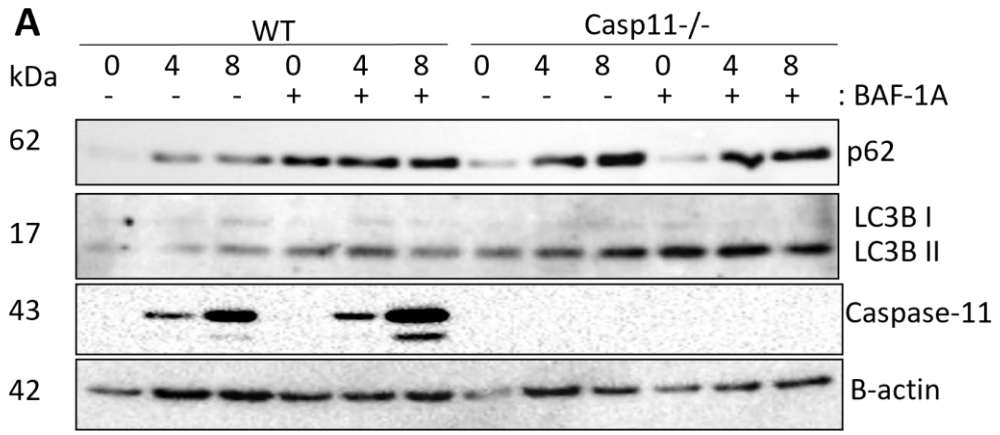

Figure 3.16: Autophagy inhibitor Bafilomycin A1 (BAF-A1) induces the accumulation of p62 and LC3-II in WT, but not *Casp11*$^{-/-}$, BMDM.

WT and *Casp11*$^{-/-}$ BMDM were seeded at 10^6 cells/ mL in 24 well plate 24 h prior treatment. Cells were stimulated with LPS (1 ug/mL) over 8 h, as indicated, and treated with BAF-A1 (inhibitor of autophagy) 2 h prior to collection. Whole cell lysates of WT and *Casp11*$^{-/-}$ BMDM (20 µg) were analysed by western blot for expression of (A) LC3B, p62, caspase-11 and β-actin, as loading control. Blots are representative of three independent experiments.

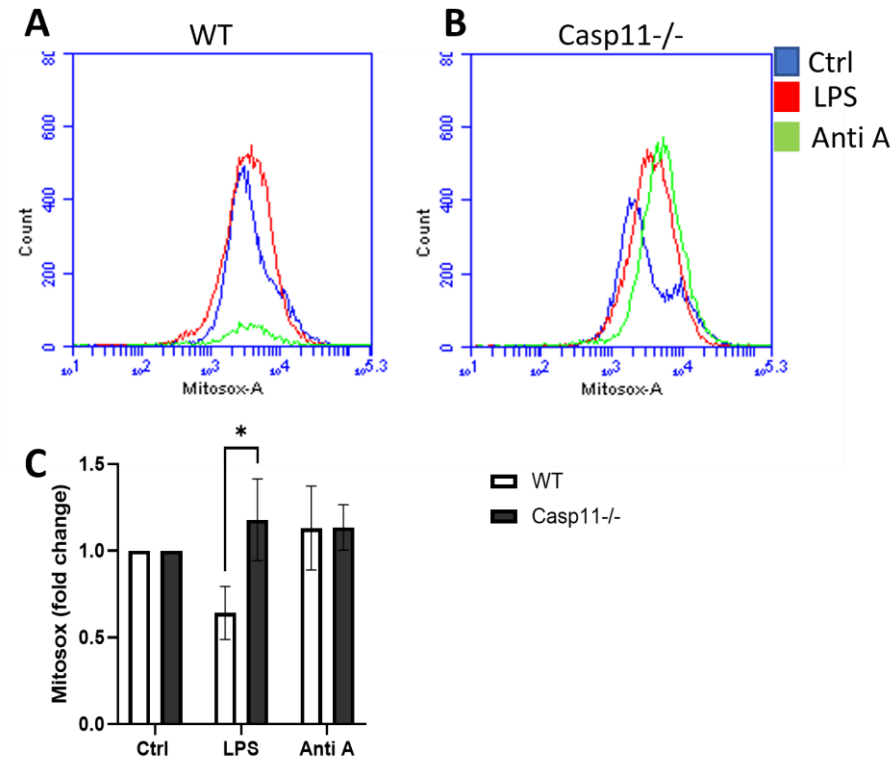

Figure 3.17: Caspase-11 regulates mtROS production in LPS stimulated BMDM

(A) WT and (B) *Casp11*$^{-/-}$ BMDM were seeded at 10^6 cells/ mL in 24 well plate 24h prior treatment. Cells were stimulated with LPS (1 mg/mL) or Antimycin A (1mM, positive control) and after 24 h cells were collected for analysis of mtROS, using the Mitosox assay. (B) Graph represents a fold change of mitosox staining relative to control. Data represent mean ± SEM (*n=3*). Statistical analysis was performed using two-way ANOVA **p<0.01 (Tukey post test).

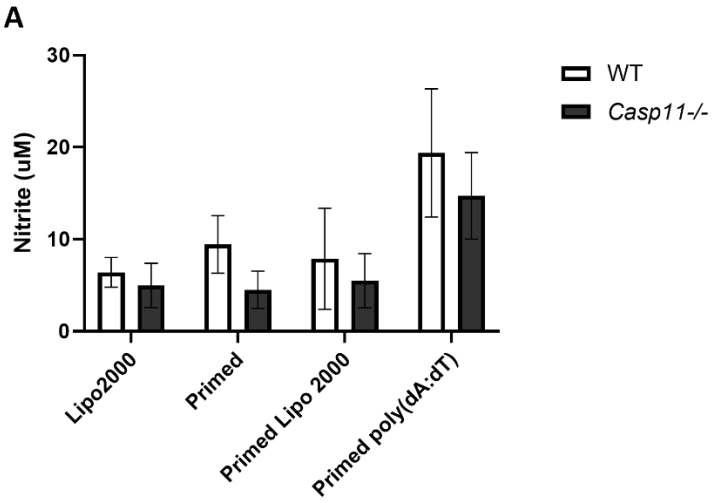

Figure 3.18: Poly(dA:dT) recuses caspase-11 deficient and NO production

WT and *Casp11*$^{-/-}$ BMDM were seeded at 10^6 cells/ mL in 24 well plate 24h prior treatment. Cells were primed with LPS (1 ug/mL) for 4 hours. After 4 h cells were washed before lipofectamine 2000 transfected with poly(dA:dT) overnight Supernatants were collected after 24 h and analysed for the production of (A) Nitrite by Griess assay. Data represents mean ± SEM values from 3 independent experiments. Statistical analysis was performed using two-tailed *ANOVA* test to compare WT and Casp11-/- BMDM *p<0.05 (Tukey post test).

4.Chapter 4: Caspase-11 regulated Nitric Oxide (NO) production mediates the glycolytic shift during M1 ‘Classical’ macrophage polarisation

4.1. Introduction

4.1.1. Caspase-11 mediated NO production drives M1 macrophage glycolytic commitment

Metabolic reprogramming plays a key role in innate immunity, of which macrophages are important players. Macrophages undergo a bioenergetic switch towards glycolytic commitment which is necessary for their inflammatory activation, regulating antigen presentation, inflammatory cytokine secretion and bacterial clearance. Nitric oxide (NO) is a fundamental electro-negative free radical molecule essential for immune modulation during inflammatory events. NO is produced from available intracellular L-arginine by catalytic activity of NADPH-dependent enzymes known as NO synthases (NOS)[298]. During inflammatory responses or tissue injury, 'classically' activated M1 macrophages synthesise NO via the inducible NOS (iNOS). NO has many functions, several of which are involved in immune cell signalling, biochemical reactions and post-translational modifications by which immune cells defend against infection. NO production has direct cytostatic and cytotoxic activity against viruses, bacteria, fungi, and protozoa, assisting host defence[299].

NO produced by macrophages is responsible for their altered energy metabolism during inflammatory responses. NO-mediated inhibition of ETC complex I, II, III, and IV was originally described as the mechanism to regulate M1 macrophage cell death[300]. NO competitively binds cytochrome c oxidase, the terminal acceptor in the mitochondrial ETC, preventing O_2 reduction to H_2O, and inhibiting ATP production[301,302]. NO is responsible for the TCA cycle break by targeting key metabolic enzymes, pyruvate dehydrogenase (PDH) which catalyses pyruvate to acetyl CoA, and aconitase-2 (ACON2) which catalyses citrate to iso-citrate[303]. Metabolic enzyme inhibition leads to stalled carbon transition and causes metabolite profile alterations of citrate, itaconate and succinate. Accumulation of these metabolites is closely associated with macrophage function.

iNOS is the main bactericidal pathway employed by M1 macrophages. Previous studies have illustrated the importance of NO as an anti-mycobacterial molecule during host immune defence against Mtb[304]. NO is converted into reactive nitrogen species (RNS) such as nitrate and nitrite, which can act directly or in combination with superoxide to form peroxynitrite, targeting Mtb directly within the phagosome[305]. In addition to directly targeting the bacterium, host immunometabolism also plays an important role in the host-pathogen interface. During Mtb exposure, innate immune cell glycolytic metabolism regulates pathogenic intracellular replication [306,307]. Several studies document increased glycolysis and other metabolic pathways

including lipid metabolism in Mtb-infected macrophages[308]. Immunometabolic manipulation of macrophages is an important strategy to strengthen host defence, as Mtb infection can lead to increased glycolytic rates, similar to that seen in cancer cells, termed the Warburg effect. During early Mtb infection, M1 macrophage polarisation and glycolysis are dominant. However, during latent and late-stage disease M2 polarity dominates, driven by TCA propelled OXPHOS. Anti-inflammatory microRNA-21 is known to limit Mtb-mediated glycolysis, driving mycobacterial survival[309]. However, the role of NO-mediated glycolysis during Mtb clearance has not been established.

4.1.2. NO regulation of the TCA cycle

The metabolic switch in activated macrophages was revealed to be associated with the Urea cycle L-arginine biochemical pathway, during which deamination activity leads to the synthesis of L-citrulline from L-arginine and oxygenated nitrogen derivates from the imino-nitrogen removed from the guanidino group of the L-arginine, catalysed by iNOS. The generation of NO and peroxynitrites induces inhibition of DNA synthesis, 2 oxidoreductases of the ETC (NADH and succinate) and ACON2. During macrophage activation, extracellular arginine is imported into the cell, via cationic amino acid transporters (CATs; SLC7A1, SLC7A2), where it is metabolised to citrulline and NO via iNOS. Citrulline is than exported out of the cell and recycled to arginine via argininosuccinate synthase (Ass1) and argininosuccinate lyase (Asl)[310,311].

A number of studies have concisely illustrated the regulatory role of NO during macrophage metabolism via ETC complex inhibition and TCA modulation[303,312]. It is well understood that remodelling of macrophage metabolism is important for activation of this plastic cell population. However, the details of how metabolism underpins the macrophage polarisation phenotype are still being elucidated. High NO concentrations have been shown to inhibit mitochondrial respiration and skew macrophage respiration towards glycolysis, while the disturbed TCA cycle influences macrophage responses.

Bailey and colleagues showed that NO modulated essential TCA metabolites; citrate and succinate, as well as the inflammatory mediator itaconate[312]. Similarly, Palmieri *et al* revealed that, in the absence of iNOS, carbon entry into the TCA cycle is fully functioning via PDH and ACON2 leading to increased itaconate concentration[303], while iNOS expression inhibits entry of carbon to the TCA cycle generating an accumulation of citrate and limiting itaconate. NO oxidises the cubane iron-sulfur (Fe-S) cluster, 4Fe-4S, enzymatic domain of ACON2, converting

it into 3Fe-4S. This loss of iron consequently leads to an inactive enzyme. The 4Fe-4S catalytic domain participates in the non-redox reaction of reversible isomerisation of citrate to isocitrate with the intermediate cis-aconitate[313,314]. During glycolytic shift, polarised cells undergo phosphorylation and inactivation of PDH. Carbon tracing revealed a lack of carboxylation through PDH and glucose contribution to acetyl-CoA is blunted, however alterative pyruvate carboxylation into lactate is supported during glycolytic demands. NO, nitroxyl and peroxynitrites directly target the dihydrolipoamide dehydrogenase (DLD) subunit (E3) of PDH, leading to inactivation possibly by cysteine-nitrosation[303]. E3 dehydrogenases the lipoate cofactor of PDH E2 subunit, during this process E3 generates NADH. E3 is also associated with other cellular metabolic enzymes including oxoglutarate and branched chain alpha keto acid dehydrogenase. Dysfunctional TCA cycle leads to inactive mitochondrial complex and suppressed oxidative phosphorylation, significantly reducing β-oxidation of fatty acids and reducing oxygen consumption rates (OCR).

NO ability to regulate mitochondrial respiration is achieved by nitrosylation of iron-sulfur proteins present in the ETC complexes, including complex I (NADPH coenzyme Q) containing 3 4Fe-4S clusters, and complex III (ubiquinone) containing a 3 iron cluster of 3Fe-4S or completive inhibition of complex IV (cytochrome c oxidase). The kinetics of NO inhibition of ACON2 is faster than inhibition of complex I or III. Following aconitase inhibition, endogenous respiration continues at normal rates when complex I and III are still fully functional, however reduction of respiration is observed at later time points.

4.1.3. Nitrosylation of ETC complexes

4.1.3.1. Complex IV; acute NO inhibition

Cytochrome c oxidase is a multicomponent metallic enzyme which catalyses the oxidation of cytochrome c and reduction of O_2 to H_20, essential for proton gradient driven ATP linked mitochondrial respiration. Cytochrome c oxidase, located in the inner membrane of the mitochondria, is comprised of four key redox active metal centres – a binuclear copper centre (Cu_A), two redox active heme A cofactors (heme a and heme a3) and tri-histidine-coordinated copper (Cu_B)[315]. Heme a3 and Cu_B make up the catalytic site for oxygen binding, which NO competitively binds reversibly. Fe2/Cu1 centre reduces O_2 and the resulting oxidised site is reduced by electron transfer from two electron donors, regenerating the Fe2/Cu1 centre[316]. iNOS generation of NO is located near cytochrome c oxidase active site, therefore alternative pathway to avoid inhibition of this constant flux is necessary. Complex IV inhibition by NO is reversible in the presence of O_2, after initial inhibition, as the reducing activity of O_2 is slowly

regained and NO rapidly dissociates from heme a3[317]. Inhibition of cytochrome c oxidase can be seen within minutes of adding NO donor and ADP to mitochondria. Initial acute effects of NO on the mitochondrial ETC is the inhibition of respiration at cytochrome c oxidase, followed later by effects that involve the inhibition of complexes I and II by prolonged chronic NO exposure[318].

4.1.3.2. Complex I: Chronic NO inhibition

Complex I is an intricate protein comprised of 44 subunits and is over 1000kDa, formed by 4 distinct modules. 5 out of 8 subunits which make up the catalytic NADPH binding module (N-module) are decreased in macrophages following M1 stimulation[312]. Other subunits, Ndufv1 and Ndufs4, which are thought to be essential for catalysis, are also decreased although not significantly. NO functions to modulate metabolism via changes of the terminal N2 FeS cluster, N-module subunit of complex I. In the absence of NO, reduction in complex I proteins associated with NAPDH oxidation is attenuated, indicating that decreases in complex I subunits are being driven by NO, contributing to the altered maximal respiration capacity in M1 stimulated macrophages[312]. Conformational changes of complex I during its active to dormant transition, mediated by divalent cations and free fatty acids, leads to exposure of cysteine 39 of the ND3 subunit[319]. This cysteine residue is susceptible to thiol modifications by nitrosation, leading to irreversible enzyme deactivation[320]. Therefore, although NO regulates mitochondrial respiration via complex IV, long term NO exposure persistently inhibits complex I[318].

4.1.4. NO driven metabolic shift

Studies by Bailey and Palmieri have highlighted the importance of NO in remodelling macrophage metabolism using NOS2-deficient murine macrophages stimulated with typical M1 stimuli, LPS and IFNγ[303,312]. Typically, murine macrophages treated with LPS and IFNγ have upregulated expression of iNOS and generate large quantities of NO, leading to the inhibition of mitochondrial respiration. Proinflammatory, M1-skewed macrophages respire by glycolysis while the TCA cycle is disturbed. It has been shown that the iNOS cofactor, tetrahydrobiopterin (BH_4), is involved in modulation of IL-1β and key metabolic remodelling via NO production[312].
Studies investigating the impact of NO on energy demands have revealed that basal, ATP-linked, and maximal respiration are maintained in M1 activated macrophages in the absence of NO, whereas OCR in WT M1 stimulated macrophages is completely impaired. Notably, maximal respiration measured in activated NO-deficient macrophages was of similar concentration to basal OCR and significantly lower than levels measured in unstimulated cells[312]. Due to these difference in maximal respiration even in the absence of iNOS, it was suggested that NO-

independent changes in respiratory capacity also occur after stimulation. There are, however, no disputes in the literature regarding NO-mediated modulation of complex I and the resultant metabolic switch away from oxidative metabolism towards glycolysis in M1 macrophages[321].

Investigations of glycolysis in the face of the switch away from oxidative metabolism have revealed that although alterations in the expression of glycolytic metabolites occurred in the absence of NO, there was no change in glycolytic rate after 16h M1 polarisation[312]. Glycolysis leads to the production of pyruvate which in turn is either converted into lactate or oxidised into the TCA cycle. Both processes lead to the acidification of extracellular media via proton exclusion which can thereby be used to measure glycolytic activity. Intracellular and extracellular lactate was found to be decreased in BH_4 and iNOS deficient cells. BH_4 functions as a NOS cofactor, structurally stabilising the NOS homodimer and inducing conformational changes that mediate catalytic activity[322]. GTPCH deficient cells notably do not produce NO, similarly to iNOS knockout macrophages, illustrating the need of BH_4 during NO synthesis and release. However, NO-deficient cells can still upregulate glycolysis despite the changes in glycolytic intermediates and proteins which are involved in glucose metabolism[303,312].

4.1.5. Macrophage Polarisation

iNOS-derived NO not only regulates metabolism remodelling but also proinflammatory cytokine production in macrophages. Gene Ontology term enrichment analysis revealed increased IL-1β production and responses to IFNβ in BH_4 and iNOS deficient macrophages, similarly IL-1β, IL-6, IL-12p4-, MCP1 and MIP1α secretion is increased at 24h M1 polarisation in the absence of NOS2, demonstrating an inflammatory regulatory role of iNOS during M1 polarisation[303,312,323] NO-mediated nitration of IRF5 suppresses its ability to activate the IL-12 promoter. Lu and colleagues demonstrate the importance of NO during IL-12 regulation in response to varying concentrations of LPS. Computational analysis suggests the LPS-mediated activation of two competing signalling pathways which differentially express iNOS or IL-12, both of which mutually inhibitory. An iNOS or IL-12 signalling outcome is dependent on LPS concentration[324]. Therefore, although iNOS is an important M1 marker, central to glycolytic commitment during proinflammatory responses, iNOS also negatively regulates M1 differentiation as observed by decreased inflammatory cytokine production and inflammatory disease susceptibility. Thus, in addition to being a signature marker for M1 macrophages, M1 expression of iNOS may control inflammation by dedifferentiating these cells, as in the absence of iNOS M1 polarisation is

significantly enhanced[128]. iNOS deficient mice are also more susceptible to inflammatory diseases such as EAE and sepsis[129,325].

Innate and adaptive immunity are efficient in host defence against Mtb infection, with macrophages, dendritic cells, T cells, and airway epithelial cells playing major roles in protection against infection[326]. Macrophages are the main effector cells mediating host defence against Mtb infection, with activities involving the production of antimicrobial cytokines, ROS, and phagocytosis. T lymphocyte IFNγ production and macrophage IL-1β- or TNF-α-induced NO production, a potent antimicrobial agent[327]. However, despite the robust innate and adaptive immune responses to protect the host against infection, Mtb still circumvents these defences. These immune evasive mechanisms leading to persistent Mtb replication are associated with negative regulation of host glycolysis and proinflammatory macrophage response[328]. This has led TB investigators to begin exploring strategies to control macrophage immunometabolic functions during active and latent disease.

Previous investigations from our lab have shown a role for caspase-11 during LPS-mediated STAT1 activation and subsequent iNOS mediated NO production. Therefore, we hypothesise that this role of caspase-11 during STAT1 activation and regulation of iNOS expression and NO production leads to altered mitochondrial respiration. We aim to illustrate that caspase-11 deficient M1 macrophages, due to their impaired ability to generate NO, have reduced capacity to shift respiration to glycolysis. Our initial investigations sought to assess the impact of caspase-11 and its corresponding NO mediated glycolytic metabolism during host innate immune defence against Mtb. We hypothesise that caspase-11 is important in mediating Mtb clearance via alterations in metabolism, illustrating the importance of caspase-11 mediated NO-induced glycolytic commitment during innate immune inflammatory response and host defense.

4.2. Hypothesis and aims of Chapter 4

Hypothesis: Caspase-11 regulates NO production and its associated glycolytic commitment during M1 'classical' macrophage activation.

Specific Aims:

1. Determine the role of caspase-11 during metabolic shift towards glycolysis in response to proinflammatory stimuli.
2. Identify caspase-11 dependent metabolic profile alterations during M1 polarisation.
3. Determine the immunomodulatory role of caspase-11 mediated NO production during heat-killed TB infection.
4. Determine the impact of NO during Mtb bacterial clearance in the absence of caspase-11.
5. Investigate the role of caspase-11-mediated metabolic alterations during Mtb bacterial infection.

4.3. Results

4.3.1. M1 macrophage glycolytic shift requires caspase-11 expression

Macrophage metabolic reprogramming is indicative of their functional state. Generally, 'classical M1' macrophage metabolism utilises glycolysis, whereas 'alternative M2' macrophages employ oxidative phosphorylation. iNOS, a phenotypic M1 marker, mediates NO production and promotes glycolytic commitment via modulation of mitochondrial targets, causing a stalled tricarboxylic acid (TCA) cycle[329]. To assess caspase-11 mediated NO contribution to metabolic reprogramming, we assayed oxygen consumption rates (OCR) (**Fig 4.1 A**) and extracellular acidification rates (ECAR) (**Fig 4.2 A**) in naïve and M1 polarised WT and *Casp11*$^{-/-}$ BMDM. Basal respiration was significantly reduced following M1 polarisation in both WT and Casp11-/- BMDM, with no significant alterations in reduction in basal respiration observed between WT and Casp11-/- BMDM (**Fig. 4.1 B**). Assessment of proton leakage (**Fig 4.1 C**) and ATP-linked respiration (**Figure 4.1 D**) revealed M1 polarisation significantly reduced respiration in both genotypes however, no significant difference between WT and Casp11-/- M1 polarised BMDM was observed. We observed a significant reduction in WT maximal respiration rates following M1 polarisation, which was not observed in *Casp11*$^{-/-}$ BMDM (**Fig 4.1 E**). Lastly, we measured spare respiratory capacity (SRC) as a measure of percentage (**Fig. 4.1 F**). SRC is the amount of extra ATP that can be produced by OXPHOS due to increased energy demands. Our data shows that Casp11-/- M1 BMDM have increased SRC compared to WT M1 BMDM, which is reflective of mitochondrial capacity to meet energy demands beyond basal levels, in response to stress and to avoid ATP crisis. This finding suggests that mitochondrial fitness or "health" is more adaptable in response to inflammatory stimuli in the absence of caspase-11. **Fig 4.1** results show that, while significant OCR reductions are observed in both WT and *Casp11*$^{-/-}$ M1 polarised BMDM relative to M0, the reduction in oxygen consumption is not as powerful in the absence of caspase-11. Therefore, we wished to further investigate ECAR (**Fig 4.2**) and OCR/ECAR ratio (**Fig 4.3**).

ECAR analysis revealed that, while basal glycolysis increased following M1 polarisation in WT and Casp11-/- BMDM, significantly lowers levels of increased basal glycolysis occurred in *Casp11*$^{-/-}$, compared to WT, M1 BMDM (**Fig. 4.2 A, B**). Analysis of glycolytic capacity also revealed increased rates in WT and *Casp11*$^{-/-}$ M1 BMDM relative to M0 (**Fig. 4.2 C**). However, no

differences were observed between WT and *Casp11*$^{-/-}$ M1 BMDM. Although, corresponding to OCR alterations observed, the increased glycolytic capacity is more pronounced in WT M1 BMDM compared to *Casp11*$^{-/-}$ M1 BMDM (**Fig. 4.2 C**).

Lastly, OCR versus ECAR was plotted on an energy map (**Fig. 4.3 A**) and OCR/ECAR ratios were calculated (**Fig 4.3 B**) to generate a bioenergetic profile of caspase-11 effects in M0 and M1-polarised BMDM. Both WT and *Casp11*$^{-/-}$ M0 BMDM were situated in the Aerobic quadrant of the energy map, confirming that both genotypes metabolise by OXPHOS during normal conditions (**Fig. 4.3 A**). M1 polarisation of WT BMDM caused a shift towards glycolysis with higher ECAR to OCR rates, whereas M1 polarised *Casp11*$^{-/-}$ BMDM are positioned between glycolytic and energetic on the map, with a less pronounced reduction in OCR than that observed in WT (**Fig 4.3 A**). OCR/ECAR ratio analysis indicated a similar commitment to OXPHOS in naïve macrophages of both genotypes (**Fig 4.3 B**). As expected, wildtype M1 polarised BMDM favour a glycolytic metabolism, whereas there is significantly less preference toward glycolytic reprogramming in the absence of caspase-11 (**Fig.4.3 B**), complementing the visible illustration of the energy map. These data suggest that while caspase-11 plays a role in glycolytic commitment in M1 polarised BMDM and has a role in energy metabolism, absence of caspase-11 does not completely abolish the M1 macrophage shift to glycolysis. This corresponds with our findings that NO production is impaired, although not abolished, in the absence of caspase-11.

To further validate the Seahorse findings, similar experiments were analysed using 2P fluorescent lifetime imaging microscopy (2P-FLIM), which detects fluorescence of intracellular free and protein-bound NA(P)DH. Free NADH, with a short fluorescent half-life, is associated with glycolysis while the protein-bound form, with a longer fluorescent lifetime, is associated with OXPHOS. The distinct fluorescent lifetime of each form of NADH allows for metabolic profile shifts to be evaluated as a ratio of bound NADH/Free NADH[330]. To initially determine basal metabolic profiles, naïve wildtype and *Casp11*$^{-/-}$ BMDM were assessed. Consistent with seahorse assay data, untreated WT and *Casp11*$^{-/-}$ BMDM favour OXPHOS (**Fig. 4.4 A, B**). Following M1 stimulation, FLIM analysis revealed increased free NADH fluorescence detection in WT, compared to *Casp11*$^{-/-}$ BMDM, illustrated as a decreased average lifetime of excitation of NADH (τavg) (**Fig. 4.4 A, B**). The observed decreased τavg defined WT M1 BMDM as glycolytic while the maintained τavg levels in M1 *Casp11*$^{-/-}$ BMDM shows metabolic profile commitment to OXPHOS.

Taken together these data confirm a regulatory role for caspase-11 in the metabolic profile shift to glycolysis that occurs in macrophages during M1 polarisation.

4.3.2. Caspase-11 mediates stall in TCA and Urea cycle

Continuing our investigation of caspase-11 regulated macrophage metabolism in response to M1 polarisation, we utilised (1)H nuclear magnetic resonance (NMR) metabolomic profiling to identify differences in metabolite abundance. Intracellular and extracellular fractions from unstimulated and M1-stimulated WT and Casp11$^{-/-}$ BMDM were subjected to (1)H NMR-based metabolomic analysis. The generated spectra were analysed using two pattern recognition methods, principal component analysis (PCA) and Bruker AssureNMR with SIMBA, to identify individual metabolites responsible for genotype differences. Untargeted analysis of NMR spectra by PCA allowed for comparison of each group's global intracellular and extracellular metabolite profile. We identified 4 distinct quadrants of separation, dependent on treatment and fraction. Naïve macrophages display similar profiles, however once M1 polarised, enhanced variations between genotypes were observed within intracellular fraction (**Fig. 4.5 A**). This analysis led us to identify individual metabolite differences associated with OXPHOS and arginine metabolism pathways.

TCA cycle dysfunction is diagnosed by detecting the accumulation of citrate, succinate and itaconate. Reduced carbon entry to TCA via PDH and reduced transition from citrate to α-ketoglutarate due to targeting mitochondrial ACON-2 during macrophage activation is NO-dependent[6]. Therefore, we proposed that caspase-11, via its regulation of NO production, similarly induces TCA cycle dysfunction. H(1) NMR was utilised to measure several metabolites involved in TCA metabolism.

During glycolysis, glucose breaks down to produce pyruvate and net energy in the form of 2 ATP and 2 NADH. If the cell is poorly oxygenated and energy demands exceed the rate of OXPHOS, pyruvate is converted to lactate via lactate dehydrogenase. Equally, pyruvate produced can enter the TCA cycle in the mitochondria to form acetyl CoA as step 1 of the TCA cycle. From our NMR metabolite data, we observed no difference in lactate or pyruvate production in intracellular or extracellular fractions between WT and *Casp11*$^{-/-}$ M1 BMDM (**Fig. 4.6 A**). However, during step 2 of the TCA involving citrate production, we observed differences in its intracellular accumulation. Fusion of acetyl CoA with oxaloacetate, catalysed by citrate synthase, produces citrate. We observed reduced citrate accumulation in both M0 and M1 *Casp11*$^{-/-}$ BMDM compared to WT (**Fig. 4.6 A**). Analysis of extracellular citrate levels, compared to cell culture media, suggests extracellular citrate consumption by BMDM, regardless of activation state. Citrate is subsequently converted to cis-aconitate and D-isocitrate, catalysed by aconitase-

2. We hypothesise that the increased citrate levels observed in WT BMDM are in response to impairment of this 3rd step of the TCA cycle, via reduced ACON2. In the absence of caspase-11, citrate levels are further reduced following M1 stimulation, suggesting that citrate metabolism continues, leading to the production of α-ketoglutarate, catalysed by isocitrate dehydrogenase.

Therefore, as expected, WT classical activated macrophages had an accumulation of intracellular citrate, whereas in the absence of caspase-11 this accumulation is abolished (**Fig. 4.6 A**). α-ketoglutarate and glutamate undergo reversible reactions, involving the enzymes, glutamate dehydrogenase and aspartate aminotransferase, required for glutamine to enter the TCA cycle. From our data we observe differences in intracellular glutamate levels in unstimulated BMDM, with WT having higher levels than *Casp11*$^{-/-}$ BMDM (**Fig. 4.6 A**). However, following M1 stimulation, intracellular glutamate levels decrease in WT but increase in *Casp11*$^{-/-}$ M1 BMDM. Increased intracellular glutamate levels in *Casp11*$^{-/-}$ M1 BMDM are accompanied by a corresponding decrease their extracellular glutamate level (**Fig 4.6 A**).

In rapidly dividing cells, glutamine is a major source of energy. M1 macrophages depend on glutamine input into the TCA to support succinate accumulation mediated glycolysis. We hypothesise that the decreased glutamate levels detected in WT M1 BMDM is due to glutamate supplying the TCA, compensating for citrate stalling, serving as an anaplerotic pathway. Glutamine thereby serves as a source of carbon and nitrogen for M1 macrophage rewiring. Alternatively, the glutaminase pathway is reversible, α-ketoglutarate transamination leads to production of glutamate. Therefore, in WT M1 BMDM, citrate accumulation is predictive of reduced α-ketoglutarate production and reduced glutamate generation. However, under lower ammonia concentrations or higher acidification conditions, glutamate dehydrogenase is expected to operate towards glutamate oxidative deamination to generate α-ketoglutarate.

The next step of the TCA cycle involves α-ketoglutarate dehydrogenase catalysing the oxidation and carboxylation of α-ketoglutarate to succinate by the formation of unstable intermediate succinyl-CoA (**Fig. 4.6 C**). As previously mentioned, carbon flux through the TCA cycle is typically stalled by reduced ACON-2 activity, however glutaminase pathway downstream serves as a carbon source. Therefore, we would not expect this step in the cycle to be impaired during M1 polarisation. From our preliminary data we did not observe ay differences in succinate between genotypes after M1 stimulation (**Fig. 4.6 B**). However, similarly we did not observe increased succinate compared to M0 naïve macrophages, which is unexpected. Although we did observe differences in fumarate. Succinate dehydrogenase converts succinate to fumarate, and loss of

activity leading to succinate accumulation to a shift towards aerobic glycolysis. We observed increased fumarate following M1 stimulation in WT BMDM, which is not found in *Casp11-/-* (**Fig 4.6 B).** Although we expected succinate dehydrogenase inhibition to reduce fumarate production, previous reports suggest that fumarate is converted from alternatives routes[331]. We suggest that interconnectivity between the TCA cycle and urea cycle, via the asparate-argininosuccinate shunt, maybe be accounting for this production of fumarate. During citrulline recycling, arginosuccinate synthase catalyses the condensation of citrulline and aspartate to form argininosuccinate, which argininosuccinate lysase spilt to release fumarate and arginine[332]. As we reported increased NO in WT M1 BMDM, compared to *Casp11-/- ,* we suggest that WT M1 BMDM have higher fumarate levels due to production from asparate-argininosuccinate of the urea cycle.

Mitochondrial ACON2 catalyses the interconversion of citrate to isocitrate via cis-aconitate in the second step of the TCA cycle. The citrate accumulation and TCA cycle stall that occurs following M1 polarisation has been reported to occur as a consequence of NO-mediated inhibition of ACON2 expression and activity[303]. To confirm whether differences in ACON2 expression could account for the selective accumulation of citrate in WT M1 BMDM, compared with *Casp11*$^{-/-}$ M1 BMDM, we measured their ACON2 protein expression levels by western blot. We observed increased ACON-2 expression following M1 stimulation in both WT and *Casp11-/-* BMDM. However, WT M1 BMDM had reduced ACON-2 expression compared to *Casp11-/-* M1 BMDM. (**Fig 4.7 A**), reflective of the decreased citrate level as a measure of TCA impairment in the absence of caspase-11 (**Fig 4.6 A**). These data implicate caspase-11 expression in TCA cycle dysfunction during metabolic reprogramming in response to inflammatory stimuli.

Utilising 1(H) NMR Bruker AssureNMR and SIMBA quantitative analysis, intracellular and extracellular arginine metabolites from unstimulated and polarised WT and *Casp11*$^{-/-}$ BMDM were evaluated. As previously shown, caspase-11 mediates iNOS expression in BMDM following inflammatory stimulation, leading to nitric oxide production (**Fig. 3.1**). L-arginine is catalysed by iNOS to produce NO and L-citrulline. Measurement of intracellular L-citrulline levels revealed that citrulline increased following M1 polarisation in WT BMDM, however, in the absence of caspase-11 a dampened production of intracellular L-citrulline was observed (**Fig. 4.8 A**). Levels of L-arginine, the substrate required to produce NO and L-citrulline, were shown to be low intracellularly, but high extracellularly, in unstimulated macrophages (both WT and *Casp11*$^{-/-}$). However, L-arginine levels were found to be altered in M1-stimulated WT compared to *Casp11*$^{-/-}$ BMDM, with a switch in L-arginine availability observed in WT macrophages - with high levels

detected intracellularly and low levels extracellularly- yet no similar switch in L-arginine availability was observed in *Casp11*$^{-/-}$ BMDM (**Fig. 4.8 A**). The high extracellular L-arginine levels observed in unstimulated WT and *Casp11*$^{-/-}$ BMDM, and M1 *Casp11*$^{-/-}$ BMDM appears to be secreted from BMDM, rather than being sourced from the cell culture media (**Fig. 4.8 A**). This is supported by other findings which show that WT M1 BMDM require L-arginine uptake to produce NO[310]. Lee and colleagues also suggest that iNOS translation is governed by L-arginine uptake into the cell[333], which coincides with our findings which suggest that L-arginine uptake does not occur following M1 polarisation of *Casp11*$^{-/-}$ BMDM, which have impaired iNOS upregulation and NO production. Measurement of other products of L-arginine metabolism, creatine and urea, also reveal a dependence on caspase-11. While creatine levels were detectable in cell culture medium alone, we found these levels to be reduced in WT BMDM, potentially by consumption (**Fig. 4.8 A**). Intracellular creatine is only detectable in M1 polarised WT BMDM, as expected, as these were the only cells with available L-arginine for metabolism. Similar observations were made when intracellular urea was measured, WT BMDM polarised to M1 have increased intracellular urea levels, whereas only low levels were detected in the absence of caspase-11 (**Fig. 4.8A**). These data illustrate that L-arginine uptake, which is essential for (i) metabolism by iNOS for NO production or (ii) hydrolysis by arginase for urea and ornithine production, is impaired in the absence of caspase-11, in response to M1 polarising cytokines.

Next, we investigated the mRNA expression levels of markers associated with arginine metabolism including SLC7A1, SLC7A2, NOS2, ARG1 and ARG2 in WT and *Casp11*$^{-/-}$ BMDM stimulated for 24 hours with M1 polarising cytokines. SLC7A family members are involved in L-arginine uptake, NOS2 catalyses L-arginine conversion to NO and L-citrulline, while ARG1 catalyses the hydrolysis of L-arginine to ornithine and urea. Cationic amino acid transporters, SLC7A1 (CAT-1) and SLC7A2 (CAT-2), are involved in the y^+ transport system, which L-arginine transport is primarily dependent upon. SLC7A1 is constitutively expressed and involved in basic metabolism, and **Fig 4.9 A** shows that its expression remains relatively low following M1 polarisation, with a slight decrease in expression in both wild-type and *Casp11*$^{-/-}$ BMDM. SLC7A2 is inducible and is known to be abundant in macrophages[311]. Thus, M1 macrophage L-arginine uptake by CAT-2 is essential for the production of NO and L-citrulline. In contrast to SLC7A1, SLC7A2 upregulation was found to be impaired in M1 polarised *Casp11*$^{-/-}$ BMDM in comparison to WT (**Fig. 4.9 B**). These data correspond with previous findings which show that *Casp11*$^{-/-}$ M1 BMDM have decreased L-arginine uptake compared to WT M1 BMDM (**Fig. 4.8 A**), suggesting that this decrease is due to caspase-11 regulated CAT-2 expression. Western blot results which show that caspase-11 regulates iNOS upregulation (**Fig 3.1 A**) are supported by results which

show that caspase-11 also regulates NOS2 at the transcriptional level (**Fig 4.9 C**). These observations suggest that the impaired NO production in *Casp11*$^{-/-}$ M1 BMDM is due not only to the decreased expression of iNOS, but also the lack of L-arginine trafficking due to reduced CAT2 expression. Further supporting data comes from the metabolic analysis, which showed that the iNOS product L-citrulline is also reduced in absence of caspase-11 due to reduced iNOS expression (**Fig 4.8**).

There are two arginases, ARG1 and ARG2 which although both convert L-arginine to L-ornithine reside in separate intracellular compartments. Arg1 is localised in the cytosol, while Arg2 is localised to the inner mitochondrial membrane[334]. It is difficult to separate the functional effects of ARG1 and ARG2, as they retain 60% amino acid sequence homology and specific inhibitors are not available. Furthermore, *Arg1*$^{-/-}$ mice do not survive more than 14 days postnatally establishing the importance of its specific function[326]. However, previous reports have demonstrated an inhibitory impact of ARG2 on NO production[327,334]. Arg1 mRNA M1 BMDM expression relative to M0 BMDM increased following polarisation, however, in the absence of caspase-11 this inducible expression is significantly decreased **(Fig. 4.9 D**). This coincides with arginine metabolism data, which illustrated reduced urea and creatine intracellular detection in the absence of caspase-11 (**Fig. 4.8 A**). In contrast, Arg2 mRNA induction by LPS is modest relative to M0 BMDM (**Fig. 4.9 E**). Previous reports have similarly shown Arg1 more highly expressed following LPS stimulation, while LPS mediated IL-10 drives Arg2 expression[334]. However, in the absence of caspase-11 we observed increased Arg2 mRNA expression. Therefore, we aimed to investigate the impact of caspase-11 on IL-10 production in response to LPS.

During the inflammatory response, iNOS-mediated NO production from available intracellular L-arginine is limited by IL-10, either by inhibition of NOS2 transcription or mediating iNOS degradation[328,334]. This suppression of NO via IL-10 was shown to preserve OXPHOS[335], similar to observations made in the absence of caspase-11. IL-10 plays a dual role in regulation of the urea cycle. While IL-10 limits iNOS catalytic activity, IL-10 enhances arginase expression, involved in L-arginine conversion to L-ornithine, typically considered an M2-like marker. Previous reports have illustrated a negative regulatory effect of iNOS on IL-10 expression, as *Nos2*$^{-/-}$ BMDM responses to M1 stimuli have increased IL-10 production[303]. IL-10 also inhibits NO production via the suppression of CAT-2, the inducible L-arginine transporter[336]. However, absence of CAT2 does not directly impact arginase activity in macrophages[337]. As we had similar observations regarding caspase-11 regulation of CAT2 and Arg1 levels (**Fig 4.9 B**), we hypothesised that

caspase-11 may negatively regulate IL-10 production to enhance iNOS and NO production and reduce arginase activity. In support of our hypothesis, Carnerio and colleagues previously reported that caspase-11 regulates IL-1α ability to inhibit *il10* expression in a Th17 CD4+ T cell population[87].

We therefore aimed to determine whether caspase-11 has a regulatory role on IL-10 production and arginase expression following LPS stimulation. LPS stimulated WT and *Casp11*$^{-/-}$ BMDM were assessed for ARG1 and ARG2 protein expression over a 24 h timecourse. ARG1 expression levels were similar in WT and *Casp11*$^{-/-}$ BMDM (**Fig. 4.10 A**). We had previously shown reduced Arg1 mRNA expression following 24 h M1 polarisation in *Casp11*$^{-/-}$ BMDM (**Fig 4.9 D**). In contrast, results identify a negative regulatory role of caspase-11 on ARG2 expression in response to LPS. In WT BMDM, Arg2 was induced following 24 h LPS stimulation (**Fig. 4.10 A**). Whereas in the absence of caspase-11 we observe basal expression of ARG2 with significantly elevated expression at 24 h LPS, compared to WT BMDM (**Fig. 4.10 A**). IL-10 ELISA of cell supernatants at 24 h was performed to determine whether the elevated ARG2 expression observed in LPS-stimulated *Casp11*$^{-/-}$ BMDM was due to a negative regulatory role of caspase-11 on IL-10 production. However, no differences in IL-10 production were observed between WT and *Casp11*$^{-/-}$ BMDM (**Fig. 4.10 B**), suggesting that caspase-11 regulation of ARG2 is IL-10 independent[324]. Lu and colleagues also showed that IL-10 mRNA expression was similarly expressed in WT and *Nos2*$^{-/-}$ M1 BMDM.

Previous studies have reported that TLR4-mediated miR-155 induction can dampen Arg2 expression [334]. IL-10 inhibits LPS induced miR-155, leading to increased Arg2 expression[334]. As we observed that caspase-11 expression negatively regulates Arg2 expression, we hypothesised that caspase-11 may be inducing miR-155, resulting in Arg2 suppression during TLR4 signalling. A dataset containing WT and *miR-155*$^{-/-}$ BMDM gene expression, generated by Affymetrix array (GSE151835)[334], was analysed for caspase-11 expression (**Fig 4.11 A**). The dataset, which consists of BMDM stimulated in biological duplicate with LPS or LPS + IL10, showed that IL-10 stimulation did not impact LPS induced Casp11 expression in WT BMDM (**Fig. 4.11 A**). However, in the absence of miR-155 there was a significant reduction in Casp11, suggesting a regulatory role for miR-155 during LPS induced Casp11 expression (**Fig. 4.11 A**). Additionally, we investigated the expression of NOS2, Arg1 and Arg2 in the absence of miR-155, to determine whether miR-155 regulation of Casp11 coincided with alterations to NOS2 and Arg expression. Although we expected to similarly see a loss of NOS2 expression, we found that NOS2 expression was similarly elevated in both WT and *miR-155*$^{-/-}$ BMDM stimulated with LPS + IL-10, anti-inflammatory

macrophages (**Fig. 4.11 B**). Arg1 expression was not significantly reduced in *miR-155*$^{-/-}$ BMDM (**Fig. 4.11 C**), while Arg2 was increased in LPS stimulated *miR-155*$^{-/-}$ BMDM. These observations, utilising the Dowling *et al.* GSE151835 dataset, supports observations from our study, as impaired caspase-11 expression and increased Arg2 expression occurs *miR-155-/-* BMDM. However, increased NOS2 expression observed in LPS stimulated *miR-155*$^{-/-}$ BMDM suggests that miR-155 has opposing effects on caspase-11 and iNOS expression, as it appears to negatively regulates NOS2 following LPS stimulation (**Fig. 4.11 B**).

We have yet to directly implicate caspase-11 mediated NO production for the altered metabolism observed during M1 polarisation. Therefore, to confirm that the caspase-11-dependent glycolytic shift observed during M1 stimulation was caused by NO production, we used the NO donor DETANO to supplement exogenous NO in *Casp11*$^{-/-}$ M1 BMDM. Addition of DETANO to *Casp11*$^{-/-}$ M1 BMDM recovered the metabolic shift, as shown by the reduction in OCR (**Fig. 4.12 A**). In parallel, the NO scavenger cPTIO was used to scavenge NO produced by WT M1 BMDM, this resulted in impaired ability of WT M1 BMDM to reduce OCR (**Fig 4.12 B**). We observed significantly increased basal and maximal respiration in WT M1 BMDM treated with cPTIO compared to WT M1 BMDM (**Fig. 4.12 C, D**). Results also showed significantly reduced basal and maximal respiration of DETANO treated *Casp11*$^{-/-}$ M1 BMDM, compared to control *Casp11*$^{-/-}$ M1 BMDM (**Fig. 4.12 C, D**). As NO donation to *Casp11*$^{-/-}$ M1 BMDM rescues the metabolic phenotype to that of WT BMDM, these results confirm that caspase-11 regulated NO production drives the glycolytic shift that occurs during M1 polarisation in BMDM.

4.3.3. Caspase-11 mediates Mycobacterium tuberculosis (Mtb) clearance in murine macrophages

Macrophage detection of Mtb involves several receptors which facilitate phagocytosis, including scavenger receptors, cytosolic DNA sensors, Fc Receptors, mannose receptors, surfactant protein A receptors, CD14, Ig receptors, CLRs, and TLRs[338]. Recognition by these PRRs mediates multiple different innate responses, such as antigen presentation, inflammasome activation, autophagy, phagosome maturation, reactive nitrogen species generation and apoptosis[339]. During Mtb infection, macrophage phagocytosis is facilitated by activation of TLRs. During phagocytosis, Rab GTPases facilitate phagolysosome formation and maturation, creating an acidic environment ideal for hydrolytic enzyme activity and pathogen clearance[340].

The role of caspase-11 during bacterial defence is not yet fully understood. The majority of works investigating the role of caspase-11 during Gram negative bacterial infection have illustrated the impact of caspase-11 during pyroptosis and the non-canonical inflammasome activation. However, many new studies have come to light revealing additional roles for caspase-11, including modulation of actin dynamics and initiation of blood coagulation[341]. Caspase-11 has been reported to functionally interact with actin interacting protein 1 (Aip1), an activator of cofilin-mediated actin depolymerisation, which ultimately regulates cytoskeleton remodelling, such as during cell migration and phagocytosis[91]. Similarly, Akhter and colleagues observed caspase-11 role in phagosome-lysosome fusion[88].

iNOS activity and NO production play a key role in innate immunity and host defence against mycobacteria. It is generally recognised that macrophage production of NO is pivotal for defence during murine TB infection models and *in vitro*, demonstrating cytostatic and cytotoxic functions[299]. NOS2-deficient mice infected with Mtb have drastically reduced survival compared to their WT littermates[342]. In light of our novel observation regarding the role of caspase-11 in NO regulation and production in M1 stimulated murine macrophages, we hypothesised that caspase-11 mediated NO production would be important for defence against Mtb infection.
Previous unpublished investigation from the Creagh Lab have illustrated the ability of γ-irradiated avirulent Mtb (H37Ra, MOI 5) to induce caspase-11 and NO production after 24-72h infection and regulate bacterial clearance[343]. Therefore, we aimed to assess the role of caspase-11 mediated NO production during Mtb infection in BMDM. WT and *Casp11*$^{-/-}$ BMDM were infected with avirulent Mtb and left to replicate for: (i) 3 hours to determine Mtb uptake by macrophages, considered the bacterial growth baseline or (ii) left to replicate for 24 - 72 hours to determine replication potential. Mtb infected WT and *Casp11*$^{-/-}$ BMDM were supplemented with the NO donor, DETANO or the NO scavenger, cPITO. Analysis of caspase-11 expression by western blot confirmed the ability of 24 h Mtb infection to induce caspase-11 expression in BMDM, which was blunted by either DETANO or cPTIO supplementation (**Fig 4.13**). Upregulation of iNOS was also observed in WT BMDM, which was impaired in the absence of caspase-11 (**Fig 4.13**). Notably, cPTIO pre-treatment followed by Mtb infection in *Casp11*$^{-/-}$ BMDM caused the induction of iNOS expression (**Fig 4.13**). cPTIO is a nitronyl nitroxide which functions as a cell permeating NO scavenger, reacting with NO to form carboxy-TIO derivatives and NO_2 which in turn inhibit iNOS. Analysis of NO production following Mtb infection was indirectly determined, by measuring nitrite levels in cell supernatants using the Greiss assay. As the NO scavenger, cPTIO converts NO into nitrite on a mole to mole basis[344], we observed increased nitrite levels detected in Mtb treated cPTIO WT BMDM, as nitrite is released into the supernatant as cPTIO

functions to scavenge NO (**Fig 4.14**). The NO donor DETANO, which is reported to release NO into the supernatant with a half-life of 20 h, was confirmed as an exogenous source of NO at similar concentrations to those induced by Mtb (**Fig. 4.14**). As part of this experiment, we next assessed the Mtb bacterial growth over a 72h time course in WT and *Casp11*$^{-/-}$ BMDM, in combination with DETANO or cPTIO. This was carried out to determine the role of caspase-11-mediated NO in the pathogenesis and replication of Mtb. Infection levels of Mtb in WT and *Casp11*$^{-/-}$ BMDM were assessed by lysing BMDM at timepoints to determine bacterial uptake and replication potential. Colony Forming Units (CFUs) from infected WT and *Casp11*$^{-/-}$ BMDM lysates were assessed to determine levels of bacterial uptake/growth. Results show that Mtb infected *Casp11*$^{-/-}$ BMDM exhibited higher levels of bacterial replication at 24 h, with significantly higher bacterial numbers following 72 h infection, compared to WT (**Fig 4.15 A, B**), implicating a role for caspase-11 during host defence against Mtb. DETANO treated *Casp11*$^{-/-}$ BMDM were found to have significantly less bacterial growth than the *Casp11*$^{-/-}$ BMDM infection control group (**Fig 4.15 B, C**). Whereas WT BMDM pre-treated with cPTIO had a trend of increased bacterial growth (**Fig 4.15 A, C**). These data illustrate the role of caspase-11 dependent NO production during Mtb clearance.

NO is converted into reactive nitrogen species (RNS) such as nitrate and nitrite, which can act directly or in combination with superoxide to form peroxynitrite to target Mtb directly within the phagosome[305]. In addition to directly targeting bacterium, host immunometabolism plays an important role in the host-pathogen interface[306]. During Mtb exposure, regulation of pathogenic intracellular replication is mediated by host innate immune cell glycolytic metabolism. Several studies document increased glycolysis and other metabolic pathways including lipid metabolism in Mtb-infected macrophages[306,308,309]. Immunometabolic manipulation in macrophages is an important strategy to strengthen host defence, as Mtb can persist in the host by altering the Warburg effect[345]. As we have previously shown a role for caspase-11-mediated NO production during Mtb clearance and observed a role for caspase-11 during glycolytic commitment, we next aimed to evaluate the importance of caspase-11 mediated NO induced glycolysis during Mtb clearance.

Firstly, we aimed to demonstrate the ability of heat-killed Mtb (HKMtb) to induce caspase-11 expression and induce NO production, using HKMtb prepared from the avirulent strain H37Ra. Western blot analysis confirms the ability of HKMtb to induce caspase-11 expression at 24 h post infection (MOI 1 or 5) (**Fig 4.16 A**). The cell wall glycolipid of HKMtb, TDM, is sensed by Mincle and other lipoproteins and lipomannan are recognised by TLR2, leading to NF-κB activation[346].

We also measured HKMtb ability to induce iNOS and NO production in the absence of caspase-11. Following 24 h infection with HKMtb (MOI 1 or 5) in WT and *Casp11*$^{-/-}$ BMDM, we observed HKMtb induced iNOS expression in WT BMDM at both concentrations (**Fig 4.16 A**), while NO production was only detected by Griess assay in WT BMDM following MOI 5 (**Fig 4.16 B**). This data confirms that HKMtb induced iNOS expression and NO production is mediated by caspase-11, as previously observed during avirulent H37Ra infection of BMDM.

Previous reports suggest that macrophages induce aerobic glycolysis following Mtb infection to promote bacterial clearance[306]. We therefore wanted to determine the ability of caspase-11 to regulate metabolic alterations in BMDM during HKMtb infection, using Seahorse technology to assay OCR (**Fig 4.17**) and ECAR (**Fig 4.18**) in naïve and HKMtb infected (MOI 1 or 5) WT and *Casp11*$^{-/-}$ BMDM. Basal respiration (**Fig 4.17 B**) was decreased following HKMtb infection in WT BMDM, whereas in the absence of caspase-11 we observed significantly higher OCR levels compared to WT infected BMDM (**Fig 4.17 B**). Assessment of maximal respiration yielded similar results. Data shows decreased maximal respiration in infected WT BMDM relative to uninfected WT BMDM (**Fig 4.17 C**). While in the absence of caspase-11, HKMtb infected BMDM have increased maximal respiration relative to uninfected controls (**Fig. 4.17 C**). ECAR measurements revealed increased basal glycolysis following HKMtb infection in WT and *Casp11*$^{-/-}$ BMDM relative to uninfected BMDM (**Fig 4.18 A**). However, in the absence of caspase-11 increased basal glycolysis was modest relative to uninfected BMDM. We observed significantly higher basal glycolysis and glycolytic capacity in HKMtb infected WT, compared to *Casp11*$^{-/-}$, BMDM (**Fig 4.18 B, C**). In summary, WT BMDM exposed to HKMtb had increased basal glycolysis and glycolytic capacity, whereas in the absence of caspase-11 this shift towards glycolysis was diminished, illustrating the ability of caspase-11 to regulate metabolism towards glycolysis in response to HKMtb infection.

Next, we aimed to evaluate the role of caspase-11 mediated NO-induced glycolytic commitment during Mtb bacterial clearance. Succinate supplementation was used as a mechanism to induce glycolysis in Mtb infected BMDM. WT and Casp11-/- BMDM were treated with succinate 3 hour post Mtb infection and 72 hours post-infection, Mtb DNA was measured to determine replication potential. Preliminary findings show that treatment with succinate to induce glycolysis led to increased bacterial clearance in *Casp11*$^{-/-}$ BMDM after 72h, illustrating that immunometabolic regulated bacterial clearance is a critical factor during host defence against infection (**Fig. 4.19**).

Previously, we showed that LPS mediated caspase-11 regulated NO production involved autocrine type I IFN signalling. Therefore, we aimed to determine whether Mtb mediated NO production similarly required caspase-11 regulated type I IFN signalling. Measurement of IFNβ secretion in WT and *Casp11*$^{-/-}$ BMDM following Mtb infection reveals that Mtb induces IFNβ secretion at 24 hour, which is sustained at 72 hours (**Fig 4.20**). In the absence of caspase-11, IFNβ secretion was reduced compared to WT at 72 hours (**Fig. 4.20**). Other data from the Creagh lab utilising pharmacological inhibitor of Jak1/2, ruxolitinib, to block STAT1-dependent iNOS expression in BMDM, showed that Mtb induced caspase-11 regulation of iNOS is STAT1 dependent[343]. These results complement this data, revealing that Mtb induced IFNβ secretion is caspase-11 dependent, confirming that a similar caspase-11 regulated autocrine type I IFN signal is required for STAT1 mediated iNOS expression and NO production during Mtb infection.

Lastly, we wanted to determine if our findings were translational to human alveolar macrophages infected with Mtb. Analysis of a publicly available dataset from Lavalett and colleagues showed the expression of human *Casp4, Casp5* and *Nos2* mRNA expression in splenic and alveolar macrophages of healthy controls and patients with active pulmonary Mtb infected *ex vivo* with two clinical isolates of Mtb (UT127 and UT205)[347]. Total RNA from splenic macrophages obtained from deceased donors infected with Mtb clinical isolates were compared to noninfected splenic macrophages as a model of extrapulmonary infection[347]. This study was designed to compare total RNA obtained from alveolar macrophages from TB patients infected with clinical isolates of Mtb to alveolar macrophages from control subjects. Analysis of both Casp4 and Casp5 mRNA revealed increased expression following infection with Mtb clinical isolates of both healthy control alveolar macrophages and from TB patients infected with clinical isolates UT127 and UT205 of TB (**Fig. 4.21 A, B**). However, this upregulation of Casp4 and Casp5 following infection *ex vivo* was not observed in splenic macrophages of deceased donors (Fig. 4.22 A, B). From this dataset we also analysed NOS2 expression in both alveolar and splenic macrophages following Mtb infection. However, we observed no increased expression of NOS2 in any macrophage subtype following infection (Fig. 4.22 C). The lack of NOS2 mRNA detected from *ex vivo* human macrophage infection with Mtb isolates is unsurprising as for many years determining the relevance of iNOS to human TB has been hindered by inability to induce human macrophage iNOS expression *in vitro* as they are observed *in vivo.* Macrophages in lungs of patients with clinically active Mtb infection have been shown to express catalytically competent NOS2[51].

4.4. Summary of main findings of Chapter 4

- Caspase-11 regulates glycolytic commitment in M1 'classically' activated murine macrophages.
- During M1 polarisation, caspase-11 alters macrophage metabolism by inducing citrate accumulation via aconitase-2 inhibition and increasing intracellular arginine levels by increasing expression of its transporter, CAT-2.
- Caspase-11 limits arginase-2 expression, which is associated with M2-like polarisation and OXPHOS metabolism, during M1 polarisation.
- Caspase-11 mediated NO production drives the M1-glycolytic switch, as reconstituting *Casp11*$^{-/-}$ BMDM with exogenous NO rescues their ability to alter metabolism towards glycolysis.
- Caspase-11-NO-glycolysis pathway mediates Mtb clearance. *Casp11*$^{-/-}$ BMDM with impaired NO production and reduced glycolysis have higher bacterial burden, however inducing glycolysis in the absence of NO inhibits bacterial growth.

4.5. Discussion

4.5.1. Caspase-11 mediated NO induced Glycolytic commitment

Nathan, Stuehr and Hibbs identified L-arginine-mediated NO as the M1 macrophage product responsible for cytostasis and reduced mitochondrial respiration via aconitase inhibition. Initially, ETC regulation by NO was identified by several groups, as competitive inhibition of cytochrome c oxidase decreased oxygen consumption[301]. Prior to the identification of NO, Drapier and Hibbs discovered that the iron-sulfur cluster enzyme aconitase was inhibited by the removal of labile iron atoms from the 4Fe-4S cluster by products of activated macrophages[301]. Inhibition of the TCA cycle mitochondrial enzyme aconitase-2 was found to be faster than either complex I or complex II of the ETC. However, endogenous respiration continued until the complexes were inhibited[298]. Our study found in *Casp11*$^{-/-}$ M1 BMDM, where there is impaired NO production, ACON-2 is highly expressed. Additionally, we observe ACON2 increased expression in WT M1 BMDM, although there is an accumulation of intracellular citrate. We suggest although ACON-2 protein expression is increased, activity may be impaired by s-nitrosylation at Cys594 or succination possibly by interfering with iron chelation[348],[349]. Reports have illustrated increased ACON-2 protein expression in the presence of fumarate, although activity is inhibited by succination of iron chelation. These reports further support our preliminary findings showing increased intracellular fumarate in the WT M1 stimulated macrophages, which is reduced in the absence of caspase-11. We suggest these PTM impaired ACON-2 activity, leading to the stalled TCA cycle and citrate accumulation.

NO-targeted enzymes, ACON2 and PDH, lead to disruptions in TCA carbon flow, which modulates the levels of essential metabolites, including citrate, itaconate, and succinate. Our preliminary results for Krebs cycle metabolites support our findings that ACON-2 expression is increased in *Casp11*$^{-/-}$ BMDM and correlated with intracellular citrate flux. In the absence of caspase-11, citrate did not accumulate, as ACON2expression increased in *Casp11*$^{-/-}$ BMDM after M1 polarisation, preventing a stall in TCA cycle carbon flow, as described by Palmieri and colleagues[325]. Reduced aconitase-2 enzymatic activity leads to citrate accumulation, which is reflective of stalled TCA cycle activity, forcing cellular energy demand to shift to glycolysis. These findings support reports of NO-mediated TCA cycle impairment, thereby reinforcing the pathological role of caspase-11 mediated NO production, as *Casp11*$^{-/-}$ M1 BMDM with impaired NO production have a reduced capacity to switch metabolism towards a glycolytic phenotype.

Drapier and Hibbs described a compensatory increase in glycolysis in activated macrophages following L-arginine-induced alterations to the intracellular macrophage environment, later referred to as glycolytic commitment[313]. However, the effect of NO on glycolysis appears to be context-dependent. Bailey and colleagues revealed that NO production did not affect the rate of glycolysis, despite the absence of NO, while observing changes in the expression of glycolytic proteins[312]. In the absence of NOS2, a rapid burst of glycolysis was observed approximately 40 min following LPS stimulation, before returning to the pre-activation state. The glycolytic burst was found to be correlated with the rate of proinflammatory cytokine production. Rapid TLR induced glycolysis independent of iNOS, was reported to be controlled by HK-II, glycolytic rate limiting enzyme, via TBK1, IKKε and Akt, to support *de novo* fatty acid synthesis required for Golgi and endoplasmic reticulum expansion integral to population expansion[350]. However, during long-term glycolytic commitment, there is a second upregulation of glycolysis, dependent on NO, which is mediated by mTOR, HIF1α, and NOS2, and is described as activated macrophage biphasic glycolytic response[128,329]. Our data revealed caspase-11 role in NO production modulated activated macrophage metabolism to favour glycolytic commitment. We observed that the reduction in maximal respiration, observed during M1 polarisation in WT BMDM, was impaired in *Casp11*$^{-/-}$ BMDM, as was the reduction in glycolysis (as measured by ECAR and τavg).

As previously described NO targets enzymes of the TCA cycle to stall carbon flux and investigations have also reported that complex I and complex II sensitivity to NO leads to inhibited mitochondrial respiration[321.] During M1 polarisation, NO has been demonstrated to affect the expression of mitochondrial proteins of the ETC, such as complex subunits, containing NADH binding domains. Therefore, NO targeted complex activity leads to reduced NADH oxidation and decreased oxygen reduction to H_2O, as electron transportation generated by complex mediated redox reactions is impaired. Additionally, reduced NADH or $FADH_2$ generation due to decreased activity of enzymes involved in the TCA cycle, alters the ketoglutarate/citrate ratio and limits acetyl-CoA entry into the TCA cycle which further slows respiratory chain activity. Therefore, reduced detection of NADH compared to NAD+ is associated with impaired OXPHOS. NADH/NAD+ ratio measuring glycolytic flux, with a high NADH/NAD+ ratio (τavg) associated with OXPHOS and a low NADH/NAD+ ratio (τavg) associated with glycolysis. Utilising 2P FLIM, we measured changes in lifetime of protein-bound NADH and free cytosolic NAD+. OXPHOS is impaired when NADH/NAD+ levels are elevated[151], as during the Kreb's cycle NAD+ is reduced to NADH, which consequently binds complexes of ETC to form ATP. This supports our findings, illustrating increased free-oxidized form of NAD+ with a shorter half-life in WT M1 BMDM, associated with glycolysis. While in the absence of *Casp11*$^{-/-}$ and reduced NO production, we

found NADH generation was not impaired and OXPHOS metabolism is maintained. This confirms seahorse OCR and ECAR data illustrating WT M1 BMDM are more glycolytic, whereas *Casp11*$^{-/-}$ M1 BMDM undergo OXPHOS metabolism.

4.5.2. Arginine Metabolism pathway divergence influence on macrophage metabolism

M1 polarised macrophages predominantly catabolise arginine to produce NO and citrulline via NOS2, which is associated with glycolytic commitment, while during M2 polarisation, arginine catabolism is diverted to Arg1 to produce L-ornithine, associated with OXPHOS. Therefore, the dominant pathway of arginine metabolism is considered to be a key regulator of macrophage polarisation and function. The results presented in Chapters 3 and 4 demonstrate caspase-11 role in the urea cycle at several stages. We observed caspase-11 dependence in urea cycle metabolism at several steps, including L-arginine uptake via regulation of CAT2 and utilization of L-arginine for NO production via regulation of iNOS expression and negative regulation of Arg2. These regulatory roles of caspase-11 in arginine metabolism and NO production are required for the regulation of aerobic glycolysis and functional plasticity in inflammatory macrophages.

The L-arginine paradox is an important phenomenon associated with arginine metabolism, which refers to the exogenous L-arginine control of NO-mediated biological effects, thereby influencing macrophage polarisation. Although the intracellular L-arginine physiological concentration far exceeds the Km of NOS, supplying exogenous L-arginine still increases NO production[351]. Additionally, utilising arginine supplementation, it was discovered that arginase activity and urea production diverting from NOS are associated with supplementation[333]. Therefore, excessive arginine availability leads to impaired nitric oxide production. There are many hypotheses to explain this phenomenon, including the concept that, rather than intracellular L-arginine, extracellular L-arginine becomes the NOS substrate when the γ+ transport system regulates uptake[333]. This is supported by CAT-2 overexpression enhancing arginine uptake six-fold and NO production two-fold, suggesting iNOS-mediated NO production depends on the recycling of arginine-derived citrulline back to arginine, and not arginine supplementation. This complements our preliminary data which shows high levels of extracellular L-arginine in *Casp11*$^{-/-}$ M1 BMDM, while NO production was reduced.

Historically, ARG2 has been viewed as having the same function as ARG1 because of the limited available information. Emerging evidence suggests a differential role for ARG2 during inflammatory macrophage activation. There are incongruences regarding ARG1 and ARG2 expression in M1 polarised macrophages, although their metabolising effects on L-arginine are similar, they are considered anti-inflammatory and pro-inflammatory, respectively. However, ARG1 expression was impaired in the absence of caspase-11 and NO, whereas ARG2 was increased. Reports have shown ARG1 reduced expression coincides with reduced NOS2 expression, as S-nitrosylation activates ARG1 by stabilizing its active homotrimer. Disruption of this interaction leads to decreased ARG1 enzymatic activity. Previous reports have illustrated the importance of M1 polarisation for M2-priming, to support response to M2-like cytokine-induced plasticity transition[324], reflective of an inflammatory-wound repair macrophage model. Sequentially, maximal Nos2 precedes Arg1 maximal expression in LPS-induced macrophages. LPS has higher arginase activity than IL-4, whereas NO is only generated by LPS[352]. This supports our findings that in the absence of caspase-11, ARG1 expression and activity are impaired, leading to reduced urea and creatine, coinciding with impaired iNOS-mediated NO and citrulline. In contrast, other studies have reported the upregulation of ARG1 and other M2-like markers in the absence of iNOS, establishing an anti-inflammatory milieu[353]. HIF isoforms are responsible for regulating iNOS and ARG by functional antagonism, where HIF1α induces iNOS-mediated NO production and HIF-2α suppresses NO via Arg1 activation. HIF1α is a known transcription factor of iNOS gene expression in response to cytokine stimulation as well as intermediates of glycolysis and pentose phosphate pathway. Suppression of HIF-1α is required to promote the switch from aerobic glycolysis to OXPHOS, and subsequently trigger an anti-inflammatory response[354].

IL-10, an important cytokine that mediates arginine metabolism, promotes arginase expression and polyamine production[334,355] and simultaneously limits inflammation via NOS2 degradation to regulate mitochondria respiration[,342],[335]. IL-10 reduces CAT-2 transcription, leading to NO reduction due to the decreased availability of intracellular arginine[336], contributing to the arginine paradox. Additionally, intracellular arginine availability has a regulatory role in iNOS expression, as decreased iNOS expression is observed in *CAT2*$^{-/-}$ M1 BMDM[310,336]. Therefore, CAT-2 is a major regulator of M1 macrophage NO production, whereas IL-10 shifts polarisation to an anti-inflammatory phenotype. LPS-driven IL-10 autocrine activity has been suggested to relieve TCA cycle break via ARG2, mediating the transition from aerobic glycolysis to OXPHOS. In the absence of Arg2, HIF-1α and IL-1β are elevated, which is associated with the maintenance of glycolysis. These data suggest that ARG2 resolves glycolysis-mediated inflammation following

LPS exposure through IL-10 autocrine signalling, as IL-10 signalling alone does not induce ARG2 expression. We propose that, in the absence of caspase-11, LPS-driven IL-10 accelerates ARG2 inflammatory resolution, driving an anti-inflammatory phenotype.

MiR-155 is of great importance for M1 polarisation, targeting inducer and inhibitory genes to promote inflammation. ARG2 is a known target of miR-155 negative regulation. Previous reports have illustrated that miR-155 amplifies NO production and cGMP signalling[357] while negatively regulating Arg2 induced L-ornithine expression. As previously discussed, ARG2, which is located in the mitochondria, mediates mitochondrial dynamics and promotes fission associated with mitophagy and OXPHOS. In contrast, miR-155 inhibits mitophagy via the PINK1 partner protein Bcl2 associated athanogene 513, leading to the accumulation of damaged mitochondria and glycolysis[358]. Our data illustrate that miR-155 is a regulator of caspase-11, as *miR-155*$^{-/-}$ BMDM have reduced Casp11 translation. Patoli et al., described how caspase-11 inhibits mitophagy during classical M1 macrophage activation via PINK1 degradation[256]. These data suggest a potential link between miR-155 and caspase-11 during M1 deregulated mitophagy. In parallel, arginase produced polyamines are associated with autophagy and spermidine hypusination-mediated reduction of NOS2 and CAT-2 expression and play a protective role against aging-related mitochondrial dysfunction[359], suggesting that arginine metabolism divergence towards arginase actively downregulates CAT-2 mediated NO production and is associated with increased mitophagy. We hypothesise that miR-155 regulation of caspase-11, associated with inhibition of mitophagy, results in iNOS catabolism of L-arginine, which is associated with glycolysis. We propose that miR-155 associated inhibition of mitophagy affects the expression of mitochondrial proteins including ARG2.

Caspase-11 role in diverting arginine metabolism towards NO production underpins the M1 macrophage shift towards glycolytic commitment. Additionally, we suggest caspase-11 role in M1 polarisation is required for M2-priming for inflammatory resolution, reflecting the macrophage inflammation-wound healing dogma.

4.5.3. Glycolysis-mediated Mtb Clearance

Many reports have demonstrated the impact of NO and immunometabolism on Mtb restriction. However, to our knowledge, NO-mediated alterations in mitochondrial respiration have not been described in Mtb infection clearance. Multiple reports have shown that NOS2 affects

bacterial survival via its cytostatic and cytotoxic effects. Chan J and colleagues reported that the L-arginine-dependent cytotoxic pathway effectively inhibits growth and kills Mtb[360]. Similarly, iNOS inhibitors and NOS2 deficiency increase mortality, bacterial burden, and pathological tissue damage, confirming the role of NO in resistance against Mtb[304,361]. These studies support our observation that caspase-11 mediated NO reduced Mtb growth, as *Casp11*$^{-/-}$ Mtb-infected BMDM had increased bacterial loads compared to WT BMDM. However, treatment with the NO donor DETANO increased bacterial clearance in *Casp11*$^{-/-}$ to levels similar to those observed in WT BMDM. Treatment with DETANO also restored the glycolytic switch in *Casp11*$^{-/-}$ BMDM, this shift in immunometabolism toward glycolysis is central to Mtb containment. Studies from the Sheedy group and others suggest that the anabolic M1 macrophage metabolism in response to Mtb is important for the antimicrobial oxidative burst and increased transcriptional/translational activity required for cytokine production[362–364]

Following exposure to iNOS-inducing agents such as LPS, upregulation of ASS and constitutive expression of ASL mediate the citrulline-NO cycle. L-citrulline uptake and ASS-mediated recycling to argininosuccinate, followed by ASL mediated arginine and fumarate synthesis is required for arginine substrate availability from iNOS mediated NO and L-citrulline, which continuously cycles. This resynthesis of arginine and arginine uptake is important to ensure this rate limiting substrate is available for iNOS or arginase activity[13,14]. During bacterial infection *mTB* Ass-1 deficient BMDM has increased pathogenic growth whereas *H. pylori* infection expresses an arginase the inhibits NO production in activated macrophages, also leading to less effective bacterial clearance.

Gleeson and colleagues utilised glucose-deprived galactose-containing media to force ATP generation to glutamine-driven oxidative metabolism or a D-glucose mimic, 2DG, to inhibit Mtb-mediated glycolysis. Inhibition of the energetic shift impacted macrophage function, as decreased IL-1β, increased IL-10 and bacterial burden were observed. Additionally, generation of metabolic intermediates can act as signalling molecules to promote macrophage phenotype, as observed when increased intracellular levels of succinate result in the stabilisation of HIF-1α, leading to increased glycolysis and initiation of IL-1β gene transcription via binding the hypoxia response element of its promoter 45. This confirms that Mtb-driven immunometabolism is linked to macrophage functionality. Our preliminary data similarly illustrated the role of caspase-11 mediated glycolysis during Mtb clearance. As we have shown, *Casp11*$^{-/-}$ BMDM have Mtb persistence and reduced glycolytic potential. We found that induction of glycolysis with exogenous succinate facilities increased Mtb clearance in the absence of caspase-11 and NO.

These findings suggest that the immunomodulatory role of NO is more important during Mtb clearance than its direct bacterial cytotoxicity alone. The metabolic status of the macrophage therefore has a major effect on host cell fate and bacterial containment. In fact, novel approaches to enhance host defence against TB include supplementation with macronutrients in glutamine, to enhance metabolic reprogramming and arginine, to enhance NO production[365,366].

It has long been debated whether the role of NO in human defence against Mtb is critical, as has been observed in mice. While it has been shown that human TB lesion macrophages have upregulated iNOS expression[367], early studies suggested that Mtb inhibition was NO independent and failed to illustrate a role for IFNγ in inducing anti-microbial effects. However, more recent reports have shown the mycobacteriostatic activity of NO-producing Mtb-infected macrophages[368] with antimicrobial activities dependent on iNOS expression[304]. NO plays a role in alveolar macrophage modulation of IL-1β and TNFα synthesis, which subsequently amplifies NO production in a positive feedback loop during pulmonary tuberculosis[369]. Macrophage consumption of L-arginine by iNOS, but not arginase, leads to T cell CD3ζ re-expression and proliferation recovery necessary for a robust adaptive immune response[370]. These data suggest that NO plays a contributory role in the human host defence against Mtb. While our studies did not observe alterations in NOS2 expression following infection with clinical isolates of Mtb, we observed that infection of both healthy and TB patient alveolar macrophages infected with Mtb induced the expression of Casp4 and Casp5, suggesting that further investigation of the human orthologs of caspase-11 during Mtb infection in macrophages could be an effective immunomodulatory therapeutic strategy against infection prevalence.

Competition for L-arginine substrates by iNOS and arginase is important during the clearance of bacterial infection. Treatment of murine peritoneal macrophages infected with T. gondii with nor-NOHA, an inhibitor of arginase activity, resulted in increased NO production and reduced bacterial growth[371]. Caspase-11, in addition to regulating iNOS expression and NO production, appears to be a key regulator of arginine metabolism associated with macrophage functionality, as we observed increased Arg2 levels, in addition to impaired iNOS upregulation following LPS stimulation of in caspase-11 deficient macrophages. Corresponding with our observations that caspase-11 deficient macrophages retain OXPHOS-dependent metabolism following M1 cytokine stimulation related to impaired NO production, Arg2 activation may be contributing to this OXPHOS metabolism. Additionally, Arg2 mediated L-ornithine production leads to

spermidine conversion to hypusine, and eif5A hypusination is associated with altered bacterial clearance[359,372].

Coinciding with the contribution of iNOS and NO to the host defence against Mtb, previous reports have investigated the role of type I IFN during infection. Banks and colleagues found that IFNβ signalling mediates a protective capacity against Mtb via increased NO production[373]. These data support our previous findings showing caspase-11 mediated type I IFN autocrine activity mediates NO production. Additionally, type II IFN, which increases aerobic glycolysis, plays a protective role against Mtb infection. As type I and type II IFNs can induce STAT1 activation, this can obscure their individual antimicrobial effects. Therefore, Desvignes et al. used IFNAR- and IFNGR-deficient mice to investigate two overlapping signalling pathways during Mtb infection, with the cofounding factor STAT1 illustrated to be important for host survival[374]. Type I IFNs play an early non-redundant protective role in the absence of IFNγ, whereas loss of type I IFN signalling alone did not lead to infection, similar to WT mice[374]. Type I IFN is essential for the recruitment, differentiation, and survival of macrophages and is crucial for mycobacterial containment. However, excess type I IFNs can be detrimental to infection control. Many studies contradict the role of type I IFNs during host defence with time- and cell-dependent distinct effects of type I IFN.

Nutrient utilisation and metabolic pathway engagement determine immune cell function. It is well established that, during an infection switch, increased glycolysis is critical for macrophage Mtb containment during early infection. The key players in the host innate immune defence, including proinflammatory cytokine secretion, autophagy, and trained immunity, are all linked to immunometabolism. These breakthroughs have driven the exploration of future therapeutics to manipulate host metabolism to reduce infection rates and mortality. The data presented here indicate a novel role for caspase-11 in controlling macrophage metabolism to aid bacterial clearance. This process involves caspase-11 regulation of type I IFN driving STAT1 mediated iNOS expression. Our data show that caspase-11 mediates the availability of nutrients required for the urea cycle production of NO. These observations enhance our understanding of classical M1 macrophage regulation of NO production and caspase-11 mediated NO glycolysis as well as the immunomodulatory function caspase-11 mediated NO in host defence during mycobacterial infection.

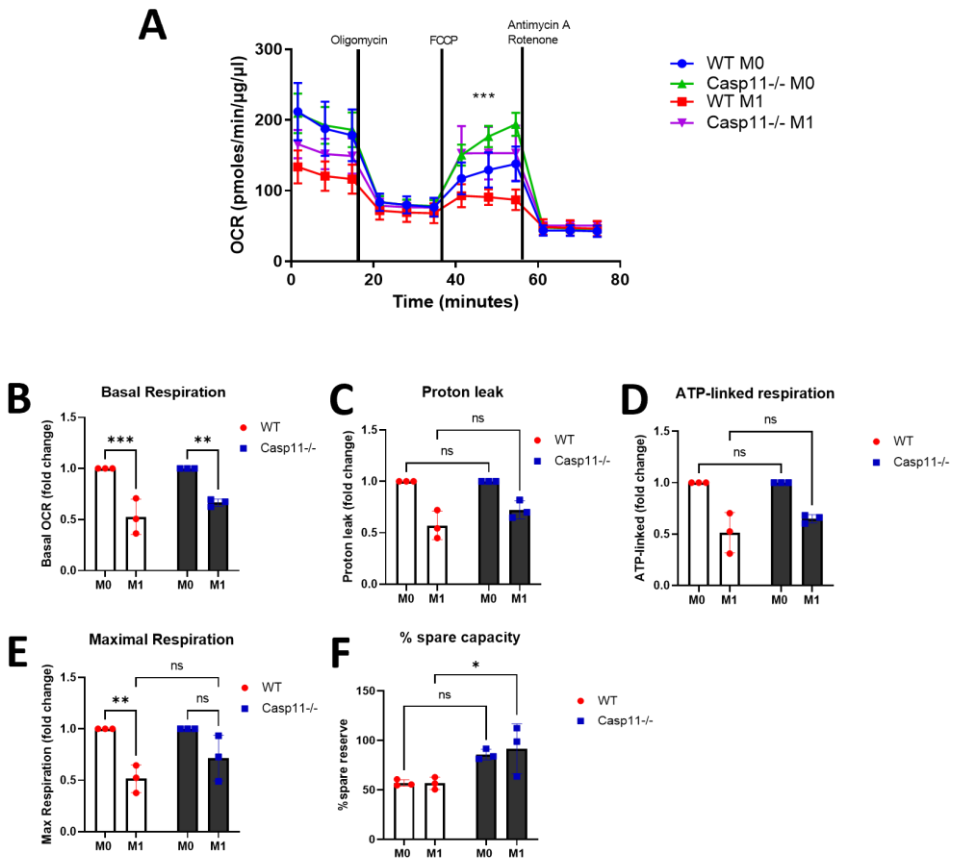

Figure 4.1: Absence of caspase-11 during M1 polarisation sustains Oxidative Phosphorylation

WT and *Casp11*$^{-/-}$ BMDMs were seeded at 80,000 cells/well in Seahorse XF96 cell culture plates O/N prior to 48h stimulation with LPS (100 ng/ml) and IFNγ (50 ng/mL). Prior to analysis on Seahorse XFp Extracellular Flux Analyser (Aligent Technologies), media was exchanged for serum free non-buffered DMEM and incubated for 1 h in non-CO_2 incubator. Wells were sequentially treated with oligomycin (Oligo), FCCP, and rotenone plus antimycin A (Rot/AA) by injection during seahorse requisition of: (A) Oxygen Consumption Rate (OCR). (B) Basal respiration; (C) proton leakage; (D) ATPlinked respiration; (E) Maximal respiration; and (F) % Spare capacity were measured as fold change relative to naïve M0 BMDM. Values represent the mean ± S.E.M of n=3. Statistical analysis was performed using two-way ANOVA ; *p<0.05, **p <0.01, ***p<0.001 (Sidak post-test).

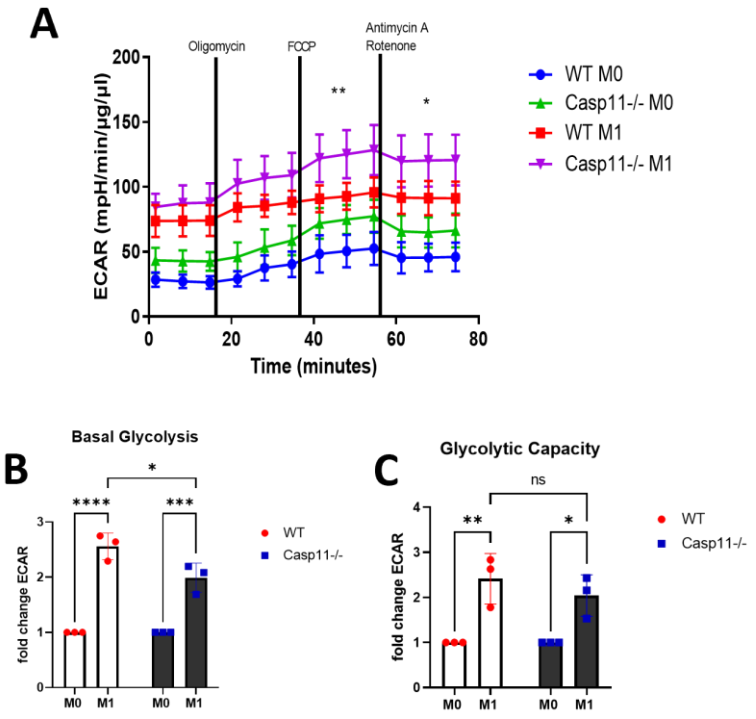

Figure 4.2: Absence of caspase-11 during M1 polarisation impairs the shift to glycolysis

WT and *Caspase-11*$^{-/-}$ BMDMs were seeded at 80,000 cells/well in Seahorse XF96 cell culture plates O/N prior to stimulation with LPS (100 ng/ml) and IFNγ (50 ng/mL) for 48 h. Prior to seahorse analysis, media was exchanged for serum free non-buffered DMEM and incubated for 1 h in non-CO_2 incubator. Wells were sequentially treated with oligomycin (Oligo), FCCP, and rotenone plus antimycin A (Rot/AA) by injection during seahorse requisition of (A) Extracellular Acidification Rate (ECAR). (B) Basal glycolysis and (C) Glycolytic capacity were analysed as fold change relative to naïve M0 macrophages. Values represent the mean ± S.E.M of n=3. Statistical analysis was performed using two-way ANOVA ; *p<0.05, **p <0.01, ***p<0.001 (Sidak post-test).

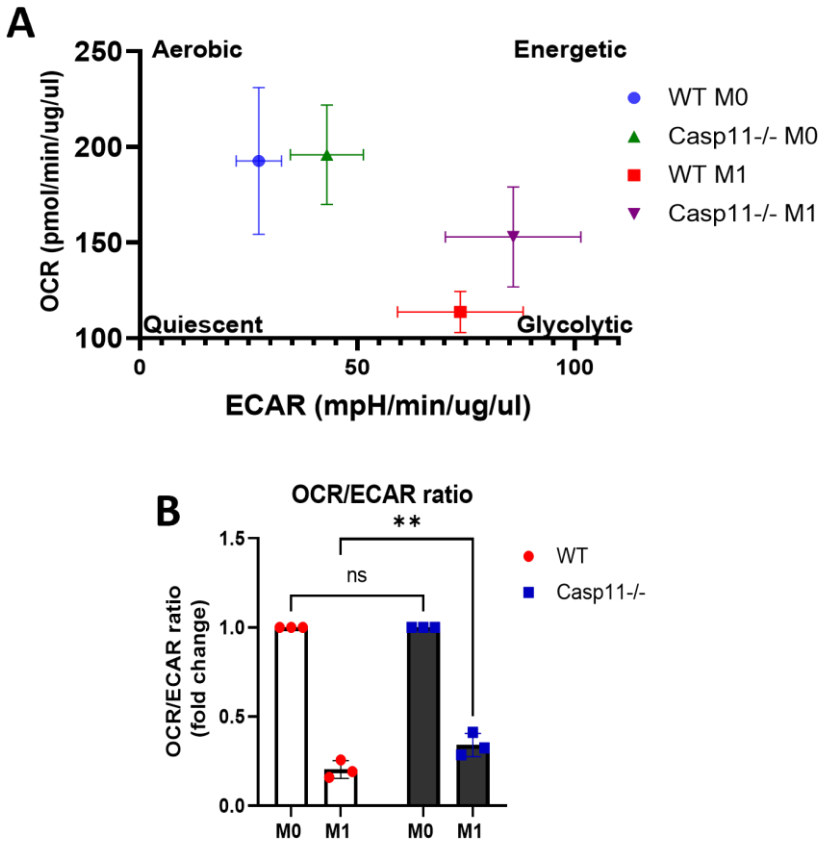

Figure 4.3: Caspase-11 regulates M1 macrophage shift towards glycolytic commitment

WT and *Casp11*$^{-/-}$ BMDM were seeded at 80,000 cells/well in Seahorse XF96 cell culture plates O/N prior to stimulation with LPS (100 ng/mL) and IFNγ (50 ng/mL) for 48 h. Prior to seahorse analysis, media was exchanged for serum free non-buffered DMEM and incubated for 1 h in a non-CO_2 incubator. Wells were sequentially treated with oligomycin (Oligo), FCCP, and rotenone plus antimycin A (Rot/AA) by injection during seahorse requisition of OCR and ECAR. (A) Energy demands were graphed as (A) OCR vs ECAR and (B) OCR/ECAR ratio. Values represent the mean ± S.E.M of 3 independent experiments. Statistical analysis was performed using two-way ANOVA ; **p <0.01 (Sidak post-test).

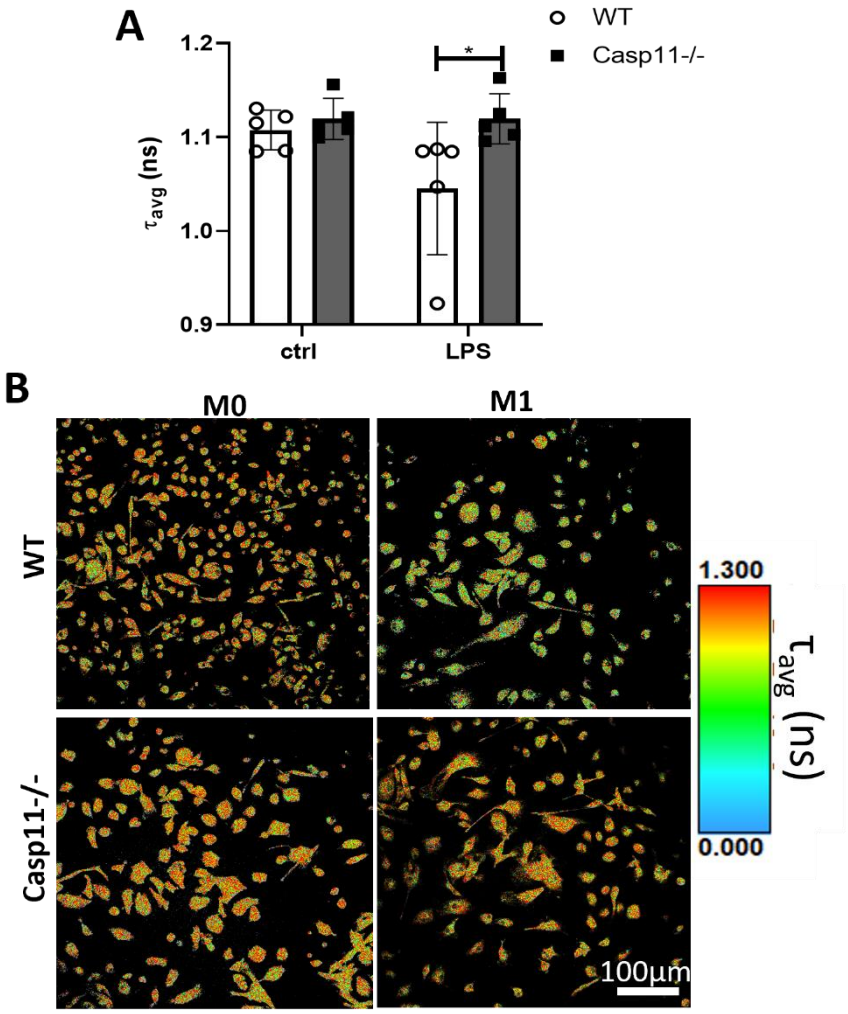

Figure 4.4: Caspase-11 during M1 stimuli alters bound-NADH to free-NADH states, associated with glycolysis

WT and *Casp11*$^{-/-}$ BMDM were seeded at 10^6 cells/ml in $3cm^3$ dish O/N prior treatment. Cells were unstimulated (M0) or stimulated with LPS (100 ng/ml) and IFNγ (50 ng/mL) (M1) for 6 h. Single cell 2P FLIM imaging analysis of NAD(P)H and FAD^+ autofluorescence to infer cellular metabolism as a measure of average fluorescence lifetime (A)τ_{avg}. (B) Representative FLIM images of WT and Casp11-/- BMDM untreated or M1 stimulated for 6 h. Values represent the mean ± S.E.M of n=3. Statistical analysis was performed using two-way ANOVA ; *p<0.05 (Sidak post-test).

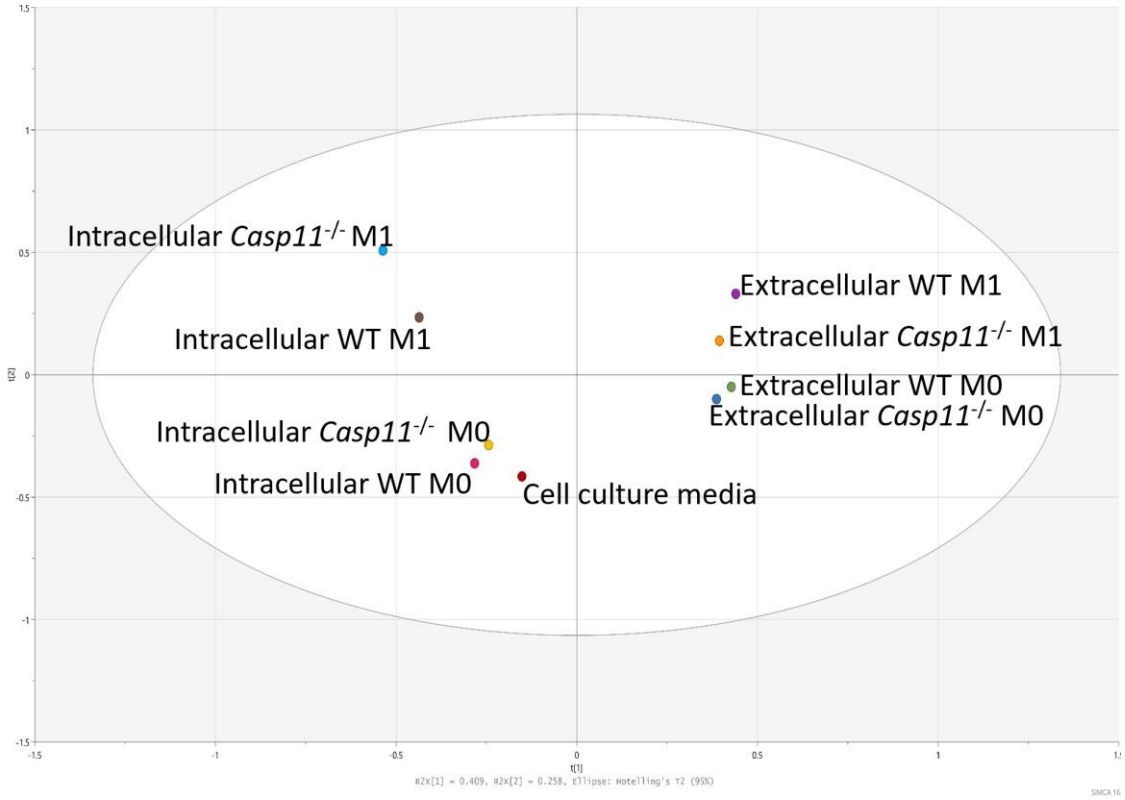

Figure 4.5: Intracellular and extracellular metabolite profiles are distinct in M1 polarised macrophages from WT and caspase-11-deficient BMDM

WT and *Casp11*$^{-/-}$ BMDM were seeded at 10^7 cells/10cm^3 dish O/N prior treatment. Cells were stimulated with LPS (100 ng/ml) and IFNγ (50 ng/mL) for 48 h. Culture supernatants and complete culture media were collected and filtered using 10kDa molecular weight cut-off centrifugal filter. Supernatants were diluted 1:3 in H_2O/D_2O for NMR analysis of extracellular metabolites. Intracellular metabolites were extracted from whole cell lysates using 9:1 methanol:chloroform precipitation. Organic solvent was removed using rotor vacuum and dried product was resuspended in H_2O/D_2O for NMR analysis of intracellular metabolites. Metabolites spectra was measured by 600Hz H^1 NMR. Prinicipal component analysis (PCA) score plots were generated by analysis of metabolic profiles from intracellular and extracellular extract spectra profiles.

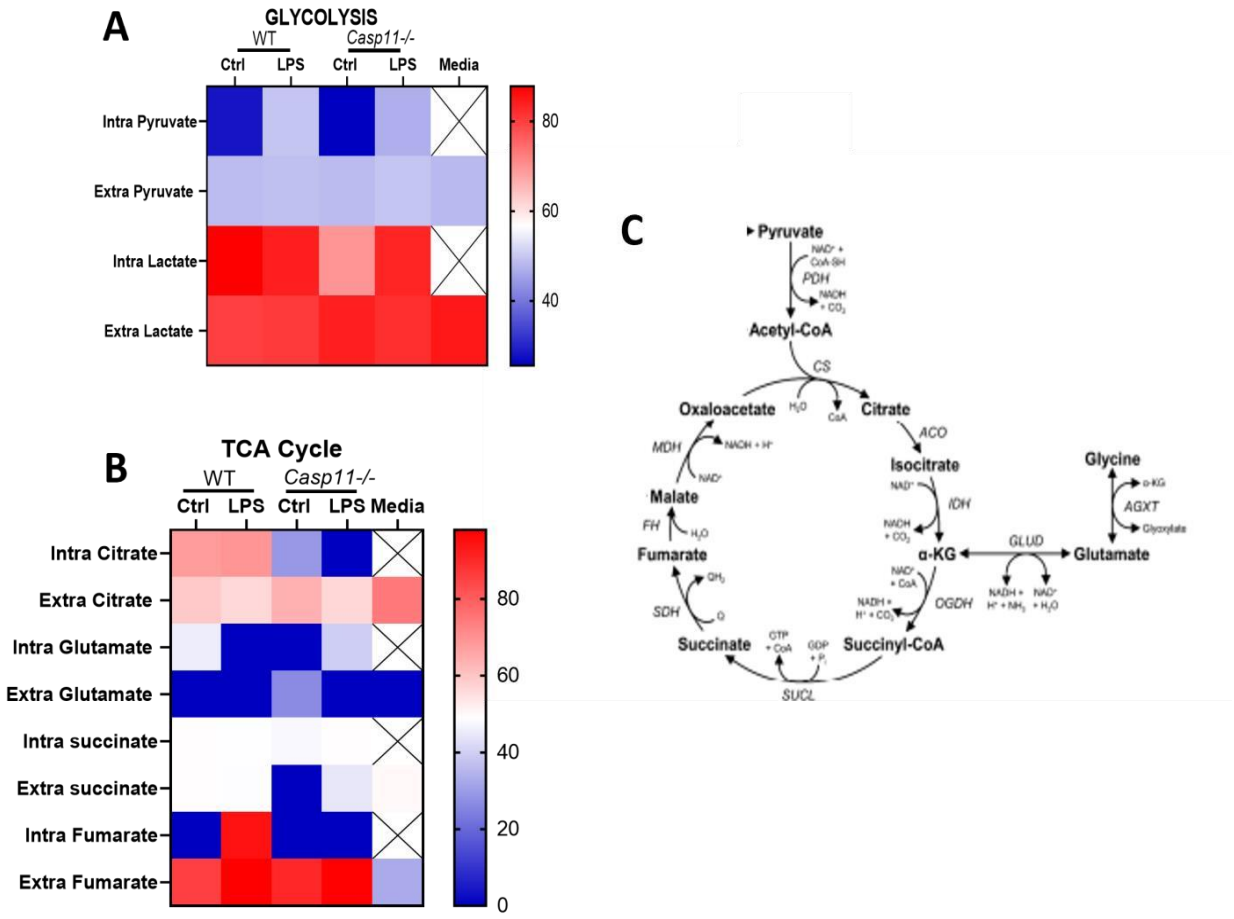

Figure 4.6: M1 macrophage-associated citrate accumulation does not occur in the absence of caspase-11.

Heat Map of metabolites spectra measured by 600Hz H^1 NMR with analysis of metabolites by AssureNMR (Bruker) and SIMBA software. Heatmap associated with intracellular and extracellular metabolites of (A) glycolysis and (B) TCA cycle from BMDMs from WT and *Casp11*$^{-/-}$ mice activated with M1 cytokines; LPS (100ng/mL) and IFNγ (50ng/mL) for 24 h compared to unstimulated (M0). (C) Schematic illustration of the TCA cycle. Colour scale represents the scaled abundance of each metabolite, with red indicating high abundance and blue indicating low abundance. Results are based on n=1 experiments and need to be repeated.

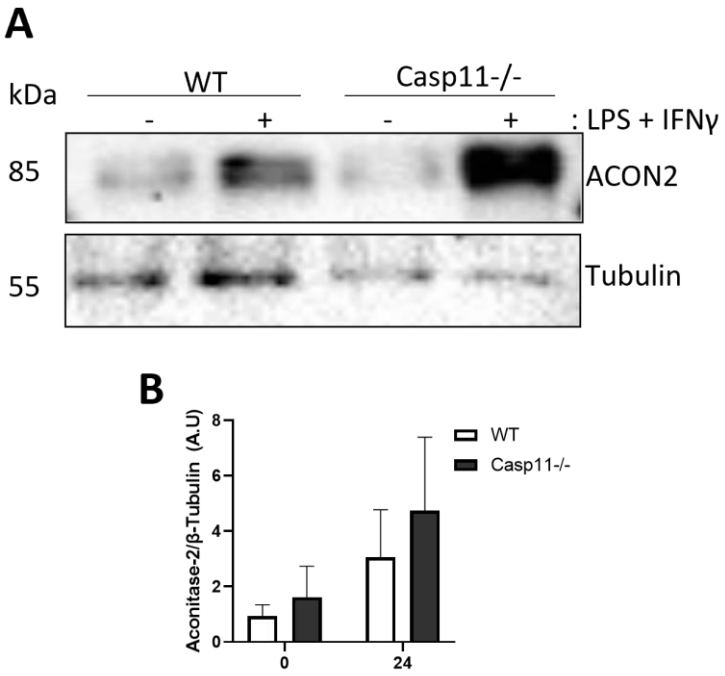

Figure 4.7: Aconitase-2 (ACON2) expression remains elevated in M1 polarised caspase-11-deficient BMDM

WT and *Casp11*$^{-/-}$ BMDM were seeded at 10^6 cells/ mL in 24 well plate 24 h prior to stimulation with LPS (100 ng/mL) and IFNγ (50 ng/mL) for 24 h. Whole cell lysates of WT and *Casp11*$^{-/-}$ BMDM (20 µg) were analysed by western blot for expression of aconitase-2 and β-tubulin, as loading control. Blots are representative of three independent experiments. Densitometry analysis was performed of aconitase-2 (relative to β-tubulin) Values represent the mean ± S.E.M of n=3. Statistical analysis was performed by two-way ANOVA; *p<0.05, **p <0.01 (Sidak post-test).

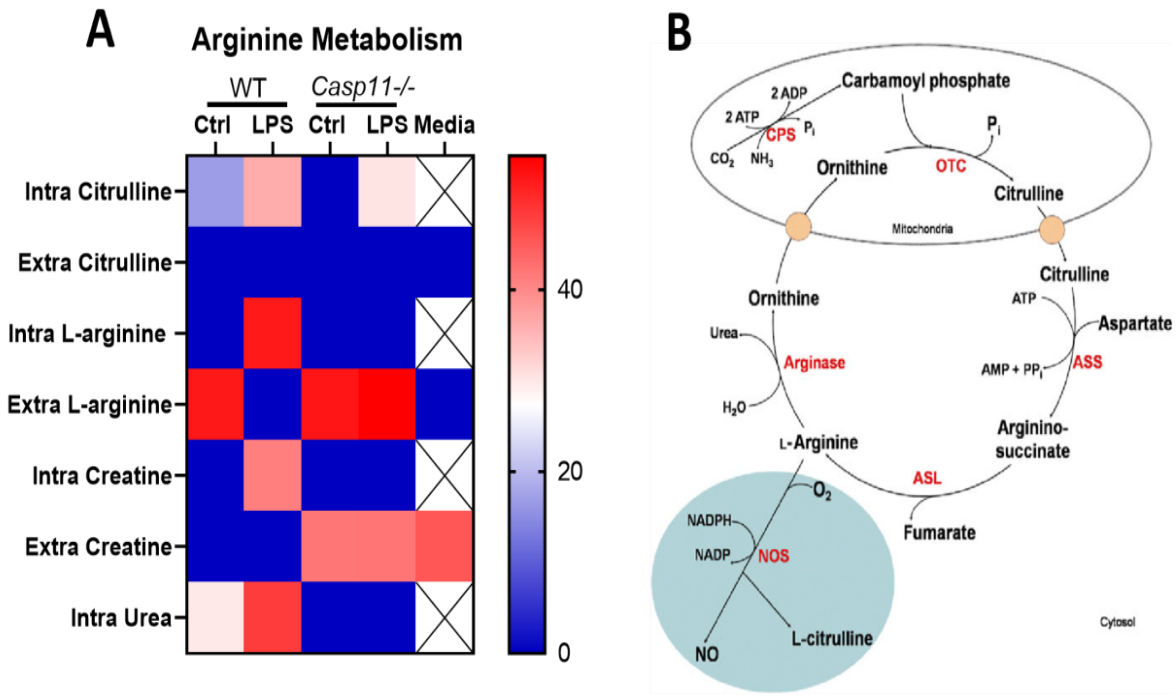

Figure 4.8: L-arginine intracellular/extracellular distribution is impacted in the absence of caspase-11

Heat Map of metabolites spectra measured by 600Hz H^1 NMR with analysis of metabolites by AssureNMR (Bruker) and SIMBA software. Heatmap associated with intracellular and extracellular metabolites of (A) arginine metabolism from BMDMs from WT and *Casp11*$^{-/-}$ mice activated with M1 cytokines; LPS (100ng/mL) and IFNγ (50ng/mL) for 24 h compared to unstimulated (M0). (B) Schematic illustration of the Urea cycle. Colour scale represents the scaled abundance of each metabolite, with red indicating high abundance and blue indicating low abundance. Results are based on n=1 experiments and need to be repeated.

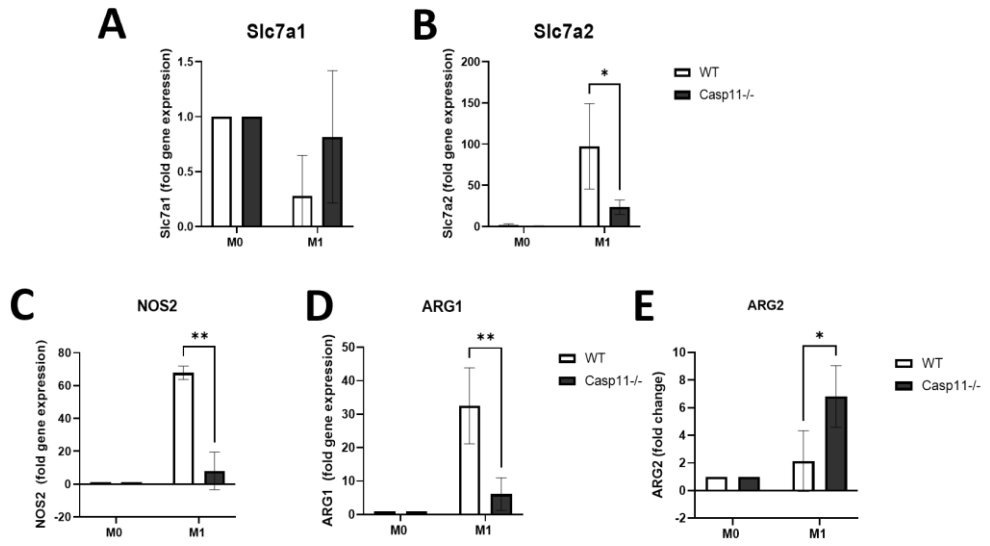

Figure 4.9: Upregulation of the L-Arginine membrane bound transporter CAT-2 (Slc7a2) is impaired in M1 polarised *Casp11*$^{-/-}$ BMDM

WT and *Casp11*$^{-/-}$ BMDM were seeded at 10^6 cells in 6 well plate O/N prior to stimulation with LPS (100 ng/mL) and IFNγ (50 ng/mL) for 24 h. RNA was isolated and converted to cDNA for mRNA expression analysis. CAT-1 (Slc7a1), CAT-2 (Slc7a2), NOS2 ARG1 and ARG2 were measured and quantified by qPCR. Data are normalized to the endogenous reference gene, GAPDH, and relative gene expression ΔΔCT was calculated relative to untreated sample. Values represent the mean ± S.E.M of three independent experiments run in triplicate. Statistical analysis was performed using two-way ANOVA ; *p<0.05, **p <0.01, ***p<0.001 (Sidak post-test).

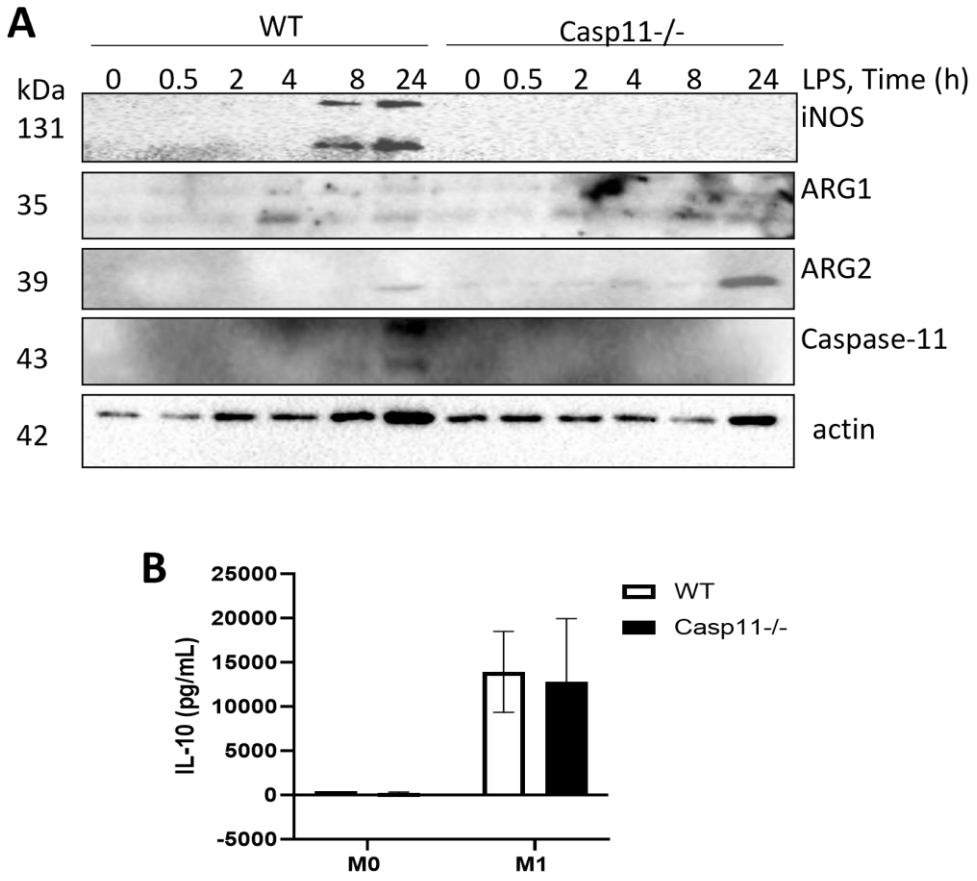

Figure 4.10: Caspase-11 regulates ARG2 expression during proinflammatory stimulation

WT and *Casp11*$^{-/-}$ BMDM were seeded at 10^6 cells/mL. After 24 h, BMDM were stimulated with 1µg/mL LPS over a 24 h timecourse, as indicated. (A) Whole cell lysates of WT and *Casp11*$^{-/-}$ BMDM (20 µg) were analysed by western blot for expression of iNOS, ARG1, ARG2, caspase-11 and β-actin, as loading control. Blots are representative of three independent experiments. (B) Supernatants collected 24 h following LPS stimulation were analysed for the expression of IL-10 by ELISA. Graphed values represent the mean ± S.E.M of three independent experiments. Statistical analysis was performed using two-way ANOVA.

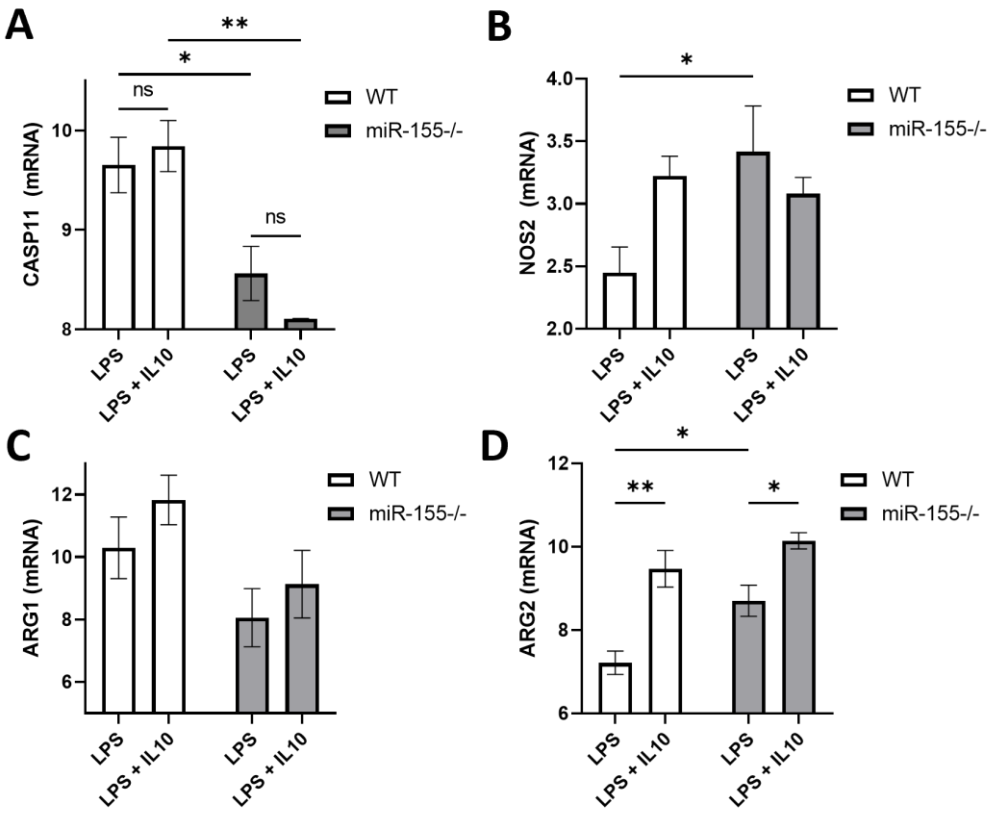

Figure 4.11: miR155 regulates Casp11 expression

Graph represents relative Casp11 mRNA expression values analysed using publicly available data set (GSE151835). WT and *miR155*$^{-/-}$ BMDM were stimulated in biological duplicate with LPS (100ng/mL) or LPS + IL10 (20ng/mL) to generate 4 groups; WT LPS, WT LPS + IL10, miR155-/- LPS and miR155-/- LPS + IL10. RNA was analysed by Affymetrix microarray and (A) Casp11, (B) NOS2, (C) ARG1 and (D) ARG2 mRNA expression across each group was mined from GSE151835 dataset. Graphed values represent the mean ± S.E.M. Statistical analysis was performed using two-way ANOVA ; *p<0.05, **p <0.01 (Tukey post-test).

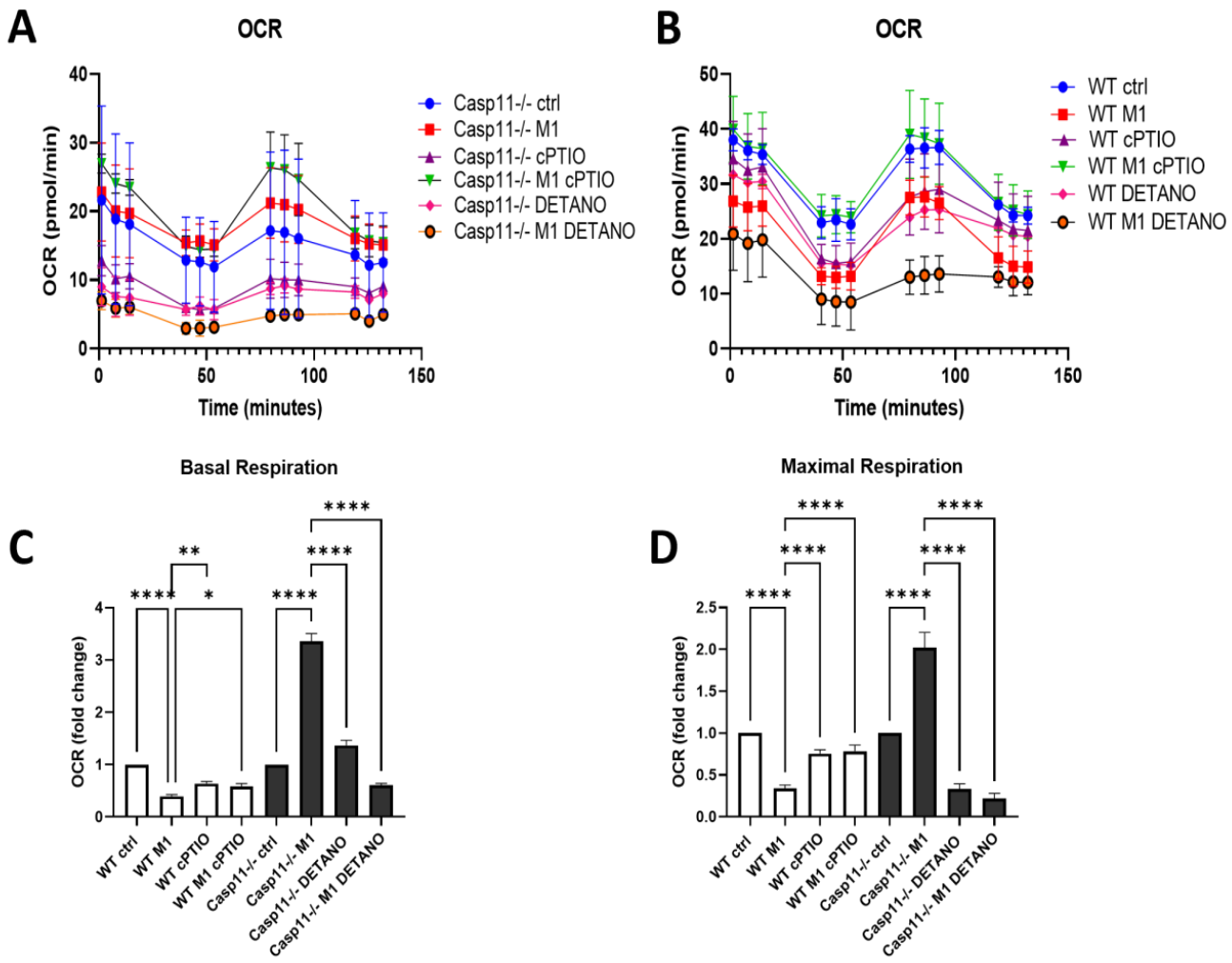

Figure 4.12: Caspase-11-mediated NO production impairs oxidative phosphorylation during M1 polarisation

WT and *Casp11*$^{-/-}$ BMDMs were seeded at 80,000 cells/well in Seahorse XF96 cell culture plates O/N prior treatment. BMDM were pretreated with 50µM c-PTIO (NO scavenger) and stimulated with LPS (100 ng/ml) and IFNγ (50 ng/mL) for 48 h, while BMDMs were post-treated with DETANO (NO donor). One hour prior to seahorse analysis media was exchanged for serum free non-buffered DMEM with 50µM c-PTIO or 25µM DETANO and incubated for 1 hour in non-CO_2 incubator. Wells were sequentially treated with oligomycin (Oligo), FCCP, and rotenone plus antimycin A (Rot/AA) by injection during Oxygen Consumption Rate (OCR) requisition by Seahorse XFp Extracellular Flux Analyser (Aligent Technologies). OCR of was measured from (A) WT and (B) *Casp11-/-* BMDM. (C) Basal respiration and (D) maximal respiration were measured as fold change relative to naïve M0 BMDM. Values represent the mean ± S.E.M of n=3. Statistical analysis was performed using one-way ANOVA comparing groups to M1 treated BMDM; *p<0.05, **p <0.01, ***p<0.001, ****p<0.0001 (Sidak post-test)

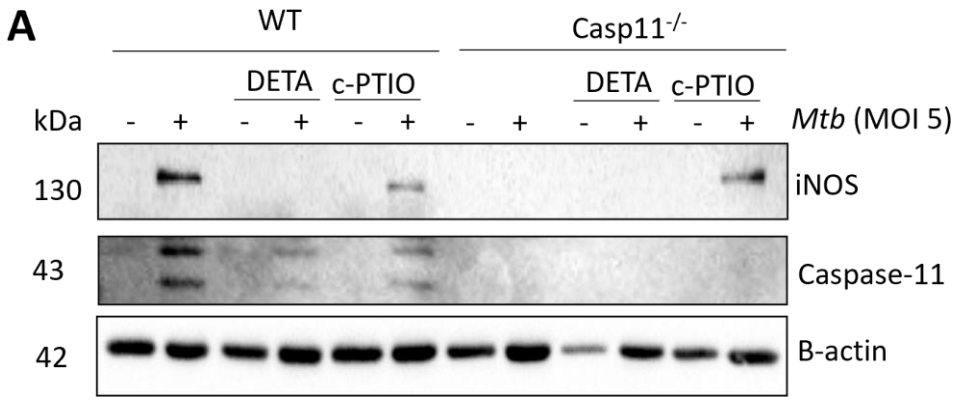

Figure 4.13: Caspase-11 regulates NO production during *Mtb* infection

WT and *Casp11*$^{-/-}$ BMDM were seeded at 10^6 cells/mL (in antibiotic-free DMEM supplemented with 10% FBS). After 24 h, BMDM were pre-treated with 50µM c-PTIO (NO scavenger). After 1 hour BMDMs were infected with *Mycobacterium tuberculosis* (*Mtb*) strain H37Ra (MOI 5) for 72 h. 3 h post infection BMDM were post-treated with 25 µM DETANO (NO donor) every 24 h. 72 h after infection whole cell lysates of WT and *Casp11*$^{-/-}$ BMDM (20 µg) were resolved by SDS-PAGE, wet transferred to nitrocellulose and were analysed for expression of iNOS, caspase-11 and β-actin, as loading control. Blots are representative of four independent experiments.

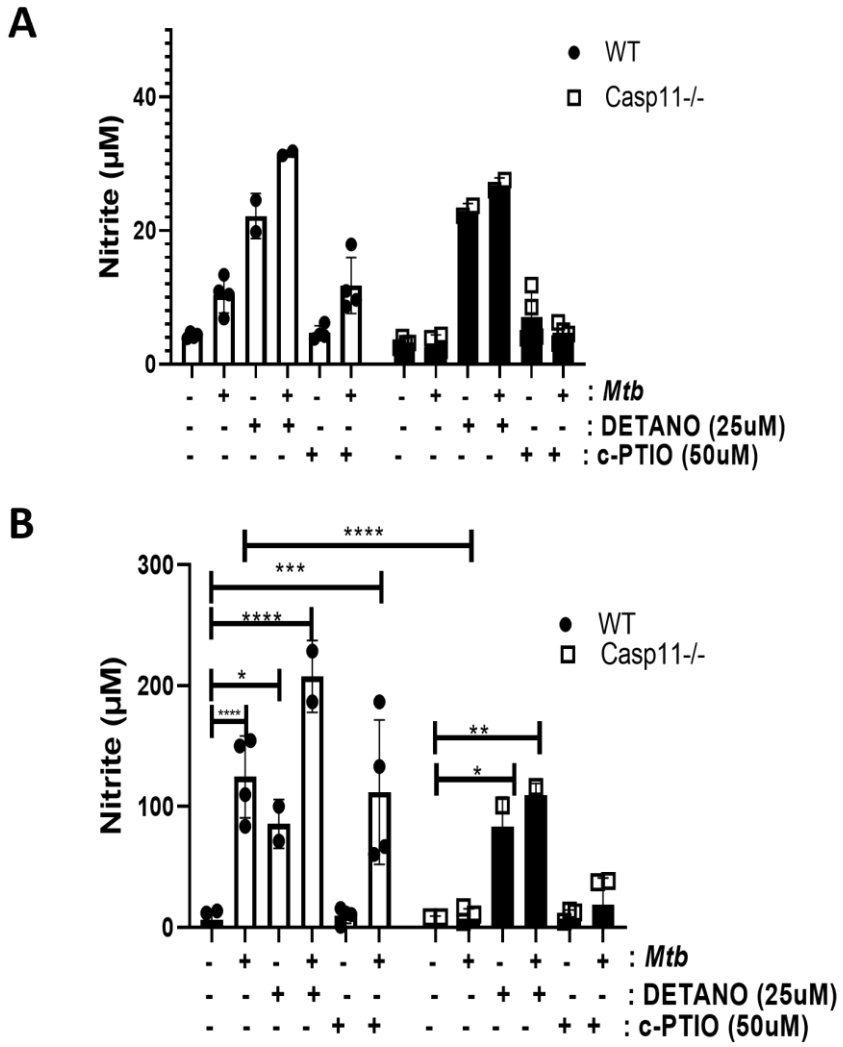

Figure 4.14: The NO donor, DETANO (25µmM), releases NO at similar concentrations to those observed during *Mtb* infection.

WT and *Casp11*$^{-/-}$ BMDM were seeded at 10^6 cells/mL (in antibiotic-free DMEM supplemented with 10% FBS). After 24 h, BMDM were pretreated with 50µM c-PTIO (NO scavenger). After 1 hour BMDMs were infected with *Mycobacterium tuberculosis* (*Mtb*) strain H37Ra (MOI 5) for 24 or 72h.. 3 h post infection BMDMs were post-treated with 25 µM DETANO (NO donor) every 24 h. After infection, supernatants were collected and nitrite was determined with Griess assay for (A) 24 or (B) 72h. Statistical analysis was performed using two-way *ANOVA* test to compare mean ± SEM of each row and column. *p<0.05, **p<0.01; ***p<0.001, ****p<0.0001 (Tukey post-test).

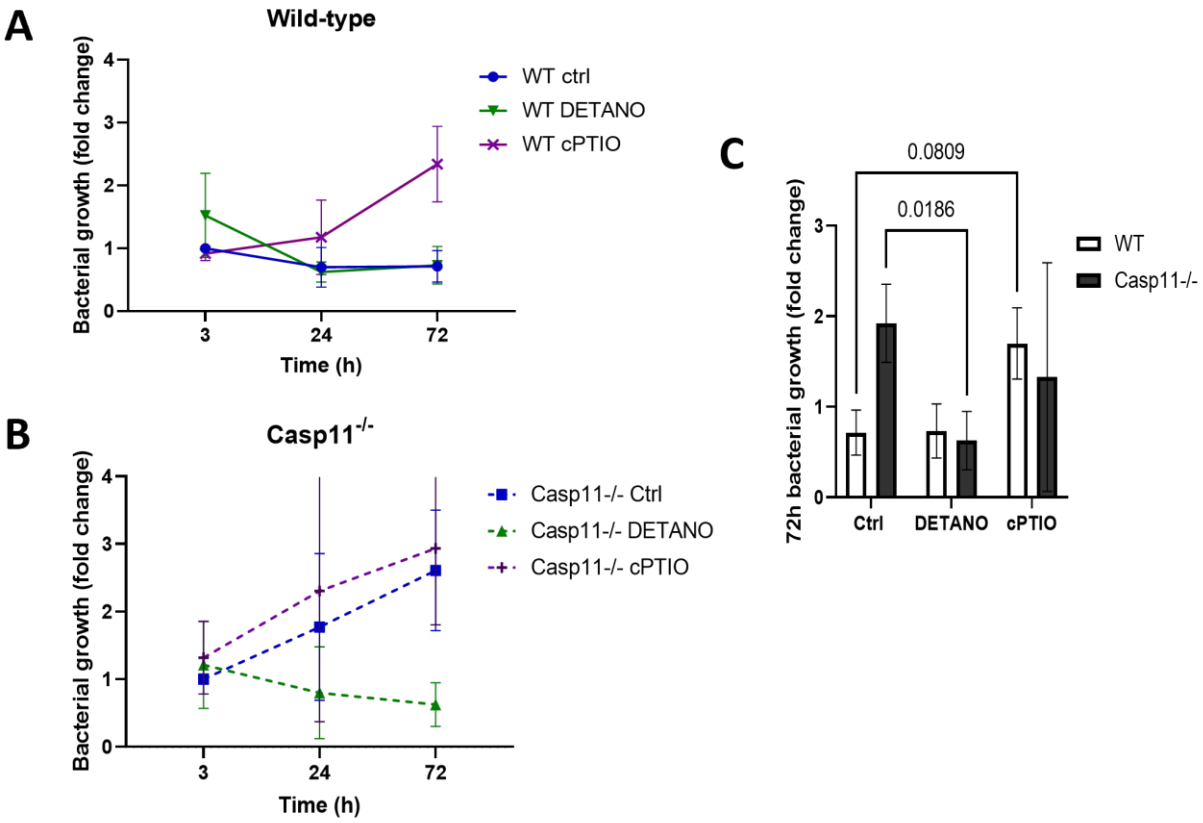

Figure 4.15: Caspase-11 mediated NO production regulates bacterial clearance during *Mtb* infection.

WT and *Casp11*$^{-/-}$ BMDM were seeded at 10^6 cells/mL (in antibiotic-free DMEM supplemented with 10% FBS). After 24 h, BMDM were pretreated with 50µM c-PTIO (NO scavenger). After 1 hour BMDMs were infected with *Mycobacterium tuberculosis* (*Mtb*) strain H37Ra (MOI 5) for 24 or 72h. 3 h post infection BMDMs were post-treated with 25 µM DETANO (NO donor) ever 24h. Macrophages were infected wit *Mtb* strain H37Ra at an MOI of 5 bacilli per cell for 3 h. Then extracellular bacteria were removed by collecting the supernatants and centrifugation to pellet extracellular bacteria. Bacteria-free media were returned to macrophages and cells were incubated for 24 h and 72 h. Baseline growth was assessed by lysing 3 h time-point in 0.1 % Triton-X for 10 min. Serial dilution were plated on 7H10 Middlebrook Agar in triplicate and colony-forming units (CFU) of (A) WT and (B)*Casp11-/-* were analysed after incubation at 37°C for 14-21 days after plating. (C) Bacterial growth after 72h, fold change relative to baseline at 3 h. Values represent the mean ± S.E.M of n=3. Statistical analysis was performed using two-way *ANOVA* test to compare mean ± SEM *p<0.05 (Tukey post-test).

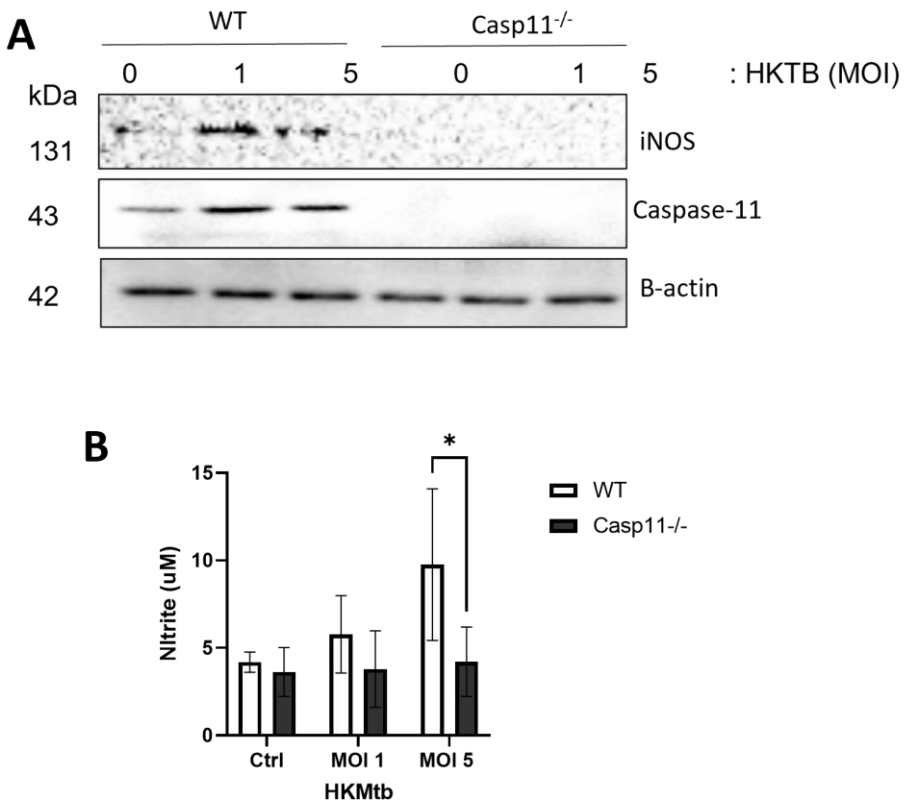

Figure 4.16: HKTB infection induces caspase-11 expression, which is required for iNOS expression and NO production, in BMDM

WT and *Casp11*$^{-/-}$ BMDM were seeded at 10^6 cells/mL (in antibiotic-free DMEM supplemented with 10% FBS). After 24 h, BMDM were infected with heat killed *Mycobacterium tuberculosis* (HKTB) strain H37Ra (MOI 1 or 5) for 24h. Cell lysates of WT and *Casp11*$^{-/-}$ BMDM (20 µg) were analysed for expression of (A) iNOS, caspase11 and β-actin, as loading control. Blots are representative of three independent experiments Supernatants were analysis for the production of (B) Nitrite by Griess assay. Values represent the mean ± S.E.M of n=3. Statistical analysis was performed using two-way ANOVA. *p<0.05 (Tukey post-test).

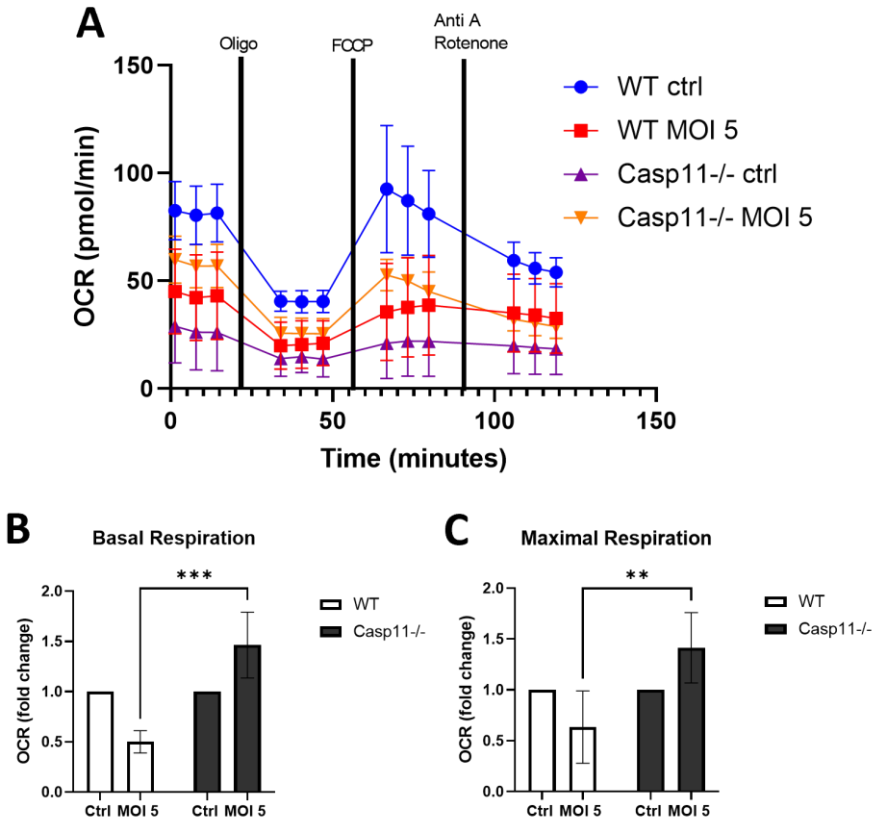

Figure 4.17: Caspase-11 mediates the inhibition of respiration during heat killed Mtb infection

WT and *Casp11*$^{-/-}$ BMDM were seeded at 80,000 cells/well in Seahorse XF96 cell culture plates O/N prior treatment BMDM were infected with HKMtb (MOI 5) for 48 h. One hour prior to seahorse analysis media was exchanged for serum free non-buffered DMEM and incubated for 1 hour in non-CO_2 incubator. Wells were sequential treated with oligomycin (Oligo), FCCP, and rotenone plus antimycin A (Rot/AA) by injection during seahorse requisition of (A) Oxygen Consumption Rate (OCR) by Seahorse XFp Extracellular Flux Analyser (Aligent Technologies). (B) Basal respiration and (C) Maximal respiration were measured as a fold change relative to uninfected BMDM. Values represent the mean ± S.E.M of three biological replicates. Statistical analysis was performed using two-way ANOVA ; **p <0.01, ***p<0.001 (Sidak post-test).

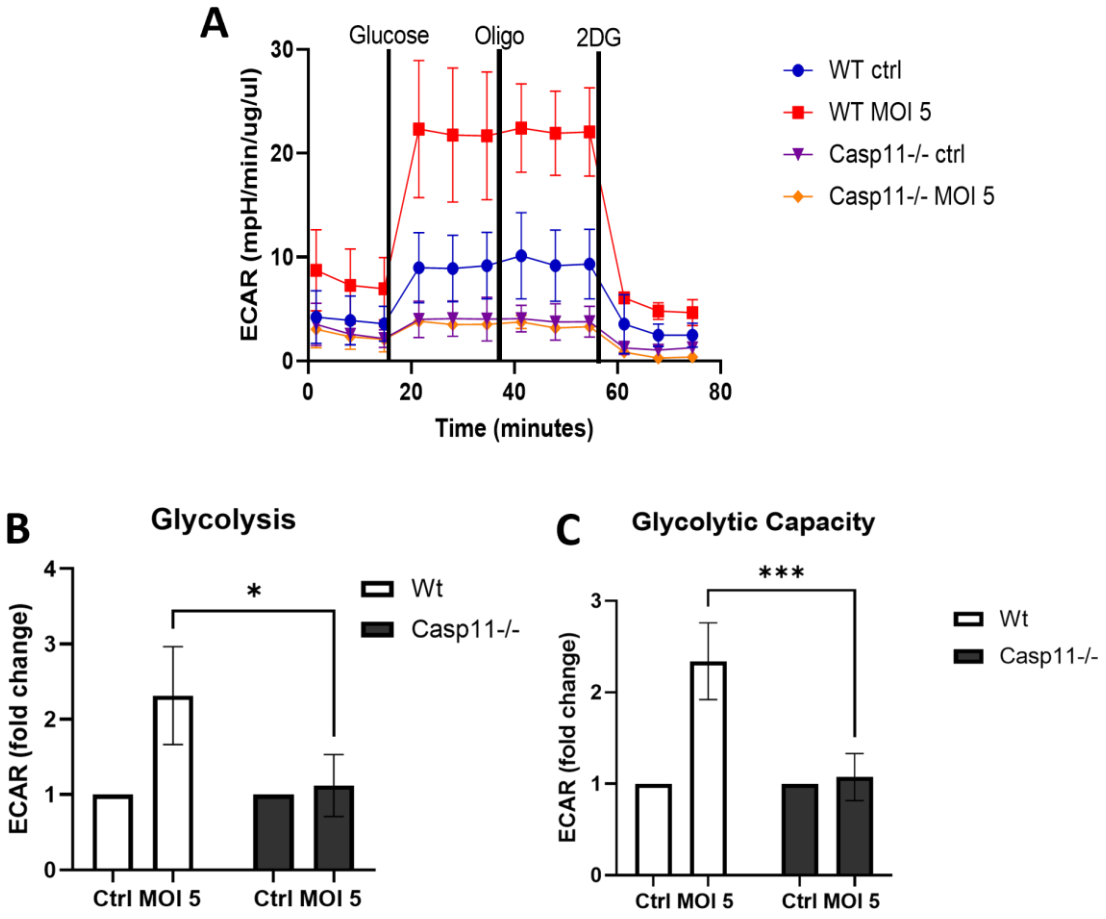

Figure 4.18: Caspase-11 mediates the glycolytic shift during heat killed Mtb infection

WT and *Casp11*$^{-/-}$ BMDM were seeded at 80,000 cells/well in Seahorse XF96 cell culture plates O/N prior treatment. BMDM were infected with HKMtb (MOI 5) for 48 h. One hour prior to seahorse analysis media was exchanged for serum free non-buffered DMEM and incubated for 1 hour in non-CO_2 incubator. Wells were sequential treated with oligomycin (Oligo), FCCP, and rotenone plus antimycin A (Rot/AA) by injection during seahorse requisition of Extracellular Acidification Rate (ECAR) by Seahorse XFp Extracellular Flux Analyser (Aligent Technologies). (B) Basal glycolysis and (C) Glycolytic capacity were analysed as fold change relative to uninfected macrophages. Values represent the mean ± S.E.M of n=3. Statistical analysis was performed using two-way ANOVA ; *p<0.05, **p <0.01, ***p<0.001 (Sidak post-test).

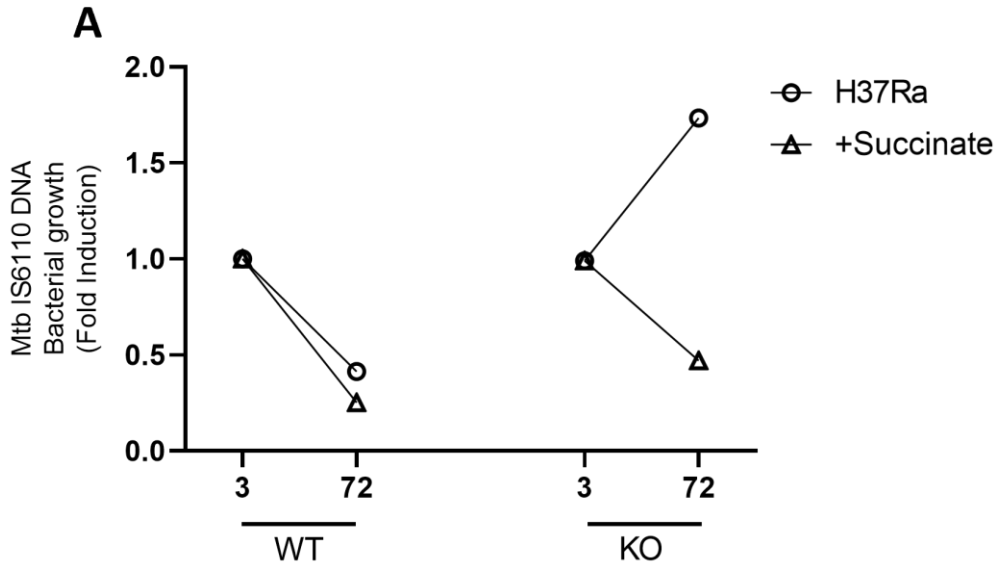

Figure 4.19: Glycolysis enhances *Mtb* clearance in BMDM

WT and *Casp11*$^{-/-}$ BMDMs were seeded at 10^6 cells/ml (in antibiotic-free DMEM supplemented with 10% FBS). After 24h BMDM were infected with *Mycobacterium tuberculosis* (*Mtb*) strain H37Ra (MOI 5) for 3 h or 72 h. 3 h post infection BMDMs were treated with 10µM succinate every 24 h. For quantification, Mtb IS6110 expression in genomic DNA was normalized to bacterial housekeeping 16 s rRNA and HPRT macrophage housekeeping RNA expression in RNA samples and expressed relative to 3h post-infection as a baseline bacterial uptake. Results are based on n=1 experiments and need to be repeated.

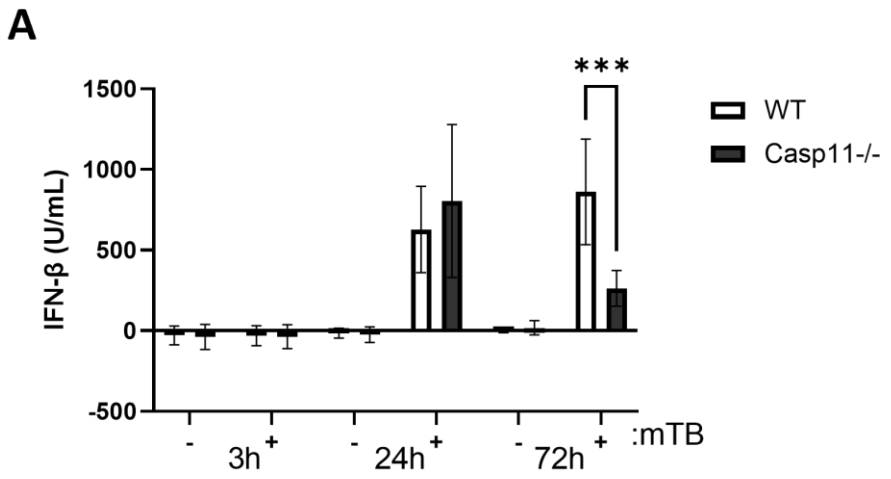

Figure 4.20: Caspase-11 regulates type I IFN responses in Mtb infected BMDM

WT and *Casp11*$^{-/-}$ BMDM were seeded at 10^6 cells/ml (in antibiotic-free DMEM supplemented with 10% FBS). After 24 h, BMDM were infected with *Mycobacterium tuberculosis* (*Mtb*) strain H37Ra (MOI 5) for 3, 24 or 72h. At 3 h, extracellular bacteria were removed by collecting the supernatants and centrifuging to pellet extracellular bacteria. Bacteria-free media were returned to macrophages and cells were incubated for 24 h and 72 h. Culture supernatants were analysed for the expression of IFNβ by ELISA. Values represent the mean ± S.E.M of n=3. Statistical analysis was performed using two-way ANOVA; ***p<0.001 (Tukey post-test).

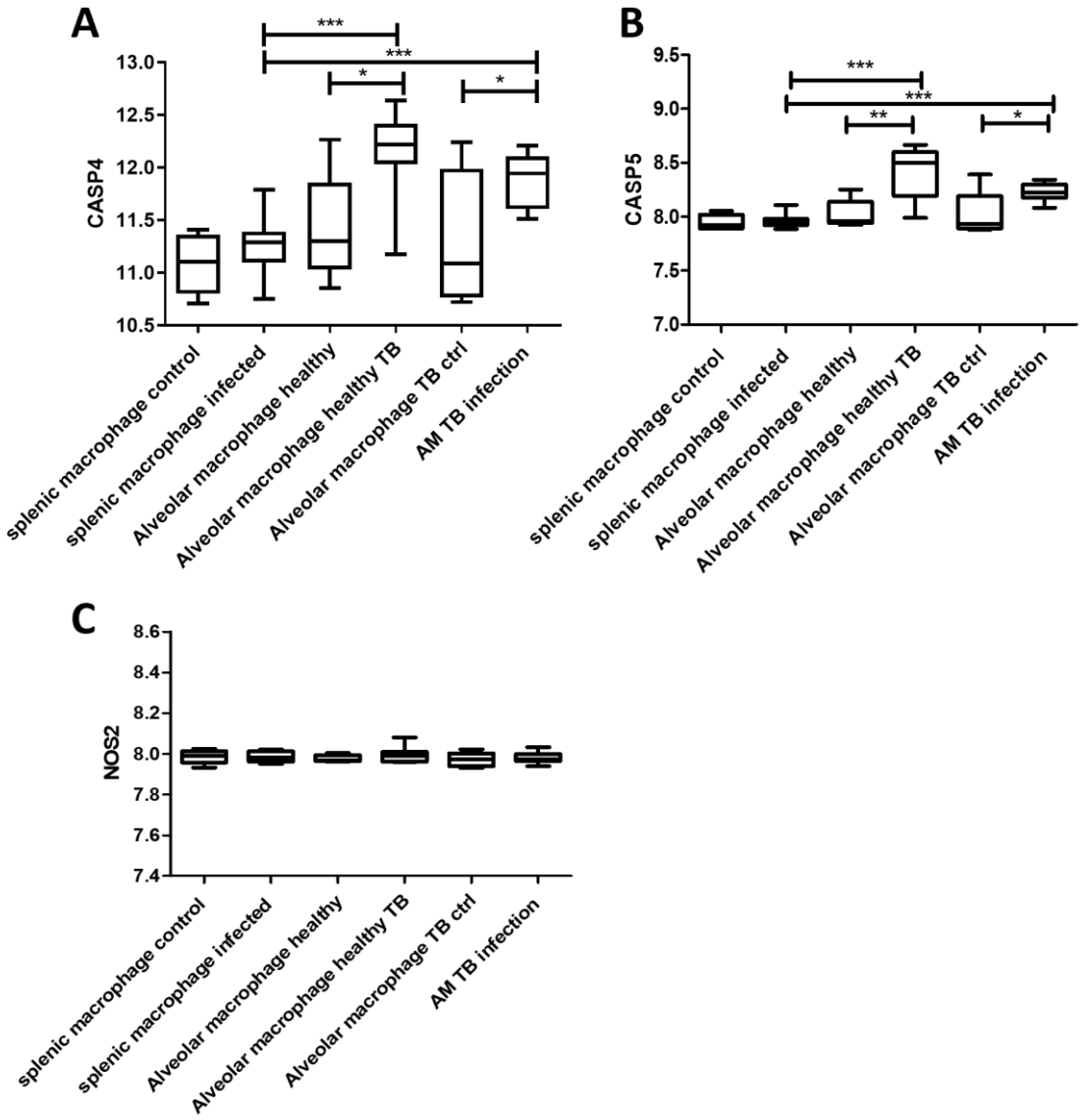

Figure 4.21: Alveolar macrophages infected with clinical isolates of Mtb have upregulated CASP4 and CASP5

Graphs represent relative mRNA inflammatory CASP4 and CASP5, and NOS2 expression values analysed using publicly available data set (Series GSE139825). mRNA from splenic macrophages obtained from spleen of a deceased donor, control (n=6) and infected *in vitro* with Mtb clinical isolates (n=12). mRNA obtained from alveolar macrophages from TB patients (n=5) infected with clinical isolates of Mtb (n=9) to compared to alveolar macrophages from healthy control subjects (n=5) infected with clinical isolates of Mtb ex-vivo (n=7). (Lavalett L *et al.,* 2020 [GSE139825]). Data represents mean ± SEM. Wilcoxon signed-rank test was used to evaluate significant differences between two groups. *p<0.05, **p<0.01; ***p<0.001

5.Chapter 5: Caspase-5/11 modulates NO production from macrophages within the TME of Basal-like Breast Cancer

5.1. Introduction

Breast cancer is a heterogeneous group of malignancies, typically adenocarcinomas, derived from ductal epithelial cells. TME is a critical participant that influences both tumour progression and therapeutic response. The infiltrating immune populations within the tumour microenvironment (TME) are dependent on the molecular cancer subtype, particularly ER status[259]. TNBC and HER2+ breast cancers are characterized by a highly inflammatory microenvironment, evidenced by elevated cytokines and growth factors, and an influx of infiltrating immune cells that support a tumour-promoting microenvironment, and are considered 'hot tumours'[375]. HR- breast cancer has a weak immunological response, termed a 'cold tumour'. Sex differences in immune responses typically result in differential disease susceptibility and development in males and females[376]. Steroid hormone signalling pathways can regulate subpopulation composition[377]. Immune infiltration patterns in breast cancer that are dependent on ER status influence treatment efficacy[378]. The ER+ breast cancer TME composition typically has a strong presence of NK cells associated with good prognosis and a smaller proportion of CD8+ and CD4+ T cells. ER- TME Tregs and M2 TAMs are the most abundant immune infiltrates associated with poor prognosis, while CD8+, CD4+ T cells, and DCs are often observed in smaller proportions and are associated with favourable neoadjuvant chemotherapy outcome[378]. The construction of immune infiltration ratios in the microenvironment is more important than the presence of immune cells alone263,264. Therefore, it is important to understand the impact of hormone receptor expression on immune cell phenotypes in the breast cancer TME.

Emerging data further suggest that the spatial orientation of immune cell populations among tumour cells is equally important to the immune cell ratio and activation within the TME. The utilisation of laser capture microdissection gene expression profiles has classified several tumour immune microenvironments (TIME). These subtypes include inflamed, indicated by CD8+ T cells distributed equally across stromal and tumour epithelial cells with high immune gene expression; compared with the less immune-activated margin and stroma restricted-TIME subtypes, and the least immune-activated group, the "immune desert," in which there were few CD8+ T cells, and only at the margin[379].

Smouldering inflammation is the seventh proposed hallmark of cancer. Inflammation in the TME consists of infiltrating immune cells and fibroblast-secreting cytokines, chemokines and growth factors. Understanding the bidirectional influence of tumour and stromal cells on the promotion

of a pro-inflammatory metastatic environment is important for predicting patient disease development and therapeutic responses. It is well acknowledged that tumour-educated stromal cells affect drug efficiency; therefore, re-education of the TME and enhancement of immune cell function is a viable therapeutic strategy for combatting cancer. Innate leukocytes can promote malignant epithelial cell survival and establish a state of chronic inflammation[191]. Although most immunotherapeutic strategies target the adaptive immune response, strategies to initiate innate immunity led to subsequent adaptive long-term cancer immune defence. Many clinically effective innate immune-targeted therapeutics involve monoclonal antibodies that mediate complement-dependent cytotoxicity or antibody-dependent cell cytotoxicity, recruiting innate immune cells to the tumour cell surface. In breast cancer, Trastuzmab binds the extracellular domain and inhibits HER2 homodimerisation in Her2 amplified breast cancer patients. This treatment strategy prevents Her2 signalling, leading to antibody-dependent cell cytotoxicity. Additionally, the effect of trastuzumab on the immune landscape has been proposed to influence innate immune effector activity, including NK cells, and alter the Treg to Th17 cell ratio in circulation[380].

The inflammatory cytokines, IL-1β, IL-6 and TNFα are strongly associated with an inflammatory breast cancer microenvironment. In general, elevated circulating IL-6 levels in the serum of breast cancer patients are associated with poor prognosis[209]. IL-6 production from malignant epithelial cells is highest in ER-breast cancer cell lines[200]. IL-6 from TNBC has been shown to mediate CCL5 signalling in lymphatic endothelial cells, promote TNBC epithelial-stromal crosstalk, and enhance tumour proliferation and metastasis[381]. Similarly, IL-1β and TNFα were highly expressed in the serum of patients with metastatic TNBC. TNBC and mesenchymal stem cell co-cultures stimulated with IL-1β and TNFα caused significantly increased expression of the pro-metastatic chemokines, CXCL8, CCL2 and CCL5, which were significantly higher in TNBC patients than in luminal A[382]. Highlighting the link between inflammatory cytokines and metastatic chemokines in TNBC-tumour-stromal networks. The TME enriched with these pro-inflammatory cytokines influences the tumour-mediated education of stromal cells to promote cancer progression.

Tumour-associated macrophages (TAMs) are the predominant leukocyte population found in the TME of breast cancer. Breast cancer-secreted factors typically induce TAM phenotypes with many M2-like features. Macrophages are highly plastic and respond to environmental signals by participating in the innate immune response. TAM M2-like macrophages are typically involved

in angiogenesis, reorganization of the extracellular matrix, recruitment of leukocytes to the TME, and tumour cell EMT[383].

TAM subpopulations on a spectrum of macrophage phenotypes are thought to comprise the TME at different ratios depending on the breast cancer molecular subtype. An investigation of immune infiltration patterns in breast cancer uncovered therapeutic implications and immune cell signatures, which can be defined by the proportions of M0, M1, and M2 macrophages within the TME[384]. M0 and M2 macrophage infiltration in ER+ disease is associated with a poor clinical outcome, and M2 macrophage subpopulation accumulation in ER- TME is also associated with poor prognosis and correlates with a lack of predicted response to chemotherapy[384]. M2 macrophage-mediated resistance to chemotherapy is highly relevant for TNBC patients, who have a poor response to treatment and a high density of infiltrating M2 macrophages. Therefore, it is important to interpret macrophage diversity when investigating their involvement in disease development and treatment responses. Therapeutic approaches exploiting macrophage plasticity to adapt their functional state towards an anti-tumour phenotype include inhibition of the CSF-1 receptor to promote M1-like differentiation[385].

Inflammasome activity in breast cancer can be indirectly measured by IL-1β production and has been demonstrated to promote tumour progression. Murine cancer models lacking inflammasome components and IL-1R signalling show decreased tumour proliferation and infiltrating myeloid cells in the TME[207]. However, delayed myeloid cell infiltration could be partially restored by IL-6 production. IL-6 is a downstream mediator of IL-1R signalling and is involved in myeloid cell expansion[386]. Treatment with anakinra, an IL-1R antagonist, impairs the growth of both ER+ and ER- human breast cancer tumours subcutaneously injected in murine xenograft models[387]. These data suggest that IL-1R signalling or IL-1β production promotes breast cancer development and represents targetable pathways that inhibit tumour growth. Treatment with anakinra controlled tumour-promoting inflammation in breast cancer. Anakinra-mediated inhibition of IL-1R1 signalling can impair Treg cell migration[388]. Treg cells are associated with poor outcomes in all the molecular subtypes of breast cancer. In a murine 4T1 breast cancer model, tumour IL-1β inhibition impaired splenocyte CCL22 signalling to control Treg recruitment[388], illustrating the diverse effects of IL-1β signalling on TME cellular composition. Additionally, IL-1β expression in breast cancer is a predictive biomarker for an increased risk of bone metastasis. Macrophage-derived, caspase-1 dependent, IL-1β promotes breast cancer endothelial adhesion and transmigration. TAM caspase-1 activation drives breast cancer cell migration and metastasis to secondary sites[389].

Although there is a vast body of research investigating caspase-1-mediated IL-1β signalling, very little research has been carried out on the involvement of the non-canonical inflammasome and pyroptotic cell death during breast cancer development. Inflammatory caspases cleave GSDMD to mediate pore formation in the cell membrane during pyroptosis, which facilitates the passive release of IL-1β, IL-18, alarmins IL-1α, and HMGB1[390]. GSDMD is a substrate of human caspases-1, -4, and -5 (and murine caspases-1 and-11)[391]. In breast cancer, GSDMB is associated with low survival and high metastasis[392]. Similar to GSDMD, GSDMB N-terminal domains can form pores that mediate pyroptosis[276]. GSDME/DFNA5 is inversely correlated with ER expression in breast cancer[277]. However, these GSDMB/GSDME family members do not contain the caspase cleavage sites found in GSDMD, suggesting a different activation mechanism.

A recent publication by Xia et al. suggested GSDMD as a potential prognostic marker and target for invasive breast cancer. The data revealed increased GSDMD expression in invasive breast cancer compared to normal mammary tissue, with the highest levels observed in luminal B and HER2+ subtypes. The expression of GSDMD is negatively associated with overall survival and is a predictor of therapeutic response[393]. Cisplatin has been demonstrated to contribute to antitumour effects in TNBC, while current treatment regimens include anthracycline, taxane, or fluorouracil. Cisplatin-induced pyroptosis via MEG3/NLRP3/caspase-1/GSDMD signalling exerts antitumour effects in TNBC cells[394]. Wang et al. developed a nanoparticle delivery system to promote tumour cell pyroptosis using an ortho-carbamoylmethylene silyl phenol ether system conjugated to GSDMA3 that can selectively be delivered to tumour cells with 90% payload within 24 h of intravenous injection. Ziroconium [Zr89] nanoparticles enhance permeabilization and internalization retention within cancer cells, while the cancer imaging probe phenylalanine trifluoroborate (Phe-BF3), fluoride ion, catalyzes desilylation, leading to the release of the conjugated GSDMA3 antibody. This bioorthogonal system was applied to a subcutaneous 4T1 murine mammary tumour model to illustrate GSDMA3 selectivity to tumour cells in an in vivo model. This study revealed that 20% tumour cell pyroptosis induces an inflammatory TME to promote tumour clearance, enhanced by combination with anti-PD1 therapy[395]. Thus, gasdermin-mediated tumour cell pyroptosis mediates the TME to improve the efficacy of immunotherapeutics in otherwise cold cancers.

A clinical trial using disulfiram and copper active therapy (NCT03323346) is currently underway for patients with metastatic breast cancer who have otherwise failed to respond to conventional systemic and/or locoregional therapies. The results of this trial are expected to be released in

December 2022. Disulfiram was originally approved by the FDA more than 55 years ago for the treatment of alcohol addiction by inducing acute sensitivity to ethanol. Studies on disulfiram have revealed its action as a proteasome inhibitor and DNA demethylating agent, which opens new potential avenues to redistribute FDA-approved drugs for therapeutic use in malignancy and infection. Disulfiram is a member of the dithiocarbamate family capable of binding copper, which promotes anticancer activity[263]. High-throughput screening of 3185 compounds against a range of TNBC cell lines identified disulfiram and the related compound thiram as potent growth inhibitors. Drug affinity responsive target stability analysis identified IQ motif-containing GTPase activating protein 1 (IQGAP1) and myosin heavy chain 9 (MYH9) as the direct targets of disulfiram. Combination studies revealed synergistic activity with disulfiram and doxorubicin induced cell death, and targeted cancer stem cell populations[396].

Similarly, there is little insight into the role of non-canonical inflammatory caspases -4, -5, and -11 in breast cancer. Caspase-4 and -5 are often investigated interchangeably, with little known about their independent inflammatory functions. In human monocyte cells, caspase-4 is constitutively expressed by basal transcriptional regulation by IRF1, caspase-4 has also been reported to be constitutively activated in macrophages, neutrophils, and various epithelial and endothelial cells. While caspase-5 is inducible with low or undetectable levels in tissues and resting macrophages. Caspase-5 expression is analogous to that of caspase-11, as both require induction. This divergent regulation supports that inflammatory caspases are non-redundant, while questioning the translation of murine caspase-11 observation to human orthologs caspase-4 and -5[397].

Genomic studies investigating acquired uniparental disomy pinpoint regions of mutated genes in cancers and found that CASP1/4/5 are predictors of TNBC[398]. Additional genomic studies using the Illumina HumanExome SNP array found the most significant associations between single code variants and breast cancer risk included CASP5. CASP5 Leu17Arg, although ranked among the top 10 SNP associated with breast cancer, is a non-significant variant for altering function or increased risk[399]. Molecular studies which modulated estrogen-mediated miR-191 regulation of chromatin remodelling (SATB1), found that estrogen signalling inhibited CASP4 mRNA transcription in the MCF-7 cell line[400]. ER/miR-191 signalling cascades in breast cancer have been identified as oncogenic players. Caspase-4 has previously been associated with the occurrence and development of breast cancer, with abnormal methylation of the CASP4 promoter region, as well as increased resistance to therapeutics[401]. Given this limited information on the role of caspase-4 and-5 in breast cancer, we aimed to investigate the molecular impact of inflammatory caspases.

Caspase-11 has been implicated in a range of inflammatory diseases, including infectious diseases, neurodegenerative diseases, IBD, inflammatory respiratory diseases, and cancer[278]. A previous investigation from the Creagh lab observed increased caspase-4 and -5 in inflamed and dysplastic stroma tissue from CRC patients, and epithelial expression was restricted to neoplastic tissue[402]. Therefore, we aimed to investigate the expression profiles of non-canonical inflammatory caspases and their potential functional involvement in breast carcinoma.

As previously shown in chapters 3 and 4, caspase-11 regulates iNOS expression and NO production in M1 activated macrophages and during mycobacterial infection. As iNOS has been observed to be markedly increased in 60% of adenomas[403] we aimed to investigate inflammatory caspase association with iNOS in breast cancer. NO has been implicated in the modulation of multiple cancer-related events, such as angiogenesis, invasion and metastasis, the cell cycle, and apoptosis, with strategies for manipulating NO production and exogenous delivery for therapeutic invention. Initial studies by Thomsen and colleagues found that NO biosynthesis is higher in invasive mammary tumours than in benign tissue, with significantly higher expression in less differentiated tumour grade III than in grade II. It was originally determined that NO production occurs predominantly from peritumoural macrophages, located adjacent to invasive tumour islands, as well as intracellular macrophages[404]. Previous studies have reported that NO biosynthesis in breast cancer is expressed not only in macrophages and stroma, but also in tumour cells themselves, and is associated with increased apoptotic index and microvessel denisty[405],[222]. As iNOS is an important prognostic indicator of breast cancer, we hypothesise that caspase-11 expression in breast cancer drives poor prognosis associated with NO in the TIME.

5.2. Hypothesis and Aims of Chapter 5

Hypothesis: The TNBC microenvironment induces caspase-5 expression in macrophages, leading to iNOS signalling and pyroptosis.

Specific Aims:

1. Determine the expression pattern of caspase-4 and -5 in areas of tumour and adjacent normal in resection tissue from breast cancer patients.
2. Examine inflammatory caspase expression profiles across different hormone receptor subtypes of breast cancer.
3. Investigate *in vitro* macrophage expression of caspase-4 and -5 in response to conditioned media (CM) from ER+ and ER- cell lines.
4. Investigate the role of caspase-11 in triple negative breast cancer (TNBC)-associated macrophages iNOS signalling and pyroptosis.
5. Investigate the impact of COX-2 and NOS2 on TNBC induced caspase-11 expression.

5.3. Results

5.3.1. Increased caspase-5 expression and intensity in tumour, compared to adjacent normal, breast cancer patient tissue.

Previous findings from the Creagh Lab have demonstrated an association between caspase-4 and -5 during active inflammatory disease activity in IBD and its progression to CRC. Histological inflammation in patients with ulcerative colitis (UC) is correlated with the stromal expression of caspases-4 and -5[402]. Infiltrating immune cells within the lamina propria were identified as stromal expressing cells, which included macrophages, neutrophils, and lymphocytes. Creagh Lab further investigated expression in CRC, regardless of subtype. Similar to actively inflamed regions of IBD, CRC is associated with upregulated expression of caspases-4 and -5 within infiltrating immune cells. In addition, malignant intestinal epithelial cells (IEC) demonstrate a striking switch to express caspases-4 and -5, which are not expressed in the IECs of normal or inflamed intestinal tissue. Therefore, malignant epithelium-specific expression of caspase-4 and caspase-5 may represent a potential biomarker for colon adenocarcinoma[402]. However, caspase-4 and caspase-5 involvement in other adenocarcinomas, including breast cancer, has yet to be established. Given the dramatic switch in the expression of caspase-4 and -5 in neoplastic IECs, we sought to determine whether malignant-specific expression of caspase-4 and -5 also occurs in mammary ductal cells during breast adenocarcinoma. As both breast cancer and colon adenocarcinoma demonstrate similar inflammatory profiles[183] we hypothesised that caspase-4 and -5 expression may also be specific to neoplastic breast carcinoma tissue.

To test this hypothesis, histologically defined regions of adjacent normal tissue (n=9) and breast adenocarcinoma tissue (n=7) from patients who underwent tumour resection were identified by a pathologist (E. Kay, RCSI & Beaumont hospital, Dublin). The tissues were immunohistochemically examined for caspase-4 and caspase-5. Each full-face section was stained and blindly scored for caspase-4 and -5 using a semi-quantitative method involving a measure of the percentage of stromal and epithelial cells positive for expression (percentage positivity) and intensity of the stain (intensity score) (K. Sheehan and J. Fay, RCSI & Beamount hospital, Dublin). The percentage positivity was scored as 0 = 0-24%, 1= 25-49%, 2= 50-74% and 3= 75-100%.

IHC staining revealed that caspase-4 is constitutively expressed in normal adjacent epithelial cells (**Fig. 5.1 A-B**), and therefore the malignant-specific expression of caspase-4 which is

observed in intestinal adenocarcinoma epithelial cells, is not observed in breast adenocarcinomas. However, IHC data revealed a significant ($p<0.05$) increase in caspase-5 positivity in neoplastic breast epithelia compared to adjacent normal epithelia (**Fig. 5.1 A**).

Similarly, examining epithelial expression of caspase-4, we observed no alterations in caspase-4 expression in tumour stroma compared to normal adjacent tissues (**Fig. 5.1 D-E**). Examination of stromal cells within breast adenocarcinoma tissue revealed a similar trend of increased caspase-5 expression, which was not statistically significant. Although a similar percentage of stromal cells expressed caspase 5, it was observed to be expressed more strongly ($p<0.05$) in the tumour stroma than in the adjacent normal stroma, as demonstrated by a significantly higher intensity score (**Fig. 5.1 D, E**).

5.3.2. Analysis of a publicly available dataset revealed increased expression of caspase-4 and -5 in basal-like breast adenocarcinoma.

Breast cancer is a highly heterogeneous disease broadly defined by four molecular subtypes: luminal A, luminal B, Her2-enriched and basal-like, all of which demonstrate phenotypic variability with different inflammatory profiles, responses to treatment, and 5-year survival rates[406]. Luminal A is the most frequently diagnosed breast cancer subtype. However, it is the least common subtype identified in patients with inflammatory breast cancer (IBC) patients[407]. IBC is more commonly associated with basal-like breast cancer, which is considered the most aggressive molecular subtype and has a poor prognosis with short disease-free and overall survival (OS) rates. Basal-like breast cancers have increased expression of genes associated with migration, immune activation and inflammatory response[408]. Therefore, there may be similar variations in inflammatory caspase expression in breast adenocarcinoma subtypes.

To investigate the expression of caspase-4 and-5 among the four molecular subtypes, we first explored their transcriptomic profiles in the METABRIC dataset. The Molecular Taxonomy of Breast Cancer International Consortium (METABRIC) investigated the genomic and transcriptomic profiles of 2,433 primary breast tumours[409]. To compare the relative mRNA levels of CASP4 and CASP5, data were mined from the METABRIC gene array and analysed by molecular subtype using PubMed Geo Dataset software.

In silico analysis of primary breast adenocarcinoma tissue revealed a significant decrease ($p < 0.05$) in relative CASP4 mRNA levels in the basal-like subtype compared to those in the luminal A subtype (**Fig. 5.2 A**). Analysis of relative CASP5 mRNA levels demonstrated a more varied expression profile among the molecular subtypes, with luminal A demonstrating significantly lower ($p < 0.001$) CASP5 mRNA expression than the 3 other subtypes, with the highest CASP5 expression observed in basal-like breast cancer patients (**Fig. 5.2 B**).

As previously shown by IHC in Fig. 5.1, tumour epithelial positivity of caspase-5 and stromal intensity of caspase-5 are significantly higher in tumour tissue than in normal adjacent tissue. Therefore, we investigated the expression of caspase-4 and -5 in normal healthy mammary tissues. To determine caspase expression in healthy tissue, mRNA from breast reduction surgery was mined from the public dataset GSE4825, which used laser capture microdissection to obtain normal epithelium and stroma from breast reduction surgery, as well as epithelium and stroma from invasive ductal carcinoma, which was classified as ER+ or ER- (**Fig. 5.2 B**). From these data, we observed no significant differences in the expression of Casp4 or Casp5 in normal mammary tissue compared to normal tumour-adjacent tissue, suggesting that the tumour cells do not induce inflammation in the surrounding tissue. Normal tumour-adjacent tissues were therefore used as a valid normal-like control.

There was also variation in the expression of ERα across the four molecular subtypes. Luminal A breast carcinoma has the highest expression of ERα, and this expression is lost in basal-like, hormone receptor-negative breast cancer. As estrogen is a known anti-inflammatory molecule, we examined Casp4 and Casp5 expression in ER+ and ER- breast carcinoma mined from the METABRIC dataset. From these data, we found significantly higher levels of CASP4 ($p < 0.001$) and Casp5 ($p < 0.05$) in ER- breast cancer patients, when compared with ER+ breast cancer patients (**Fig. 5.3 A-B**). Collectively, these data demonstrate that increased CASP5 mRNA levels in basal-like breast adenocarcinoma are associated with the TME, which appear to inversely correlate with ER expression.

5.3.3. Basal-like breast cancer TME has increased expression of caspase-5.

Having observed differences in CASP5 mRNA expression across breast cancer subtypes, with a negative association with ER expression, we examined caspase-4 and caspase-5 expression by IHC in a range of breast cancer subtypes.

Tissue microarrays (TMA) were constructed from 26 breast cancer patient tumours consisting of a mixture of hormone receptor-positive and-negative expressing malignancies (**Table 5.1**). TMAs were stained for the expression of caspase-4 and caspase-5 using IHC. Stromal and epithelial expression were assessed by two blinded scorers (K. Sheehan and J. Fay, Beaumont Histopathology) and semi-quantitatively scored, as previously described. IHC analysis revealed that epithelial expression of caspase-4 and -5, as a measure of percentage positivity or intensity, was not altered by hormone receptor status, either ER or PR (**Fig. 5.4 A-D**). Analysis of stromal cell caspase-4 positivity also revealed a non-significant ($p < 0.0972$) trend of increased expression in ER- tumours compared to that in ER+ tumours (**Fig. 5.5 A**), and no significant difference in caspase-5 expression was dependent on the PR status (**Fig. 5.5B**). Similar to the *in silico* results (**Fig. 5.3 B**), stromal caspase-5 positivity increased ($p < 0.05$) in ER-negative tumours (**Fig. 5.5 C**), suggesting that ER-negative tumours have a higher population of caspase-5 expressing infiltrating immune cells than ER-positive tumours. Collectively, these data suggest that increased infiltration of immune cells expressing caspase-5 occurs in basal-like breast cancer.

5.3.4. Basal-like Breast Cancer expressing high CASP5 mRNA is associated with an inflammatory innate immune profile.

As previously observed by IHC, ER- breast cancer patients have significantly higher caspase-5 expression in their stroma, comprising infiltrating immune cells, vasculature, and tissue matrix. This led us to investigate the impact of caspase-5 expression in basal-like breast cancer using the breast invasive carcinoma TGCA and PanCancer Atlas dataset. This dataset contains information from 1,084 samples, of which 171 are categorised as basal-like. To investigate the influence of caspase-5 expression in basal-like breast cancer, we first separated these patient samples into $CASP5^{hi}$ and $CASP5^{lo}$ expressing tumours. Basal-like samples were analysed for CASP5 mRNA expression and divided into four quartiles, of which the 1st quartile (A) was considered $CASP5^{lo}$ expressing (n=42), and the 4th quartile (D), $CASP5^{hi}$ expression (n=43) (**Fig. 5.6 A**). We continued with these two groups for the remaining analyses.

Previous investigations revealed that high levels of NLRP3 inflammasomes positively expressing infiltrating macrophages correlate with poor survival, lymph node invasion, and metastasis in invasive breast cancer patients[410]. As we observed caspase-5 to be most highly expressed in the stroma of ER- breast cancer, we aimed to determine the influence of caspase-5 on patient survival. We examined the overall survival of basal-like breast cancer patients with either

CASP5^{hi} or CASP5^{lo} expressing tumours, to determine the prognostic value of CASP5, as basal-like is the most aggressive molecular subtype. Based on previously mined patient data from TCGA PanCancer Atlas, basal-like breast cancer patients with low and high CASP5 expression survival data were applied to a Kaplan-Meier curve as a measure of overall survival over all events recorded. However, there was no significant difference in survival between the two groups (**Fig. 5.6 B**). We determined the median survival time of basal-like breast cancer patients with CASP5^{hi} expression to be 114.15 months, whereas that of Casp5^{lo} was undetermined (**Fig. 5.6 C**).

To further investigate the impact of CASP5^{hi} versus CASP5^{lo} mRNA expression in basal-like breast cancer, we investigated the differentially expressed genes (DEG) between these two groups. Returning to the PanCancer Atlas, CASP5^{hi} and CASP5^{lo} expressing basal-like breast cancer patients, we examined differentially expressed genes. The volcano plot shows differentially expressed genes by red dots, while black dots under the-log of the false discovery threshold (<2) are not significantly differentially expressed (**Fig. 5.7 A**). Among the 4,319 differentially expressed genes, 1683 were upregulated in CASP5^{lo} basal-like tumours, whereas 2,636 genes were upregulated in CASP5^{hi} basal-like tumours (**Fig 5.7A**).

Genes such as IFNG, CD163, CD86, STAT1, and IRF1, highlighted in blue, were among the genes associated with M1-like inflammatory macrophages upregulated in CASP5^{hi} tumours (**Fig. 5.7A**). To evaluate the relevance of these differentially expressed genes, gene enrichment analysis was performed using Qiagen Ingenuity Pathway Analysis (IPA) to determine the upregulation and activation of canonical pathways. Blue bars indicate pathways upregulated in CASP5^{hi} tumours, and red bars indicate pathways upregulated in CASP5^{lo} tumours. Colour intensity corresponds to activity, with more grayscale bars signifying no activity pattern. From these data, we observed multiple M1 macrophage pathways associated with CASP5^{hi} tumours, including pathogen-induced cytokine storm signalling, macrophage classical activation signalling pathway, phagosome formation, pyroptosis signalling, iNOS signalling, and the production of NO and ROS in macrophages (**Fig. 5.8 A**).

EIF2 signalling, PD-1/PD-L1 cancer immunotherapy pathway, and oxidative phosphorylation are upregulated and activated in CASP5^{lo} basal-like tumours (**Fig. 5.8 A**). Eukaryotic initiation factor 2 (eIF2) phosphorylation has been shown to negatively correlate with iNOS and predict disease-free survival in TNBC[411]. Additionally, we previously observed that in the absence of caspase-11, M1 macrophages failed to shift towards glycolytic commitment and retained OXPHOS

metabolism, similar to observations in CASP5^{lo} basal-like tumours, which are enriched with genes activating OXPHOS metabolism.

As we observed that increased M1 polarization and pyroptotic signalling are associated with CASP5^{hi} basal-like breast cancer, we aimed to investigate the impact of caspase-5 on iNOS, which is central to M1 polarization, within the breast cancer TME. Caspase-11 regulates NO mediated glycolysis in response to inflammatory stimuli. Therefore, we hypothesise caspase-5 expressing TAM in basal-like breast cancer mediate iNOS signalling.

5.3.5. Basal-like breast cancer tumour conditioned media promotes caspase-4 and -5 upregulation in primary monocyte derived macrophages.

IHC analysis suggested that the epithelial expression of caspase-4 and -5 was not influenced by hormone receptor expression status (**Fig. 5.4**). To further validate this finding *in vitro*, a panel of luminal A and basal-like breast cancer cell lines were examined for caspase-4 and -5 expression. MCF-7, T47D, CAMA-1, and ZR-75-1 represent ER+ expressing luminal A breast cancer, and BT549, HS578T, and MDA-MB-231 represent ER- basal-like breast cancer (**Fig. 5.9 A**). Western blot analysis of cell lysates confirmed the ER status of the cell lines (**Fig. 5.9 B**). In agreement with the IHC data, *in vitro* cell lines expressed varied levels of inflammatory caspase expression in luminal A and basal-like cell lines.

Having observed increased caspase-5 expression in the stromal tissue of breast cancers, particularly ER- cancers, we investigated the influence of secreted factors from ER+ and ER- breast cancers on inflammatory caspase expression in primary human macrophages. The TME comprises a heterogeneous assortment of endothelial cells, fibroblasts, adipocytes, and highly active immune cells. In breast cancer, there is an abundance of TAMs that constitute more than 50% of all tumour associated cells[412]. High TAM infiltration density correlates with a poorer patient prognosis, and their phenotype is dictated by the TME in which they reside, which can skew polarization from tumour promoting to destructive[412]. Macrophage plasticity is highly sensitive to intratumoural localization and environmental cues. During normal breast tissue development, macrophages are recruited to the ductal structure of the mammary gland, where they play a role in reorganizing tissue architecture, regulating vascular growth, and maintaining mammary stem cells. A similar tissue repair and construction phenotype during invasive ductal adenocarcinoma mediates tumour progression[413]. An investigation of the clinical relevance of TAMs according to hormone receptor status demonstrated that high TAM infiltration is associated with hormone receptor negativity[414]. These reports suggest that infiltrating

macrophages are the most abundant immune cells in the breast cancer microenvironment, particularly in hormone receptor-negative breast cancers. Additionally, we observed that, in Casp5^{hi} basal-like tumours, macrophage genes were highly differentially expressed (**Fig. 5.7**). As we observed that a higher percentage of infiltrating immune cells express caspase-5 in ER- carcinoma microenvironments (**Fig 5.5 C**), we investigated the primary macrophage response to tumour conditioned media (CM) from ER+ and ER- breast cancer cell lines.

In vitro analysis of primary macrophages cultured with CM from a panel of luminal A and basal-like cell lines found higher capase-5 expression in the presence of CM from basal-like cells, similar to LPS induction (**Fig. 5.10 A**). However, the ER+ luminal A CM from several cell lines did not induce caspase-5 MDM expression (**Fig. 5.10 A**). Additionally, we observed that caspase-4 expression, which is basally expressed in unstimulated MDM, was dampened when cultured with luminal A CM. Primary macrophages cultured in basal-like CM showed higher GSDMD expression than those cultured in CM from luminal A cells (**Fig. 5.10 A**), suggesting that basal-like breast CM mediates caspase-5-induced pyroptosis in TAM. Data from both IHC staining and CM cultured with primary macrophages suggest that the TNBC microenvironment has higher levels of non-canonical inflammasome proteins, including caspase-4, caspase-5 and GSDMD.

5.3.6. Basal-like breast cancer tumour conditioned media promotes caspase-11 expression in BMDM, which mediates iNOS expression and pro-IL-1β and GSDMD upregulation.

Following the observation that CM from basal-like breast cancer induces caspase-5 expression in primary macrophages, we next determined the functional impact of TAM caspase-5 expression. To understand the functional impact of caspase-4 and -5 upregulation in breast cancer TAM, we carried out a series of experiments in BMDM from WT and *Casp11*$^{-/-}$ mice. As caspase-11 is the murine ortholog of human caspases-4 and -5, the use of *Casp11*$^{-/-}$ BMDM should indicate the effect of caspase-4 and -5 in macrophages stimulated with CM from ER+ and ER- breast cancers. First, CM from unstimulated MCF-7 and MDA-MB-231 cells was used to stimulate the BMDMs. The results showed that, similar to observations from human MDM, CM from MDA-MB-231 cells induced caspase-11, whereas this was not observed in MCF-7 CM in murine BMDM (**Fig. 5.11 A**). We also analysed pro-IL-1β and GSDMD expression, as these components are related to non-canonical inflammasome activity. We observed that MDA-MB-231 CM induced pro-IL-1β and GSDMD upregulation in a caspase-11-dependent manner, as

Casp11$^{-/-}$ BMDM did not express pro-IL-1β or GSDMD following culturing with MDA-MB-231 CM (**Fig. 5.11 A**).

As our previous findings have shown that iNOS expression is partly regulated by caspase-11 in BMDMs, we therefore also examined iNOS expression in response to MDA-MB-231 CM in WT and *Casp11*$^{-/-}$ BMDM. Furthermore, pathway enrichment analysis identified iNOS signalling and the production of NO and ROS in macrophages infiltrating CASP5^{hi} basal-like breast cancer. We found that the absence of caspase-11 impaired the expression of iNOS in response to basal-like CM and MCF-7 CM did not induce iNOS expression (**Fig. 5.11 A**). iNOS is a pro-inflammatory enzyme associated with chronic inflammation and wound healing, and in the context of breast cancer, is associated with poor survival and basal-like gene signatures[356].

The mammary TME propagates an M2-like TAM phenotype. Clinical studies have associated a high infiltration of M2 macrophages with fast-proliferating ER- breast cancer[224]. Additionally, *in vitro* studies have found that MDA-MB-231 cells secrete more M-CSF than MCF-7 cells and skew macrophage polarization towards an M2 phenotype[223]. Breast cancer macrophage populations are highly heterogeneous, depending upon the molecular subtype and localization within the tumour stroma or tumour nest[221,384]. To assess the effects of macrophage differentiation on the ability of CM from breast cancer cells to induce caspase-11 expression, we cultured WT and *Casp11*$^{-/-}$ BMDMs for 24 hours with 50% MCF-7 or MDA-MB-231 CM, in the presence/absence of M1 (LPS + IFN-γ) or M2 (M-CSF + IL-4) macrophage differentiation cytokines. This experimental approach attempts to mimic the plasticity that macrophages undergo within the tumour, as macrophages residing and infiltrating the TME are functionally plastic in response to environmental cues. We aimed to illustrate the effects of macrophage-polarizing cytokines on the expression of caspase-11 and its downstream signatures in response to breast cancer CM.

M1 polarising cytokines LPS and IFN-γ are known stimulants for caspase-11 upregulation in BMDM[115]. Therefore, we similarly observe caspase-11 induced expression in M1 BMDM either alone or in combination with MDA-MB-231 CM. MCF-7 CM did not appear to dampen caspase-11 levels in the presence of M1 differentiation factors, as previously we observed dampened caspase-5 expression in MDM cultured with CM from luminal A cells. We did not observe the ability of M2 polarizing cytokines to upregulate caspase-11 expression. However, M2 polarizing cytokines in combination with MDA-MB-231 CM induced a more modest upregulation of caspase-11 compared to the levels induced by M1 differentiating cytokines (**Fig. 5.11 B**). As macrophages are not binary, it is unsurprising that M2-like TAMs retain M1-associated gene

expression. GSDMD expression was observed in both M1 and M2-like BMDM, alone or in combination with CM. We found that GSDMD expression in M2 MDA-MB-231 CM-treated BMDM was the only stimulus in which GSDMD was dependent on caspase-11 expression (**Fig. 5.11 B**), suggesting MDA-MB-231 induced pyroptosis is dependent on caspase-11. Investigating iNOS expression in TAM, we found that M1 cytokines alone and cultured with CM induced iNOS expression. However, in the absence of caspase-11, iNOS expression was impaired in both MCF-7 CM and MDA-MB-231 CM-cultured M1 BMDM (**Fig. 5.11 B**), revealing that M1 polarised BMDM with CM-mediated iNOS expression is dependent on caspase-11. Caspase-11 regulation of iNOS, GSDMD, and pro-IL1β in TNBC-associated macrophages supports our previous finding that pro-inflammatory M1-like pathways associated with pyroptosis and iNOS signalling are activated in $CASP5^{hi}$ basal-like breast cancer (**Fig. 5.8**).

Next, we investigated the effect of breast cancer CM on cytokine secretion by macrophages. WT and *Casp11*$^{-/-}$ BMDM were stimulated with M1 or M2 cytokines in the absence or presence of MCF-7 or MDA-MB-231 CM. MDA-MB-231 CM induced secretion of IL-1α and NO compared to naïve BMDM, which was not observed following culture with MCF-7 CM (**Fig. 5.12 A-B**). Following M1 stimulation, we also observed that IL-1α secretion was dependent on caspase-11 expression, following stimulation with M1 stimuli alone or in combination with MDA-MB-231 CM (**Fig. 5.12 D**). We also observed that MCF-7 CM dampened IL-1α secretion by M1 BMDM (**Fig. 5.12 D**), which corresponds with previous findings illustrating the ability of ER + CM to dampen the inflammatory response. NO production during M1 polarization in combination with CM was found to be dependent on caspase-11 expression (**Fig. 5.12 E**). Finally, IL-1α and NO, and M2 BMDM were produced independently of caspase-11 (**Fig. 5.12 G-I**). These data suggest that: (1) IL-1α secretion from BMDM, mediated by the MDA-MB-231 secretome, is dependent on caspase-11; (2) caspase-11 influences IL-1α expression in M1 polarised macrophages in the presence of CM from ER-breast cancers; (3) NO production is mediated by the MDA-MB-231 secretome and is dependent on caspase-11 expression, similar to previous observations using LPS. These results confirm that factors secreted from breast cancers modulate the macrophage phenotype and suggest that caspase-11 can regulate their pro-inflammatory phenotype, demonstrating how the functional plasticity of macrophages is dependent on the signals mediated by the environment in which they reside.

As previously shown, caspase-11 driven NO production following LPS stimulation is type I IFN-STAT1 dependent. We previously observed that transfection with synthetic dsDNA, poly(dA:dT), rescued NO production following LPS stimulation in caspase-11 deficient BMDM. We proposed

that STING activation-mediated type I IFN-driven NO production in response to LPS. To strengthen this proposal, we aimed to determine whether caspase-11 mediated STING activation induced NO production in response to M1 stimuli and MDA-MB-231 CM. To illustrate the importance of caspase-11 during STING activation, we cultured WT and *Casp11*$^{-/-}$ BMDM with MDA-MB-231 CM or M1 cytokines. We observed that MDA-MB-231 CM and M1 cytokines induced pTBK1, pIRF3, and STING expression in BMDM (**Fig. 5.13 A**). However, in the absence of caspase-11, the expression of these STING complex proteins was impaired (**Fig. 5.13 A**). These data show that secreted factors from MDA-MB-231, a basal-like cancer cell line, induce STING complex activation, which we hypothesise mediates type I IFN-dependent iNOS activity. We also found that the MDA-MB-231cell line secretome mediates IL-1α related pyroptosis, as we observed that these pathways were impaired in the absence of caspase-11.

5.3.7. Basal-like Breast Cancer CASP5 expression decreases with tumour stage, inversely correlating with NOS2 expression

Pathway enrichment analysis and *in vitro* studies showed that iNOS signalling and the production of NO were activated in CASP5^{hi} basal-like breast cancer. Therefore, we investigated CASP5 and NOS2 expression across basal-like breast cancer tumour stages, as well as COX2, to determine their association with tumour progression. COX2 has been shown to promote NOS2 expression in a positive feedback cycle[415], while the COX2 product PGE2 inhibits caspase-11 expression in LPS stimulated macrophages[79]. We hypothesized that caspase-5 expression is important during basal-like breast cancer initiation but becomes negatively regulated during disease progression once iNOS is expressed and the NOS2/COX2 positive feedback cycle is initiated, inhibiting caspase-5 expression, which is not required for disease progression. This inactivation of caspase-5 limits anti-tumour pyroptosis.

To investigate gene expression across tumour grades, we mined public data from the PanCancer Atlas and TCGA, Nature 2012, basal-like breast cancer subtype, and examined CASP5, IL1A, NOS2, and PTGES2 expression over four tumour stages (T1-T4) defined by the American Joint Committee on Cancer Tumour Stage Code. From these data, we observed that CASP5 expression decreased as the tumour stage increased. We observed that CASP5 expression was significantly lower in the highest grade (T4) compared to the lowest grade (T1) (**Fig. 5.14 A**). Similarly, we found a trend of reduced IIL1A expression with increased tumour grade (**Fig. 5.14 B**). In contrast, we observed that both NOS2 and PTGES2 expression increased with increasing tumour stage (**Fig. 5.14 C-D**). We observed increased NOS2 expression in the T4 grade compared to the T1 and

T3 grade (**Fig. 5.14 C**). These data suggest that caspase-5 expression is higher at basal-like cancer initiation stages, with its expression decreasing inversely with NOS2 and PTGES2 as the disease progresses. Previous unpublished data from the Creagh Lab has observed, in a wound healing model, that Casp11 expression levels are significantly increased 12-24 h following wound initiation. However, expression levels resolve after 3-10 days to levels similar to those observed in control mice. The relationship between wound healing and cancer has long been recognised, as mechanisms regulating wound healing have been shown to promote transformation and growth of malignant cells. These data suggest that caspase-11 may be involved in the initial stages of wound repair, similar to that observed during breast cancer initiation.

We hypothesised that caspase-5/11 expression is elevated during cancer initiation and functions to mediate NO production and pyroptosis to promote immune cell infiltration. However, as we observed that CASP5 expression decreased inversely with NOS2 and COX2 across increased tumour grade, we suggest caspase-11 mediated NO production is switched off during disease progression. To further investigate the role of caspase-11 in inflammation-induced cancer we examined caspase-11 mediated iNOS expression during disease initiation and progression in an AOM/DSS model of CRC. WT and *Casp11*$^{-/-}$ mice were treated with the DNA methylating agent AOM and repeatedly exposed to DSS to induce chronic colitis-associated CRC (**Fig. 5.14 A**). Animals were sacrificed on days 17, week 6, and week 15 to assess caspase-11 activity during CRC development[234]. On day 17, colon pathology showed increased inflammation and reduced epithelial barrier integrity; week 6 was reflective of epithelial dysplasia and metaplasia transformation, and week 15 tumour adenocarcinoma was fully formed with increased angiogenesis. On day 17, after one AOM intraperitoneal injection and the first cycle of 2% DSS, strong caspase-11 expression was observed (**Fig. 5.14 B**). This timepoint of the AOM/DSS model is associated with epithelial injury, immune cell activation, and consequently, cytokine and chemokine production. We showed that iNOS expression is impaired in the absence of caspase-11 from distal colon homogenates at this early time point (**Fig. 5.14 B**). At week 6, when neoplastic transformation of colon epithelial cells was underway, we observed a reduction in caspase-11 mediated iNOS expression. At week 6, the WT and *Casp11*$^{-/-}$ colon lysates expressed similar levels of iNOS (**Fig. 5.14 C**). These data suggest that the dependence of iNOS expression on caspase-11 was reduced during malignant transformation. Lastly, at week 15, macroscopic evaluation indicated well-developed adenomatous and formed tumours, and iNOS expression was found to be independent of caspase-11 (**Fig. 5.14 D**). These data illustrate that iNOS expression dependent on caspase-11 is required during chronic inflammation to initiate tumour

development. However, once tumours are formed, iNOS expression occurs in a caspase-11 independent manner.

5.3.8. NOS2/COX2 loop negatively regulates Caspase-11 expression in Macrophages during Inflammation

Our investigation of CASP5 and NOS2 expression during basal-like breast cancer revealed an inverse correlation, with CASP5 decreasing across tumour stages, while NOS2 increased with tumour stage. Additionally, utilising AOM/DSS induced model of CRC we were able to monitor caspase-11 mediated iNOS expression across disease progression, to reveal iNOS dependency on caspase-11 at chronic inflammation inducing cancer initiation. As we have shown, MDA-MB-231 CM induces caspase-5 and caspase-11 mediated NO production, however we hypothesise that during tumour development, NO negatively regulates caspase-5 expression via an inhibitory feedback loop, leading to decreased CASP5 and GSDMD during tumour development. To explore the potential negative regulatory role of iNOS during caspase-5 expression, we utilised *Nos2*$^{-/-}$ BMDM. To demonstrate the inhibitory role of iNOS, firstly we examined Casp11 mRNA expression in WT and *Nos2*$^{-/-}$ BMDM treated for 8 h with M1 cytokines (LPS 100ng/mL and IFNγ 50ng/mL) mined from public dataset GSE115120[303]. Results showed no differences in Casp11 transcription in *Nos2*$^{-/-}$ BMDM compared to WT BMDM (**Fig. 5.15 A**). Next, we treated WT and *Nos2*$^{-/-}$ BMDM with LPS over a 24 h time course. Similarly, we observed no differences caspase-11 expression in the absence of NOS2 from 4h to 24 h compared to WT BMDM (**Fig. 5.15 B**). Additionally, we measured IL-1α secretion in WT and *Nos2-/-* BMDM following 24 h LPS stimulation. We showed IL-1α secretion in the absence of Nos2 is not impaired (**Fig. 5.15C**), suggesting NO does not feedback to negatively impact caspase-11 mediated IL-1α secretion. Since cyclooxygenases are stimulated by NO and previous reports have suggested PGE2 is a negative regulated of caspase-11 mediated pyroptosis[416,417], the potential role of NO during caspase-11 regulation maybe mediated by the COX-2 product, PGE2.

Previous reports by Zaslona *et al.* have illustrated the inhibitory role of PGE2 during LPS-induced caspase-11 expression[79]. PGE_2 can inhibit IFN-β production and caspase-11 transcription, as well as caspase-11 activation by LPS, thereby limiting pyroptosis. This study also reported basal caspase-11 expression in cells deficient in the PGE2 receptor, EP2, demonstrating the negative impact of COX-2 mediated PGE2 during caspase-11 induction. To confirm these findings, BMDM were pre-treated with PGE2 for 30 minutes prior to LPS stimulation for 24h. We similarly observed that PGE2 pre-treatment reduced LPS mediated caspase-11 expression (**Fig. 5.16 A**).

There are conflicting reports in the literature regarding the influence of PGE_2 on NO production. One study found that PGE_2 in combination with LPS, promotes an anti-inflammatory phenotype in macrophages, characterized by high expression of IL-10, meditating arginase activation and decreasing nitrite levels[355]. However, Basudhar *et al.,* found that NO and PGE2, products of iNOS and COX-2, promote a feedforward NOS2/COX-2 crosstalk in basal-like breast cancer[415]. We found that PGE2 pre-treatment did not significantly impair LPS mediated NO production in WT BMDM (**Fig. 5.16 B**). We hypothesised that PGE2, which inhibits caspase-11 expression, would cause impaired NO production in macrophages. However, we did not observe reduced NO production following PGE2 treatment, suggesting that a NOS2/COX2 feedforward loop has been established when caspase-11 is impaired. Previous studies have shown that in BMDM, LPS induced PGE2 production by 8 h and continued increasing in the late phase (16-24 h). In response to LPS-treatment, the expression of both COX-2 and iNOS was detected within 2 to 4 h[418].

In parallel to these experiments, we aimed to inhibit the negative regulatory role of COX-2 on LPS-induced caspase-11 expression. Therefore, we pre-treated BMDM with varying concentrations of indomethacin (10-1μM), followed by LPS stimulation. Indomethacin is a widely used clinical NSAID, which blocks PGE2 production to relieve inflammation. We observed increased caspase-11 expression when BMDM were pre-treated with indomethacin compared to LPS stimulation alone, with the lowest indomethacin concentration inducing the highest caspase-11 expression (**Fig. 5.16 C**). Indomethacin is considered a time-dependent, nonselective inhibitor of COX-1 and COX-2 at low doses, while at higher doses >100um it inhibits NF-κB activation [419]. Therefore, we suggest that at higher concentrations of indomethacin, NF-κB is inhibition leads to altered caspase-11 expression and NO production via reduced NF-κB transcriptional activity. While at lower doses of indomethacin, inhibition of PGE2 increased caspase-11 expression. We observed that indomethacin, across all concentrations, led to reduced levels of nitrite in BMDM (**Fig. 5.16 D**). Previous studies also report that indomethacin inhibits NO production in murine macrophages[417]. These data suggest COX-2 mediated NO production is downstream of caspase-11, as in the presence of exogenous PGE2, the impaired caspase-11 expression did not affect NO production. We observed that inhibition of COX-2 using indomethacin increased caspase-11 expression and impaired NO production. These findings support our hypothesis that caspase-11 mediated NO production is switched off once the NO-induced COX-2 feedback loop is activated.

Our findings are consistent with those of previous studies, which illustrate that indomethacin treatment of murine peritoneal macrophages inhibits LPS mediated NO production. Therefore,

during COX-2 inhibition, NO production is supressed while caspase-11 expression is increased. Previous studies have reported $COX2^{lo}/NOS2^{lo}$ basal-like breast cancer have improved 5-year survival compared to $NOS2^{hi}/COX2^{hi}$ which is reported to have poor 5-year OS. We proposed this $COX2^{lo}/NOS2^{lo}$ cohort of patients have increased caspase-5 induced pyroptosis and IL-1α expression during advanced tumour stage.

Therefore, to determine the influence of COX2/NOS2 on macrophage caspase-11 mediated IL-1α secretion in the TNBC microenvironment, we utilised *Nos2*$^{-/-}$ BMDM cultured with MDA-MB-231 CM. We cultured WT and *Nos2*$^{-/-}$ BMDM with MDA-MB-231 CM or LPS, with or without PGE2 or indomethacin, to determine whether altering NOS2/COX2 signalling could enhance or reverse expression of caspase-11 or pyroptosis markers, GSDMD and IL-1α. Consistent with previous reports, PGE_2 induced upregulated iNOS expression following LPS stimulation or exposure to MDA-MB-231 CM (**Fig. 5.17 A**). As previously observed, treatment with PGE_2 inhibited caspase-11 expression in WT and *Nos2*$^{-/-}$ BMDM following LPS stimulation and exposure to MDA-MB-231 CM (**Fig. 5.17 A**), illustrating that PGE_2 impairs caspase-11 expression independently of NOS2. While we did not observe any alterations in full-length GSDMD protein expression following PGE_2 treatment or in the absence of Nos2 (**Fig. 5.17 A**), we did observe that LPS and MDA-MB-231 CM induced IL-1α independent of Nos2 expression (**Fig. 5.17 B**). However, we observed reduced IL-1α expression following PGE2 treatment, which reduced caspase-11 expression (**Fig. 5.17 B**). Previously we observed MDA-MB-231 CM mediated IL-1α secretion in M0 and M1 BMDM was dependent on caspase-11 (**Fig. 5. 13 A, B**). Therefore, these data suggest that PGE_2 impairs caspase-11 mediated IL-1α production in TNBC TAMs, while supporting iNOS expression.

Investigations into whether the COX2 inhibitor indomethacin could potentially rescue caspase-11 mediated IL-1α expression in the absence of NO mediated COX-2 regulated PGE2 production were performed. Similar to previous findings showing reduced LPS-mediated nitrite levels in indomethacin treated BMDM (**Fig. 5.16 D**), we observed that iNOS expression was increased in LPS and, to a lesser extent, MDA-MB-231 CM stimulated BMDM that had been pre-treated with indomethacin (**Fig. 5.17 C**). Indomethacin increased caspase-11 expression in LPS stimulated WT and *Nos2-/-* BMDM, as previously shown. However, we found that indomethacin treatment impaired caspase-11 expression in WT and *Nos2-/-* BMDM cultured with MDA-MB-231 CM (**Fig. 5.17 C**), consistent with IL-1α secretion findings. As previously mentioned Nos2 expression did not impact LPS or MDA-MB-231 CM induced IL-1α secretion (**Fig. 5.17 D**). However, as indomethacin elevated LPS mediated caspase-11 expression in BMDM, we also observed

increased IL-1α secretion (**Fig. 5.17 D**). Similarly, under conditions where indomethacin reduced MDA-MB-231 CM induced caspase-11 expression we did not observe detectable IL-1α (**Fig. 5.17 D**). We suggest that the composition of the TCM secretome may be impacting the ability of indomethacin to enhance IL-1α production.

These data suggest that the TNBC secretome induces caspase-5 expression in the TIME, which is responsible for increased macrophage infiltration, iNOS signalling and pyroptosis. We propose that caspase-5 expression during cancer initiation is important for the wound healing phenotype, promoting IL-1α secretion and iNOS mediated NO production. However, we suggest that the NOS2/COX2 cycle negatively regulates caspase-5 and subsequent IL-1α release via PGE_2, while continuing to promote NO production during tumour progression.

5.4. Summary of Findings from Chapter 5

- Caspase-5 expression is elevated in breast tumour tissue compared to normal adjacent tissues, and significantly higher levels of CASP5 mRNA are observed in basal-like breast cancers compared to the other molecular subtypes. TMAs showed that stromal tissue from ER- cancers had significantly higher caspase-5 expression than ER+ stromal tissue.
- $CASP5^{hi}$ TNBC tumours are associated with activation of the inflammatory macrophage classical activation signalling pathway, pyroptosis signalling, iNOS signalling, and production of NO and ROS in macrophages. In contrast, $CASP5^{lo}$ TNBC tumour differentially activated pathways include EIF2 signalling, PD-1 PD-L1 cancer immunotherapy pathway, and OXPHOS.
- The TNBC secretome induces iNOS-mediated NO and IL-1α production in TAM in a caspase-11 dependent manner.
- Caspase-11 dependent regulation of iNOS expression following macrophage stimulation with CM from TNBCs or M1 stimuli appears to be mediated by the STING-type I IFN pathway.
- CASP5 and GSDMD expression is high at early tumour stages, whereas NOS2 and COX2 expression increase with tumour stage.
- In a murine colorectal cancer model (AOM-DSS), caspase-11 mediated iNOS expression occurs during early-stage disease and is associated with inflammation and reduced barrier integrity. However, once tumours are fully formed, there is less iNOS expression and it is independent of caspase-11 expression.
- The COX-2 product, PGE2, inhibits caspase-11 expression and caspase-11 mediated IL-1α production while maintaining iNOS-mediated NO production.

.

5.5. Discussion

In this Chapter, IHC analysis of breast carcinoma tissue resections demonstrated increased expression of caspase-5 in epithelial and stromal compartments, compared to normal adjacent tissue. This observation is similar to inflammatory caspase expression patterns in IBD and CRC patient samples[402]. However, the dramatic upregulation of inflammatory caspases observed in malignant IECs during CRC was not observed in breast malignant epithelial cells, suggesting that this phenomenon may be specific to the colon[402]. Breast carcinoma is a heterogeneous disease with different molecular subtypes, governing exposure to a range of microenvironmental factors, which may contribute to the stromal expression of caspase-5. Emerging data demonstrate that differences in the TME are dependent on the molecular subtype of breast cancer, and their role in cancer progression is influenced by environmental signals[224,420,421]. *In silico* dataset analysis of CASP4 and CASP5 mRNA levels across the main molecular subtypes (luminal A, luminal B, Her2-enriched and basal-like) demonstrated significantly higher CASP5 expression in basal-like breast cancer. This stepwise increase in CASP5 expression suggests an inverse relationship with ESR1 expression across breast cancer molecular subtypes, with luminal A expressing the highest ESR1 levels and basal-like cancers defined by the lack of ER expression. Estrogen activity has previously been implicated in modulation of the stromal environment, inhibition of T and B cell development, and macrophage phagocytic activity[377]. Estrogen signalling is also implicated in autoimmune diseases, particularly systemic lupus erythematosus, which disproportionally affects women[422]. These studies therefore implicate estrogen signalling in TME modulation. However, basal-like breast cancers which lack ER status demonstrate significantly higher immune infiltration than luminal breast cancers. The TNBC microenvironment is abundantly populated with TIL subsets, CD8+ and Treg cells, and TAMs, which contribute to the aggressive inflammatory and metastatic phenotype[423].

Previous studies have demonstrated the effect of ER expression on inflammasome activity in inflammatory diseases. Murine allergic airway inflammation is enhanced by estrogen regulation of the NLRP3 inflammasome[424]. The inflammasome components caspase-1 and pro-IL-1β increase simultaneously with ERβ reduction during ovalbumin airway inflammation in an ovariectomized murine model, similar to our observations of increased CASP5 expression in breast cancers lacking expression of ESR1. Treatment with 17β-estradiol ameliorates airway inflammation by reducing leukocyte recruitment and decreased secretion of pro-inflammatory cytokines IL-1β, IL-6, and TNFα[424]. In addition to decreased leukocyte infiltration and pro-inflammatory cytokine secretion, suppression of inflammasome-associated components has

been observed following ER signal transduction[424]. Similarly, ERα downregulation occurred in an estrogen-deficient rat aneurysm model, whereas NLRP3, caspase-1, pro-IL-1β, and MMP9 were increased[305]. These studies demonstrate a negative regulatory role of ER signalling during inflammasome activity. We hypothesize that ER- breast cancer therefore facilitate a more inflammatory profile and can influence capase-5 expression in leukocyte populations.

Further investigation of caspase-4 and -5 expression *in vivo* by IHC staining revealed an increased percentage of cells positive for caspase-5 expression in the stroma of ER- breast tissues. Stromal cellular composition varies significantly in breast cancer molecular subtypes, particularly with regard to macrophage dependence on ER status[384], supporting the hypothesis that ERα-expressing tumour cells may negatively influence leukocyte recruitment of caspase-5 positive macrophages. M2 macrophages are strongly associated with Ki67 high, poorly differentiated and ER- breast cancer[223]. Luminal A breast cancer co-cultured macrophages polarize to an M1-like phenotype[224]. Previous studies have demonstrated caspase-5 expression following inflammatory stimuli in M2 primed macrophages. M2 polarised macrophages primed and treated with LPS followed by heme express caspase-5 similarly to M1 polarised macrophages[425].We have shown CM induces caspase-11 in M2 primed macrophages suggesting that in the M2 predominant population associated with ER- breast cancer, caspase-5 is positively expressed in this stromal cell population.

A Phase II clinical trial (NCT03323346)[426] aimed at establishing clinical evidence for introducing disulfiram and copper as an active therapy for metastatic breast cancer upon failure of conventional therapies is currently underway. As previously described, disulfiram covalently modifies catalytic cysteine residues and inhibits GSDMD-mediated pyroptosis. High-throughput screening of multiple TNBC cell lines revealed that disulfiram and the related compound thiram are strong candidates for tumour growth inhibition with tumour-specific targeting in combination with copper to inhibit proteasomal activity in TNBC. Xenograft models of athymic nude mice injected with MDA-MB-231 cells have shown up to 74% tumour growth inhibition when treated with disulfiram after tumour establishment (~ 200 mm3), associated with decreased proteasome activity and induced apoptosis[427]. Interestingly, a Danish retrospective study examining the association of long-term disulfiram usage with cancer risk found epidemiological evidence to support a protective effect against breast and prostate cancer development[428]. In a study of 108 breast cancers and 23 benign lesions, pathological grade and TNM stage were associated with pyroptotic proteins. High GSDMD expression is associated with poor prognosis. Similarly, we observed that IL1A expression in the stroma of ER-breast cancer

patients was a strong predictor of poor survival, as indicated by a hazard ratio of 40.6 (False discovery rate = 0.499, p = 0.0167) (Appendix). Therefore, while we initially observed IL1A to be a good indicator of prognosis, FDR was too high to be used as a single marker. However, in combination with other studies, this could be a useful prognostic marker. Contrastingly, Wang *et al.* developed a bioorthologonal chemical system using phenylalanine trifluoroborate (Phe-BF_3), a cancer imaging probe that can cleave a designed linker containing a silyl ether[395]. This system was used to release active GSDM selectively into tumour cells in mice. Results showed that induction of pyroptosis in less than 15% of tumour cells was sufficient to clear the entire 4T1 tumour graft. Tumour clearance was absent in immune-deficient mice, suggesting that anti-tumour pyroptotic effects are immune response-driven. Therefore, tumour cell-specific pyroptosis and immune cell infiltration was anti-tumourigenic in this model. Elevated levels of pyroptosis-associated genes are associated with immune filtration and high immune activity[429]. Similarly, we observed elevated pyroptotic signalling and increased classical macrophage activation signalling in $CASP5^{hi}$ basal-like tumours, suggesting a link between pyroptosis and immune activity. The pro-tumour or anti-tumour role of pyroptosis during disease seems to be cell type-specific and tumour stage-dependent during disease progression. An investigation of CASP5 and GSDMD expression across tumour grades revealed that they were more highly expressed during disease initiation. During breast cancer disease progression, we observed that CASP5 and GSDMD mRNA levels decreased with tumour stage, inverse of NOS2 and COX2 expression, which is more highly expressed at later stages.

Further examination of caspase-11 role during iNOS signalling in TNBC TAMs brought us back to our working hypothesis of Chapter 3, which suggested that mitochondrial dynamics mediated by caspase-11 led to accumulation of cytosolic mtDNA, triggering STING activation and type I IFN responses to promote iNOS expression. Induction of type I IFN requires STING activation and recruitment of TBK1, important for IRF3 mediated type I IFN induction[430]. Recent studies have observed elevated levels of autophagy related genes expressed in breast cancer, with a higher dependency of TNBC on mitophagy for survival, compared to ER+ breast cancer[431]. Elevated IFI16 in TNBC inhibited DNA repair, promoting a STING/TBK1/IRF3 induced type I IFN signalling pathway[432]. Our investigations revealed that STING/TBK1/IRF3 complex activation is induced by M1 cytokines and MDA-MB-231 CM, which is impaired in the absence of caspase-11. LPS priming with Poly(dA:dT) was capable of inducing NO production in *Casp11*$^{-/-}$ BMDM, suggesting that caspase-11 mediated STING activation induces iNOS signalling in TAM in TNBC.

DEGs analysis of CASP5^{lo} expressing basal-like breast cancer revealed the activation of EIF2 signalling, PD-1, PDL-1 cancer immunotherapy pathway, and OXPHOS. NO mediates kinases that phosphorylate the alpha subunit of eIF2a, which plays an important role in gene regulation. Four EIF1AKs were found (EIFAK2 - EIF2KA4) to be involved in EIF2 signalling pathway activation in CASP5^{lo} basal-like breast cancer. Each EIF2AK has a unique effect mediated by NO. EIF2KA2 can mediate iNOS expression and NO production, and EIF2AK4 is activated by the depletion of L-arginine used during arginine metabolism[411,433]. Lee *et al.* suggested that eIF2α phosphorylation mediates a proximal step in iNOS mRNA translation by regulating the availability of L-arginine, thereby inhibiting NO production[333]. Phosphorylation of eIF2α has been associated with better disease-free survival in patients with TNBC[411], and peIF2α expression is inversely correlated with iNOS[333]. Another elongation initiation factor, eIF5A, was also highly expressed in CASP5^{lo} basal-like cancer with Arg2 mRNA expression. Although Arg2 mediated the EIF5A hypusination pathway, it was not found to be significantly activated in CASP5^{lo} TNBC. We have previously shown that caspase-11 regulates NO-mediated aerobic glycolysis; therefore, in CASP5^{lo} TNBC, where iNOS signalling is decreased relative to CASP5^{hi}, we found that OXPHOS metabolism was activated. As we demonstrate CASP5 expression reduces with tumour grade, this would suggest OXPHOS metabolism corresponds with advanced disease stage, although this is a NO high environment. Although cancer usually has a glycolytic metabolism, previous reports suggest that TNBC has the highest occurrence of OXPHOS[434]. Alternatively, quiescent, and non-stimulated immune cells primarily utilise OXPHOS for energy production, indicating increased reliance on OXPHOS over glycolysis is necessary for wound healing and an immunosuppressive response in immune cells during advanced stage TNBC. The OXPHOS expression signature in TNBC following neoadjuvant chemotherapy was found to be associated with worse outcome[435]. Targeting metabolism is a promising approach for the treatment of TNBC, although individually targeting OXPHOS or glycolysis appears to be ineffective[436]. However, combination treatment with a selective oligomycin A derivative, 2DG, and 3-bromopyruvate effectively inhibited MDA-MB-231 migration[437].

Factors secreted from ER+ and TNBC tumours mediate differential gene expression profiles in macrophages. TNBC educates macrophages towards an M2-like phenotype by downregulating citrulline metabolism[224]. MDA-MB-231 and MCF-7 breast cancer cell lines have different secretory profiles, which lead to differential polarization of TAM. Conversely, TAM populations derived from breast soluble factors influence breast epithelial cells in different ways. MDA-MB-231 cells produce high levels of M-CSF, which skews macrophage differentiation towards M2. However, macrophage isolation protocols often use M-CSF to cultivate macrophages derived

from the murine bone marrow. Stimulation of these M2 primed macrophages with LPS induces a strong M1 proinflammatory response[438]. However, defining TAM subpopulations is complex because of the plethora of stimuli expressed in breast cancer CM. Therefore, although TNBC secretes copious levels of M-CSF and induces the M2 macrophage marker CD163+, the pro-inflammatory cytokines also secreted from TNBC may mediate an M1-like response and inflammatory caspase activation. This contributes to the concept of macrophage plasticity and a polarizing spectrum within the TME, with TAM expressing both M1 and M2-associated genes. TAM heterogeneity has been previously observed in a mouse model of spontaneous breast cancer, in which distinct TAM subsets were identified. Monocytic TAM precursors were found to populate the TME exclusively, consisting of inflammatory CCR2+ $Ly6C^{hi}$ $CX3CR1^{low}$ monocytes. Despite the pro-M1 predisposition of monocytes, M2-like TAMs are enriched in hypoxic areas, inducing angiogenesis and cancer progression[439]. *In vivo* monocyte labelling demonstrated the differentiation of inflammatory monocyte precursors into distinct pro- and anti-inflammatory TAM subsets within the TME[413]. However, other studies have reported that TNBC secretory factors influence TAM polarization compared to cytokine-induced M2 macrophages and that TNBC CM upregulates both M1 and M2-associated genes, including IL-6, TNFα, and IL-10. These *in vitro* models are consistent with TCGA and METABRIC dataset analysis, which observed that M1-associated genes, CXCL10 and IL1B, were expressed in TNBC compared to non-TNBC. TNBC-induced TAMs enhance tumour cell growth and aggressiveness[169]. These reports support our findings revealing increased expression of inflammatory M1-associated genes in TNBC TAMs, of which iNOS is a central regulator of M1 polarisation.

Induction of iNOS by MDA-MB-231 CM has previously been demonstrated in the murine RAW264.7 macrophage cell line[440]. This study observed that MCF-7 cells secrete lower CSF-1 levels than MDA-MB-231 cells, which potentially contribute to the poorer iNOS regulation and macrophage migration induced by CM from MCF-7 cells compared to CM from MDA-MB-231 cells. NO production and macrophage migration are regulated by c-Jun-N-terminal protein kinase (JNK) and NF-κB[440]. Our findings identified similar differences between the ability of CM from MDA-MB-231 and MCF-7 cells to induce iNOS expression in macrophages. The involvement of caspase-11 in the regulation of iNOS expression in breast cancer TAMs has not been previously observed. These findings are corroborated by those previously discussed in Chapter 4, regarding the ability of caspase-11 to induce NO production and enhance disease clearance in Mtb-infected BMDM. Our data investigating pro- and anti-inflammatory effects on breast CM macrophage activity suggest that, while M2 anti-inflammatory cytokines alone do not induce caspase-11, M2 cytokines reduce MDA-MB-231 CM-mediated caspase-11 expression and NO

production. Additionally, M0 and M1 macrophage NO production mediated by MDA-MB-231 CM is mediated by caspase-11. These data suggest that basal-like breast cancer soluble factors mediate macrophage caspase-11 regulation of NO in the TME. Additionally, we observed that IL-1α induced by MDA-MB-231 CM is regulated by caspase-11 in both naïve and M1 cytokine-exposed macrophages. IL-1α secretion in M2 cytokine-induced BMDM treated with MDA-MB-231 CM was negligible. Therefore, depending on environmental cues, TNBC secretory factors can induce varied macrophage activities.

Our analysis of CASP5 expression across basal-like tumour grades showed that CASP5 expression decreased with tumour stage, while NOS2 expression continues to increase with tumour progression. This study demonstrates a regulatory role for caspase-11, the human ortholog of caspase-5, in the initiation of iNOS signalling. Therefore, we hypothesized that when iNOS expression was established, caspase-11 was no longer required to mediate NO production. Previous studies have observed caspases to be important s-nitrosylation targets, with s-nitrosylation of catalytic cysteine residues serving as an on/off switch of caspase activity[441]**. S-nitrosylation involves covalent attachment of a nitrogen monoxide group to the thiol side chain of cysteine.** Mannick *et al*. suggested that mitochondrial, but not cytoplasmic, caspase-3 is S-nitrosylated, preventing its activity[442]. Similarly, COX-2 resides in mitochondria and undergoes S-nitrosylation-mediated activation[443]. Therefore, caspase localization is important for NO-mediated PTM regulation. Although we found that caspase-11 expression was not altered in *Nos2*$^{-/-}$ BMDM localization-specific activity may play a role in caspase-11 mediated mitophagy. Therefore, examination of caspase-11 localization in the mitochondria compared to cytoplasm may reveal differences in nitrosylation patterns.

While NO mediates the regulation of caspases, studies have illustrated that PGE2, the product of COX2, can alter caspase activity[79,444]. iNOS can selectively bind COX-2, targeting it for s-nitrosylation which activates COX-2 and leads to prostaglandin formation[445]. Reports from Zaslona have shown that PGE2 suppresses caspase-11-dependent pyroptosis in murine and human macrophages, while treatment with indomethacin promotes caspase-11 expression[79]. These reports support our observations that indomethacin increases caspase-11 expression following LPS stimulation in WT and *Nos2*$^{-/-}$ BMDM. PGE2 inhibits caspase-11 expression in WT and *Nos2*$^{-/-}$ BMDM cultured in MDA-MB-231 CM, suggesting that NO-mediated PGE2 formation inhibits caspase-11 activity. Previous reports from Basudhar et al. found that NOS2 and COX2 products, NO and PGE2, promote a feedforward NOS2/COX2 crosstalk in basal-like breast cancer

cells[415]. This highlights the redundance of caspase-11 mediated NO production once COX-2 mediated NO production is established at later disease stages.

Similar to CASP5, there was a trend of reduced GSDMD expression during basal-like breast cancer tumour progression, supporting our claim that caspase-5 mediated pyroptosis is important during breast cancer initiation. Pyroptosis is closely associated with tumour development and metastasis which has both pro-tumour and anti-tumour roles. On one hand, pyroptosis can inhibit the occurrence and development of tumours; on the other hand, as a type of proinflammatory death, pyroptosis can form a suitable microenvironment to promote tumour cell growth[446]. During TNBC Wang *et al.,* have illustrated induction of pyroptosis enhances anti-tumour immune response[395]. Therefore, pyroptotic activity during breast cancer initiation may support immune cell infiltration and activity. Dysregulation prevents pyroptosis-mediated tumour clearance as disease advances. We found caspase-11 dependent IL-1α secretion from BMDM cultured with MDA-MB-231 CM. We evaluated whether caspase-11 dependent IL-1α secretion in TNBC TAMS could be enhanced by indomethacin, to find reduced NO production and increased IL-1α secretion. These data suggest that COX-2 activity impairs caspase-11-dependent pyroptosis in murine macrophages treated with MDA-MB-231 CM.

To date, our findings suggest breast cancer ER status influences stromal expression of caspase-5 in the TIME. TAM populations within the tumour stroma are heterogeneous, and predisposition for polarisation influences the impact of the TME on macrophage cytokine secretion. The role of caspase-11 expression in macrophages exposed to CM from basal-like breast cancer suggests that caspase-11 regulates the expression of iNOS, IL-1α, and GSDMD, which are known for their invasive and migratory activity in TNBC. TNBC is the most aggressive molecular subtype, and high TAM infiltration is associated with poor prognosis. Therefore, targeting and re-educating TAM associated with TNBC and determining the involvement of inflammatory caspases in these processes are current areas of investigation.

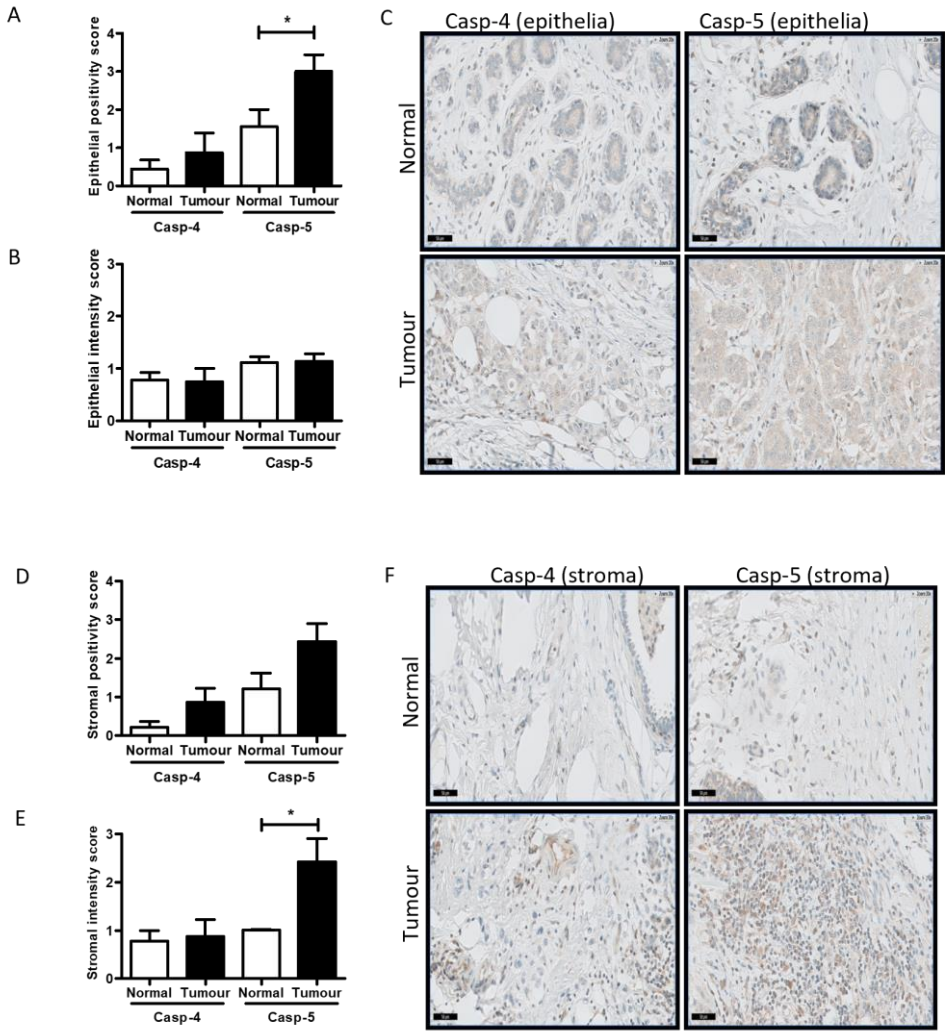

Figure 5.1: Increased caspase-5 expression in tumour, compared to adjacent normal tissue, in breast cancer patients

Tumour and adjacent normal tissue from invasive breast cancer patient resection tissue were immunohistochemically stained and scored for (A-C) epithelial or (D-F) stromal caspase-4 and caspase-5 expression. (A) epithelial percentage positivity; (B) epithelial intensity; (C) representative epithelial staining; or (D) stromal percentage positivity; (E) stromal intensity; (F) representative stromal staining. Data represent mean ± SEM; *$p < 0.05$ (paired t- test). Adjacent normal tissue (n=9), tumour tissue (n=7) for both caspase-4 and -5. Magnification 20X (scale bar = 50µm) for representative images of normal and tumour tissues stained for caspase-4 and caspase-5.

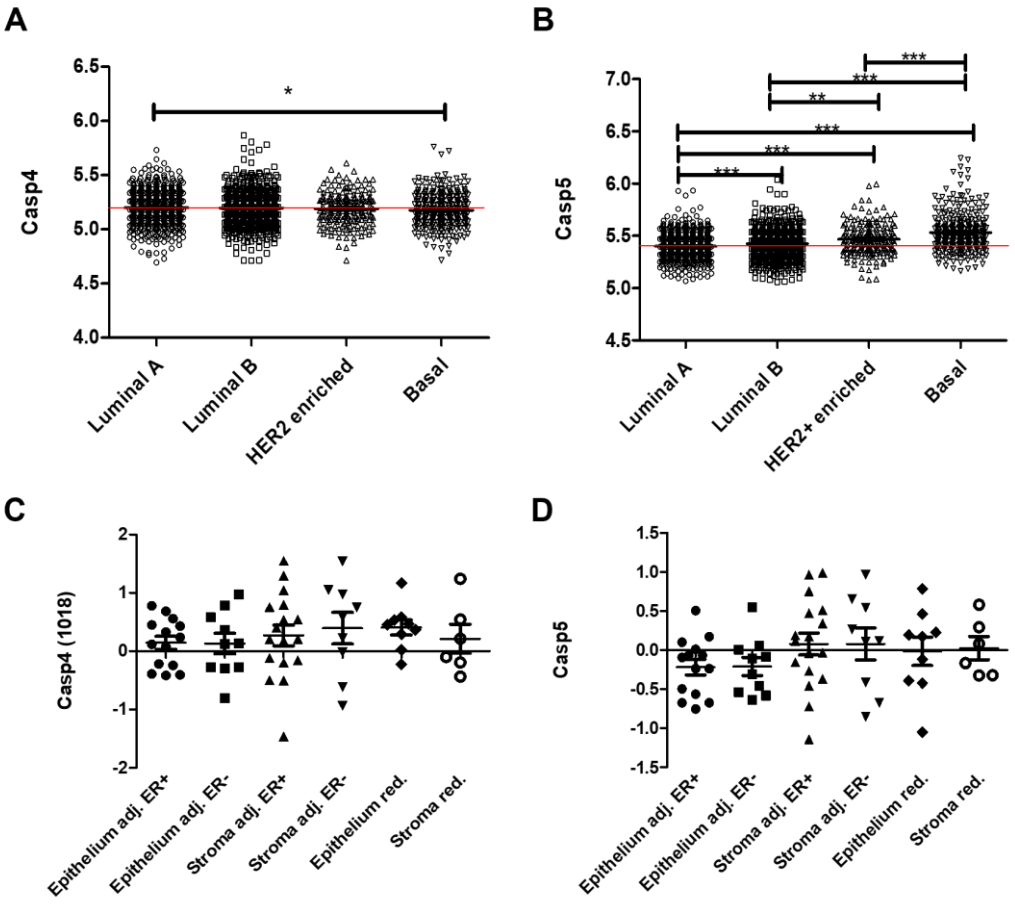

Figure 5.2: Increased CASP4 and CASP5 mRNA levels in Basal Invasive Breast Carcinoma

Graph represents relative (A) CASP4 and (B) CASP5 mRNA levels measured in different breast cancer subtypes: luminal A, luminal B, Her2-enriched and basal. mRNA expression was mined from publicly available datasets (**METABRIC**, Nature 2012 & Nat Commun 2016). (C) CASP4 and (D) CASP5 mRNA analysis was performed using the published dataset GSE4823 (Finak G. et al. (2006) Breast Cancer Res.), which obtained histologically normal breast epithelium and stroma from breast reduction specimens and from specimens of invasive ductal carcinoma, using laser capture microdissection techniques). Data represent mean ± SEM. Mann-Whitney U 2-tailed t test $^{**}p < 0.01$, $^{***}p < 0.001$.

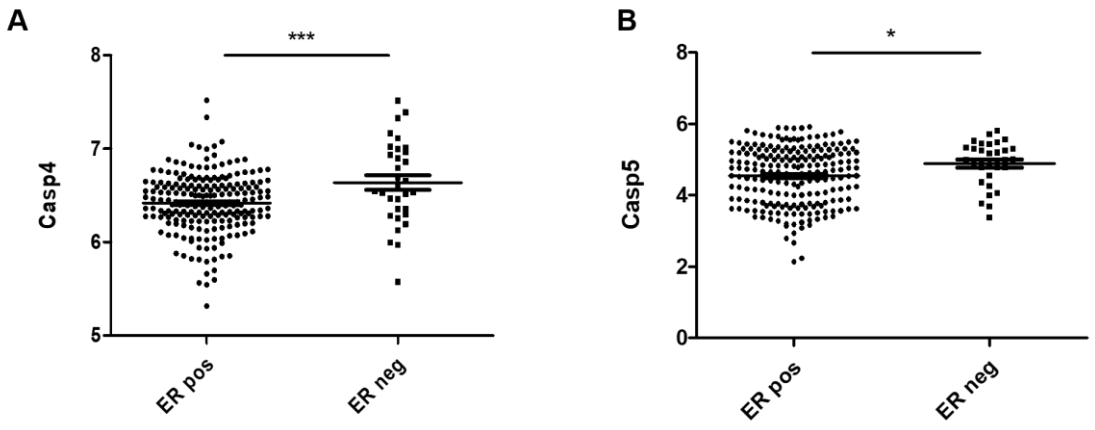

Figure 5.3: CASP4 and CASP5 are more highly expressed in oestrogen receptor negative (ER–) breast cancer, compared to oestrogen receptor positive (ER+) breast cancer

Graph represents relative (A) CASP4 and (B) CASP5 mRNA levels measured in ER positive or ER negative breast cancer tissue. mRNA expression was mined from publicly available dataset (**METABRIC**, Nature 2012 & Nat Commun 2016). Data represent mean ± SEM. Mann-Whitney U 2-tailed t test *$p < 0.05$, ***$p < 0.001$.

Table 5.1: Characteristics of breast cancer patient tumours examined for caspases-4 and -5 expression by immunohistochemistry (IHC)

Patient no	Tumour type	Grade	ER	PR	Her2 IHC	TNM stage
1	Invasive ductal carcinoma	2	Negative	Negative	3+	-
2	Invasive ductal carcinoma	2	Positive	Positive	2+	pN1
3	Invasive ductal carcinoma	2	Positive	Negative	1+	pT2 N1 (SN, Mi) Mx
4	Invasive ductal carcinoma	2	Positive	Positive	0	pT1 N1 Mx
5	Invasive ductal carcinoma	2	Positive	Positive	1+/2+	pT2 N2
6	Invasive ductal carcinoma	2	Negative	Negative	2+	-
7	Ductal + lobular carcinoma	3	Positive	Positive	2+	pT1c N0 Mx
8	Invasive ductal carcinoma	1	Positive	Positive	0	pT1 N0
9	Invasive ductal carcinoma	3	Positive	Positive	2+	pT2 N1 Mx
10	Invasive ductal carcinoma	2	Positive	Positive	0	pT1 N0
11	Invasive ductal carcinoma	1	Positive	Positive	0	pT1c N0
12	Invasive lobular carcinoma	2	Positive	Negative	0	pT3 N0
13	Invasive ductal carcinoma	2	Positive	Positive	0	pT2 N1 Mx
14	Invasive ductal carcinoma	2	Negative	Negative	0	pT2 N0 Mx
15	Invasive ductal carcinoma	2	Positive	Positive	1+	pT1 N1
16	Invasive ductal carcinoma	2	Positive	Positive	1+	pT2 N0 Mx
17	Invasive ductal carcinoma	3	Negative	Negative	3+	pT3 N3 Mx
18	Invasive ductal carcinoma	3	Positive	Positive	0	-
19	Invasive ductal carcinoma	2	Positive	Positive	3+	pT3 N2a
20	Atypical medullary carcinoma	3	Negative	Negative	1+	T3 pN1bII Mx
21	Invasive ductal carcinoma	3	Positive	Positive	2+	pT2 N0 Mx
22	Invasive lobular carcinoma	Not given	Positive	Positive	2+	pT2 N1 Mx
23	Invasive ductal carcinoma	2	Negative	Negative	3+	pT1b N1
24	Invasive ductal carcinoma	3	Negative	Negative	Neg	pT3 N3 Mx
25	Invasive ductal carcinoma	3	Positive	Positive	1+	pT2 N3a Mx
26	Invasive ductal carcinoma	3	Positive	Positive	2+	pT1c N0

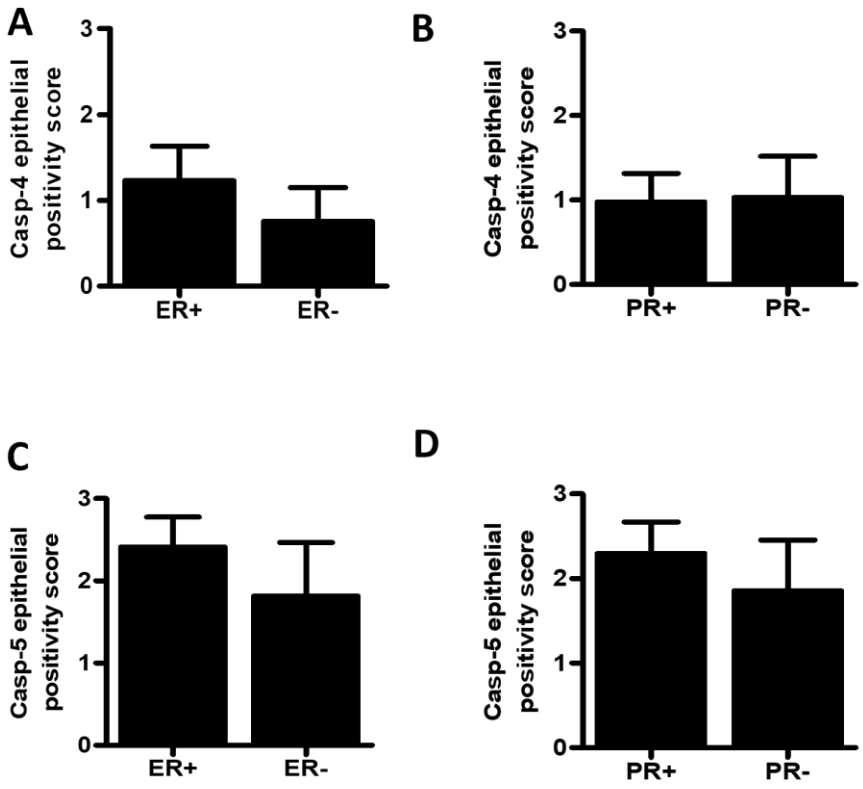

Figure 5.4: Epithelial caspase-4/-5 expression levels are independent of hormone receptor status

TMA of breast adenocarcinomas with known hormone receptor status was immunohistochemically stained and analysed for caspase-4 and -5 expression. Epithelial caspase-4 expression levels are shown as a measure of percentage positivity in (A) ER- vs. ER+ and (B) PR- vs PR+. Epithelial caspase-5 expression levels shown as a measure of percentage positivity in (C) ER- vs. ER+ and (D) PR- vs PR+ (ER negative (n=7); positive (n=18)); PR negative (n=9); positive (n=15)). Data represent mean ± SEM. Student unpaired t-test.

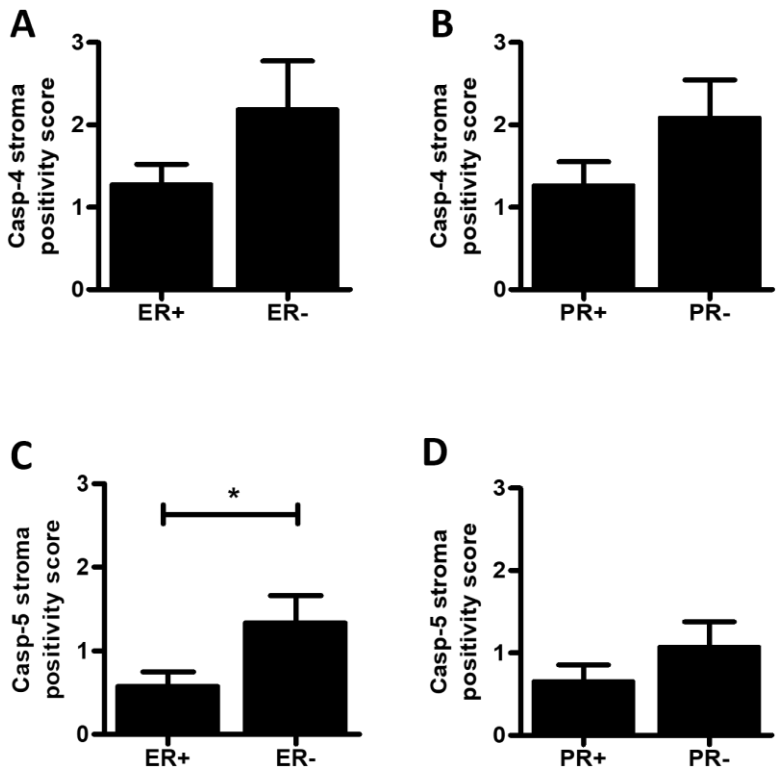

Figure 5.5: Increased stromal Caspase-5 expression in ER- breast cancer tissue, compared to ER+ tissue

TMA of breast adenocarcinomas with known hormone receptor status was immunohistochemically stained and analysed for caspase-4 and -5 expression. Stromal caspase-4 expression as a measure of percentage positivity in (A) ER- vs. ER+ and (B) PR- vs PR+. Stromal caspase-5 expression as a measure of percentage positivity in (C) ER- vs. ER+ and (D) PR- vs PR+ (ER negative (n=7); positive (n=18)); PR negative (n=9); positive (n=15)). Data represent mean ± SEM. Student unpaired t-test *$p < 0.05$.

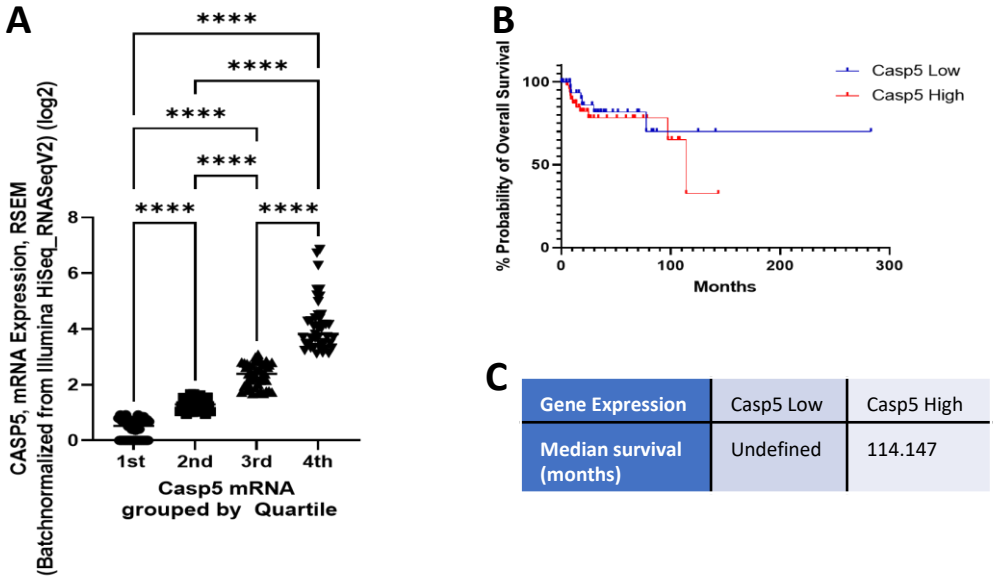

C

Gene Expression	Casp5 Low	Casp5 High
Median survival (months)	Undefined	114.147

Figure 5.6: CASP5^{hi} tumours from TNBC patients show a trend of worse overall survival rate compared to CASP5^{lo} TNBC tumours

Breast invasive carcinoma data from publicly available TCGA, PanCancer Altas was mined for CASP5 mRNA expression in basal-like breast cancer. From PanCancer Atlas, (**A**) basal-like breast cancer CASP5 mRNA expression was separated across 4 quartiles. Group (A) 0-0.89 was considered CASP5 low and (D)7.65-114.57 was considered CASP5 high. Extracting patient survival data from CASP5 low and CASP5 high expressing basal-like tumours (**B**) Overall Survival as a measure of % probability was assessed. Table (**C**) shows the median survival (in months) of each group.

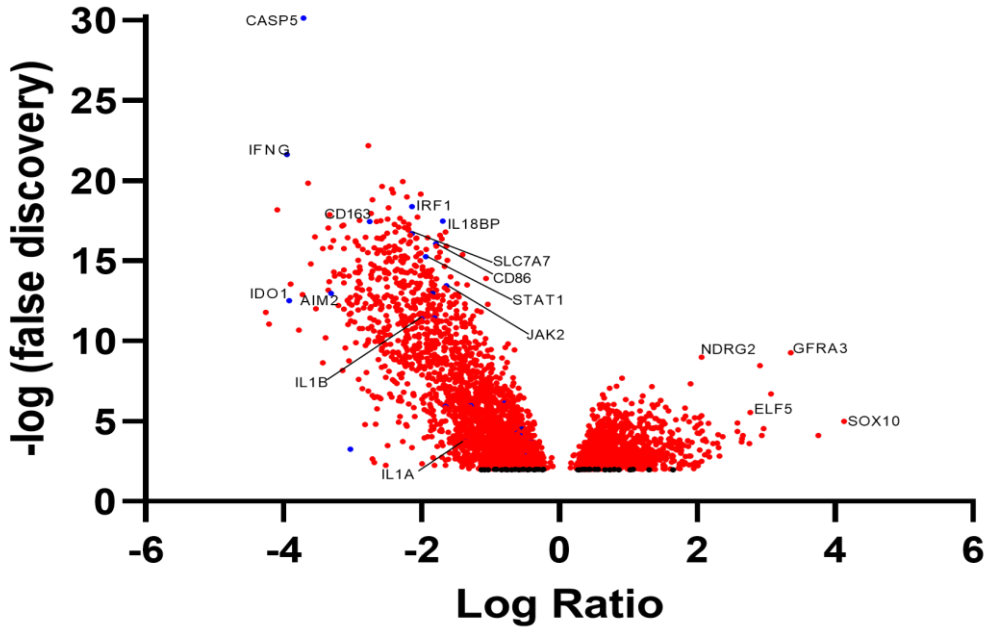

Figure 5.7: CASP5^{hi} expressing tumours from TNBC patients compared to CASP5^{lo} have differential mRNA expression profiles

Breast invasive carcinoma data from publicly available TCGA, PanCancer Altas was mined for CASP5 mRNA expression in basal-like breast cancer subtype. Differential gene expression from CASP5^{lo} and CASP5^{hi} expressing tumours was analysed and significantly altered expression between each group were plotted on Volcano plot.

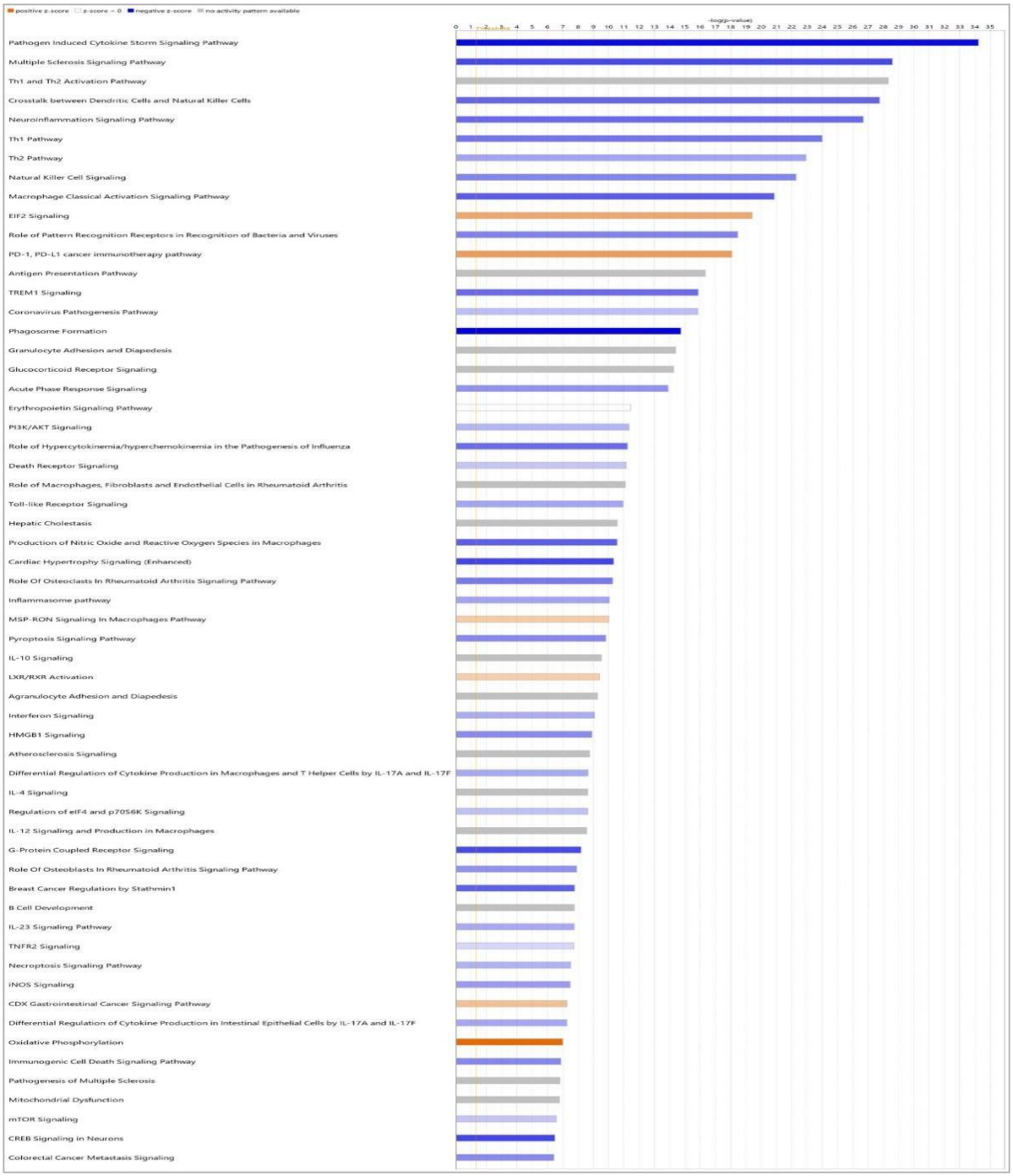

Figure 5.8: CASP5^{hi} TNBC patients are enriched for canonical pathways involved in M1 inflammatory macrophage polarisation and pyroptosis

Significantly differentially expressed genes between CASP5^{lo} and CASP5^{hi} TNBC were entered into Ingenuity Pathway Enrichment (IPA) (Qiagen) to score for the likelihood that genes belonging to a specific canonical pathway category were different between CASP5^{lo} and CASP5^{hi} (blue) TNBC. Positive or negative *z*-score value indicates that a function is predicted to be associated with CASP5^{lo} (positive z-score; red) or CASP5^{hi} (negative z-score; blue) TNBC. The significance of canonical pathways were determined by IPA's default threshold [–log (*p*-value) > 1.3] ($p < 0.05$), indicated by threshold in the graph.

A

Cell line name	Cancer type	Classification	Hormone Status	Morphology	Characteristic
MCF-7	mammary gland adenocarcinoma	Luminal A	ER+, PR+, Her2-		differentiated mammay epithelial
T47D	infiltrating ductal carcinoma	Luminal A	ER+, PR+, Her2-	rounded, epithelial-like	
CAMA-1	mammary adenocarinoma	Luminal A	ER+, PR+, Her2-	rounded	poorly differentiated grade III tumors
ZR-75-1	infiltrating ductal carcinoma	Luminal B	ER+, PR+, Her 2 +	epithelial	
BT549	mammary gland ductal carcinoma	Claudin-low (TNBC)	ER-, PR-, HER2-	polymorphic with epithelial like and multinucleated giant cells	mucin like material secreted into culture medium
HS578T	carcinsacroma	Claudin-low (TNBC)	ER-, PR-, HER2-	inititally polygonal, stellate morphology emerges	
MDA-MB-231	metastatic mammary adenocarcinoma	Claudin-low (TNBC)	ER-, PR-, HER2-	spindlemesenchymal-like	highly aggressive, poorly differentiated

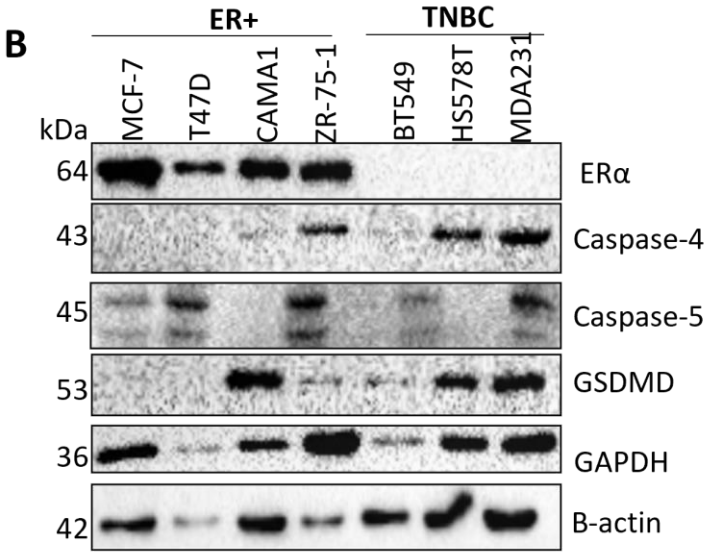

Figure 5.9: Caspase-4 and -5 expression in breast cancer epithelial cell lines is not determined by estrogen receptor status

(A) Table summarising breast cancer cell line panel: ER+ cells: MCF-7, CAMA-1, T47D, ZR-75-1 and triple negative breast cancer (TNBC): BT549, HS578T and MDAMB231. (B) Whole cell lysates (20 µg) from each cell line were analysed for expression of ERα, Caspase-4, Caspase-5, GSDMD, GAPDH and β-actin, as loading control. Blots are representative of three independent experiments.

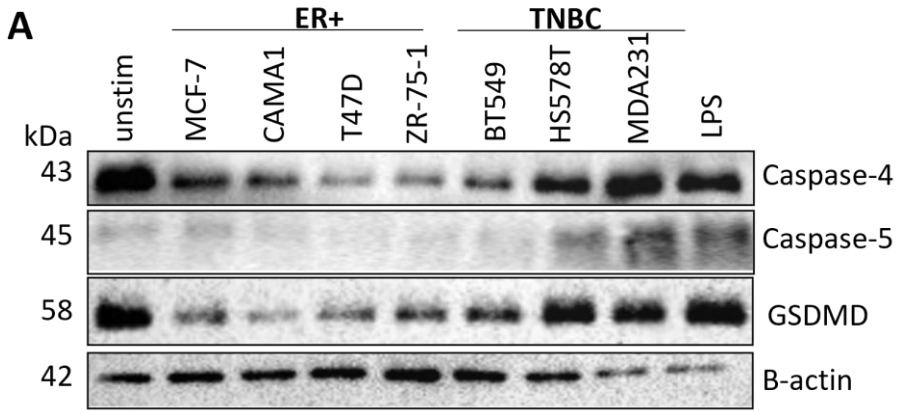

Figure 5.10: Conditioned media from TNBC breast carcinoma cell lines induce expression of Caspases-4, -5 and their substrate GSDMD in primary human monocyte derived macrophages

Monocyte derived macrophages (MDM) were stimulated for 24 h with TCM (50%) from unstimulated ER+ (MCF-7, CAMA-1, T47D, ZR-75-1) and TNBC (BT549, HS578T and MDAMB231) cell lines or LPS (1µg/mL). Whole cell lysates (20 µg) were were analysed for expression of caspase-4, caspase-5, GSDMD, and β-actin, as loading control.

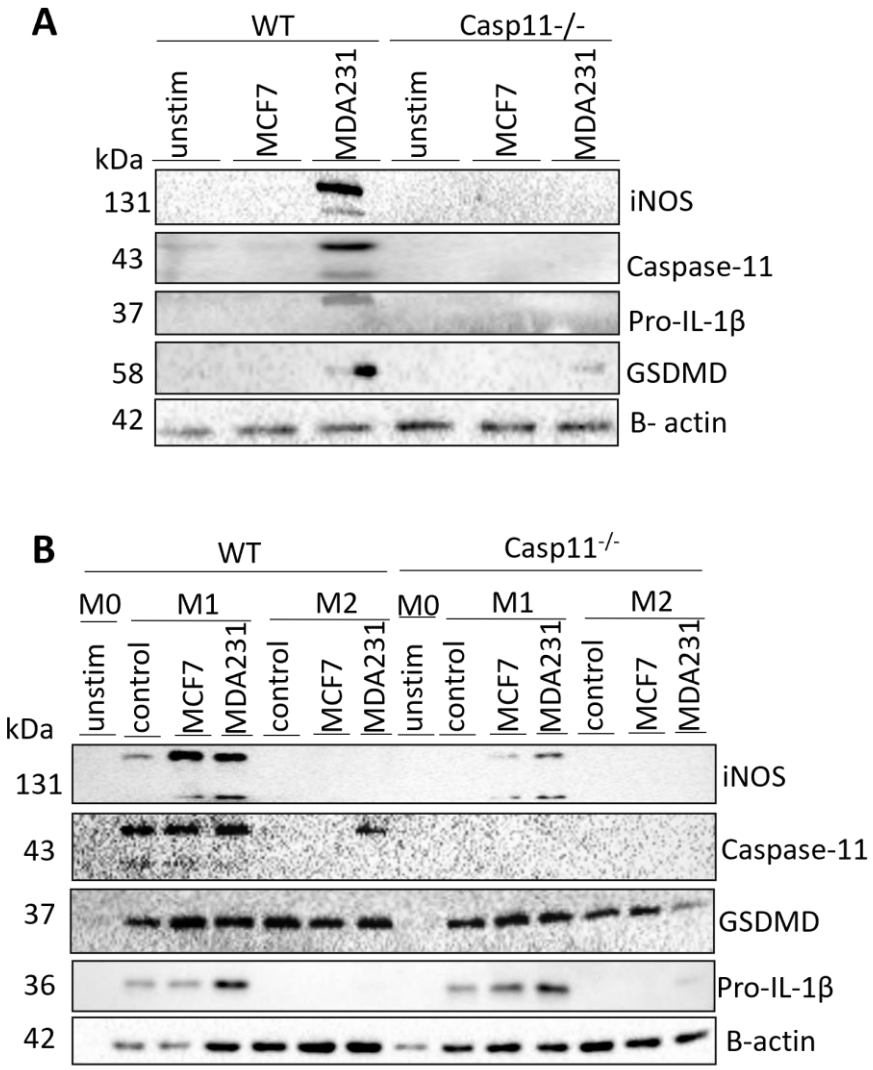

Figure 5.11: Tumour conditioned media (TCM) from TNBC cell line MDA-MB-231 induces caspase-11 expression in BMDM, which regulates iNOS, pro-IL-1β and GSDMD expression

(A) WT and Casp11$^{-/-}$ BMDM stimulated (24 h) with 50% TCM from MCF-7 (ER+) and MDA-MD-MB-231 (TNBC). (B) BMDM were stimulated (24 h) with 50% TCM as in (A) in combination with polarising cytokines for M1 (50ng/mL LPS, 20ng/mL IL-1β) or M2 (50ng/mL M-CSF, 20ng/mL IL-4). (A, B) BMDM lysates (20 µg) were analysed for expression of iNOS, caspase-11, GSDMD and pro-IL-1β, and β-actin, as loading control. Blots are representative of three independent experiments.

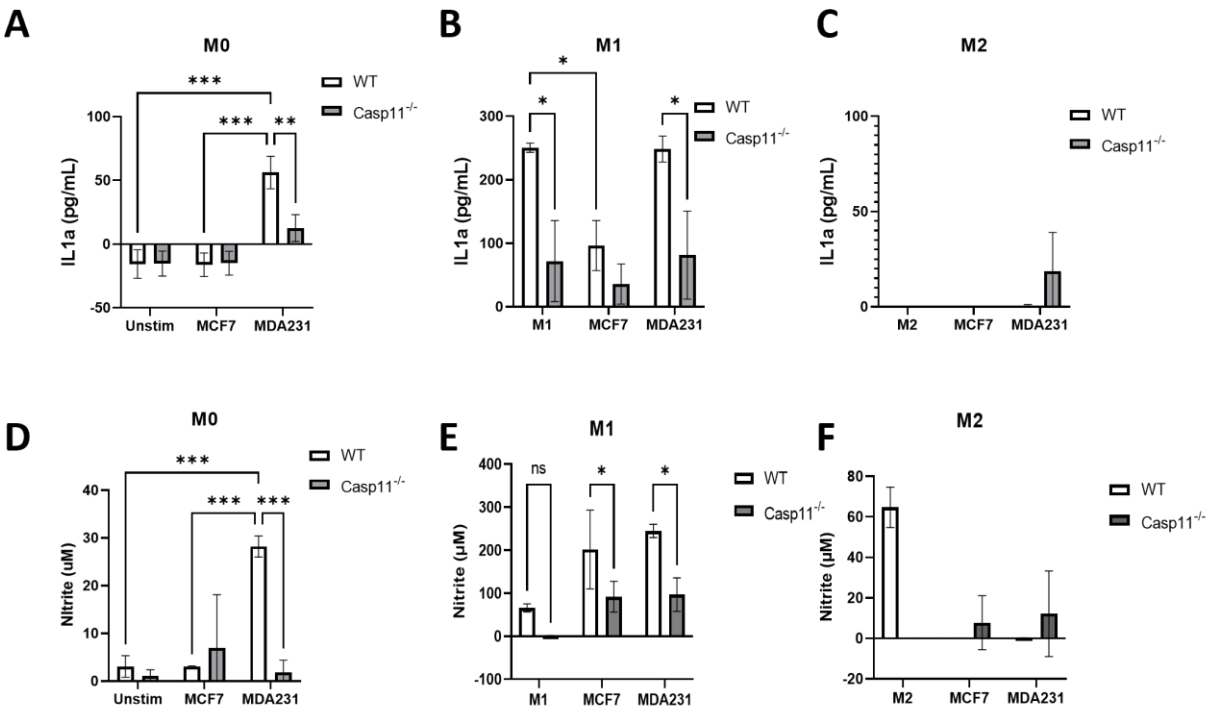

Figure 5.12: MDA-MB-231 CM induces IL-1α and NO production in TAM-like macrophages, which is dependent on caspase-11

WT and Casp11$^{-/-}$ BMDM stimulated (72 h) with 50% TCM from MCF-7 (ER+) and MDA-MB-231 (TNBC). BMDM were also stimulated with or without (M0) polarisation cytokines M1 (100ng/mL LPS, 50ng/mL IFN-γ) or M2 (50ng/mL M-CSF, 20ng/mL IL-4) in combination with 50% TCM. BMDM supernatants were analysed by ELISA for (A-C) IL-1α, (D-F) Nitrite levels by Griess assay in M0, M1 or M2-like BMDM. Data represent mean ± SEM. Statistical analysis was performed using two-way ANOVA ; *p<0.05, **p <0.01, ***p<0.001 (Tukey's post-test).

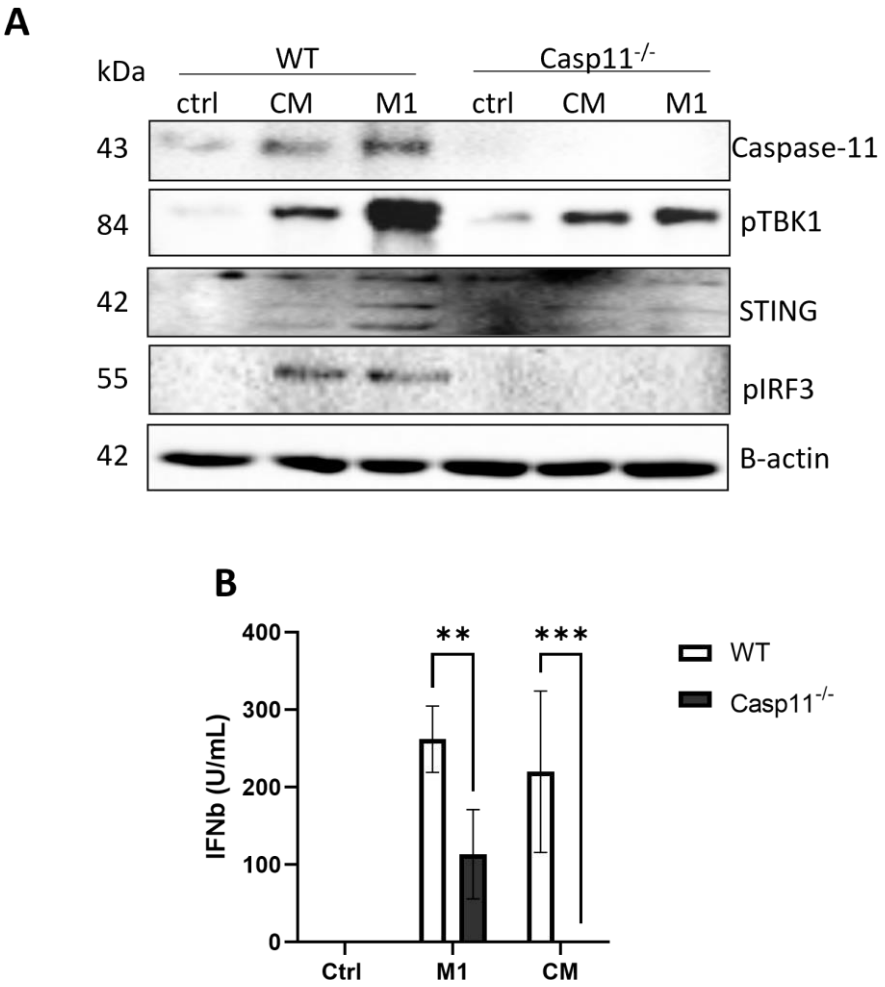

Figure 5.13: TCM from TNBC cell line MDA-MB-231 induces pTBK1, STING and pIRF3 expression in a caspase-11 dependent manner

WT and Casp11$^{-/-}$ BMDM stimulated (24 h) with 50% TCM MDA-MD-MB-231 (TNBC) or M1 cytokines (100ng/mL LPS, 50ng/mL IFNγ). WT and Casp11$^{-/-}$ BMDM lysates (20 µg) were analysed for expression of (A) caspase-11, pTKB1, STING, pIRF3, and β-actin, as loading control. Blots are representative of three independent experiments.

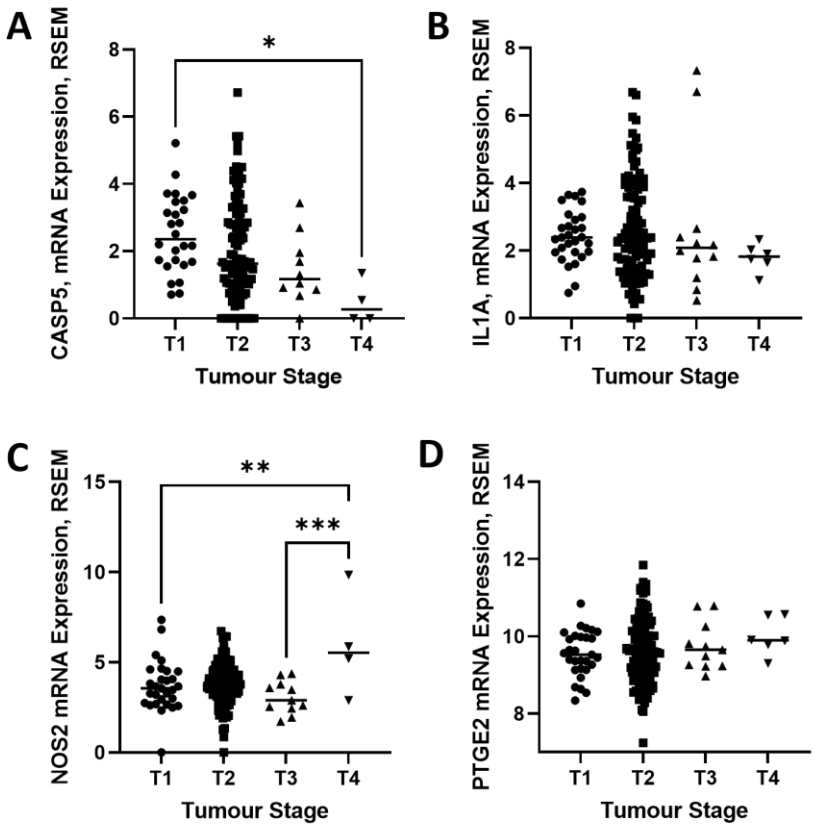

Figure 5.14: CASP5 expression decreases across tumour grade of basal-like breast carcinoma, while NOS2 and COX2 expression increases across tumour grade

Breast invasive carcinoma data from combined publicly available TCGA, PanCancer Altas, and TCGA, Nature 2012, (A) CASP5 (B) IL1A (C) NOS2 and (D) PTGES2 mRNA expression across tumour stage as defined by the American Joint Committee on Cancer Tumour Stage Code; T1 (n=29), T1 (n=107), T3 (n=11), T4 (n=6). Data represent mean ± SEM. Statistical analysis was performed using one-way ANOV ; *p<0.05, **p <0.01, ***p<0.001 (Tukey's post-test).

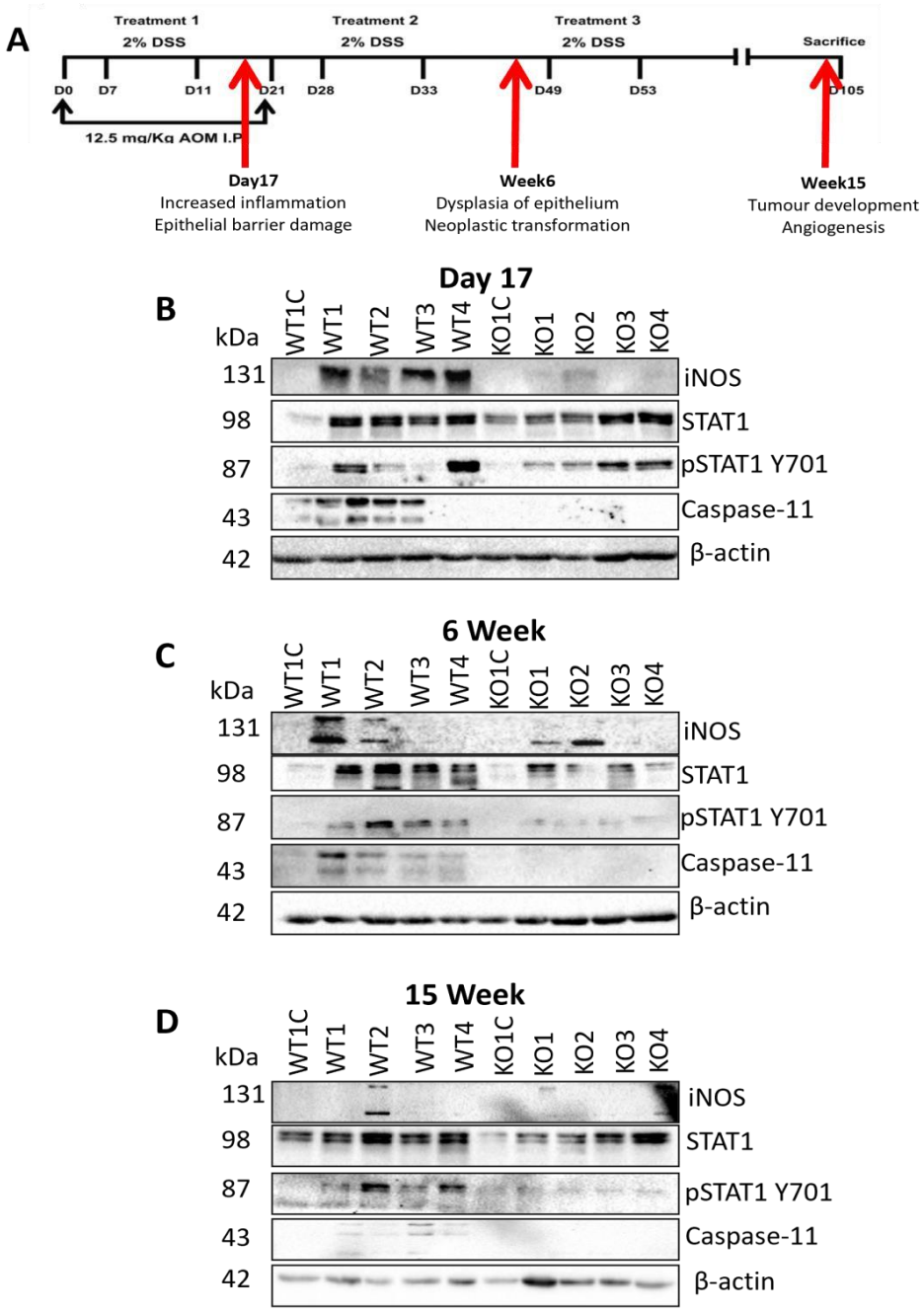

Figure 5.15: Caspase-11 mediates iNOS expression during early-stage disease in a murine model of colorectal cancer (CRC)

(A) WT and Casp11$^{-/-}$ mice were injected intraperitoneally with 12.5 mg/kg AOM on days 0 and 21 followed by the administration of 3 cycles of 2% (w/v) DSS. WT and Casp11$^{-/-}$ colons harvested from mice at (B) day 17, (C) week 6 and (D) week 15 following initial AOM injection were homogenised (20 µg) and analysed for expression of iNOS, pSTAT1 y701, tSTAT1, caspase-11 and β-actin (loading control). Each lane represents an individual mouse.

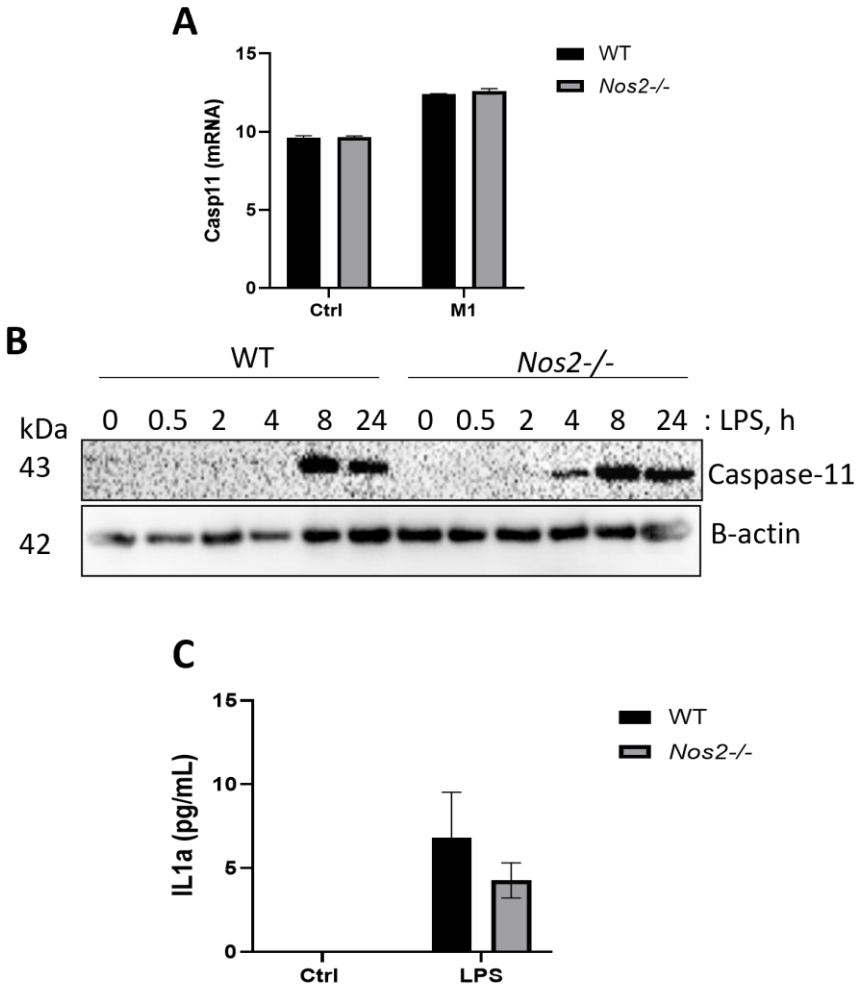

Figure 5.16: NOS2 does not regulate caspase-11 expression or IL-1α secretion

(A) Casp11 mRNA analysis was performed using the published dataset GSE115120 (Palmieri E. et al. (2020) Nature Communications), which compared WT and *Nos2*$^{-/-}$ BMDM treated for 8h with M1 cytokines (LPS 100ng/mL and IFNγ 50ng/mL). WT and *Nos2*$^{-/-}$ BMDM were stimulated with LPS (1μg/mL) over a 24 h timecourse, as indicated. Whole cell lysates of WT and *Nos2*$^{-/-}$ BMDM (20 μg) were analysed for expression of (B) caspase-11 and β-actin, as loading control. Blots are representative of three independent experiments. Supernatants were analysed for (C) IL-1α secretion following 24h LPS stimulation. Statistical analysis was performed using two-way ANOVA ; (Sidak post-test).

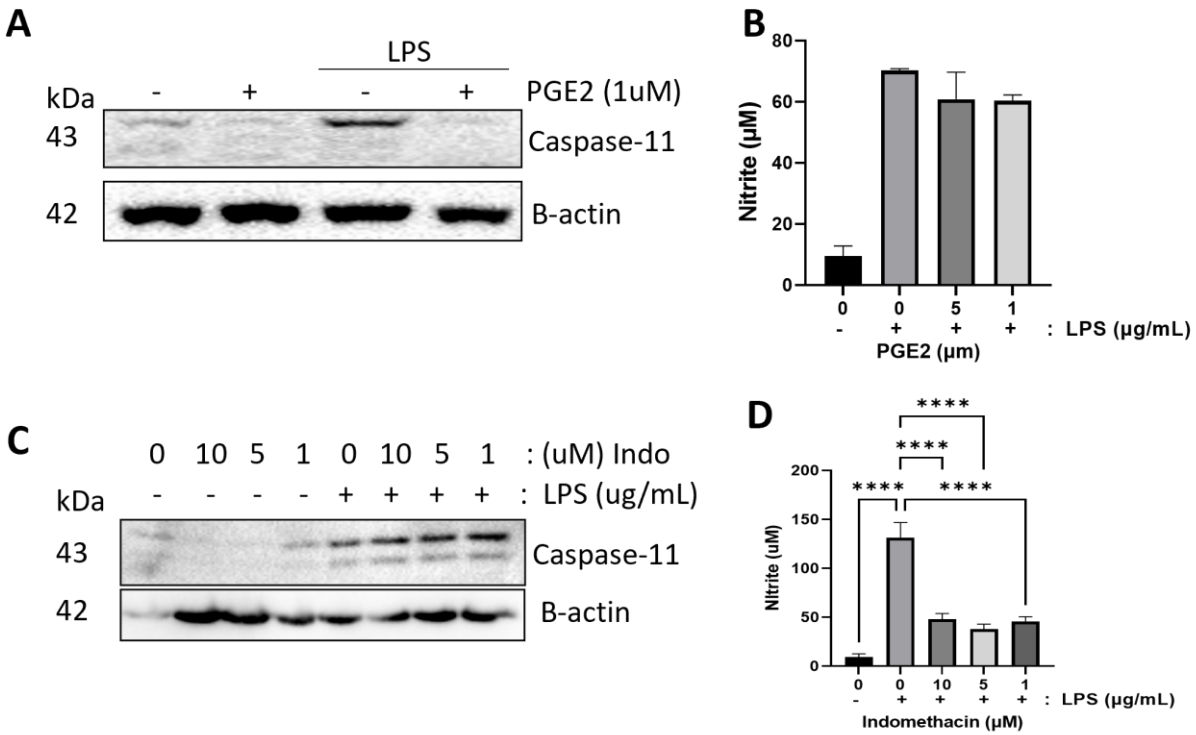

Figure 5.17: The inflammatory mediator PGE2 negatively regulates caspase-11 expression, whereas COX-2 inhibition reduces LPS-induced NO production

BMDM were pre-treated (30 min) with PGE_2 at the indicated concentrations prior to stimulation with LPS (1µg.mL) for 24 h. (A) Whole cell lysates (20 µg) were analysed for protein expression of caspase-11 and β-actin, as loading control. (B) Supernatants were analysed for nitrite production by Griess assay. BMDM were pre-treated (30 min) with indomethacine, at indicated concentrations prior to LPS stimulation (1µg.mL, 24 h). (C) Whole cell lysates (20 µg) were analysed for expression of caspase-11 and β-actin, as loading control. (D) Supernatants were analysed for nitrite production by Griess assay (n=3) and analysed by two-way ANOVA; *p <0.05 (Sidak post-test). Blots are representative of three independent experiments.

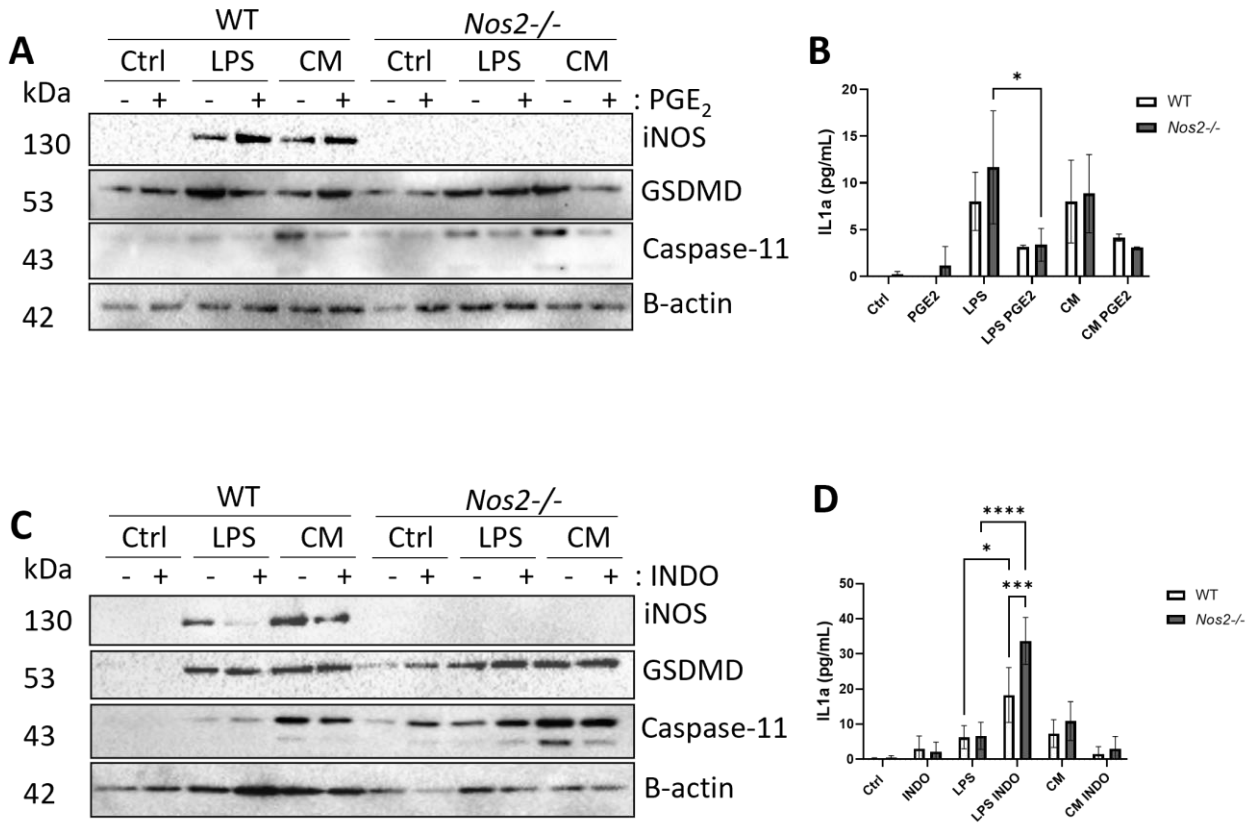

Figure 5.18: Conditioned media from TNBC cell line, MDA-MB-231, induces caspase-11 expression in BMDM, which is regulated by iNOS and COX2

WT and *Nos2*$^{-/-}$ BMDM were pre-treated (30 min) with PGE_2 (1µM) prior to stimulation with 50% TCM from MDA-MB-231 cells or LPS (1µg/mL) for 24 h. BMDM lysates (20 µg) were analysed for expression of (A) iNOS, GSDMD, caspase-11 and housekeeping protein β-actin. (B) Supernatants were analysed by ELISA for IL-1α secretion. WT and *Nos2*$^{-/-}$ BMDM were pre-treated (30 min) with indomethacin (1µM) prior to stimulation with 50% TCM from MDA-MD-MB-231 (TNBC) or LPS (1µg/mL) for 24 h. (C) BMDM lysates (20 µg) were analysed for expression of iNOS, GSDMD, caspase-11 and housekeeping protein β-actin expression. (D) Supernatants were analysed by ELISA for the secretion of IL-1α. Blots are representative of three independent experiments. Statistical analysis was performed using two-way ANOVA; *p<0.05, ***p <0.001, ****p<0.0001 (Tukey's post-test).

6. Chapter 6: General Discussion & Future Work

6.1. General Discussion

The term Immunometabolism, which has been a rapidly accelerating area of interest, was coined by Mathis and Shoelson in 2011[447]. Immunometabolism describes the interplay between metabolic and immunological processes. This term encompasses two concepts: how leukocyte function is regulated by internal metabolism; and how pathologies, such as obesity, promote metabolic abnormalities and increase the risk of type 2 diabetes, cardiovascular diseases, and cancer. Immunometabolism has been described as a nexus between therapeutic efficacy and resistance[448]. Therefore, understanding the molecular activities underlying immunological-metabolic crosstalk is important.

In this study, we investigated the role of caspase-11 mediated NO production during alterations in intracellular metabolic pathways and immune cell function. The dysregulation of the NO gasotransmitter has been implicated in many diseases, including cancer. In Chapter 3, we investigated the mechanism by which caspase-11 mediates NO production to understand how it becomes dysregulated during disease. Results have shown that LPS-induced caspase-11 leads to autocrine type I IFN signalling, mediating iNOS expression and NO production via mitophagy inhibition and potential cGAS-STING activity. Chapter 4 links caspase-11 driven NO to glycolytic commitment during M1 polarisation, demonstrating its importance for immune defence against TB. In Chapter 5, results suggest that in the context of TNBC, caspase-mediated NO production becomes redundant, once the COX2/NOS2 positive feedback loop promoting NO production has been established, while PGE2 inhibits caspase-11 expression.

6.1.1. STING is a nexus for Mitophagy-Type I IFN crosstalk

Aberrant immune activation, leading to chronic inflammation, has emerged as a hallmark of cancer. Therefore, strict control of inflammation induction and resolution must be maintained to support a homeostatic environment and to avoid excessive or deficient responses. Recent studies have illustrated that maintenance of mitochondrial health by mitophagy and recycling of mitochondrial contents by dynamic processes of fission and fusion are important for the regulation of innate immunity, and their dysfunction may contribute to inflammatory disorders[155,268]. However, the relationship between autophagy and immunity is complex and reciprocal, with autophagy both inducing and suppressing inflammation, while inflammation mediates the induction and suppression of autophagy. In cancer, aging, and neurodegenerative diseases, defective autophagy via gene mutation or antagonism may be the underlying route of pathogenesis.

The cGAS-STING pathway has been characterised as an inflammatory response mechanism to the presence of cytosolic dsDNA. Evidence indicates that STING promotes autophagy and a robust type I IFN response[430]. Reciprocally, the type I IFN response enables cGAS to sense dsDNA and form cGAMP, a STING agonist. cGAMP activation of STING promotes downstream inflammatory signalling, as defined by the induction of ISGs[449]. Based on our observations, we hypothesise that STING promotes M1 polarisation via type I IFN autocrine signalling. Initial studies investigating STING focused on pro-inflammatory and antiviral defence mechanisms. Later evidence depicted STING activation as being anti-tumourigenic, with STING agonist-mediated IFN signalling supporting anti-tumour immunity in the TME[450]. However, further studies have challenged the anti-tumour role of STING, with a tumour-promoting role contributing to progression and metastasis[451].

Cancer and aging are closely associated with mitochondrial fitness, as abundant evidence implicates loss of function, mtDNA mutations, and alterations in mitochondrial respiration during disease. During aging, a decline in PINK1/Parkin mediated mitophagy of defective mitochondria facilitates macrophage mtDNA leakage to promote STING activation[156]. Loss of function mutations of PINK1 induce mitochondrial dysfunction, such as morphological abnormalities, reduced membrane potential, and increased mtROS, as PINK1 kinase activity to phosphorylate Parkin Ser65 is impaired, preventing mitophagy. PINK1 deficiency induces an increase in LC3-II puncta and p62 accumulation, suggesting that autophagy is stalled under this condition[275]. Although the leakage of mtDNA into the cytosol is not well understood, reports have shown that significantly increased levels of cytosolic mtDNA are present in macrophages after LPS stimulation[452,453]. mtDNA engages cGAS-STING to induce type I IFN production while activating TLR9 to induce proinflammatory cytokine and chemokine production[454]. STING activation and type I IFN production induce a profound shift in the tumour immune landscape, promoting a robust immune response, T cell priming, and NK cell-mediated tumour regression6. STING agonists co-administered with other cancer immunotherapies, including immune checkpoint inhibitors such as anti-PD1, hold promise for treating medium and advanced cancers[455]. Similarly, in a TLR9 dependent-manner, the TIME landscape shifts - mounting an anti-tumourigenic CD8 T cell response[456]. Our data demonstrates a regulatory role for caspase-11 during STING activity and late IFNβ production, suggesting that caspase-11 expression influences an anti-tumour immune landscape. Previous reports illustrate that pyroptosis and IL-1β exert tumour supressing effects and anti-tumour immunity, established by inflammatory immune infiltration into the microenvironment. In a model of *Chlamydia muridarum,* caspase-11

contributes to disease clearance, independently of caspase-1. In the absence of caspase-11, neutrophil recruitment during early infection was reduced, however in late stage disease the $CD4^+$ T cell population remained elevated, as infection did not clear[457]. Caspase-11 mediated IL-1α release during *Paracoccidioides Brasiliense* infection boosted neutrophil and Th17 lymphocyte infiltration in lungs[87]. These observations strengthen our proposal that caspase-11 is required during TNBC initiation to generate an infiltratory, tumour suppressive environment. Moreover, within an allergic airway inflammation (AAI) model, caspase-11 has been illustrated to influence immune infiltration. Zaslona *et al.,* found that, in the absence of caspase-11, leukocyte and eosinophil populations in the bronchoalveolar lavage fluid were decreased. Th2 cytokines, IL-4 and IL-5, which are typically a hallmark of AAI, were abolished or diminished[79].

In agreement with our observations, Wu *et al.,* reported that pyroptosis-related proteins inversely correlated with tumour grade, size, clinical stage and risk of death in breast cancer[458]. However, the tumour promoting or inhibiting role of pyroptosis in cancer remains ambiguous. Release of pyroptosis-produced cytokines alter the immune microenvironment and promote the development of tumours by evading immune surveillance. Alternatively, pyroptosis-produced cytokines can also collect immune cells and ignite the immune system to improve the efficiency of tumour immunotherapies. Breast cancer studies have found that GSDMD-mediated pyroptosis and IL-1β release triggers myeloid cell infiltration into the TME[459],[206]. Studies have found GSDMA3-NT triggered pyroptosis and IL-18 increased T-cell anti-tumour responses. Pyroptosis is also related to some immune checkpoints, especially programmed death-1 (PD-1) or programmed death- ligand 1 (PD-L1). Pyroptosis-induced inflammation combined with anti-PD-1 sensitised breast cancer cells to the tumour microenvironment. Therefore, while we observed TNBC-induced STING in TAM in Chapter 5, it is important to monitor these expression levels during disease progression, as we reported caspase-5 suppression during advanced disease.

Although we observed TNBC CM-induced STING complex activation in TAM, cGAS-STING signalling was suppressed in association with DNMT1-mediated epigenetic regulation of MYC in TNBC[460]. Parkes et al. reported that perinuclear STING does not provide prognostic significance in ER-breast cancer, as it becomes uncoupled from the IFN response[461]. In contrast, in ER+ breast cancer, low perinuclear STING detection is associated with immunosuppressive TIME and M2-like macrophage infiltration. However, investigation of STING activation in HCC patients revealed that low STING levels correlated with advanced TNM staging and poorer OS, compared to high STING[462]. Reports have suggested that the STING pathway may be selectively suppressed during

cancer development. Similarly, we propose that caspase-5 expression during TNBC, driving the type I IFN response and NO production, is negatively regulated during advanced disease stages. Our results indicate that caspase-5/11 expression becomes supressed during TNBC development, as CASP5 expression inversely correlates with tumour stage. Additionally, COX-2 product PGE2, which is associated with tumour progression, supresses caspase-11 mediated IL-1α in TNBC-mediated TAMs. We suggest during the establishment of the TNBC TIME, caspase-11 promotes STING activation to induce IFN-β production (**Fig. 6.1**). Therefore, it would be interesting to further investigate the role of PGE2 suppression of caspase-11 during STING activation as well as pyroptosis. We propose that during tumour development, as PGE2 inhibits caspase-11 expression, the STING-IFN pathway will become downregulated. Therefore, as mentioned, STING agonist treatment in medium and advanced disease or treatment of late stage TNBC with pyroptotic-inducing compounds would promote a cytotoxic anti-tumorigenic TIME, and in combination with anti-PD1 potential facilitates tumour clearance.

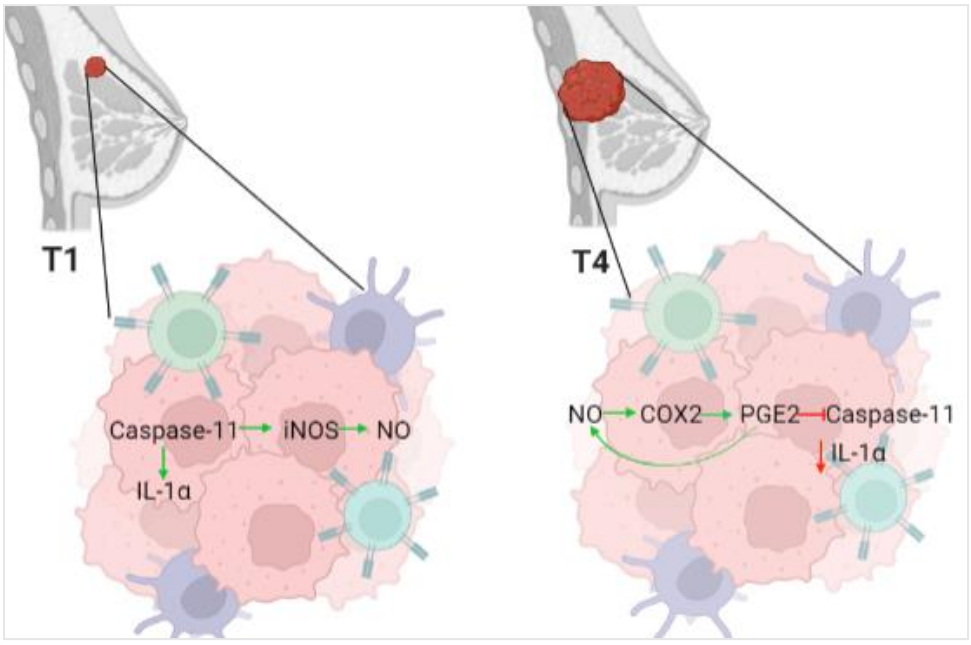

Figure 6.1: TAM expression of caspase-11 mediated by basal-like breast cancer secretome drives iNOS expression and NO production. Once expressed NO mediates COX-2 induced PGE2 expression which feedbacks in a positive loop. PGE2 inhibits caspase-11 expression which is no longer required for iNOS regulation.

LPS mediates the downregulation of the mitochondrial outer membrane proteins TOMM20 and VDAC1[453], which are typically associated with fusion. Impaired mitochondrial fission results in mitophagy initiation, and mtDNA inhibition regulated by EtBr, prevents STING phosphorylation

and TBK1 activity[453]. Importantly, the clearance of damaged mitochondria serves as an intrinsic negative feedback loop to prevent excessive STING-induced inflammation, thereby acting as a control mechanism for the resolution of inflammation. Similarly, our data suggest caspase-11 inhibition of mitophagy in response to LPS in murine macrophages leads to a type I IFN response, which we propose is mediated by STING activation, leading to NO production (**Fig. 6.2**). However, cytosolic DNA activation of cGAS-STING-induced type I IFNs is a target of AIM2 mediated GSDMD-driven K+ efflux to reinforce the type I IFN response[463]. Therefore, the disruption of ionic homeostasis by pore-forming pyroptosis can suppress type I IFN. In Chapter 3, we observed that NO production is independent of GSDMD following LPS stimulation, which we demonstrated to be dependent on autocrine IFNβ signalling. Previous reports have also found that the pyroptosis inhibitor dimethyl fumarate inhibited M1 polarisation[464]. Similar to findings showing increased inflammatory cytokine production in Nos2-/- BMDM, Aim2-deficiency compromised pyroptosis and accelerated aberrant inflammation, as evidenced by increased macrophage accumulation and TBK1-IRF3/NFκB signalling. In the absence of AIM2, macrophages escape pyroptosis in response to dsDNA, and dsDNA engages the STING-TBK1-IRF3 signalling pathway, leading to aggravated inflammation[465].

Mitophagy has been described as a major regulator of OXPHOS, and mitochondrial dynamics contribute to the metabolic status. Melser et al. showed that OXPHOS enhances mitophagy to promote renewal in a cycle to maintain mitochondrial health[466]. mtDNA and STING are emerging drivers of inflammation, energy metabolism, and disease progression. PINK1 deficiency and DJ1, markers of mitochondrial integrity, have been implicated in promoting glycolysis[467,468], suggesting that impaired mitophagy is involved in metabolic rewiring. Our data support these reports, as we observed that in the absence of caspase-11, increased PINK1 expression correlates with defective M1 shift to glycolysis. Additionally, reduced mtDNA during aging or mutation of mtDNA mediates a shift in energy metabolism towards OXPHOS[469].

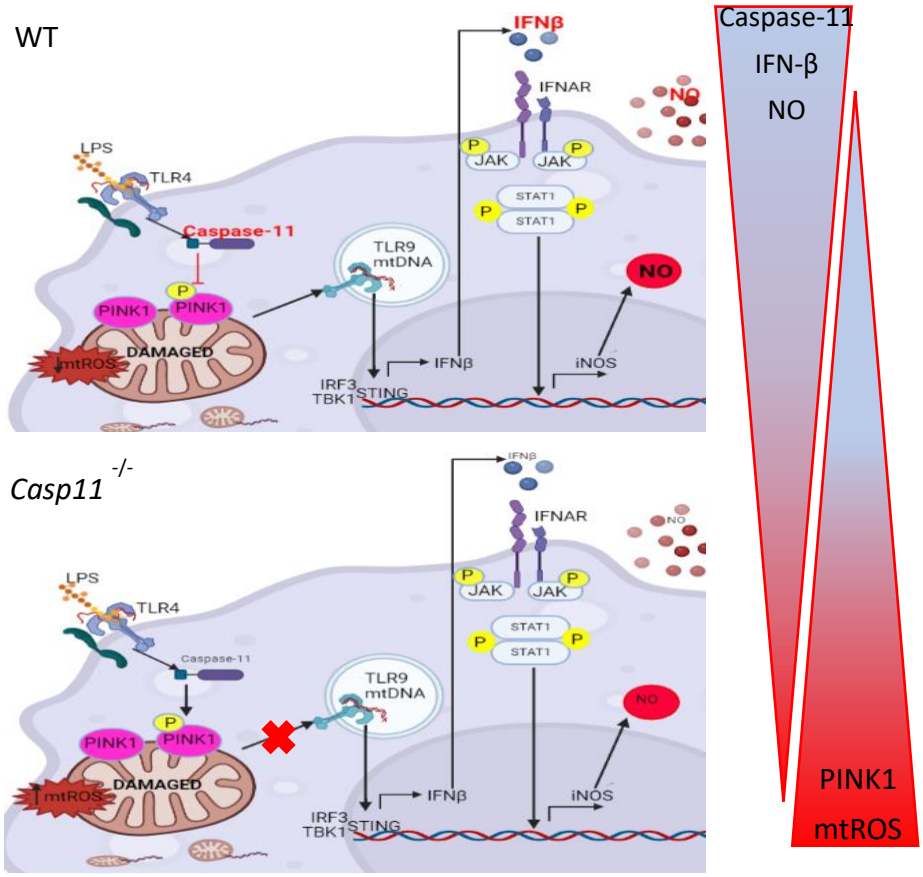

Figure 6.2: Caspase-11 inhibition of mitophagy induces macrophage type I IFN response. IFNβ autocrine activity via STAT1 activation regulated NO production. Caspase-11 inhibits PINK1-mediated mitophagy in response to LPS leading to the accumulation of damaged mitochondria in WT BMDM. mtDNA from damaged mitochondria induce STING-mediated type I IFN response. IFNβ autocrine signalling feedbacks to induced STAT-regulated iNOS expression and NO production. In caspase-11 deficient BMDM, PINK-1 mitophagy clears dysfunctional mitochondria leading to reduced type I IFN response and NO production.

6.1.2. Macrophage metabolism and phenotype crosstalk

Chapter 4 investigated the impact of caspase-11 mediated NO during inflammatory macrophage metabolic reprogramming. The central dogma of macrophage polarisation suggests M1 'classically' activated macrophages induced glycolysis drives the inflammatory phenotype. Traditionally, macrophages have been classified as M1 by their preferential expression of iNOS, which we found to be partially regulated by caspase-11, suggesting that caspase-11 links inflammation via non-canonical inflammasome activation and metabolism via mitophagy-induced type I IFN-mediated NO production. However, we observed that the role of caspase-11

in mediating glycolysis via NO production is independent of the non-canonical inflammasome and identifies a novel functional role for caspase-11 during inflammation.

6.1.3. Macrophage metabolism and phenotype crosstalk

Chapter 4 investigated the impact of caspase-11 mediated NO during inflammatory macrophage metabolic reprogramming. The central dogma of macrophage polarisation suggests M1 'classically' activated macrophages induced glycolysis drives the inflammatory phenotype. Traditionally, macrophages have been classified as M1 by their preferential expression of iNOS, which we found to be partially regulated by caspase-11, suggesting that caspase-11 links inflammation via non-canonical inflammasome activation and metabolism via mitophagy-induced type I IFN-mediated NO production. However, we observed that the role of caspase-11 in mediating glycolysis via NO production is independent of the non-canonical inflammasome and identifies a novel functional role for caspase-11 during inflammation.

TNBC displays the highest frequency of mitochondrial defects; therefore, it is typically characterized by lower mtDNA content and decreased mitochondrial respiration. Reports suggest that lower OXPHOS in TNBC may be a consequence of mtDNA mutations or reduced mtDNA coding for ETC complexes[434]. While glycolysis supports malignancy in TNBC under the influence of the Warburg effect, alterations in OXPHOS have also been reported in TNBC, with OXPHOS associated with a higher risk of recurrence and death in TNBC[435]. Hence, the dual targeting of metabolism is required for the effective treatment of TNBC. Using multi-omics approaches, TNBC has been classified into three heterogeneous metabolic pathway-based subtypes with distinct metabolic characteristics[470], enabling personalised therapies against metabolic profiles. These metabolic-pathway based subtypes include; MPS1, the lipogenic subtype with upregulated lipid metabolism; MPS2, the glycolytic subtype with upregulated carbohydrate and nucleotide metabolism; and MPS3, the mixed subtype with partial pathway dysregulation[470]. Therefore, caspase-5 may be a targetable feature of metabolically mediated immune regulation in the TNBC TIME.

Recently, avenues of investigation have also indicated that STING is a nexus between inflammation and metabolism. Overactive cGAS-STING signalling in mice deficient in the nucleic acid metabolism enzyme, 3' repair exonuclease 1 (TREX1) is associated with chronic systemic inflammation and glycolytic commitment. Additional studies investigating the effects of genes on systemic inflammation versus metabolism found that IRF3 regulates inflammation but not

glycolysis, whereas STING expression mediates both the metabolic switch and inflammatory response[471]. Similarly, although NO has been found to negatively regulate TCA and ETC by targeting metabolic enzymes and complexes to shift metabolism towards glycolysis, it was discovered that NO dampened the expression of pro-inflammatory cytokines. Therefore, these reports support the hypothesis that the inhibition of mitochondrial respiration is not critical for a complete inflammatory response. These congruences have unravelled the previously conceived dogma of macrophage polarisation mediated by glycolysis, which drives inflammation. However, NO inhibition of NF-κB-mediated inflammation suggests a potential negative feedback mechanism to prevent excessive inflammation. Our data suggests that caspase-11 mediated NO regulation of glycolysis is important for the bactericidal function of Mtb-infected macrophages (**Fig. 6.3**). However, it would be interesting to investigate the impact of caspase-11 during latent Mtb, as control of NO-mediated glycolysis and pyroptosis is impaired.

Although M1 associated glycolysis is impaired in caspase-11-NO deficient BMDM, our data showed reduced Arg1 expression in these cells. As previously mentioned, Arg1 is a marker of 'alternative' M2 polarisation, driving arginine conversion to urea and polyamines associated with an OXPHOS metabolism. An emerging area of interest is the influence of M1 activation on M2 behaviour. Recent publications have reported differential gene expression in M0-M2 polarized macrophages compared to M1-M2 polarised macrophages with distinct phenotypes[472]. Therefore, we propose that the impact of caspase-11 on glycolysis and M2-associated genes in M1 polarised macrophages may affect inflammatory resolution, which is important for mitigating inflammatory diseases, such as cancer progression. Restoring mitochondrial function, for example, through iNOS inhibition, might be useful for improving the reprogramming of M1 macrophages into M2 macrophages as a method of controlling inflammatory diseases.

Notably, mitochondrial dysfunction prevents repolarisation of inflammatory macrophages to an anti-inflammatory M2 phenotype. Van den Bossche *et al.,* suggest that inflammation induces glycolysis to trigger rapid energy production for clearance of intracellular pathogens by NO and ROS, which due to impaired mitochondrial function, repolarisation to M2 is hampered[473]. Impaired iNOS expression improved mitochondrial function in M1 macrophages, by pronounced increased OCR, as previously discussed. Decreased iNOS mediated mitochondrial dysfunction markedly improved subsequent M2 activation[473]. Therefore, a healthy mitochondrial status is

important for mediating macrophage phenotypic plasticity, preventing chronic inflammation and inducing tissue repair.

These observations imply that the apparent switch from M1 to M2 macrophages during infection, when mitochondria become dysfunctional and switch to healing responses is probably not caused by actual M1/M2 repolarization of the macrophages that are present, but rather by the repopulation and M2 polarization of newly recruited blood monocytes in the healing-promoting environment.

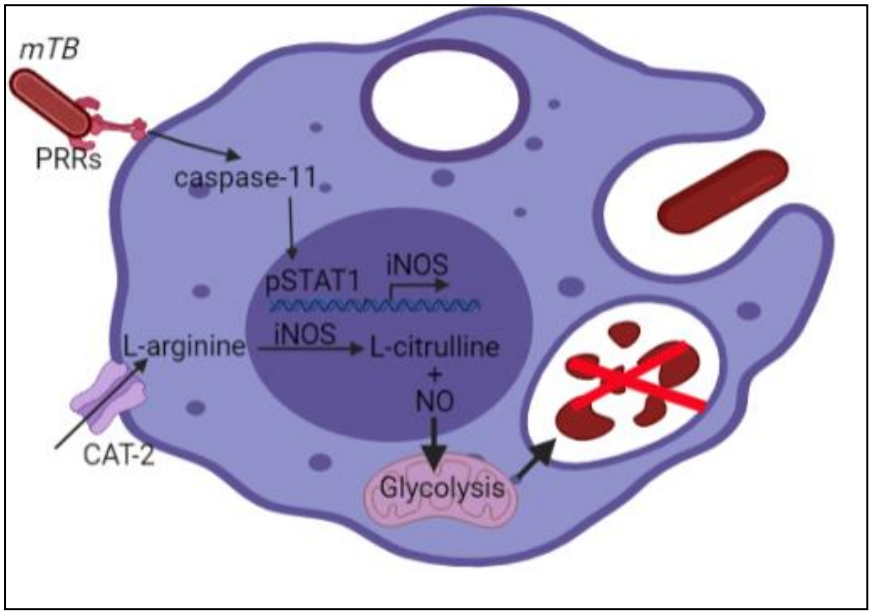

Figure 6.3: Caspase-11 mediated NO production drives glycolytic commitment in M1 BMDM and during Mtb infection, enhancing immune defence and Mtb clearance. Mtb infection induced caspase-11 expression leading to iNOS upregulation and NO production via IFNβ-STAT1 pathway. L-arginine uptake via CAT-2, regulated by caspase-11, is catabolised by iNOS to produce NO and L-citrulline. NO mediated glycolytic reprogramming to aid in Mtb clearance.

6.1.4. Alteration in TIME during disease progression

Classical basal-like TNBC has been classified further into several distinct populations dependent on the tumour immune microenvironment (TIME), categorised as inflamed, immunologically active, and non-inflamed, including immune-excluded and immune-desert associated with low immune infiltration and reduced cytolytic activity. LPS upregulated the expression of transcription factor c-Myc, which subsequently enhanced the activity of STING promoter and promoted its expression without affecting its phosphorylation. While, in the non-inflamed subtype, MYC overexpressing TNBC have supressed cyclic cGAS-STING pathway activation[460].

MYC amplification and overexpression led to low immune infiltration and cytolytic activity in TIME. MYC bound to DNA-methyltransferase-1 (*DNMT1)* promoter and activated *DNMT1* transcription in TNBC cells, thus suppressing the cGAS-STING pathway via an epigenetic regulatory way[460]. Inhibition of MYC induced DNMT1, with decitabine, a DNA methyltransferase inhibitor, restored STING and IFNβ expression, and enhanced $CD8^+$ T cell infiltration. Thereby illustrating the role of STING-IFN within the TIME for generating an active inflamed immune response. As PD-L1 expression is downstream of IFN signalling, decitabine significantly enhanced PD-L1 expression in TNBC. Decitabine-mediated STING-IFN activation alters the TNBC TIME for combination treatment with anti-PD-1 to increase cytotoxic $CD8^+$ T cell activity and decrease tumour volume[460]. Our study found that $CASP5^{hi}$ basal-like breast cancer is associated with increased proinflammatory macrophage associated pathways, which express STING and type I IFN genes. Additionally, caspase-11 induced STING activation in TNBC-associated TAMs, which we propose to be classified as immune-inflamed in early disease. This subset of TNBC is characterised by abundant T cell infiltration.

Whereas, in $NOS2^{hi}$/$COX2^{hi}$ TNBC tumours, spatial orientation restricts $CD8^+$ T cell infiltration, described as an immune desert. Targeted NOS2/COX2 blockade improved $CD8^+$ T cell penetration into the tumour epithelium associated with tumour growth delays[474]. We propose that caspase-11 importance during iNOS expression in cancer initiation becomes redundant as NOS2/COX2 feeds back to inhibit caspase-11 expression. As we observe, in the absence of COX2 and NOS2, caspase-11 expression is increased, there may potentially be higher CD8 infiltration. High pyroptosis links with “hot tumour” characteristics and high response rates to PD1/PDL1 inhibitors derived from clinical trials. In a bioorthogonal system targeting GSDM, 15% tumour cells undergoing pyroptosis is sufficient to clear the tumour in 4T1 model[395]. In this model GSDM induced pyroptosis induced inflammation triggered an anti-tumour immune response. M1 macrophage population increased in percentage compared to decreased M2-like macrophages following pyroptosis, as well as increased $CD4^+$, $CD8^+$ T cells. Thereby, low level pyroptosis induced in tumour cells synergise with anti-PD-1 to increase anti-tumour immunity[395]. Our study found that NO production, pivotal to M1 metabolic rewiring toward glycolysis, is independent of GSDMD. We demonstrate evidence of a negative feedback loop, in which PGE2 suppresses caspase-11 mediated IL-1α in advanced disease stages, once NO production is established. Therefore, in parallel with the opposing effect of NO and pyroptosis on the TIME, we suggest that the early activation of caspase-11 mediated IL-1α recruits inflammatory infiltration, with NO contributing to M1 metabolic reprogramming. However, as disease progresses CASP5

reduction and NOS2 elevation may potentially shift the TIME landscape to a pro-tumorigenic immune desert.

In conclusion, this study illustrated a key role for caspase-11 as a nexus to mitophagy and metabolism during inflammation. Caspase-11 contribution to mitochondrial dysfunction driving type I IFN responses underpins our molecular understanding of caspase-11 mediated NO production regulating glycolytic commitment. Arginine metabolism divergence is a major classifier of macrophage polarisation and we demonstrate that caspase-11 is involved at several steps including L-arginine uptake via CAT-2, and iNOS and Arg expression for L-arginine catabolism. NO mediated by caspase-11 is central to M1 macrophage polarisation and immunometabolism. Investigation of caspase-11 mediated NO production in TNBC led us to hypothesise that this relationship is important during tumour initiation and becomes redundant during progression. Therefore, targeting and re-education of TAM is stage dependent, requiring understanding of the immune infiltrate landscape.

6.2. Study Limitations

In humans, the ortholog of mouse caspase-11 may be either caspase-4 or caspase-5, based on amino acid sequence. However, only caspase-5 appears to be regulated in a similar way to murine caspase-11 in relation to response to extracellular stimuli including LPS and interferons[47]. Subtle differences have been reported between caspase-4 and -5 which are influenced by types of activators delivered into the cell and appear to cell-type and species-specific dependent[397]. Although caspase-4 amino acid sequence identifies with 60% of caspase-11 sequence it has been suggested that caspase-4 is unlikely to be the human homologue of mouse caspase-11 due to the high basal expression levels of CASP4 mRNA in tissues and cells, in contrast to the low expression of caspase-11 in unstimulated mouse colonic tissue[39]. Therefore, while our findings utilising *Casp11*$^{-/-}$ BMDM appear to correspond with human caspase-5, there is a need to differentiate the role of caspse-4 and caspase-5 during disease. However, currently separating the role of caspase-4 and -5 mechanistically comes with challenges due to their close homology, with no peptide inhibitors available which selectively targets one without the other. Similarly, using murine models to investigate iNOS expression and NO production comes with limitations as many reports have demonstrated restricted induction of iNOS in human macrophages and epithelial cells, thereby questioning the importance of its role during immunometabolism and inflammatory disease progression in a human system. Growing evidence has revealed that chromatin hypermethylation of Nos2 locus around the transcriptional start site may contribute to limited iNOS induction[475] and modest NO concentrations produced in human macrophages in comparison to rodent macrophages[476]. Accordingly, these difference in iNOS induction and NO concentrations are reflective upon human macrophage M1 glycolytic commitment. After 40 minutes LPS stimulation human and murine macrophages, independent of NO, shift to glycolysis in parallel with rapid proinflammatory cytokine production[477]. Whereas NO-dependent metabolic reprogramming towards glycolysis in murine macrophages is during late stage (>4h). NO targeted PDH and ACON-2 to stall glucose-driven TCA cycle flux and substitute carbon source as glutamine is not observed in human macrophages[303]. Therefore, these differences in gene transcription of iNOS and metabolic role of NO during M1 polarisation indicate that further work is required to translate our proposed model to human disease.

6.3. Future Work

Further investigation of caspase-11's impact on mitophagic flux is necessary to convincingly attribute mtDNA release as the trigger of type I IFN mediated NO production. Future experiments should focus on monitoring mitophagy in real time to visualise protein localisation at the mitochondria and autophagolysome formation while examining mitochondrial dynamics. These experiments will aid in differentiating basal autophagy and autophagic flux in the absence of caspase-11. Tandem-tagged fluorescent LC3B, in which fluorescent tagged LC3 alternates colour when quenched by acidic pH of the autolysosomes is informative of LC3-I conjugation to phosphatidylethanaolamine, to form LC3-II. Soluble cytosolic LC3-I conversion to hydrolipid lysosome bound LC3-II is not necessarily indicative of complete autophagy. Therefore, monitoring LC3-II quenching by the acidic pH of the autophagosome environment is indicative of autophagic flux. In parallel, mitophagy and mitochondrial dynamics can be monitored by mitotracker staining, to determine the impact of reduced mitophagy on damaged mitochondrial accumulation. Additionally, mtDNA structures can be observed by staining with anti-dsDNA antibody, to visualise dsDNA translocation into the cytosol or colocalization within the mitochondria, following LPS stimulation, to observe mtDNA leakage in response to impaired mitophagy in WT compared to *Casp11/-* BMDM.

We propose that caspase-11 inhibition of mitophagy increases NO production via type I IFN response to shift cellular energy demands towards glycolysis. As we have previously observed, induction of mitophagy utilising the pharmacological inhibitor, ivermectin, and the NO donor DETANO supported glycolytic shift. It would be of interest to investigate the impact of mitophagy induction in WT BMDM, and inhibition in *Casp11-/-* BMDM on NO driven glycolytic commitment. As mitochondrial dysfunction and inhibited PINK1 mediated mitophagy is associated with impaired mitochondrial respiration, we hypothesise that induction of mitophagy in WT M1 BMDM will suppress glycolytic reprogramming. Whereas inhibition of mitophagy in *Casp11-/-* M1 BMDM aids the metabolic shift to glycolysis. Notably, we will also need to measure mitochondrial number after treatment with inducers of mitophagy, to ensure that changes in energy demands are not a direct impact of altered mitochondria per cell.

In this study we have performed preliminary investigations on the intracellular and extracellular metabolites of glycolysis, TCA cycle and arginine metabolism in WT and *Casp11-/-* M1 BMDM, of which biological replicates must be performed in the future. Additionally, we propose to investigate the activity of the key metabolic enzymes which we observed our preliminary

differences, including ACON-2, ketoglutarate dehydrogenase, arginosuccinate lyase/synthase as well as PDH and SDH. Investigation of enzymatic activity of these enzymes will provide further clarification of whether metabolite accumulation is a consequence of cycle stall or increased production due to inflammatory stimuli.

Although previous studies from Zaslona *et al.,* have demonstrated that PGE2 inhibition of IFNβ leads to impaired caspase-11 expression[79] we wish to further explore how PGE2 negatively regulates type I IFN production. Previously, reports have found that exogenous PGE2 supressed cGAMP-induced STING signalling and IFNβ production in murine macrophage [478,479], and the PGE2 receptor 4 agonist modulates mitophagy. Therefore, we propose investigating the impact of exogenous PGE2, and LPS stimulated *EP2-/-* BMDM, during mitophagy. We hypothesise that increased mitophagy will impair IFN-β production and caspase-11 expression. As mitophagy and inflammation reciprocally induce and supress each other, we suggest that IFN-β is involved in the positive amplification, while PGE2 suppress IFNβ activity.

Further investigation into the role of stromal caspase-5 during TNBC disease progression and its influence on the TIME is required to understand the impact of caspase-5 on TME driven progression. We proposed caspase-11 regulation of iNOS driven by impaired mitophagy and type I IFN response is important during TNBC disease progression. However, caspase-11 becomes redundant during NO production, as a result of a NOS2/COX2 positive feedback loop which subsequently inhibits caspase-11 activity. This loss of caspase-11 activity during advanced TNBC disease impairs anti-tumourigenic pyroptotic role of caspase-11, leading to immunosuppressive TIME. To investigate this regulatory loop during TNBC disease progression we propose utilising a syngeneic, orthotopic model of TNBC in WT and *Casp11*$^{-/-}$ mice in combination with indomethacin to determine the influence of caspase-11 during disease development and COX-2 inhibition of caspase-11 on pyroptotic mediated TIME. This Py8119 model of TNBC typically takes 35 days to reach a maximum volume of 1200mm^3. Therefore, we suggest harvesting tumours at several timepoints over 35 days once visible macroscopic tumours are formed at the mammary fat pad. From this trial we aim to examine the influence of caspase-11 on the rates of disease initiation, and caspase-11 mediated mitophagy and type I IFN response in early disease. Additionally, we aim to illustrate reduced caspase-11 expression and thereby mitophagy and type I IFN responses as disease stage advances, while NOS2/COX2 increases. Lastly, from this trial we hypothesise that the indomethacin treated group would have sustained caspase-11 expression and increased pyroptotic markers associated with increased CD8$^+$ T cell infiltration and reduced tumour load.

7.Bibliography

1. Hanahan D, Weinberg RA. Hallmarks of cancer: The next generation. *Cell*. Published online 2011. doi:10.1016/j.cell.2011.02.013
2. Xiao TS. Innate immunity and inflammation. *Cell Mol Immunol*. Published online 2017. doi:10.1038/cmi.2016.45
3. Gasteiger G, D'osualdo A, Schubert DA, Weber A, Bruscia EM, Hartl D. Cellular Innate Immunity: An Old Game with New Players. *J Innate Immun*. Published online 2017. doi:10.1159/000453397
4. Netea MG, Joosten LAB, Latz E, et al. Trained immunity: A program of innate immune memory in health and disease. *Science (80-)*. Published online 2016. doi:10.1126/science.aaf1098
5. Boraschi D, Italiani P. Innate immune memory: Time for adopting a correct terminology. *Front Immunol*. Published online 2018. doi:10.3389/fimmu.2018.00799
6. Blok BA, Arts RJW, van Crevel R, Benn CS, Netea MG. Trained innate immunity as underlying mechanism for the long-term, nonspecific effects of vaccines. *J Leukoc Biol*. Published online 2015. doi:10.1189/jlb.5ri0315-096r
7. Akira S, Uematsu S, Takeuchi O. Pathogen recognition and innate immunity. *Cell*. Published online 2006. doi:10.1016/j.cell.2006.02.015
8. Mogensen TH. Pathogen recognition and inflammatory signaling in innate immune defenses. *Clin Microbiol Rev*. Published online 2009. doi:10.1128/CMR.00046-08
9. Amarante-Mendes GP, Adjemian S, Branco LM, Zanetti LC, Weinlich R, Bortoluci KR. Pattern recognition receptors and the host cell death molecular machinery. *Front Immunol*. Published online 2018. doi:10.3389/fimmu.2018.02379
10. Kawai T, Akira S. The roles of TLRs, RLRs and NLRs in pathogen recognition. *Int Immunol*. Published online 2009. doi:10.1093/intimm/dxp017
11. Takeuchi O, Akira S. Pattern Recognition Receptors and Inflammation. *Cell*. Published online 2010. doi:10.1016/j.cell.2010.01.022
12. Gong T, Liu L, Jiang W, Zhou R. DAMP-sensing receptors in sterile inflammation and inflammatory diseases. *Nat Rev Immunol*. Published online 2020. doi:10.1038/s41577-019-0215-7
13. Botos I, Segal DM, Davies DR. The structural biology of Toll-like receptors. *Structure*. Published online 2011. doi:10.1016/j.str.2011.02.004
14. Kawasaki T, Kawai T. Toll-like receptor signaling pathways. *Front Immunol*. Published online 2014. doi:10.3389/fimmu.2014.00461
15. Fitzgerald KA, Rowe DC, Golenbock DT. Endotoxin recognition and signal transduction by the TLR4/MD-2 complex. *Microbes Infect*. Published online 2004. doi:10.1016/j.micinf.2004.08.015
16. Akira S, Takeda K. Toll-like receptor signalling. *Nat Rev Immunol*. Published online 2004. doi:10.1038/nri1391
17. Martinon F, Burns K, Tschopp J. The Inflammasome: A molecular platform triggering activation of inflammatory caspases and processing of proIL-β. *Mol Cell*. Published online 2002. doi:10.1016/S1097-2765(02)00599-3
18. Latz E, Xiao TS, Stutz A. Activation and regulation of the inflammasomes. *Nat Rev Immunol*. Published online 2013. doi:10.1038/nri3452
19. Du B, Jiang Q-L, Cleveland J, Liu B-R, Zhang D. Targeting Toll-like receptors against cancer. *J Cancer Metastasis Treat*. Published online 2016. doi:10.20517/2394-4722.2016.62
20. Lamkanfi M, Declercq W, Kalai M, Saelens X, Vandenabeele P. Alice in caspase land. A phylogenetic analysis of caspases from worm to man. *Cell Death Differ*. Published online 2002. doi:10.1038/sj.cdd.4400989
21. Scott AM, Saleh M. The inflammatory caspases: Guardians against infections and sepsis. *Cell Death Differ*. Published online 2007. doi:10.1038/sj.cdd.4402026
22. Nadiri A, Wolinski MK, Saleh M. The Inflammatory Caspases: Key Players in the Host Response to Pathogenic Invasion and Sepsis. *J Immunol*. Published online 2006.

doi:10.4049/jimmunol.177.7.4239
23. Black RA, Kronheim SR, Merriam JE, March CJ, Hopp TP. A pre-aspartate-specific protease from human leukocytes that cleaves pro-interleukin-1β. *J Biol Chem*. Published online 1989.
24. Thornberry NA, Bull HG, Calaycay JR, et al. A novel heterodimeric cysteine protease is required for interleukin-1βprocessing in monocytes. *Nature*. Published online 1992. doi:10.1038/356768a0
25. Cerretti DP, Kozlosky CJ, Mosley B, et al. Molecular cloning of the interleukin-1β converting enzyme. *Science (80-)*. Published online 1992. doi:10.1126/science.1373520
26. Fuentes-Prior P, Salvesen GS. The protein structures that shape caspase activity, specificity, activation and inhibition. *Biochem J*. Published online 2004. doi:10.1042/BJ20041142
27. Pop C, Salvesen GS. Human caspases: Activation, specificity, and regulation. *J Biol Chem*. Published online 2009. doi:10.1074/jbc.R800084200
28. Martinon F, Tschopp J. Inflammatory caspases: Linking an intracellular innate immune system to autoinflammatory diseases. *Cell*. Published online 2004. doi:10.1016/j.cell.2004.05.004
29. Walker NPC, Talanian R V., Brady KD, et al. Crystal structure of the cysteine protease interleukin-1β-converting enzyme: A (p20/p10)2 homodimer. *Cell*. Published online 1994. doi:10.1016/0092-8674(94)90303-4
30. Broz P, Von Moltke J, Jones JW, Vance RE, Monack DM. Differential requirement for caspase-1 autoproteolysis in pathogen-induced cell death and cytokine processing. *Cell Host Microbe*. Published online 2010. doi:10.1016/j.chom.2010.11.007
31. Wilson KP, Black JAF, Thomson JA, et al. Structure and mechanism of interleukin-lβ converting enzyme. *Nature*. Published online 1994. doi:10.1038/370270a0
32. Datta D, McClendon CL, Jacobson MP, Wells JA. Substrate and inhibitor-induced dimerization and cooperativity in caspase-1 but not caspase-3. *J Biol Chem*. Published online 2013. doi:10.1074/jbc.M112.426460
33. Boucher D, Monteleone M, Coll RC, et al. Caspase-1 self-cleavage is an intrinsic mechanism to terminate inflammasome activity. *J Exp Med*. Published online 2018. doi:10.1084/jem.20172222
34. Lopez-Castejon G. Control of the inflammasome by the ubiquitin system. *FEBS J*. Published online 2020. doi:10.1111/febs.15118
35. Groslambert M, Py BF. Spotlight on the NLRP3 inflammasome pathway. *J Inflamm Res*. Published online 2018. doi:10.2147/JIR.S141220
36. Munday NA, Vaillancourt JP, Ali A, et al. Molecular cloning and pro-apoptotic activity of ICErelII and ICErelIII, members of the ICE/CED-3 family of cysteine proteases. *J Biol Chem*. Published online 1995. doi:10.1074/jbc.270.26.15870
37. Faucheu C, Diu A, Chan AW, et al. A novel human protease similar to the interleukin-1 beta converting enzyme induces apoptosis in transfected cells. *EMBO J*. Published online 1995. doi:10.1002/j.1460-2075.1995.tb07183.x
38. Faucheu C, Blanchet AM, Collard-Dutilleul C, Lalanne JL, Diu-Hercend A. Identification of a cysteine protease closely related to interleukin-1β-converting enzyme. *Eur J Biochem*. Published online 1996. doi:10.1111/j.1432-1033.1996.t01-1-00207.x
39. Wang S, Miura M, Jung YK, et al. Identification and characterization of ich-3, a member of the interleukin-1β converting enzyme (ICE)/Ced-3 family and an upstream regulator of ICE. *J Biol Chem*. Published online 1996. doi:10.1074/jbc.271.34.20580
40. Lee BL, Stowe IB, Gupta A, et al. Caspase-11 auto-proteolysis is crucial for noncanonical inflammasome activation. *J Exp Med*. Published online 2018. doi:10.1084/jem.20180589
41. Hitomi J, Katayama T, Eguchi Y, et al. Involvement of caspase-4 in endoplasmic reticulum stress-induced apoptosis and Aβ-induced cell death. *J Cell Biol*. Published online 2004. doi:10.1083/jcb.200310015

42. Bian ZM, Elner SG, Elner VM. Dual involvement of caspase-4 in inflammatory and ER stress-induced apoptotic responses in human retinal pigment epithelial cells. *Investig Ophthalmol Vis Sci*. Published online 2009. doi:10.1167/iovs.09-3628
43. Pataer A, Hu W, Xiaolin L, et al. Adenoviral endoplasmic reticulum-targeted mda-7/interleukin-24 vector enhances human cancer cell killing. *Mol Cancer Ther*. Published online 2008. doi:10.1158/1535-7163.MCT-08-0083
44. Lakshmanan U, Porter AG. Caspase-4 Interacts with TNF Receptor-Associated Factor 6 and Mediates Lipopolysaccharide-Induced NF-κB-Dependent Production of IL-8 and CC Chemokine Ligand 4 (Macrophage-Inflammatory Protein-1β). *J Immunol*. Published online 2007. doi:10.4049/jimmunol.179.12.8480
45. Casson CN, Yu J, Reyes VM, et al. Human caspase-4 mediates noncanonical inflammasome activation against gram-negative bacterial pathogens. *Proc Natl Acad Sci U S A*. Published online 2015. doi:10.1073/pnas.1421699112
46. Lagrange B, Benaoudia S, Wallet P, et al. Human caspase-4 detects tetra-acylated LPS and cytosolic Francisella and functions differently from murine caspase-11. *Nat Commun*. Published online 2018. doi:10.1038/s41467-017-02682-y
47. Lin XY, Choi MSK, Porter AG. Expression analysis of the human caspase-1 subfamily reveals specific regulation of the CASP5 gene by lipopolysaccharide and interferon-γ. *J Biol Chem*. Published online 2000. doi:10.1074/jbc.M007255200
48. Ming Man S, Karki R, Briard B, et al. Differential roles of caspase-1 and caspase-11 in infection and inflammation. *Sci Rep*. Published online 2017. doi:10.1038/srep45126
49. Wang S, Miura M, Jung YK, Zhu H, Li E, Yuan J. Murine caspase-11, an ICE-interacting protease, is essential for the activation of ICE. *Cell*. Published online 1998. doi:10.1016/S0092-8674(00)80943-5
50. Kesavardhana S, Kanneganti TD. Mechanisms governing inflammasome activation, assembly and pyroptosis induction. *Int Immunol*. Published online 2017. doi:10.1093/intimm/dxx018
51. Dorfleutner A, Chu L, Stehlik C. Inhibiting the inflammasome: One domain at a time. *Immunol Rev*. Published online 2015. doi:10.1111/imr.12290
52. Saxena M, Yeretssian G. NOD-like receptors: Master regulators of inflammation and cancer. *Front Immunol*. Published online 2014. doi:10.3389/fimmu.2014.00327
53. Hattori M, Gouaux E. Molecular mechanism of ATP binding and ion channel activation in P2X receptors. *Nature*. Published online 2012. doi:10.1038/nature11010
54. Serna M, Giles JL, Morgan BP, Bubeck D. Structural basis of complement membrane attack complex formation. *Nat Commun*. Published online 2016. doi:10.1038/ncomms10587
55. Zhou R, Yazdi AS, Menu P, Tschopp J. A role for mitochondria in NLRP3 inflammasome activation. *Nature*. Published online 2011. doi:10.1038/nature09663
56. Campden RI, Zhang Y. The role of lysosomal cysteine cathepsins in NLRP3 inflammasome activation. *Arch Biochem Biophys*. Published online 2019. doi:10.1016/j.abb.2019.02.015
57. Muñoz-Planillo R, Kuffa P, Martínez-Colón G, Smith BL, Rajendiran TM, Núñez G. K+ Efflux Is the Common Trigger of NLRP3 Inflammasome Activation by Bacterial Toxins and Particulate Matter. *Immunity*. Published online 2013. doi:10.1016/j.immuni.2013.05.016
58. Murakami T, Ockinger J, Yu J, et al. Critical role for calcium mobilization in activation of the NLRP3 inflammasome. *Proc Natl Acad Sci U S A*. Published online 2012. doi:10.1073/pnas.1117765109
59. Green JP, Yu S, Martín-Sánchez F, et al. Chloride regulates dynamic NLRP3-dependent ASC oligomerization and inflammasome priming. *Proc Natl Acad Sci U S A*. Published online 2018. doi:10.1073/pnas.1812744115
60. Shi H, Wang Y, Li X, et al. NLRP3 activation and mitosis are mutually exclusive events coordinated by NEK7, a new inflammasome component. *Nat Immunol*. Published online 2016. doi:10.1038/ni.3333

61. Tschopp J, Schroder K. NLRP3 inflammasome activation: The convergence of multiple signalling pathways on ROS production? *Nat Rev Immunol*. Published online 2010. doi:10.1038/nri2725
62. Yang Y, Wang H, Kouadir M, Song H, Shi F. Recent advances in the mechanisms of NLRP3 inflammasome activation and its inhibitors. *Cell Death Dis*. Published online 2019. doi:10.1038/s41419-019-1413-8
63. Broz P, Monack DM. Noncanonical Inflammasomes: Caspase-11 Activation and Effector Mechanisms. *PLoS Pathog*. Published online 2013. doi:10.1371/journal.ppat.1003144
64. Rühl S, Broz P. Caspase-11 activates a canonical NLRP3 inflammasome by promoting K+ efflux. *Eur J Immunol*. Published online 2015. doi:10.1002/eji.201545772
65. Kayagaki N, Warming S, Lamkanfi M, et al. Non-canonical inflammasome activation targets caspase-11. *Nature*. Published online 2011. doi:10.1038/nature10558
66. Rathinam VAK, Vanaja SK, Waggoner L, et al. TRIF licenses caspase-11-dependent NLRP3 inflammasome activation by gram-negative bacteria. *Cell*. Published online 2012. doi:10.1016/j.cell.2012.07.007
67. Kajiwara Y, Schiff T, Voloudakis G, et al. A Critical Role for Human Caspase-4 in Endotoxin Sensitivity. *J Immunol*. Published online 2014. doi:10.4049/jimmunol.1303424
68. Huang X, Feng Y, Xiong G, et al. Caspase-11, a specific sensor for intracellular lipopolysaccharide recognition, mediates the non-canonical inflammatory pathway of pyroptosis. *Cell Biosci*. Published online 2019. doi:10.1186/s13578-019-0292-0
69. Hagar JA, Powell DA, Aachoui Y, Ernst RK, Miao EA. Cytoplasmic LPS activates caspase-11: Implications in TLR4-independent endotoxic shock. *Science (80-)*. Published online 2013. doi:10.1126/science.1240988
70. Kayagaki N, Wong MT, Stowe IB, et al. Noncanonical inflammasome activation by intracellular LPS independent of TLR4. *Science (80-)*. Published online 2013. doi:10.1126/science.1240248
71. Shi J, Zhao Y, Wang Y, et al. Inflammatory caspases are innate immune receptors for intracellular LPS. *Nature*. Published online 2014. doi:10.1038/nature13683
72. Shi J, Zhao Y, Wang K, et al. Cleavage of GSDMD by inflammatory caspases determines pyroptotic cell death. *Nature*. Published online 2015. doi:10.1038/nature15514
73. Evavold CL, Hafner-bratkovič I, Devant P, et al. Ragulator-Rag-mTORC1 pathway. 2022;184(17):4495-4511. doi:10.1016/j.cell.2021.06.028.Control
74. Xia S, Zhang Z, Magupalli VG, et al. Gasdermin D pore structure reveals preferential release of mature interleukin-1. *Nature*. 2021;593(7860):607-611. doi:10.1038/s41586-021-03478-3
75. Humphries F, Shmuel-Galia L, Ketelut-Carneiro N, et al. Succination inactivates gasdermin D and blocks pyroptosis. *Science (80-)*. 2020;369(6511):1633-1637. doi:10.1126/science.abb9818
76. Evavold CL, Ruan J, Tan Y, Xia S, Wu H, Kagan JC. The Pore-Forming Protein Gasdermin D Regulates Interleukin-1 Secretion from Living Macrophages. *Immunity*. 2018;48(1). doi:10.1016/j.immuni.2017.11.013
77. Schauvliege R, Vanrobaeys J, Schotte P, Beyaert R. Caspase-11 gene expression in response to lipopolysaccharide and interferon-γ requires nuclear factor-κB and signal transducer and activator of transcription (STAT) 1. *J Biol Chem*. Published online 2002. doi:10.1074/jbc.M207852200
78. Broz P, Ruby T, Belhocine K, et al. Caspase-11 increases susceptibility to Salmonella infection in the absence of caspase-1. *Nature*. Published online 2012. doi:10.1038/nature11419
79. Zasłona Z, Flis E, Wilk MM, et al. Caspase-11 promotes allergic airway inflammation. *Nat Commun*. Published online 2020. doi:10.1038/s41467-020-14945-2
80. Yang D, He Y, Muñoz-Planillo R, Liu Q, Núñez G. Caspase-11 Requires the Pannexin-1 Channel and the Purinergic P2X7 Pore to Mediate Pyroptosis and Endotoxic Shock.

Immunity. Published online 2015. doi:10.1016/j.immuni.2015.10.009
81. Chen KW, Demarco B, Heilig R, et al. Extrinsic and intrinsic apoptosis activate pannexin-1 to drive NLRP 3 inflammasome assembly . *EMBO J*. Published online 2019. doi:10.15252/embj.2019101638
82. Demarco B, Chen KW, Broz P. Pannexin-1 channels bridge apoptosis to NLRP3 inflammasome activation. *Mol Cell Oncol*. Published online 2019. doi:10.1080/23723556.2019.1610324
83. Deng M, Tang Y, Li W, et al. The Endotoxin Delivery Protein HMGB1 Mediates Caspase-11-Dependent Lethality in Sepsis. *Immunity*. 2018;49(4). doi:10.1016/j.immuni.2018.08.016
84. Deng M, Scott M, loughran P, Wang Q, Lu B, Billiar TR. Caspase-11-mediated HMGB1 release from the liver drives immune cell pyroptosis in sepsis. *J Immunol*. 2017;198(1 Supplement):75.16 LP-75.16. http://www.jimmunol.org/content/198/1_Supplement/75.16.abstract
85. Watanabe N, Kobayashi Y. SELECTIVE RELEASE OF A PROCESSED FORM OF INTERLEUKIN la. 1994;l(6):597-601.
86. Wiggins KA, Parry AJ, Cassidy LD, et al. IL-1α cleavage by inflammatory caspases of the noncanonical inflammasome controls the senescence-associated secretory phenotype. *Aging Cell*. Published online 2019. doi:10.1111/acel.12946
87. Ketelut-Carneiro N, Souza COS, Benevides L, et al. Caspase-11-dependent IL-1α release boosts Th17 immunity against Paracoccidioides brasiliensis. *PLoS Pathog*. 2019;15(8):1-28. doi:10.1371/journal.ppat.1007990
88. Akhter A, Caution K, Abu Khweek A, et al. Caspase-11 Promotes the Fusion of Phagosomes Harboring Pathogenic Bacteria with Lysosomes by Modulating Actin Polymerization. *Immunity*. Published online 2012. doi:10.1016/j.immuni.2012.05.001
89. Guérin I, De Chastellier C. Pathogenic mycobacteria disrupt the macrophage actin filament network. *Infect Immun*. 2000;68(5):2655-2662. doi:10.1128/IAI.68.5.2655-2662.2000
90. Dawe HR, Minamide LS, Bamburg JR, Cramer LP. ADF/cofilin controls cell polarity during fibroblast migration. *Curr Biol*. 2003;13(3):252-257. doi:10.1016/S0960-9822(03)00040-X
91. Li J, Brieher WM, Scimone ML, et al. Caspase-11 regulates cell migration by promoting Aip1-Cofilin-mediated actin depolymerization. *Nat Cell Biol*. 2007;9(3):276-286. doi:10.1038/ncb1541
92. Caution K, Gavrilin MA, Tazi M, et al. Caspase-11 and caspase-1 differentially modulate actin polymerization via RhoA and Slingshot proteins to promote bacterial clearance. *Sci Rep*. 2015;5(December):1-13. doi:10.1038/srep18479
93. Krause K, Caution K, Badr A, et al. CASP4/caspase-11 promotes autophagosome formation in response to bacterial infection. *Autophagy*. 2018;14(11). doi:10.1080/15548627.2018.1491494
94. Bergsbaken T, Bevan MJ. HHS Public Access. 2016;195(1):41-45. doi:10.4049/jimmunol.1500812.Cutting
95. Caution K, Young N, Robledo-Avila F, et al. Caspase-11 Mediates Neutrophil Chemotaxis and Extracellular Trap Formation During Acute Gouty Arthritis Through Alteration of Cofilin Phosphorylation. *Front Immunol*. Published online 2019. doi:10.3389/fimmu.2019.02519
96. Sachdev U, Ferrari R, Cui X, et al. Caspase1 / 11 signaling affects muscle regeneration and recovery following ischemia , and can be modulated by chloroquine. Published online 2020.
97. Krause K, Daily K, Estfanous S, et al. Caspase-11 counteracts mitochondrial ROS-mediated clearance of Staphylococcus aureus in macrophages . *EMBO Rep*. 2019;20(12):1-17. doi:10.15252/embr.201948109

98. Chen R, Zeng L, Zhu S, et al. CAMP metabolism controls caspase-11 inflammasome activation and pyroptosis in sepsis. *Sci Adv*. Published online 2019. doi:10.1126/sciadv.aav5562
99. Wu C, Lu W, Zhang Y, et al. Inflammasome Activation Triggers Blood Clotting and Host Death through Pyroptosis. *Immunity*. 2019;50(6):1401-1411.e4. doi:10.1016/j.immuni.2019.04.003
100. Grover SP, Mackman N. Tissue Factor: An Essential Mediator of Hemostasis and Trigger of Thrombosis. *Arterioscler Thromb Vasc Biol*. 2018;38(4):709-725. doi:10.1161/ATVBAHA.117.309846
101. Yang X, Cheng X, Tang Y, et al. Bacterial Endotoxin Activates the Coagulation Cascade through Gasdermin D-Dependent Phosphatidylserine Exposure. *Immunity*. 2019;51(6):983-996.e6. doi:10.1016/j.immuni.2019.11.005
102. Rühl S, Shkarina K, Demarco B, Heilig R, Santos JC, Broz P. ESCRT-dependent membrane repair negatively regulates pyroptosis downstream of GSDMD activation. *Science (80-)*. 2018;362(6417):956-960. doi:10.1126/science.aar7607
103. Bevilacqua MP, Pober JS, Majeau GR, Cotran RS, Gimbrone MA. Interleukin 1 (IL-1) induces biosynthesis and cell surface expression of procoagulant activity in human vascular endothelial cells. *J Exp Med*. 1984;160(2):618-623. doi:10.1084/jem.160.2.618
104. Peng Y, Gao M, Liu Y, et al. Bacterial outer membrane vesicles induce disseminated intravascular coagulation through the caspase-11-gasdermin D pathway. *Thromb Res*. 2020;196(138):159-166. doi:10.1016/j.thromres.2020.08.013
105. Perlee D, de Beer R, Florquin S, van der Poll T, van't Veer C, de Vos AF. Caspase-11 contributes to pulmonary host defense against klebsiella pneumoniae and local activation of coagulation. *Am J Physiol - Lung Cell Mol Physiol*. 2020;319(1):L105-L114. doi:10.1152/ajplung.00422.2019
106. Wang J, Shao Y, Wang W, et al. Caspase-11 deficiency impairs neutrophil recruitment and bacterial clearance in the early stage of pulmonary Klebsiella pneumoniae infection. *Int J Med Microbiol*. 2017;307(8):490-496. doi:10.1016/j.ijmm.2017.09.012
107. Claushuis TAM, de Stoppelaar SF, Stroo I, et al. Thrombin contributes to protective immunity in pneumonia-derived sepsis via fibrin polymerization and platelet–neutrophil interactions. *J Thromb Haemost*. 2017;15(4):744-757. doi:10.1111/jth.13625
108. Kawamoto H, Minato N. Myeloid cells. *Int J Biochem Cell Biol*. Published online 2004. doi:10.1016/j.biocel.2004.01.020
109. Marti LC, Bacal NS, Bento LC, Rocha FA. Phenotypic Markers and Functional Regulators of Myelomonocytic Cells. In: *Biology of Myelomonocytic Cells*. ; 2017. doi:10.5772/67324
110. Chávez-Galán L, Olleros ML, Vesin D, Garcia I. Much more than M1 and M2 macrophages, there are also CD169+ and TCR+ macrophages. *Front Immunol*. Published online 2015. doi:10.3389/fimmu.2015.00263
111. Mills CD, Kincaid K, Alt JM, Heilman MJ, Hill AM. M-1/M-2 Macrophages and the Th1/Th2 Paradigm. *J Immunol*. Published online 2000. doi:10.4049/jimmunol.164.12.6166
112. Martinez FO, Gordon S. The M1 and M2 paradigm of macrophage activation: Time for reassessment. *F1000Prime Rep*. Published online 2014. doi:10.12703/P6-13
113. Sans-Fons MG, Yeramian A, Pereira-Lopes S, et al. Arginine transport is impaired in C57Bl/6 mouse macrophages as a result of a deletion in the promoter of Slc7a2 (CAT2), and susceptibility to Leishmania infection is reduced. *J Infect Dis*. Published online 2013. doi:10.1093/infdis/jit084
114. Murray PJ, Allen JE, Biswas SK, et al. Macrophage Activation and Polarization: Nomenclature and Experimental Guidelines. *Immunity*. Published online 2014. doi:10.1016/j.immuni.2014.06.008
115. Fleetwood AJ, Dinh H, Cook AD, Hertzog PJ, Hamilton JA. GM-CSF- and M-CSF-dependent macrophage phenotypes display differential dependence on Type I interferon signaling. *J Leukoc Biol*. Published online 2009. doi:10.1189/jlb.1108702

116. Biswas SK, Mantovani A. Macrophage plasticity and interaction with lymphocyte subsets: Cancer as a paradigm. *Nat Immunol*. Published online 2010. doi:10.1038/ni.1937
117. Gordon S, Taylor PR. Monocyte and macrophage heterogeneity. *Nat Rev Immunol*. Published online 2005. doi:10.1038/nri1733
118. Ziegler-Heitbrock HWL, Fingerle G, Ströbel M, et al. The novel subset of CD14+/CD16+ blood monocytes exhibits features of tissue macrophages. *Eur J Immunol*. Published online 1993. doi:10.1002/eji.1830230902
119. Sunderkötter C, Nikolic T, Dillon MJ, et al. Subpopulations of Mouse Blood Monocytes Differ in Maturation Stage and Inflammatory Response. *J Immunol*. Published online 2004. doi:10.4049/jimmunol.172.7.4410
120. Mosser DM, Edwards JP. Exploring the full spectrum of macrophage activation. *Nat Rev Immunol*. Published online 2008. doi:10.1038/nri2448
121. Passlick B, Flieger D, Loms Ziegler-Heitbrock HW. Identification and characterization of a novel monocyte subpopulation in human peripheral blood. *Blood*. Published online 1989. doi:10.1182/blood.v74.7.2527.bloodjournal7472527
122. Schliefsteiner C, Peinhaupt M, Kopp S, et al. Human placental Hofbauer cells maintain an anti-inflammatory M2 phenotype despite the presence of gestational diabetes mellitus. *Front Immunol*. Published online 2017. doi:10.3389/fimmu.2017.00888
123. Dale DC, Boxer L, Conrad Liles W. The phagocytes: Neutrophils and monocytes. *Blood*. Published online 2008. doi:10.1182/blood-2007-12-077917
124. Hoshino Y, Hoshino S, Gold JA, et al. Mechanisms of Polymorphonuclear Neutrophil–Mediated Induction of HIV-1 Replication in Macrophages during Pulmonary Tuberculosis. *J Infect Dis*. Published online 2007. doi:10.1086/513438
125. Orabona C, Grohmann U, Belladonna ML, et al. CD28 induces immunostimulatory signals in dendritic cells via CD80 and CD86. *Nat Immunol*. Published online 2004. doi:10.1038/ni1124
126. Arnold CE, Whyte CS, Gordon P, Barker RN, Rees AJ, Wilson HM. A critical role for suppressor of cytokine signalling 3 in promoting M1 macrophage activation and function in vitro and in vivo. *Immunology*. Published online 2014. doi:10.1111/imm.12173
127. Förstermann U, Sessa WC. Nitric oxide synthases: Regulation and function. *Eur Heart J*. Published online 2012. doi:10.1093/eurheartj/ehr304
128. Xue Q, Yan Y, Zhang R, Xiong H. Regulation of iNOS on immune cells and its role in diseases. *Int J Mol Sci*. Published online 2018. doi:10.3390/ijms19123805
129. Niedbala W, Alves-Filho JC, Fukada SY, et al. Regulation of type 17 helper T-cell function by nitric oxide during inflammation. *Proc Natl Acad Sci U S A*. 2011;108(22):9220-9225. doi:10.1073/pnas.1100667108
130. Cobb JP, Hotchkiss RS, Swanson PE, et al. Inducible nitric oxide synthase (iNOS) gene deficiency increases the mortality of sepsis in mice. *Surgery*. Published online 1999. doi:10.1016/S0039-6060(99)70189-3
131. Xiong H, Zhu C, Li F, et al. Inhibition of Interleukin-12 p40 Transcription and NF-κB Activation by Nitric Oxide in Murine Macrophages and Dendritic Cells. *J Biol Chem*. Published online 2004. doi:10.1074/jbc.M313416200
132. Mantovani A, Sica A, Locati M. Macrophage polarization comes of age. *Immunity*. Published online 2005. doi:10.1016/j.immuni.2005.10.001
133. Sun YJ, Chang NCA, Hung SI, Chien Chang A, Chou CC, Hsiao CD. The Crystal Structure of a Novel Mammalian Lectin, Ym1, Suggests a Saccharide Binding Site. *J Biol Chem*. Published online 2001. doi:10.1074/jbc.M010416200
134. Azad AK, Rajaram MVS, Schlesinger LS. Exploitation of the Macrophage Mannose Receptor (CD206) in Infectious Disease Diagnostics and Therapeutics. *J Cytol Mol Biol*. Published online 2014. doi:10.13188/2325-4653.1000003
135. Moseman AP, Moseman EA, Schworer S, et al. Mannose Receptor 1 Mediates Cellular Uptake and Endosomal Delivery of CpG-Motif Containing Oligodeoxynucleotides. *J*

Immunol. Published online 2013. doi:10.4049/jimmunol.1301438
136. Porcheray F, Viaud S, Rimaniol AC, et al. Macrophage activation switching: An asset for the resolution of inflammation. *Clin Exp Immunol*. Published online 2005. doi:10.1111/j.1365-2249.2005.02934.x
137. Raes G, De Baetselier P, Noël W, Beschin A, Brombacher F, Hassanzadeh Gh G. Differential expression of FIZZ1 and Ym1 in alternatively versus classically activated macrophages. *J Leukoc Biol*. Published online 2002. doi:10.1189/jlb.71.4.597
138. Holcomb IN, Kabakoff RC, Chan B, et al. FIZZ1, a novel cysteine-rich secreted protein associated with pulmonary inflammation, defines a new gene family. *EMBO J*. Published online 2000. doi:10.1093/emboj/19.15.4046
139. Chen C, Hsu S, Ann DK, Yen Y, Kung H. Arginine Signaling and Cancer Metabolism. Published online 2021:1-29.
140. Munder M. Arginase: An emerging key player in the mammalian immune system: REVIEW. *Br J Pharmacol*. 2009;158(3):638-651. doi:10.1111/j.1476-5381.2009.00291.x
141. Freemerman AJ, Johnson AR, Sacks GN, et al. Metabolic reprogramming of macrophages: Glucose transporter 1 (GLUT1)-mediated glucose metabolism drives a proinflammatory phenotype. *J Biol Chem*. 2014;289(11):7884-7896. doi:10.1074/jbc.M113.522037
142. Alam MM, Lal S, FitzGerald KE, Zhang L. A holistic view of cancer bioenergetics: mitochondrial function and respiration play fundamental roles in the development and progression of diverse tumors. *Clin Transl Med*. 2016;5(1). doi:10.1186/s40169-016-0082-9
143. Braverman J, Sogi KM, Benjamin D, Nomura DK, Stanley SA. HIF-1α Is an Essential Mediator of IFN-γ–Dependent Immunity to Mycobacterium tuberculosis . *J Immunol*. 2016;197(4):1287-1297. doi:10.4049/jimmunol.1600266
144. Kelly B, O'Neill LAJ. Metabolic reprogramming in macrophages and dendritic cells in innate immunity. *Cell Res*. 2015;25(7):771-784. doi:10.1038/cr.2015.68
145. Rogatzki MJ, Ferguson BS, Goodwin ML, Gladden LB. Lactate is always the end product of glycolysis. *Front Neurosci*. 2015;9(FEB):1-7. doi:10.3389/fnins.2015.00022
146. Haas R, Smith J, Rocher-Ros V, et al. Lactate Regulates Metabolic and Pro-inflammatory Circuits in Control of T Cell Migration and Effector Functions. *PLOS Biol*. 2015;13(7):e1002202. https://doi.org/10.1371/journal.pbio.1002202
147. Colegio OR, Chu N-Q, Szabo AL, et al. Functional polarization of tumour-associated macrophages by tumour-derived lactic acid. *Nature*. 2014;513(7519):559-563. doi:10.1038/nature13490
148. Errea A, Cayet D, Marchetti P, et al. Lactate Inhibits the Pro-Inflammatory Response and Metabolic Reprogramming in Murine Macrophages in a GPR81-Independent Manner. *PLoS One*. 2016;11(11):e0163694. doi:10.1371/journal.pone.0163694
149. Nasi A, Fekete T, Krishnamurthy A, et al. Dendritic Cell Reprogramming by Endogenously Produced Lactic Acid. *J Immunol*. 2013;191(6):3090-3099. doi:10.4049/jimmunol.1300772
150. Li JL, Lin TY, Chen PL, et al. Mitochondrial Function and Parkinson's Disease: From the Perspective of the Electron Transport Chain. *Front Mol Neurosci*. 2021;14(December):1-15. doi:10.3389/fnmol.2021.797833
151. Tannahill GM, Curtis AM, Adamik J, et al. Succinate is a danger signal that induces IL-1β via HIF-1α. *Nature*. 2013;496(7444):238-242. doi:10.1038/nature11986.Succinate
152. Viola A, Munari F, Sánchez-Rodríguez R, Scolaro T, Castegna A. The metabolic signature of macrophage responses. *Front Immunol*. 2019;10(JULY):1-16. doi:10.3389/fimmu.2019.01462
153. Ge P, Dawson VL, Dawson TM. PINK1 and Parkin mitochondrial quality control: A source of regional vulnerability in Parkinson's disease. *Mol Neurodegener*. 2020;15(1):1-18. doi:10.1186/s13024-020-00367-7
154. Zhu CL, Yao RQ, Li LX, et al. Mechanism of Mitophagy and Its Role in Sepsis Induced Organ

Dysfunction: A Review. *Front Cell Dev Biol*. 2021;9(June):1-13. doi:10.3389/fcell.2021.664896
155. Song Y, Zhou Y, Zhou X. The role of mitophagy in innate immune responses triggered by mitochondrial stress. *Cell Commun Signal*. 2020;18(1):1-14. doi:10.1186/s12964-020-00659-x
156. Zhong W, Rao Z, Xu J, et al. Defective mitophagy in aged macrophages promotes mitochondrial DNA cytosolic leakage to activate STING signaling during liver sterile inflammation. *Aging Cell*. 2022;21(6):1-16. doi:10.1111/acel.13622
157. Hu X, Peng X, Lu C, et al. Type I IFN expression is stimulated by cytosolic MtDNA released from pneumolysin-damaged mitochondria via the STING signaling pathway in macrophages. *FEBS J*. 2019;286(23):4754-4768. doi:10.1111/febs.15001
158. Bray F, Ferlay J, Soerjomataram I, Siegel RL, Torre LA, Jemal A. Global cancer statistics 2018: GLOBOCAN estimates of incidence and mortality worldwide for 36 cancers in 185 countries. *CA Cancer J Clin*. Published online 2018. doi:10.3322/caac.21492
159. NCRI. Cancer in Ireland 1994-2016 with estimates for 2016-2018: Annual Report of the National Cancer Registry | National Cancer Registry Ireland. Published online 2018. https://www.ncri.ie/sites/ncri/files/pubs/annualreport2018_26112018.pdf
160. Ataollahi MR, Sharifi J, Paknahad MR, Paknahad A. Breast cancer and associated factors: a review. *J Med Life*. Published online 2015.
161. Gethins M. Breast cancer in men. *J Natl Cancer Inst*. Published online 2012. doi:10.1093/jnci/djs172
162. Travis RC, Key TJ. Oestrogen exposure and breast cancer risk. *Breast Cancer Res*. Published online 2003. doi:10.1186/bcr628
163. Greenwald P. Role of dietary fat in the causation of breast cancer: Point. *Cancer Epidemiol Biomarkers Prev*. Published online 1999.
164. De Blok CJM, Wiepjes CM, Nota NM, et al. Breast cancer risk in transgender people receiving hormone treatment: Nationwide cohort study in the Netherlands. *BMJ*. Published online 2019. doi:10.1136/bmj.l1652
165. Momenimovahed Z, Salehiniya H. Epidemiological characteristics of and risk factors for breast cancer in the world. *Breast Cancer Targets Ther*. Published online 2019. doi:10.2147/BCTT.S176070
166. Beral V, Bull D, Doll R, et al. Familial breast cancer: Collaborative reanalysis of individual data from 52 epidemiological studies including 58 209 women with breast cancer and 101 986 women without the disease. *Lancet*. Published online 2001. doi:10.1016/S0140-6736(01)06524-2
167. Hall JM, Lee MK, Newman B, et al. Linkage of early-onset familial breast cancer to chromosome 17q21. *Science (80-)*. Published online 1990. doi:10.1126/science.2270482
168. Wooster R, Neuhausen SL, Mangion J, et al. Localization of a breast cancer susceptibility gene, BRCA2, to chromosome 13q12-13. *Science (80-)*. Published online 1994. doi:10.1126/science.8091231
169. Stratton MR, Rahman N. The emerging landscape of breast cancer susceptibility. *Nat Genet*. Published online 2008. doi:10.1038/ng.2007.53
170. Sinn HP, Kreipe H. A brief overview of the WHO classification of breast tumors, 4th edition, focusing on issues and updates from the 3rd edition. *Breast Care*. Published online 2013. doi:10.1159/000350774
171. Perou CM, Sørile T, Eisen MB, et al. Molecular portraits of human breast tumours. *Nature*. Published online 2000. doi:10.1038/35021093
172. Sørlie T, Perou CM, Tibshirani R, et al. Gene expression patterns of breast carcinomas distinguish tumor subclasses with clinical implications. *Proc Natl Acad Sci U S A*. Published online 2001. doi:10.1073/pnas.191367098
173. Vuong D, Simpson PT, Green B, Cummings MC, Lakhani SR. Molecular classification of breast cancer. *Virchows Arch*. Published online 2014. doi:10.1007/s00428-014-1593-7

174. Prat A, Cheang MCU, Martín M, et al. Prognostic significance of progesterone receptor-positive tumor cells within immunohistochemically defined luminal a breast cancer. *J Clin Oncol*. Published online 2013. doi:10.1200/JCO.2012.43.4134
175. Prat A, Pineda E, Adamo B, et al. Clinical implications of the intrinsic molecular subtypes of breast cancer. *Breast*. Published online 2015. doi:10.1016/j.breast.2015.07.008
176. Goldhirsch A, Winer EP, Coates AS, et al. Personalizing the treatment of women with early breast cancer: Highlights of the st gallen international expert consensus on the primary therapy of early breast Cancer 2013. *Ann Oncol*. Published online 2013. doi:10.1093/annonc/mdt303
177. Tang P, Tse GM. Immunohistochemical surrogates for molecular classification of breast carcinoma: A 2015 update. In: *Archives of Pathology and Laboratory Medicine*. ; 2016. doi:10.5858/arpa.2015-0133-RA
178. Casalini P, Iorio M V., Galmozzi E, Ménard S. Role of HER receptors family in development and differentiation. *J Cell Physiol*. Published online 2004. doi:10.1002/jcp.20007
179. Prat A, Carey LA, Adamo B, et al. Molecular features and survival outcomes of the intrinsic subtypes within HER2-positive breast cancer. *J Natl Cancer Inst*. Published online 2014. doi:10.1093/jnci/dju152
180. Carey LA, Berry DA, Cirrincione CT, et al. Molecular heterogeneity and response to neoadjuvant human epidermal growth factor receptor 2 targeting in CALGB 40601, a randomized phase III trial of paclitaxel plus trastuzumab with or without lapatinib. *J Clin Oncol*. Published online 2016. doi:10.1200/JCO.2015.62.1268
181. Gierach GL, Burke A, Anderson WF. Epidemiology of triple negative breast cancers. *Breast Dis*. Published online 2010. doi:10.3233/BD-2010-0319
182. Schmidt M, Böhm D, Von Törne C, et al. The humoral immune system has a key prognostic impact in node-negative breast cancer. *Cancer Res*. Published online 2008. doi:10.1158/0008-5472.CAN-07-5206
183. Aaltomaa S, Lipponen P, Eskelinen M, et al. Lymphocyte infiltrates as a prognostic variable in female breast cancer. *Eur J Cancer*. Published online 1992. doi:10.1016/0959-8049(92)90134-N
184. Huebner RJ, Ewald AJ. Cellular foundations of mammary tubulogenesis. *Semin Cell Dev Biol*. Published online 2014. doi:10.1016/j.semcdb.2014.04.019
185. Visvader JE, Stingl J. Mammary stem cells and the differentiation hierarchy: Current status and perspectives. *Genes Dev*. Published online 2014. doi:10.1101/gad.242511.114
186. Meyer DS, Brinkhaus H, Müller U, Müller M, Cardiff RD, Bentires-Alj M. Luminal expression of PIK3CA mutant H1047R in the mammary gland induces heterogeneous tumors. *Cancer Res*. Published online 2011. doi:10.1158/0008-5472.CAN-10-3827
187. Zhou J, Chen Q, Zou Y, Chen H, Qi L, Chen Y. Stem cells and cellular origins of breast cancer: Updates in the rationale, controversies, and therapeutic implications. *Front Oncol*. Published online 2019. doi:10.3389/fonc.2019.00820
188. Feng Y, Spezia M, Huang S, et al. Breast cancer development and progression: Risk factors, cancer stem cells, signaling pathways, genomics, and molecular pathogenesis. *Genes Dis*. Published online 2018. doi:10.1016/j.gendis.2018.05.001
189. Kalimutho M, Parsons K, Mittal D, López JA, Srihari S, Khanna KK. Targeted Therapies for Triple-Negative Breast Cancer: Combating a Stubborn Disease. *Trends Pharmacol Sci*. Published online 2015. doi:10.1016/j.tips.2015.08.009
190. Pizato N, Luzete BC, Kiffer LFMV, et al. Omega-3 docosahexaenoic acid induces pyroptosis cell death in triple-negative breast cancer cells. *Sci Rep*. Published online 2018. doi:10.1038/s41598-018-20422-0
191. DeNardo DG, Coussens LM. Inflammation and breast cancer. Balancing immune response: Crosstalk between adaptive and innate immune cells during breast cancer progression. *Breast Cancer Res*. Published online 2007. doi:10.1186/bcr1746
192. Mazzurana L, Rao A, Van Acker A, Mjösberg J. The roles for innate lymphoid cells in the

human immune system. *Semin Immunopathol*. Published online 2018. doi:10.1007/s00281-018-0688-7
193. He D, Li H, Yusuf N, et al. IL-17 Promotes Tumor Development through the Induction of Tumor Promoting Microenvironments at Tumor Sites and Myeloid-Derived Suppressor Cells. *J Immunol*. Published online 2010. doi:10.4049/jimmunol.0902574
194. Weber GF, Gaertner FC, Erl W, et al. IL-22-Mediated Tumor Growth Reduction Correlates with Inhibition of ERK1/2 and AKT Phosphorylation and Induction of Cell Cycle Arrest in the G 2 -M Phase . *J Immunol*. Published online 2006. doi:10.4049/jimmunol.177.11.8266
195. Varner JA, Schmid MC. Myeloid cells in the tumor microenvironment: Modulation of tumor angiogenesis and tumor inflammation. *J Oncol*. Published online 2010. doi:10.1155/2010/201026
196. Toor SM, Syed Khaja AS, El Salhat H, et al. Myeloid cells in circulation and tumor microenvironment of breast cancer patients. *Cancer Immunol Immunother*. Published online 2017. doi:10.1007/s00262-017-1977-z
197. Coffelt SB, Kersten K, Doornebal CW, et al. IL-17-producing γδ T cells and neutrophils conspire to promote breast cancer metastasis. *Nature*. Published online 2015. doi:10.1038/nature14282
198. Granot Z, Henke E, Comen EA, King TA, Norton L, Benezra R. Tumor entrained neutrophils inhibit seeding in the premetastatic lung. *Cancer Cell*. Published online 2011. doi:10.1016/j.ccr.2011.08.012
199. DeNardo DG, Barreto JB, Andreu P, et al. CD4+ T Cells Regulate Pulmonary Metastasis of Mammary Carcinomas by Enhancing Protumor Properties of Macrophages. *Cancer Cell*. Published online 2009. doi:10.1016/j.ccr.2009.06.018
200. Fasoulakis Z, Kolios G, Papamanolis V, Kontomanolis EN. Interleukins Associated with Breast Cancer. *Cureus*. Published online 2018. doi:10.7759/cureus.3549
201. Baker KJ, Houston A, Brint E. IL-1 family members in cancer; two sides to every story. *Front Immunol*. Published online 2019. doi:10.3389/fimmu.2019.01197
202. Bent R, Moll L, Grabbe S, Bros M. Interleukin-1 beta—A friend or foe in malignancies? *Int J Mol Sci*. Published online 2018. doi:10.3390/ijms19082155
203. Sutton CE, Lalor SJ, Sweeney CM, Brereton CF, Lavelle EC, Mills KHG. Interleukin-1 and IL-23 Induce Innate IL-17 Production from γδ T Cells, Amplifying Th17 Responses and Autoimmunity. *Immunity*. Published online 2009. doi:10.1016/j.immuni.2009.08.001
204. Wu TC, Xu K, Martinek J, et al. IL1 receptor antagonist controls transcriptional signature of inflammation in patients with metastatic breast cancer. *Cancer Res*. Published online 2018. doi:10.1158/0008-5472.CAN-18-0413
205. Kuan EL, Ziegler SF. A tumor-myeloid cell axis, mediated via the cytokines IL-1α and TSLP, promotes the progression of breast cancer. *Nat Immunol*. Published online 2018. doi:10.1038/s41590-018-0066-6
206. Kaplanov I, Carmi Y, Kornetsky R, et al. Blocking IL-1β reverses the immunosuppression in mouse breast cancer and synergizes with anti–PD-1 for tumor abrogation. *Proc Natl Acad Sci U S A*. Published online 2019. doi:10.1073/pnas.1812266115
207. Guo B, Fu S, Zhang J, Liu B, Li Z. Targeting inflammasome/IL-1 pathways for cancer immunotherapy. *Sci Rep*. Published online 2016. doi:10.1038/srep36107
208. Raut PK, Kim SH, Choi DY, Jeong GS, Park PH. Growth of breast cancer cells by leptin is mediated via activation of the inflammasome: Critical roles of estrogen receptor signaling and reactive oxygen species production. *Biochem Pharmacol*. Published online 2019. doi:10.1016/j.bcp.2019.01.006
209. Knüpfer H, Preiß R. Significance of interleukin-6 (IL-6) in breast cancer (review). *Breast Cancer Res Treat*. Published online 2007. doi:10.1007/s10549-006-9328-3
210. Sullivan NJ, Sasser AK, Axel AE, et al. Interleukin-6 induces an epithelial-mesenchymal transition phenotype in human breast cancer cells. *Oncogene*. Published online 2009. doi:10.1038/onc.2009.180

211. Aeschlimann D, Knäuper V. P2X7 receptor-mediated TG2 externalization: a link to inflammatory arthritis? *Amino Acids*. Published online 2017. doi:10.1007/s00726-016-2319-8
212. Oh K, Lee OY, Park Y, Seo MW, Lee DS. IL-1β induces IL-6 production and increases invasiveness and estrogen-independent growth in a TG2-dependent manner in human breast cancer cells. *BMC Cancer*. Published online 2016. doi:10.1186/s12885-016-2746-7
213. Wang YY, Liu XL, Zhao R. Induction of pyroptosis and its implications in cancer management. *Front Oncol*. Published online 2019. doi:10.3389/fonc.2019.00971
214. Bates JP, Derakhshandeh R, Jones L, Webb TJ. Mechanisms of immune evasion in breast cancer. *BMC Cancer*. Published online 2018. doi:10.1186/s12885-018-4441-3
215. Yun EJ, Song KS, Shin S, et al. Docosahexaenoic acid suppresses breast cancer cell metastasis by targeting matrix-metalloproteinases. *Oncotarget*. Published online 2016. doi:10.18632/oncotarget.10266
216. Noy R, Pollard JW. Tumor-Associated Macrophages: From Mechanisms to Therapy. *Immunity*. Published online 2014. doi:10.1016/j.immuni.2014.06.010
217. Franklin RA, Liao W, Sarkar A, et al. The cellular and molecular origin of tumor-associated macrophages. *Science (80-)*. Published online 2014. doi:10.1126/science.1252510
218. Cassetta L, Fragkogianni S, Sims AH, et al. Human Tumor-Associated Macrophage and Monocyte Transcriptional Landscapes Reveal Cancer-Specific Reprogramming, Biomarkers, and Therapeutic Targets. *Cancer Cell*. Published online 2019. doi:10.1016/j.ccell.2019.02.009
219. Olingy CE, San Emeterio CL, Ogle ME, et al. Non-classical monocytes are biased progenitors of wound healing macrophages during soft tissue injury. *Sci Rep*. Published online 2017. doi:10.1038/s41598-017-00477-1
220. Zhang Q wen, Liu L, Gong C yang, et al. Prognostic Significance of Tumor-Associated Macrophages in Solid Tumor: A Meta-Analysis of the Literature. *PLoS One*. Published online 2012. doi:10.1371/journal.pone.0050946
221. Jeong H, Hwang I, Kang SH, Shin HC, Kwon SY. Tumor-associated macrophages as potential prognostic biomarkers of invasive breast cancer. *J Breast Cancer*. Published online 2019. doi:10.4048/jbc.2019.22.e5
222. Ch'Ng ES, Tuan Sharif SE, Jaafar H. In human invasive breast ductal carcinoma, tumor stromal macrophages and tumor nest macrophages have distinct relationships with clinicopathological parameters and tumor angiogenesis. *Virchows Arch*. Published online 2013. doi:10.1007/s00428-012-1362-4
223. Sousa S, Brion R, Lintunen M, et al. Human breast cancer cells educate macrophages toward the M2 activation status. *Breast Cancer Res*. Published online 2015. doi:10.1186/s13058-015-0621-0
224. Hollmén M, Roudnicky F, Karaman S, Detmar M. Characterization of macrophage - Cancer cell crosstalk in estrogen receptor positive and triple-negative breast cancer. *Sci Rep*. Published online 2015. doi:10.1038/srep09188
225. Yang M, Ma B, Shao H, Clark AM, Wells A. Macrophage phenotypic subtypes diametrically regulate epithelial-mesenchymal plasticity in breast cancer cells. *BMC Cancer*. Published online 2016. doi:10.1186/s12885-016-2411-1
226. Liu Y, Gao X, Miao Y, et al. NLRP3 regulates macrophage M2 polarization through up-regulation of IL-4 in asthma. *Biochem J*. Published online 2018. doi:10.1042/BCJ20180086
227. Anders HJ, Suarez-Alvarez B, Grigorescu M, et al. The macrophage phenotype and inflammasome component NLRP3 contributes to nephrocalcinosis-related chronic kidney disease independent from IL-1–mediated tissue injury. *Kidney Int*. Published online 2018. doi:10.1016/j.kint.2017.09.022
228. Lumeng CN, Bodzin JL, Saltiel AR. Obesity induces a phenotypic switch in adipose tissue macrophage polarization. *J Clin Invest*. Published online 2007. doi:10.1172/JCI29881

229. Vandanmagsar B, Youm YH, Ravussin A, et al. The NLRP3 inflammasome instigates obesity-induced inflammation and insulin resistance. *Nat Med*. Published online 2011. doi:10.1038/nm.2279
230. Awad F, Assrawi E, Jumeau C, et al. Impact of human monocyte and macrophage polarization on NLR expression and NLRP3 inflammasome activation. *PLoS One*. Published online 2017. doi:10.1371/journal.pone.0175336
231. Davies JQ, Gordon S. Isolation and culture of human macrophages. *Methods Mol Biol*. Published online 2005. doi:10.1385/1-59259-838-2:105
232. Young L, Sung J, Masters JR. Detection of mycoplasma in cell cultures. *Nat Protoc*. Published online 2010. doi:10.1038/nprot.2010.43
233. Kopitar-Jerala N. The role of interferons in inflammation and inflammasome activation. *Front Immunol*. 2017;8(JUL). doi:10.3389/fimmu.2017.00873
234. Flood B, Manils J, Nulty C, et al. Caspase-11 regulates the tumour suppressor function of STAT1 in a murine model of colitis-associated carcinogenesis. *Oncogene*. Published online 2019. doi:10.1038/s41388-018-0613-5
235. Majoros A, Platanitis E, Kernbauer-Hölzl E, Rosebrock F, Müller M, Decker T. Canonical and non-canonical aspects of JAK-STAT signaling: Lessons from interferons for cytokine responses. *Front Immunol*. 2017;8(JAN). doi:10.3389/fimmu.2017.00029
236. Larkin J, Johnson HM, Subramaniam PS. Differential nuclear localization of the IFNGR-1 and IFNGR-2 subunits of the IFN-γ receptor complex following activation by IFN-γ. *J Interf Cytokine Res*. 2000;20(6):565-576. doi:10.1089/10799900050044769
237. Bach EA, Aguet M, Schreiber RD. The IFNγ receptor: A paradigm for cytokine receptor signaling. *Annu Rev Immunol*. 1997;15:563-591. doi:10.1146/annurev.immunol.15.1.563
238. Greenlund AC, Farrar MA, Viviano BL, Schreiber RD. Ligand-induced IFN(γ) receptor tyrosine phosphorylation couples the receptor to its signal transduction system (p91). *EMBO J*. 1994;13(7):1591-1600. doi:10.1002/j.1460-2075.1994.tb06422.x
239. Staab J, Herrmann-Lingen C, Meyer T. A rapid conformational rearrangement of STAT1 dimers is required for termination rather than for amplification of interferon-γ signaling. *Jak-Stat*. 2013;2(1):e23576. doi:10.4161/jkst.23576
240. Michalska A, Blaszczyk K, Wesoly J, Bluyssen HAR. A positive feedback amplifier circuit that regulates interferon (IFN)-stimulated gene expression and controls type I and type II IFN responses. *Front Immunol*. 2018;9(MAY):1-17. doi:10.3389/fimmu.2018.01135
241. Dempoya J, Matsumiya T, Imaizumi T, et al. Double-Stranded RNA Induces Biphasic STAT1 Phosphorylation by both Type I Interferon (IFN)-Dependent and Type I IFN-Independent Pathways. *J Virol*. Published online 2012. doi:10.1128/jvi.01881-12
242. Rhee SH, Jones BW, Toshchakov V, Vogel SN, Fenton MJ. Toll-like receptors 2 and 4 activate STAT1 serine phosphorylation by distinct mechanisms in macrophages. *J Biol Chem*. 2003;278(25):22506-22512. doi:10.1074/jbc.M208633200
243. Luu K, Greenhill CJ, Majoros A, Decker T, Jenkins BJ, Mansell A. STAT1 plays a role in TLR signal transduction and inflammatory responses. *Immunol Cell Biol*. 2014;92(9):761-769. doi:10.1038/icb.2014.51
244. Sheikh F, Dickensheets H, Gamero AM, Vogel SN, Donnelly RP. An essential role for IFN-β in the induction of IFN-stimulated gene expression by LPS in macrophages. *J Leukoc Biol*. 2014;96(4):591-600. doi:10.1189/jlb.2a0414-191r
245. Gao J, Morrison DC, Parmely TJ, Russell SW, Murphy WJ. An interferon-γ-activated site (GAS) is necessary for full expression of the mouse iNOS gene in response to interferon-γ and lipopolysaccharide. *J Biol Chem*. 1997;272(2):1226-1230. doi:10.1074/jbc.272.2.1226
246. Vadiveloo PK, Vairo G, Hertzog P, Kola I, Hamilton JA. Role of type I interferons during macrophage activation by lipopolysaccharide. *Cytokine*. 2000;12(11):1639-1646. doi:10.1006/cyto.2000.0766
247. Oliveira LS, De Queiroz NMGP, Veloso LVS, et al. A defective TLR4 signaling for IFN-β

expression is responsible for the innately lower ability of BALB/c macrophages to produce NO in response to LPS as compared to C57BL/6. *PLoS One*. 2014;9(6). doi:10.1371/journal.pone.0098913
248. Jacobs AT, Ignarro LJ. Lipopolysaccharide-induced Expression of Interferon-β Mediates the Timing of Inducible Nitric-oxide Synthase Induction in RAW 264.7 Macrophages. *J Biol Chem*. 2001;276(51):47950-47957. doi:10.1074/jbc.M106639200
249. Parzych KR, Klionsky DJ. An overview of autophagy: Morphology, mechanism, and regulation. *Antioxidants Redox Signal*. 2014;20(3):460-473. doi:10.1089/ars.2013.5371
250. Kaur J, Debnath J. Autophagy at the crossroads of catabolism and anabolism. *Nat Rev Mol Cell Biol*. 2015;16(8):461-472. doi:10.1038/nrm4024
251. Punctum A. Targeting NFKB by autophagy to polarize hepatoma-associated macrophage differentiation 1. 2013;(April):619-621.
252. Saitoh T, Fujita N, Jang MH, et al. Loss of the autophagy protein Atg16L1 enhances endotoxin-induced IL-1β production. *Nature*. 2008;456(7219):264-268. doi:10.1038/nature07383
253. Lee J, Kim HR, Quinley C, et al. Autophagy suppresses interleukin-1β (IL-1β) signaling by activation of p62 degradation via lysosomal and proteasomal pathways. *J Biol Chem*. 2012;287(6):4033-4040. doi:10.1074/jbc.M111.280065
254. Byrne BG, Dubuisson JF, Joshi AD, Persson JJ, Swanson MS. Inflammasome components coordinate autophagy and pyroptosis as macrophage responses to infection. *MBio*. 2013;4(1):1-12. doi:10.1128/mBio.00620-12
255. Yu J, Nagasu H, Murakami T, et al. Inflammasome activation leads to Caspase-1-dependent mitochondrial damage and block of mitophagy. *Proc Natl Acad Sci U S A*. 2014;111(43):15514-15519. doi:10.1073/pnas.1414859111
256. Patoli D, Mignotte F, Deckert V, et al. Inhibition of mitophagy drives macrophage activation and antibacterial defense during sepsis. *J Clin Invest*. 2020;130(11):5858-5874. doi:10.1172/JCI130996
257. Pestana CR, Oishi JC, Sobreiro H, Gerson SA, Rodrigues J. Inhibition of autophagy by chloroquine stimulates nitric oxide production and protects endothelial function during serum deprivation. *Cell Physiol Biochem*. 2015;37(3):1168-1177. doi:10.1159/000430240
258. Guo F, Li X, Peng J, et al. Autophagy regulates vascular endothelial cell eNOS and ET-1 expression induced by laminar shear stress in an ex vivo perfused system. *Ann Biomed Eng*. 2014;42(9):1978-1988. doi:10.1007/s10439-014-1033-5
259. Katsuyama K, Shichiri M, Marumo F, Hirata Y. NO inhibits cytokine-induced iNOS expression and NF-κB activation by interfering with phosphorylation and degradation of IκB-α. *Arterioscler Thromb Vasc Biol*. 1998;18(11):1796-1802. doi:10.1161/01.ATV.18.11.1796
260. Gutierrez MG, Munafó DB, Berón W, Colombo MI. Rab7 is required for the normal progression of the autophagic pathway in mammalian cells. *J Cell Sci*. 2004;117(13):2687-2697. doi:10.1242/jcs.01114
261. Bezbradica JS, Schroder K. TRAF6 is a nexus for TLR-STAT1 crosstalk. *Immunol Cell Biol*. 2014;92(9):737-738. doi:10.1038/icb.2014.71
262. Ramsauer K, Sadzak I, Porras A, et al. p38 MAPK enhances STAT 1-dependent transcription independently of Ser-727 phosphorylation. *Proc Natl Acad Sci U S A*. 2002;99(20):12859-12864. doi:10.1073/pnas.192264999
263. Hu JJ, Liu X, Xia S, et al. FDA-approved disulfiram inhibits pyroptosis by blocking gasdermin D pore formation. *Nat Immunol*. 2020;21(7):736-745. doi:10.1038/s41590-020-0669-6
264. Ross C, Chan AH, Von Pein J, Boucher D, Schroder K. Dimerization and auto-processing induce caspase-11 protease activation within the non-canonical inflammasome. *Life Sci Alliance*. 2018;1(6):1-10. doi:10.26508/lsa.201800237
265. Okugawa S, Ota Y, Kitazawa T, et al. Janus kinase 2 is involved in lipopolysaccharide-

induced activation of macrophages. *Am J Physiol - Cell Physiol*. 2003;285(2 54-2). doi:10.1152/ajpcell.00026.2003
266. Cruz MT, Duarte CB, Gonçalo M, Carvalho AP, Lopes MC. LPS induction of IκB-α degradation and iNOS expression in a skin dendritic cell line is prevented by the janus kinase 2 inhibitor, tyrphostin B42. *Nitric Oxide - Biol Chem*. 2001;5(1):53-61. doi:10.1006/niox.2000.0320
267. Minogue AM, Barrett JP, Lynch MA. LPS-induced release of IL-6 from glia modulates production of IL-1β in a JAK2-dependent manner. *J Neuroinflammation*. 2012;9:1-10. doi:10.1186/1742-2094-9-126
268. Ma K, Chen G, Li W, Kepp O, Zhu Y, Chen Q. Mitophagy, Mitochondrial Homeostasis, and Cell Fate. *Front Cell Dev Biol*. 2020;8(June):1-14. doi:10.3389/fcell.2020.00467
269. Harmuth T, Prell-Schicker C, Weber JJ, et al. Mitochondrial Morphology, Function and Homeostasis Are Impaired by Expression of an N-terminal Calpain Cleavage Fragment of Ataxin-3. *Front Mol Neurosci*. 2018;11(October). doi:10.3389/fnmol.2018.00368
270. Mills EL, Kelly B, Logan A, et al. Succinate Dehydrogenase Supports Metabolic Repurposing of Mitochondria to Drive Inflammatory Macrophages. *Cell*. 2016;167(2):457-470.e13. doi:10.1016/j.cell.2016.08.064
271. Zachari M, Gudmundsson SR, Li Z, et al. Selective Autophagy of Mitochondria on a Ubiquitin-Endoplasmic-Reticulum Platform. *Dev Cell*. 2019;50(5):627-643.e5. doi:10.1016/j.devcel.2019.06.016
272. Yang SNY, Atkinson SC, Wang C, et al. The broad spectrum antiviral ivermectin targets the host nuclear transport importin α/β1 heterodimer. *Antiviral Res*. 2020;177(February):104760. doi:10.1016/j.antiviral.2020.104760
273. Jia Y, Han B, Wang R. Ivermectin induces mitophagy in H9c2 cells via activation of the PINK1/Parkin pathway. *Food Sci Technol*. 2022;42:1-8. doi:10.1590/fst.65621
274. Zhang X, Song Y, Xiong H, et al. Inhibitory effects of ivermectin on nitric oxide and prostaglandin E2 production in LPS-stimulated RAW 264.7 macrophages. *Int Immunopharmacol*. 2009;9(3):354-359. doi:10.1016/j.intimp.2008.12.016
275. Gómez-Sánchez R, Yakhine-Diop SMS, Bravo-San Pedro JM, et al. PINK1 deficiency enhances autophagy and mitophagy induction. *Mol Cell Oncol*. 2016;3(2):1-10. doi:10.1080/23723556.2015.1046579
276. Song P, Li S, Wu H, et al. Parkin promotes proteasomal degradation of p62: implication of selective vulnerability of neuronal cells in the pathogenesis of Parkinson's disease. *Protein Cell*. 2016;7(2):114-129. doi:10.1007/s13238-015-0230-9
277. Lazarou M, Sliter DA, Kane LA, et al. The ubiquitin kinase PINK1 recruits autophagy receptors to induce mitophagy. *Nature*. 2015;524(7565):309-314. doi:10.1038/nature14893
278. Fujita KI, Maeda D, Xiao Q, Srinivasula SM. Nrf2-mediated induction of p62 controls Toll-like receptor-4-driven aggresome-like induced structure formation and autophagic degradation. *Proc Natl Acad Sci U S A*. 2011;108(4):1427-1432. doi:10.1073/pnas.1014156108
279. Agod Z, Fekete T, Budai MM, et al. Regulation of type I interferon responses by mitochondria-derived reactive oxygen species in plasmacytoid dendritic cells. *Redox Biol*. 2017;13(July):633-645. doi:10.1016/j.redox.2017.07.016
280. Ježek J, Cooper KF, Strich R. Review the impact of mitochondrial fission-stimulated ros production on pro-apoptotic chemotherapy. *Biology (Basel)*. 2021;10(1):1-20. doi:10.3390/biology10010033
281. Hu Z, Wang Y, Gao X, et al. Optineurin-mediated mitophagy as a potential therapeutic target for intervertebral disc degeneration. *Front Pharmacol*. 2022;13(August):1-14. doi:10.3389/fphar.2022.893307
282. Zhan X, Cui R, Geng X, et al. LPS-induced mitochondrial DNA synthesis and release facilitate RAD50-dependent acute lung injury. *Signal Transduct Target Ther*.

2021;6(1):2020-2022. doi:10.1038/s41392-021-00494-7
283. Bachmann M, Waibler Z, Pleli T, Pfeilschifter J, Mühl H. Type I interferon supports inducible nitric oxide synthase in murine hepatoma cells and hepatocytes and during experimental acetaminophen-induced liver damage. *Front Immunol*. 2017;8(JUL):1-11. doi:10.3389/fimmu.2017.00890
284. Flood B, Manils J, Nulty C, et al. Caspase-11 regulates the tumour suppressor function of STAT1 in a murine model of colitis-associated carcinogenesis. *Oncogene*. 2019;38(14). doi:10.1038/s41388-018-0613-5
285. Wienerroither S, Shukla P, Farlik M, et al. Cooperative Transcriptional Activation of Antimicrobial Genes by STAT and NF-κB Pathways by Concerted Recruitment of the Mediator Complex. *Cell Rep*. 2015;12(2):300-312. doi:10.1016/j.celrep.2015.06.021
286. Farlik M, Reutterer B, Schindler C, Greten F, Vogl C, Müller M. Supplemental Information Nonconventional Initiation Complex Assembly by STAT and NF-κB Transcription Factors Regulates Host Defense Genes. 33:1-2.
287. Hwang S-Y, Hur K-Y, Kim J-R, Cho K-H, Kim S-H, Yoo J-Y. Biphasic RLR–IFN-β Response Controls the Balance between Antiviral Immunity and Cell Damage. *J Immunol*. 2013;190(3):1192-1200. doi:10.4049/jimmunol.1202326
288. Mertens C, Zhong M, Krishnaraj R, Zou W, Chen X, Darnell JE. Dephosphorylation of phosphotyrosine on STAT1 dimers requires extensive spatial reorientation of the monomers facilitated by the N-terminal domain. *Genes Dev*. 2006;20(24):3372-3381. doi:10.1101/gad.1485406
289. Wang R, Wang W, Li A, et al. Lipopolysaccharide enhances DNA-induced IFN-β expression and autophagy by upregulating cGAS expression in A549 cells. *Exp Ther Med*. Published online 2019:4157-4164. doi:10.3892/etm.2019.8001
290. Nakahira K, Haspel JA, Rathinam VAK, et al. Autophagy proteins regulate innate immune responses by inhibiting the release of mitochondrial DNA mediated by the NALP3 inflammasome. *Nat Immunol*. 2011;12(3):222-230. doi:10.1038/ni.1980
291. Youle RJ, Van Der Bliek AM. Good for Discussion: Mitochondrial Fission, Fusion, and Stress. *Science (80-)*. 2012;337(6098):1062-1065. doi:10.1126/science.1219855.Mitochondrial
292. Twig G, Elorza A, Molina AJA, et al. Fission and selective fusion govern mitochondrial segregation and elimination by autophagy. *EMBO J*. 2008;27(2):433-446. doi:10.1038/sj.emboj.7601963
293. Caielli S, Athale S, Domic B, et al. Oxidized mitochondrial nucleoids released by neutrophils drive type I interferon production in human lupus. *J Exp Med*. 2016;213(5):697-713. doi:10.1084/jem.20151876
294. Litvinova L, Atochin DN, Fattakhov N, Vasilenko M, Zatolokin P, Kirienkova E. Nitric oxide and mitochondria in metabolic syndrome. *Front Physiol*. 2015;6(FEB):1-10. doi:10.3389/fphys.2015.00020
295. Melo GD, Lazarini F, Larrous F, et al. Attenuation of clinical and immunological outcomes during SARS-CoV-2 infection by ivermectin. *EMBO Mol Med*. 2021;13(8):1-14. doi:10.15252/emmm.202114122
296. Kawaguchi M, Aoki S, Hirao T, Morita M, Ito K. Autophagy is an important metabolic pathway to determine leukemia cell survival following suppression of the glycolytic pathway. *Biochem Biophys Res Commun*. 2016;474(1):188-192. doi:10.1016/j.bbrc.2016.04.098
297. Miyazaki N, Shiratori R, Oshima T, et al. PINK1-dependent and Parkin-independent mitophagy is involved in reprogramming of glycometabolism in pancreatic cancer cells. *Biochem Biophys Res Commun*. 2022;625:167-173. doi:10.1016/j.bbrc.2022.08.004
298. Smith TD, Tse MJ, Read EL, Liu WF. Regulation of macrophage polarization and plasticity by complex activation signals. *Integr Biol (United Kingdom)*. Published online 2016. doi:10.1039/c6ib00105j

299. MacMicking J, Xie QW, Nathan C. Nitric oxide and macrophage function. *Annu Rev Immunol*. 1997;15(1):323-350. doi:10.1146/annurev.immunol.15.1.323
300. Granger DL, Lehninger AL. Sites of inhibition of mitochondrial electron transport in macrophage-injured neoplastic cells. *J Cell Biol*. 1982;95(2):527-535. doi:10.1083/jcb.95.2.527
301. Cleeter MWJ, Cooper JM, Darley-Usmar VM, Moncada S, Schapira AHV. Reversible inhibition of cytochrome c oxidase, the terminal enzyme of the mitochondrial respiratory chain, by nitric oxide. Implications for neurodegenerative diseases. *FEBS Lett*. 1994;345(1):50-54. doi:10.1016/0014-5793(94)00424-2
302. Mason MG, Nicholls P, Wilson MT, Cooper CE. Nitric oxide inhibition of respiration involves both competitive (heme) and noncompetitive (copper) binding to cytochrome c oxidase. *Proc Natl Acad Sci U S A*. 2006;103(3):708-713. doi:10.1073/pnas.0506562103
303. Palmieri EM, Gonzalez-Cotto M, Baseler WA, et al. Nitric oxide orchestrates metabolic rewiring in M1 macrophages by targeting aconitase 2 and pyruvate dehydrogenase. *Nat Commun*. 2020;11(1). doi:10.1038/s41467-020-14433-7
304. Yang C-S, Yuk J-M, Jo E-K. The Role of Nitric Oxide in Mycobacterial Infections. *Immune Netw*. 2009;9(2):46. doi:10.4110/in.2009.9.2.46
305. Jamaati H, Mortaz E, Pajouhi Z, et al. Nitric oxide in the pathogenesis and treatment of tuberculosis. *Front Microbiol*. 2017;8(OCT):1-11. doi:10.3389/fmicb.2017.02008
306. Gleeson LE, Sheedy FJ, Palsson-McDermott EM, et al. Cutting Edge: Mycobacterium tuberculosis Induces Aerobic Glycolysis in Human Alveolar Macrophages That Is Required for Control of Intracellular Bacillary Replication . *J Immunol*. 2016;196(6):2444-2449. doi:10.4049/jimmunol.1501612
307. Gleeson LE, O'Leary SM, Ryan D, McLaughlin AM, Sheedy FJ, Keane J. Cigarette smoking impairs the bioenergetic immune response to mycobacterium tuberculosis infection. *Am J Respir Cell Mol Biol*. 2018;59(5):572-579. doi:10.1165/rcmb.2018-0162OC
308. Ouimet M, Koster S, Sakowski E, et al. HHS Public Access. 2016;17(6):677-686. doi:10.1038/ni.3434.Mycobacterium
309. Hackett EE, Charles-Messance H, O'Leary SM, et al. Mycobacterium tuberculosis Limits Host Glycolysis and IL-1β by Restriction of PFK-M via MicroRNA-21. *Cell Rep*. 2020;30(1):124-136.e4. doi:10.1016/j.celrep.2019.12.015
310. Kakuda DK, Sweet MJ, MacLeod CL, Hume DA, Markovich D. CAT2-mediated L-arginine transport and nitric oxide production in activated macrophages. *Biochem J*. 1999;340(2):549-553. doi:10.1042/0264-6021:3400549
311. Nicholson B, Manner CK, Kleeman J, MacLeod CL. Sustained Nitric Oxide Production in Macrophages Requires the Arginine Transporter CAT2. *J Biol Chem*. 2001;276(19):15881-15885. doi:10.1074/jbc.M010030200
312. Bailey JD, Diotallevi M, Nicol T, et al. Nitric Oxide Modulates Metabolic Remodeling in Inflammatory Macrophages through TCA Cycle Regulation and Itaconate Accumulation. *Cell Rep*. 2019;28(1):218-230.e7. doi:10.1016/j.celrep.2019.06.018
313. Drapier JC, Hibbs JB. Differentiation of murine macrophages to express nonspecific cytotoxicity for tumor cells results in L-arginine-dependent inhibition of mitochondrial iron-sulfur enzymes in the macrophage effector cells. *J Immunol*. 1988;140(8):2829-2838. http://www.ncbi.nlm.nih.gov/pubmed/2451695
314. Drapier JC, Hibbs JB. Murine cytotoxicity activated macrophages inhibit aconitase in tumor cells. *JClinInvest*. 1986;78(September):790-797.
315. Wikström M, Krab K, Sharma V. Oxygen Activation and Energy Conservation by Cytochrome c Oxidase. *Chem Rev*. 2018;118(5):2469-2490. doi:10.1021/acs.chemrev.7b00664
316. Cooper CE, Brown GC. The inhibition of mitochondrial cytochrome oxidase by the gases carbon monoxide, nitric oxide, hydrogen cyanide and hydrogen sulfide: Chemical mechanism and physiological significance. *J Bioenerg Biomembr*. 2008;40(5):533-539.

doi:10.1007/s10863-008-9166-6
317. Collman JP, Dey A, Decreau RA, et al. Interaction of nitric oxide with a functional model of cytochrome c oxidase. *Proc Natl Acad Sci U S A*. 2008;105(29):9892-9896. doi:10.1073/pnas.0804257105
318. Clementi E, Brown GC, Feelisch M, Moncada S. Persistent inhibition of cell respiration by nitric oxide: Crucial role of S-nitrosylation of mitochondrial complex I and protective action of glutathione. *Proc Natl Acad Sci U S A*. 1998;95(13):7631-7636. doi:10.1073/pnas.95.13.7631
319. Dröse S, Stepanova A, Galkin A. Ischemic A/D transition of mitochondrial complex i and its role in ROS generation. *Biochim Biophys Acta - Bioenerg*. 2016;1857(7):946-957. doi:10.1016/j.bbabio.2015.12.013
320. Burwell LS, Nadtochiy SM, Tompkins AJ, Young S, Brookes PS. Direct evidence for S-nitrosation of mitochondrial complex I. *Biochem J*. 2006;394(3):627-634. doi:10.1042/BJ20051435
321. Brown GC, Borutaite V. Inhibition of mitochondrial respiratory complex I by nitric oxide, peroxynitrite and S-nitrosothiols. *Biochim Biophys Acta - Bioenerg*. 2004;1658(1-2):44-49. doi:10.1016/j.bbabio.2004.03.016
322. Tayeh MA, Marletta MA. Macrophage Oxidation of L-Arginine to Nitric Oxide, Nitrite, and Nitrate. *J Biol Chem*. 1989;264(33):19654-19658. doi:10.1016/s0021-9258(19)47163-9
323. Giordano D, Li C, Suthar MS, et al. Nitric oxide controls an inflammatory-like Ly6C hi PDCA1 + DC subset that regulates Th1 immune responses . *J Leukoc Biol*. 2011;89(3):443-455. doi:10.1189/jlb.0610329
324. Lu G, Zhang R, Geng S, et al. Myeloid cell-derived inducible nitric oxide synthase suppresses M1 macrophage polarization. *Nat Commun*. 2015;6. doi:10.1038/ncomms7676
325. Mao K, Chen S, Chen M, et al. Nitric oxide suppresses NLRP3 inflammasome activation and protects against LPS-induced septic shock. *Cell Res*. 2013;23(2):201-212. doi:10.1038/cr.2013.6
326. Anakha J, Kawathe PS, Datta S, Jawalekar SS, Banerjee UC, Pande AH. Human arginase 1, a Jack of all trades? *3 Biotech*. 2022;12(10):1-9. doi:10.1007/s13205-022-03326-9
327. Lee EJ, Lee YR, Joo HK, et al. Arginase II inhibited lipopolysaccharide-induced cell death by regulation of iNOS and Bcl-2 family proteins in macrophages. *Mol Cells*. 2013;35(5):396-401. doi:10.1007/s10059-013-2332-7
328. Lang R, Patel D, Morris JJ, Rutschman RL, Murray PJ. Shaping Gene Expression in Activated and Resting Primary Macrophages by IL-10. *J Immunol*. 2002;169(5):2253-2263. doi:10.4049/jimmunol.169.5.2253
329. Palmieri EM, McGinity C, Wink DA, McVicar DW. Nitric oxide in macrophage immunometabolism: Hiding in plain sight. *Metabolites*. 2020;10(11):1-34. doi:10.3390/metabo10110429
330. Ranawat H, Pal S, Mazumder N. Recent trends in two-photon auto-fluorescence lifetime imaging (2P-FLIM) and its biomedical applications. *Biomed Eng Lett*. 2019;9(3):293-310. doi:10.1007/s13534-019-00119-7
331. Yang M, Soga T, Pollard PJ, Adam J. The emerging role of fumarate as an oncometabolite. 2012;2(July):1-7. doi:10.3389/fonc.2012.00085
332. Haines RJ, Pendleton LC, Eichler DC. Argininosuccinate synthase : at the center of arginine metabolism. 2011;2(1):8-23.
333. Lee J, Ryu H, Ferrante RJ, Morris SM, Ratan RR. Translational control of inducible nitric oxide synthase expression by arginine can explain the arginine paradox. *Proc Natl Acad Sci U S A*. 2003;100(8):4843-4848. doi:10.1073/pnas.0735876100
334. Dowling JK, Afzal R, Gearing LJ, et al. Mitochondrial arginase-2 is essential for IL-10 metabolic reprogramming of inflammatory macrophages. *Nat Commun*. 2021;12(1):1-14. doi:10.1038/s41467-021-21617-2

335. Baseler WA, Davies LC, Quigley L, et al. Autocrine IL-10 functions as a rheostat for M1 macrophage glycolytic commitment by tuning nitric oxide production. *Redox Biol*. 2016;10:12-23. doi:10.1016/j.redox.2016.09.005
336. Huang CJ, Stevens BR, Nielsen RB, et al. Interleukin-10 inhibition of nitric oxide biosynthesis involves suppression of CAT-2 transcription. *Nitric Oxide - Biol Chem*. 2002;6(1):79-84. doi:10.1006/niox.2001.0402
337. Cimen Bozkus C, Elzey BD, Crist SA, Ellies LG, Ratliff TL. Expression of Cationic Amino Acid Transporter 2 Is Required for Myeloid-Derived Suppressor Cell-Mediated Control of T Cell Immunity. *J Immunol*. 2015;195(11):5237-5250. doi:10.4049/jimmunol.1500959
338. Stamm CE, Collins AC, Shiloh MU. Sensing of Mycobacterium tuberculosis and consequences to both host and bacillus. *Immunol Rev*. 2015;264(1):204-219. doi:10.1111/imr.12263
339. Queval CJ, Brosch R, Simeone R. The macrophage: A disputed fortress in the battle against Mycobacterium tuberculosis. *Front Microbiol*. 2017;8(NOV):1-11. doi:10.3389/fmicb.2017.02284
340. Maphasa RE, Meyer M, Dube A. The Macrophage Response to Mycobacterium tuberculosis and Opportunities for Autophagy Inducing Nanomedicines for Tuberculosis Therapy. *Front Cell Infect Microbiol*. 2021;10(February):1-22. doi:10.3389/fcimb.2020.618414
341. Agnew A, Nulty C, Creagh EM. Regulation, activation and function of caspase-11 during health and disease. *Int J Mol Sci*. 2021;22(4):1-20. doi:10.3390/ijms22041506
342. John D. Macmicking, Robert J. North, Ron Lacourse, John S. Mudgett, Shrenik K. Shah§ and CFN. Identification of nitric oxide synthase as a protective locus. *Immunology*. 1997;94(May):5243-5248.
343. Flis-jankowska E. *Identification of Novel Innate Immune Mechanisms Regulating Oesophageal Adenocarcinoma (OAC) Progression and Bacterial Infection . Thesis Submitted to the University of Dublin , Trinity College*.; 2021.
344. Amano F, Noda T. Improved detection of nitric oxide radical (NO•) production in an activated macrophage culture with a radical scavenger, car□y PTIO, and Griess reagent. *FEBS Lett*. 1995;368(3):425-428. doi:10.1016/0014-5793(95)00700-J
345. Cumming BM, Pacl HT, Steyn AJC. Relevance of the Warburg Effect in Tuberculosis for Host-Directed Therapy. *Front Cell Infect Microbiol*. 2020;10(September):1-13. doi:10.3389/fcimb.2020.576596
346. Ishikawa E, Ishikawa T, Morita YS, et al. Direct recognition of the mycobacterial glycolipid, trehalose dimycolate, by C-type lectin Mincle. *J Exp Med*. 2009;206(13):2879-2888. doi:10.1084/jem.20091750
347. Lavalett L, Ortega H, Barrera LF. Infection of Monocytes From Tuberculosis Patients With Two Virulent Clinical Isolates of Mycobacterium tuberculosis Induces Alterations in Myeloid Effector Functions. *Front Cell Infect Microbiol*. 2020;10(April):1-17. doi:10.3389/fcimb.2020.00163
348. Liu R, Zhu T, Yang T, et al. NO regulates ganoderic acid biosynthesis by the S-nitrosylation of aconitase under HS in Ganoderma lucidum This article is protected by copyright . All rights reserved . This article is protected by copyright . All rights reserved . doi:10.1111/1462-2920.15109
349. Ternette N, Yang M, Laroyia M, et al. Report Inhibition of Mitochondrial Aconitase by Succination in Fumarate Hydratase Deficiency. *CellReports*. 2013;3(3):689-700. doi:10.1016/j.celrep.2013.02.013
350. Everts B, Amiel E, Van Der Windt GJW, et al. Commitment to glycolysis sustains survival of NO-producing inflammatory dendritic cells. *Blood*. 2012;120(7):1422-1431. doi:10.1182/blood-2012-03-419747
351. Dioguardi FS. To give or not to give? Lessons from the arginine paradox. *J Nutrigenet Nutrigenomics*. 2011;4(2):90-98. doi:10.1159/000327777

352. Immunology E, Menzies FM, Henriquez FL, Alexander J, Roberts CW. Sequential expression of macrophage anti-microbial / inflammatory and wound healing markers following innate , alternative and classical activation. 2009;2:369-379. doi:10.1111/j.1365-2249.2009.04086.x
353. Inducible Nitric Oxide Synthase deficiency leads to early demyelination by altering the balance between pro- and anti-inflammatory responses against Murine-β-Coronavirus. Published online 2022:1-41.
354. Tannahill GM, Curtis AM, Adamik J, et al. Succinate is an inflammatory signal that induces IL-1β through HIF-1α. *Nature*. 2013;496(7444):238-242. doi:10.1038/nature11986
355. Corraliza IM, Soler G, Eichmann K, Modolell M. Arginase induction by suppressors of nitric oxide synthesis (IL-4, IL-10 and PGE2) in murine bone-marrow-derived macrophages. *Biochem Biophys Res Commun*. 1995;206(2):667-673. doi:10.1006/bbrc.1995.1094
356. Garrido P, Shalaby A, Walsh EM, et al. Impact of inducible nitric oxide synthase (iNOS) expression on triple negative breast cancer outcome and activation of EGFR and ERK signaling pathways. *Oncotarget*. Published online 2017. doi:10.18632/oncotarget.19631
357. Vasques-Nóvoa F, Laundos TL, Cerqueira RJ, et al. MicroRNA-155 amplifies nitric oxide/cGMP signaling and impairs vascular angiotensin II reactivity in septic shock. *Crit Care Med*. 2018;46(9):E945-E954. doi:10.1097/CCM.0000000000003296
358. Tsujimoto T, Mori T, Houri K, et al. miR-155 inhibits mitophagy through suppression of BAG5, a partner protein of PINK1. *Biochem Biophys Res Commun*. 2020;523(3):707-712. doi:10.1016/j.bbrc.2020.01.022
359. Puleston DJ, Buck MD, Klein Geltink RI, et al. Polyamines and eIF5A Hypusination Modulate Mitochondrial Respiration and Macrophage Activation. *Cell Metab*. 2019;30(2):352-363.e8. doi:10.1016/j.cmet.2019.05.003
360. Chan BJ, Xing Y, Magliozzo RS, Bloom BR. Mycobacterium tuberculosis. 1992;175(April).
361. Macmicking JD, North RJ, Lacourse R, Mudgett JS, Shah SK, Nathan CF. Identification of nitric oxide synthase as a protective locus against tuberculosis. *Proc Natl Acad Sci U S A*. 1997;94(10):5243-5248. doi:10.1073/pnas.94.10.5243
362. Perona-wright G, Sheedy FJ, Divangahi M. Targeting immunometabolism in host defence against Mycobacterium tuberculosis. Published online 2021:145-159. doi:10.1111/imm.13276
363. Nagy C, Haschemi A. Time and demand are two critical dimensions of immunometabolism : the process of macrophage activation and the pentose phosphate pathway. 2015;6(April):1-8. doi:10.3389/fimmu.2015.00164
364. Infantino V, Iacobazzi V, Palmieri F, Menga A. Biochemical and Biophysical Research Communications ATP-citrate lyase is essential for macrophage inflammatory response. *Biochem Biophys Res Commun*. 2013;(September):1-7. doi:10.1016/j.bbrc.2013.09.037
365. Koeken VACM, Lachmandas E, Riza A, et al. Role of Glutamine Metabolism in Host Defense Against Mycobacterium tuberculosis Infection. 2019;219:1662-1670. doi:10.1093/infdis/jiy709
366. Rapovy SM, Zhao J, Bricker RL, Schmidt SM, Setchell KDR, Qualls JE. Member Organization Author Manuscript. 2019;195(7):3293-3300. doi:10.4049/jimmunol.1500800.Differential
367. Nicholson S, Bonecini-Almeida MDG, Lapa E Silva JR, et al. Inducible nitric oxide synthase in pulmonary alveolar macrophages from patients with tuberculosis. *J Exp Med*. 1996;183(5):2293-2302. doi:10.1084/jem.183.5.2293
368. Aston C, Rom WN, Talbot AT, Reibman J. Early inhibition of mycobacterial growth by human alveolar macrophages is not due to nitric oxide. *Am J Respir Crit Care Med*. 1998;157(6 PART I):1943-1950. doi:10.1164/ajrccm.157.6.9705028
369. Bhatt K, Salgame P. Host Innate Immune Response to Mycobacterium tuberculosis. 2007;27(4):347-362. doi:10.1007/s10875-007-9084-0
370. Rodriguez PC, Zea AH, DeSalvo J, et al. l-Arginine Consumption by Macrophages

Modulates the Expression of CD3ζ Chain in T Lymphocytes. *J Immunol*. 2003;171(3):1232-1239. doi:10.4049/jimmunol.171.3.1232

371. Li Z, Zhao ZJ, Zhu XQ, et al. Differences in iNOS and arginase expression and activity in the macrophages of rats are responsible for the resistance against T. gondii infection. *PLoS One*. 2012;7(4). doi:10.1371/journal.pone.0035834
372. Liang Y, Piao C, Beuschel CB, Liu F, Sickmann A, Sigrist SJ. Article eIF5A hypusination , boosted by dietary spermidine , protects from premature brain aging and mitochondrial dysfunction ll ll eIF5A hypusination , boosted by dietary spermidine , protects from premature brain aging and mitochondrial dysfunction. Published online 2021. doi:10.1016/j.celrep.2021.108941
373. Banks DA, Ahlbrand SE, Hughitt VK, et al. HHS Public Access. 2020;202(8):2348-2359. doi:10.4049/jimmunol.1801303.Mycobacterium
374. Desvignes L, Wolf AJ, Ernst JD. Dynamic Roles of Type I and Type II IFNs in Early Infection with Mycobacterium tuberculosis . *J Immunol*. 2012;188(12):6205-6215. doi:10.4049/jimmunol.1200255
375. Deshmukh SK, Srivastava SK, Poosarla T, et al. Inflammation, immunosuppressive microenvironment and breast cancer: opportunities for cancer prevention and therapy. *Ann Transl Med*. Published online 2019. doi:10.21037/atm.2019.09.68
376. Klein SL, Flanagan KL. Sex differences in immune responses. *Nat Rev Immunol*. Published online 2016. doi:10.1038/nri.2016.90
377. Laiosa M. Steroid Hormones and their Effect on the Immune System. In: *Encyclopedic Reference of Immunotoxicology*. ; 2006. doi:10.1007/3-540-27806-0_1383
378. Segovia-Mendoza M, Morales-Montor J. Immune tumor microenvironment in breast cancer and the participation of estrogens and its receptors into cancer physiopathology. *Front Immunol*. Published online 2019. doi:10.3389/fimmu.2019.00348
379. Gruosso T, Gigoux M, Satya V, et al. Spatially distinct tumor immune microenvironments stratify triple-negative breast cancers. 2019;129(4):1785-1800.
380. Nuti M, Bellati F, Visconti V, et al. Immune effects of Trastuzumab. *J Cancer*. 2011;2(1):317-323. doi:10.7150/jca.2.317
381. Jin K, Pandey NB, Popel AS. Simultaneous blockade of IL-6 and CCL5 signaling for synergistic inhibition of triple-negative breast cancer growth and metastasis. *Breast Cancer Res*. Published online 2018. doi:10.1186/s13058-018-0981-3
382. Liubomirski Y, Lerrer S, Meshel T, et al. Tumor-stroma-inflammation networks promote pro-metastatic chemokines and aggressiveness characteristics in triple-negative breast cancer. *Front Immunol*. Published online 2019. doi:10.3389/fimmu.2019.00757
383. Choi J, Gyamfi J, Jang H, Koo JS. The role of tumor-associated macrophage in breast cancer biology. *Histol Histopathol*. Published online 2018. doi:10.14670/HH-11-916
384. Ali HR, Chlon L, Pharoah PDP, Markowetz F, Caldas C. Patterns of Immune Infiltration in Breast Cancer and Their Clinical Implications: A Gene-Expression-Based Retrospective Study. *PLoS Med*. Published online 2016. doi:10.1371/journal.pmed.1002194
385. D.C. S, B. R, Y. O, M.J. B, L.M. C, N. P. CSF1R inhibition delays cervical and mammary tumor growth in murine models by attenuating the turnover of tumor-associated macrophages and enhancing infiltration by CD8+ T cells. *Oncoimmunology*. Published online 2013.
386. Bunt SK, Yang L, Sinha P, Clements VK, Leips J, Ostrand-Rosenberg S. Reduced inflammation in the tumor microenvironment delays the accumulation of myeloid-derived suppressor cells and limits tumor progression. *Cancer Res*. Published online 2007. doi:10.1158/0008-5472.CAN-07-2354
387. Holen I, Lefley D V., Francis SE, et al. IL-1 drives breast cancer growth and bone metastasis in vivo. *Oncotarget*. Published online 2016. doi:10.18632/oncotarget.12289
388. Wiedemann GM, Knott MML, Vetter VK, et al. Cancer cell-derived IL-1α induces CCL22 and the recruitment of regulatory T cells. *Oncoimmunology*. Published online 2016. doi:10.1080/2162402X.2016.1175794

389. Storr SJ, Safuan S, Ahmad N, El-Refaee M, Jackson AM, Martin SG. Macrophage-derived interleukin-1beta promotes human breast cancer cell migration and lymphatic adhesion in vitro. *Cancer Immunol Immunother*. Published online 2017. doi:10.1007/s00262-017-2020-0
390. Kayagaki N, Stowe IB, Lee BL, et al. Caspase-11 cleaves gasdermin D for non-canonical inflammasome signalling. *Nature*. Published online 2015. doi:10.1038/nature15541
391. Shi J, Gao W, Shao F. Pyroptosis: Gasdermin-Mediated Programmed Necrotic Cell Death. *Trends Biochem Sci*. Published online 2017. doi:10.1016/j.tibs.2016.10.004
392. Hergueta-Redondo M, Sarrió D, Molina-Crespo Á, et al. Gasdermin-B promotes invasion and metastasis in breast cancer cells. *PLoS One*. Published online 2014. doi:10.1371/journal.pone.0090099
393. Xia X, Yin W, Mao J, et al. Gasdermin D as a potential prognosis and treatment response prediction biomarker for invasive breast cancer. *J Clin Oncol*. 2021;39(15_suppl):e12548-e12548. doi:10.1200/JCO.2021.39.15_suppl.e12548
394. Yan H, Luo B, Wu X, et al. Cisplatin induces pyroptosis via activation of meg3/ nlrp3/caspase-1/gsdmd pathway in triple-negative breast cancer. *Int J Biol Sci*. 2021;17(10):2606-2621. doi:10.7150/ijbs.60292
395. Wang Q, Wang Y, Ding J, et al. A bioorthogonal system reveals antitumour immune function of pyroptosis. *Nature*. 2020;579(7799):421-426. doi:10.1038/s41586-020-2079-1
396. Robinson TJ, Pai M, Liu JC, et al. High-throughput screen identifies disulfiram as a potential therapeutic for triple-negative breast cancer cells: Interaction with IQ motif-containing factors. *Cell Cycle*. 2013;12(18):3013-3024. doi:10.4161/cc.26063
397. Smith AP, Creagh EM. Caspase-4 and -5 Biology in the Pathogenesis of Inflammatory Bowel Disease. *Front Pharmacol*. 2022;13(May):1-18. doi:10.3389/fphar.2022.919567
398. Tuna M, Smid M, Zhu D, Martens JWM, Amos CI. Association between acquired uniparental disomy and homozygous mutations and HER2/ER/PR status in breast cancer. *PLoS One*. 2010;5(11). doi:10.1371/journal.pone.0015094
399. Haiman CA, Han Y, Feng Y, et al. Genome-Wide Testing of Putative Functional Exonic Variants in Relationship with Breast and Prostate Cancer Risk in a Multiethnic Population. *PLoS Genet*. 2013;9(3). doi:10.1371/journal.pgen.1003419
400. Nagpal N, Ahmad HM, Molparia B, Kulshreshtha R. MicroRNA-191, an estrogen-responsive microRNA, functions as an oncogenic regulator in human breast cancer. *Carcinogenesis*. 2013;34(8):1889-1899. doi:10.1093/carcin/bgt107
401. Meng L, Tian Z, Long X, et al. Caspase 4 Overexpression as a Prognostic Marker in Clear Cell Renal Cell Carcinoma: A Study Based on the Cancer Genome Atlas Data Mining. *Front Genet*. 2021;11(January):1-12. doi:10.3389/fgene.2020.600248
402. Flood B, Oficjalska K, Laukens D, et al. Altered expression of caspases-4 and -5 during inflammatory bowel disease and colorectal cancer: Diagnostic and therapeutic potential. *Clin Exp Immunol*. Published online 2015. doi:10.1111/cei.12617
403. Wang H, Wang L, Xie Z, Zhou S, Li Y, Zhou Y. Targeted Therapy for Colon Cancer. Published online 2020:1-25.
404. LL T, DW M, L H, LG B, RG K, S M. Nitric oxide synthase activity in human breast cancer. *Br J Cancer*. 1995;(November 1994):41-44. https://www.ncbi.nlm.nih.gov/pmc/articles/PMC2034139/pdf/brjcancer00041-0045.pdf
405. Vakkala M, Kahlos K, Lakari E, Pääkkö P, Kinnula V, Soini Y. Inducible nitric oxide synthase expression, apoptosis, and angiogenesis in in situ and invasive breast carcinomas. *Clin Cancer Res*. 2000;6(6):2408-2416.
406. Fragomeni SM, Sciallis A, Jeruss JS. Molecular Subtypes and Local-Regional Control of Breast Cancer. *Surg Oncol Clin N Am*. Published online 2018. doi:10.1016/j.soc.2017.08.005

407. Cakar B, Surmeli Z, Gursoy Oner P, Yelim ES, Karabulut B, Uslu R. The Impact of Subtype Distribution in Inflammatory Breast Cancer Outcome. *Eur J Breast Heal*. Published online 2018. doi:10.5152/ejbh.2018.4170
408. Milioli HH, Tishchenko I, Riveros C, Berretta R, Moscato P. Basal-like breast cancer: molecular profiles, clinical features and survival outcomes. *BMC Med Genomics*. Published online 2017. doi:10.1186/s12920-017-0250-9
409. Curtis C, Shah SP, Chin SF, et al. The genomic and transcriptomic architecture of 2,000 breast tumours reveals novel subgroups. *Nature*. Published online 2012. doi:10.1038/nature10983
410. Weichand B, Popp R, Dziumbla S, et al. S1PR1 on tumor-associated macrophages promotes lymphangiogenesis and metastasis via NLRP3/IL-1ß. *J Exp Med*. Published online 2017. doi:10.1084/jem.20160392
411. Guo L, Chi Y, Xue J, Ma L, Shao Z, Wu J. Phosphorylated eIF2α predicts disease-free survival in triple-negative breast cancer patients. *Sci Rep*. 2017;7:1-9. doi:10.1038/srep44674
412. Qiu SQ, Waaijer SJH, Zwager MC, de Vries EGE, van der Vegt B, Schröder CP. Tumor-associated macrophages in breast cancer: Innocent bystander or important player? *Cancer Treat Rev*. Published online 2018. doi:10.1016/j.ctrv.2018.08.010
413. Williams CB, Yeh ES, Soloff AC. Tumor-associated macrophages: Unwitting accomplices in breast cancer malignancy. *npj Breast Cancer*. Published online 2016. doi:10.1038/npjbcancer.2015.25
414. Gwak JM, Jang MH, Kim D Il, Seo AN, Park SY. Prognostic value of tumor-associated macrophages according to histologic locations and hormone receptor status in breast cancer. *PLoS One*. Published online 2015. doi:10.1371/journal.pone.0125728
415. Basudhar D, Glynn SA, Greer M, et al. Coexpression of NOS2 and COX2 accelerates tumor growth and reduces survival in estrogen receptor-negative breast cancer. *Proc Natl Acad Sci U S A*. 2017;114(49):13030-13035. doi:10.1073/pnas.1709119114
416. Zamora R, Bult H, Herman AG. The role of prostaglandin E2 and nitric oxide in cell death in J774 murine macrophages. *Eur J Pharmacol*. 1998;349(2-3):307-315. doi:10.1016/S0014-2999(98)00211-8
417. Hrabák A, Vercruysse V, Kahán IL, Vray B. Indomethacin prevents the induction of inducible nitric oxide synthase in murine peritoneal macrophages and decreases their nitric oxide production. *Life Sci*. 2001;68(16):1923-1930. doi:10.1016/S0024-3205(01)00978-X
418. Xiao L, Ornatowska M, Zhao G, et al. Lipopolysaccharide-Induced Expression of Microsomal Prostaglandin E Synthase-1 Mediates Late-Phase PGE2 Production in Bone Marrow Derived Macrophages. *PLoS One*. 2012;7(11). doi:10.1371/journal.pone.0050244
419. Park MH, Hong JT. Roles of NF-κB in cancer and inflammatory diseases and their therapeutic approaches. *Cells*. 2016;5(2). doi:10.3390/cells5020015
420. Hwang H, Shin C, Park J, et al. Human breast cancer-derived soluble factors facilitate CCL19-induced chemotaxis of human dendritic cells. *Sci Rep*. Published online 2016. doi:10.1038/srep30207
421. Soto-Perez-de-Celis E, Chavarri-Guerra Y, Leon-Rodriguez E, Gamboa-Dominguez A. Tumor-associated neutrophils in breast cancer subtypes. *Asian Pacific J Cancer Prev*. Published online 2017. doi:10.22034/APJCP.2017.18.10.2689
422. Vidaver R. Molecular and clinical evidence of the role of estrogen in lupus. In: *Trends in Immunology*. ; 2002. doi:10.1016/S1471-4906(02)02204-4
423. Yu T, Di G. Role of tumor microenvironment in triple-negative breast cancer and its prognostic significance. *Chinese J Cancer Res*. Published online 2017. doi:10.21147/j.issn.1000-9604.2017.03.10
424. Cheng C, Wu H, Wang M, et al. Estrogen ameliorates allergic airway inflammation by

regulating activation of NLRP3 in mice. *Biosci Rep*. Published online 2019. doi:10.1042/BSR20181117
425. Bolívar BE, Rohrman BA, Charendoff CI, Yazdani V. Non-redundant roles of caspase-4 and caspase-5 in heme driven-IL-1β release and cell death. *bioRxiv*. Published online 2020.
426. NCT03323346.
427. Chen D, Cui QC, Yang H, Dou QP. Disulfiram, a clinically used anti-alcoholism drug and copper-binding agent, induces apoptotic cell death in breast cancer cultures and xenografts via inhibition of the proteasome activity. *Cancer Res*. 2006;66(21):10425-10433. doi:10.1158/0008-5472.CAN-06-2126
428. Askgaard G, Friis S, Hallas J, Thygesen LC, Pottegård A. Use of disulfiram and risk of cancer: A population-based case-control study. *Eur J Cancer Prev*. 2014;23(3):225-232. doi:10.1097/CEJ.0b013e3283647466
429. Lou X, Li K, Qian B, Li Y, Zhang D, Cui W. Pyroptosis correlates with tumor immunity and prognosis. *Commun Biol*. 2022;5(1):1-11. doi:10.1038/s42003-022-03806-x
430. Yum S, Li M, Fang Y, Chen ZJ. TBK1 recruitment to STING activates both IRF3 and NF-κB that mediate immune defense against tumors and viral infections. *Proc Natl Acad Sci U S A*. 2021;118(14):1-9. doi:10.1073/pnas.2100225118
431. Mustafa MF, Saliluddin SM, Fakurazi S, et al. Expression of Autophagy and Mitophagy Markers in Breast Cancer Tissues. *Front Oncol*. 2021;11(August):1-12. doi:10.3389/fonc.2021.612009
432. Ka NL, Lim GY, Hwang S, Kim SS, Lee MO. IFI16 inhibits DNA repair that potentiates type-I interferon-induced antitumor effects in triple negative breast cancer. *Cell Rep*. 2021;37(12):110138. doi:10.1016/j.celrep.2021.110138
433. Tong L, Heim RA, Wu S. Nitric oxide: A regulator of eukaryotic initiation factor 2 kinases. *Free Radic Biol Med*. 2011;50(12):1717-1725. doi:10.1016/j.freeradbiomed.2011.03.032
434. Sun X, Wang M, Wang M, et al. Metabolic Reprogramming in Triple-Negative Breast Cancer. 2020;10(March). doi:10.3389/fonc.2020.00428
435. Evans KW, Yuca E, Scott SS, et al. Oxidative phosphorylation is a metabolic vulnerability in chemotherapy-resistant triple-negative breast cancer. *Cancer Res*. 2021;81(21):5572-5581. doi:10.1158/0008-5472.CAN-20-3242
436. Scherbakov AM, Omelchuk O, Sorokin D, Shatskaya V, Shchekotikhin A, Krasil'nikov M. 77P Dual targeting oxidative phosphorylation and glycolysis in triple-negative breast cancers: En route to effective inhibition of tumour metabolism. *Ann Oncol*. 2020;31:S1272. doi:10.1016/j.annonc.2020.10.097
437. Yu Q, Guo M, Zeng W, et al. Interactions between NLRP3 inflammasome and glycolysis in macrophages: New insights into chronic inflammation pathogenesis. *Immunity, Inflamm Dis*. 2022;10(3):1-13. doi:10.1002/iid3.581
438. Vogel DYS, Glim JE, Stavenuiter AWD, et al. Human macrophage polarization in vitro: Maturation and activation methods compared. *Immunobiology*. Published online 2014. doi:10.1016/j.imbio.2014.05.002
439. Movahedi K, Laoui D, Gysemans C, et al. Different tumor microenvironments contain functionally distinct subsets of macrophages derived from Ly6C(high) monocytes. *Cancer Res*. Published online 2010. doi:10.1158/0008-5472.CAN-09-4672
440. Liny CW, Shen SC, Ko CH, Lin HY, Chen YC. Reciprocal activation of macrophages and breast carcinoma cells by nitric oxide and colony-stimulating factor-1. *Carcinogenesis*. Published online 2010. doi:10.1093/carcin/bgq172
441. Shantanam S, MUELLER. 乳鼠心肌提取 HHS Public Access. *Physiol Behav*. 2018;176(1):139-148. doi:10.1111/j.1524-475X.2009.00459.x.S
442. Mannick JB, Schonhoff C, Papeta N, et al. S-nitrosylation of mitochondrial caspases. *J Cell Biol*. 2001;154(6):1111-1116. doi:10.1083/jcb.200104008
443. Tian J, Kim SF, Hester L, Snyder SH. S-nitrosylation/activation of COX-2 mediates NMDA neurotoxicity. *Proc Natl Acad Sci U S A*. 2008;105(30):10537-10540.

doi:10.1073/pnas.0804852105
444. Zaslona Z, Flis E, Nulty C, et al. Caspase-4: A Therapeutic Target for Peptic Ulcer Disease. *ImmunoHorizons*. 2020;4(10):627-633. doi:10.4049/immunohorizons.2000080
445. Kim SF, Huri DA, Snyder SH. Medicine: Inducible nitric oxide synthase binds, S-nitrosylates, and activates cyclooxygenase-2. *Science (80-)*. 2005;310(5756):1966-1970. doi:10.1126/science.1119407
446. Xia X, Wang X, Cheng Z, et al. The role of pyroptosis in cancer: pro-cancer or pro-"host"? *Cell Death Dis*. Published online 2019. doi:10.1038/s41419-019-1883-8
447. Lugus JJ, Walsh K, Shoelson SE, Cantrell DA. Immunometabolism: an emerging frontier. *Nat Publ Gr*. 2011;11(FEBRuARy):81-83. doi:10.1038/nri2922
448. Traba J, Sack MN, Waldmann TA, Anton OM. Immunometabolism at the Nexus of Cancer Therapeutic Efficacy and Resistance. *Front Immunol*. 2021;12(May):1-16. doi:10.3389/fimmu.2021.657293
449. Joshi B, Joshi JC, Mehta D. Regulation of cGAS Activity and Downstream Signaling. *Cells*. 2022;11(18). doi:10.3390/cells11182812
450. Sokolowska O, Nowis D. STING Signaling in Cancer Cells: Important or Not? *Arch Immunol Ther Exp (Warsz)*. 2018;66(2):125-132. doi:10.1007/s00005-017-0481-7
451. Won JK, Bakhoum SF. The cytosolic DNA-sensing cGAS–sting pathway in cancer. *Cancer Discov*. 2020;10(1):26-39. doi:10.1158/2159-8290.CD-19-0761
452. Ning L, Ning L, Wei W. Cytosolic DNA-STING-NLRP3 axis is involved in murine acute lung injury induced by lipopolysaccharide Cytosolic DNA-STING-NLRP3 axis is involved in murine acute lung injury induced by lipopolysaccharide. 2020;(August). doi:10.1002/ctm2.228
453. Zhou L, Zhang YF, Yang FH, Mao HQ, Chen Z, Zhang L. Mitochondrial DNA leakage induces odontoblast inflammation via the cGAS - STING pathway. *Cell Commun Signal*. Published online 2021:1-11. doi:10.1186/s12964-021-00738-7
454. Zhong F, Liang S, Zhong Z. Emerging Role of Mitochondrial DNA as a Major Driver of Inflammation and Disease Progression. *Trends Immunol*. Published online 2019:1-14. doi:10.1016/j.it.2019.10.008
455. Jiang M, Chen P, Wang L, et al. cGAS-STING , an important pathway in cancer immunotherapy. Published online 2020:1-11.
456. Kang TH, Mao C, Kim YS, et al. TLR9 acts as a sensor for tumor-released DNA to modulate anti-tumor immunity after chemotherapy. 2019;2:1-8.
457. Iv JA, Gyorke CE, Tripathy MK, Zhang Y, Lovett A, Montgomery SA. crossm Caspase-11 Contributes to Oviduct Pathology during Genital Chlamydia Infection in Mice. 2019;87(8):1-12.
458. Wu X, Mao X, Huang Y, Zhu Q, Guan J, Wu L. Detection of proteins associated with the pyroptosis signaling pathway in breast cancer tissues and their significance. 2020;13(January):1408-1414.
459. Ershaid N, Sharon Y, Doron H, et al. progression and metastasis. *Nat Commun*. Published online 2019. doi:10.1038/s41467-019-12370-8
460. Wu SY, Xiao Y, Wei JL, et al. MYC suppresses STING-dependent innate immunity by transcriptionally upregulating DNMT1 in triple-negative breast cancer. *J Immunother Cancer*. 2021;9(7). doi:10.1136/jitc-2021-002528
461. Parkes EE, Humphries MP, Gilmore E, et al. The clinical and molecular signi fi cance associated with STING signaling in breast cancer. Published online 2021. doi:10.1038/s41523-021-00283-z
462. Bu Y, Liu F, Jia Q, Yu S. Decreased Expression of TMEM173 Predicts Poor Prognosis in Patients with Hepatocellular Carcinoma. Published online 2016:1-11. doi:10.1371/journal.pone.0165681
463. Banerjee I, Behl B, Mendonca M, et al. Gasdermin D Restrains Type I Interferon Response to Cytosolic DNA by Disrupting Ionic Homeostasis Article Gasdermin D Restrains Type I

Interferon Response to Cytosolic DNA by Disrupting Ionic Homeostasis. *Immunity*. 2018;49(3):413-426.e5. doi:10.1016/j.immuni.2018.07.006
464. Li N, Chen J, Geng C, et al. Myoglobin promotes macrophage polarization to M1 type and pyroptosis via the RIG-I / Caspase1 / GSDMD signaling pathway in. 2022;(February):1-14. doi:10.1038/s41420-022-00894-w
465. Baatarjav C, Komada T, Karasawa T, et al. dsDNA-induced AIM2 pyroptosis halts aberrant inflammation during rhabdomyolysis-induced acute kidney injury. *Cell Death Differ*. 2022;29(12):2487-2502. doi:10.1038/s41418-022-01033-9
466. Lavie J, Mahfouf W, Jose C, et al. Article Rheb Regulates Mitophagy Induced by Mitochondrial Energetic Status. Published online 2013:719-730. doi:10.1016/j.cmet.2013.03.014
467. Yao Z, Gandhi S, Burchell VS, Plun-favreau H, Wood NW, Abramov AY. Cell metabolism affects selective vulnerability in PINK1-associated Parkinson ' s disease. Published online 2011:4194-4202. doi:10.1242/jcs.088260
468. Requejo-aguilar R, Lopez-fabuel I, Jimenez-blasco D, Almeida A. HHS Public Access. 2016;467(2):303-310. doi:10.1042/BJ20141025.DJ1
469. Mitochondria M. Review Mammalian Mitochondria and Aging : An Update. Published online 2017:57-71. doi:10.1016/j.cmet.2016.09.017
470. Gong Y, Ji P, Yang Y, et al. Clinical and Translational Report Metabolic-Pathway-Based Subtyping of Triple- Negative Breast Cancer Reveals Potential Therapeutic Targets ll Clinical and Translational Report Metabolic-Pathway-Based Subtyping of Triple-Negative Breast Cancer Reveals Pot. Published online 2021:51-64. doi:10.1016/j.cmet.2020.10.012
471. Hasan M, Gonugunta VK, Dobbs N, Ali A, Palchik G, Calvaruso MA. Chronic innate immune activation of TBK1 suppresses mTORC1 activity and dysregulates cellular metabolism. Published online 2017. doi:10.1073/pnas.1611113114
472. Brien EMO, Spiller KL. Pro-inflammatory polarization primes Macrophages to transition into a distinct M2-like phenotype in response to IL-4. 2022;111(5):989-1000. doi:10.1002/JLB.3A0520-338R.Pro-inflammatory
473. Bossche J Van Den, Baardman J, Otto NA, et al. Mitochondrial Dysfunction Prevents Repolarization of Inflammatory Macrophages Article Mitochondrial Dysfunction Prevents Repolarization of Inflammatory Macrophages. *CellReports*. 2016;17(3):684-696. doi:10.1016/j.celrep.2016.09.008
474. Somasundaram V, Ridnour LA, Cheng RYS, et al. 1* . 1. Published online 2022.
475. Gross TJ, Kremens K, Powers LS, et al. Epigenetic Silencing of the Human. 2017;2. doi:10.4049/jimmunol.1301758
476. Albina E. On the expression of nitric oxide synthase Why no NO ? by human. 1995;58(December):643-649. doi:10.1002/jlb.58.6.643
477. Kam Y, Swain PM, Dranka BP. Abstract A67: Bi-phasic metabolic responses to in situ macrophage activation. *Cancer Immunol Res*. 2018;6(9_Supplement):A67-A67. doi:10.1158/2326-6074.tumimm17-a67
478. Jaworska J, Verway M, Tzelepis F, et al. Article Targeted Prostaglandin E 2 Inhibition Enhances Antiviral Immunity through Induction of Type I Interferon and Apoptosis in Macrophages Franc. 2011;1. doi:10.1016/j.immuni.2014.02.013
479. Mayer-barber KD, Andrade BB, Oland SD, et al. interleukin-1 and type I interferon crosstalk. *Nature*. 2014;511(7507):99-103. doi:10.1038/nature13489

8.Appendix

Table 8.1: Survival of all patients subtypes correlating to stromal expression

Parametric p-value	FDR	Hazard Ratio	SD of log intensities	Symbol	Name
0.0012187	0.0451	2.438	0.558	ARG2	arginase 2
0.121823	0.878	1.562	0.632	CASP1	caspase 1
0.130544	0.878	1.783	0.524	PANX1	pannexin 1
0.142682	0.878	1.829	0.44	CASP1	caspase 1
0.163672	0.878	3.021	0.25	CASP1	caspase 1
0.224089	0.878	0.283	0.228	IL1A	interleukin 1 alpha
0.236961	0.878	5.683	0.124	CASP5	caspase 5
0.241275	0.878	0.459	0.285	IFNG	interferon gamma
0.242835	0.878	1.747	0.381	CASP1	caspase 1
0.280323	0.878	1.278	0.751	ASS1	argininosuccinate synthase 1
0.301886	0.878	0.744	0.586	PTGS1	prostaglandinendoperoxide synthase 1
0.3262	0.878	0.614	0.363	IL18	interleukin 18
0.334663	0.878	1.459	0.408	IL1B	interleukin 1 beta
0.340812	0.878	0.768	0.618	PTGS1	prostaglandinendoperoxide synthase 1
0.356296	0.878	0.704	0.477	CASP4	caspase 4
0.429138	0.878	1.397	0.432	GSDMD	gasdermin D
0.440635	0.878	1.437	0.376	HMGB1	high mobility group box 1
0.467225	0.878	2.083	0.196	IL1A	interleukin 1 alpha
0.4757	0.878	0.887	1.046	STAT1	signal transducer and activator of transcription 1
0.505691	0.878	0.688	0.325	STAT1	signal transducer and activator of transcription 1
0.523617	0.878	1.389	0.326	IL1B	interleukin 1 beta

0.528177	0.878	0.441	0.159	NOS2	nitric oxide synthase 2
0.545931	0.878	1.645	0.212	HMGB1	high mobility group box 1
0.597265	0.9	0.824	0.534	CASP1	caspase 1
0.618952	0.9	1.2	0.534	CASP4	caspase 4
0.637769	0.9	1.251	0.371	ASL	argininosuccinate lyase
0.657857	0.9	0.917	0.881	STAT1	signal transducer and activator of transcription 1
0.681153	0.9	0.799	0.314	STAT1	signal transducer and activator of transcription 1
0.705865	0.901	0.785	0.283	IFNB1	interferon beta 1
0.765766	0.939	0.753	0.186	PTGS1	prostaglandinendoperoxide synthase 1
0.821584	0.939	1.149	0.264	ARG2	arginase 2
0.834844	0.939	0.963	0.963	PTGS2	prostaglandinendoperoxide synthase 2
0.858792	0.939	0.964	0.849	STAT1	signal transducer and activator of transcription 1
0.886354	0.939	1.19	0.15	IFNA1	interferon alpha 1
0.888498	0.939	1.171	0.177	ARG1	arginase 1

Table 8.2: Survival in ER- patients correlating to stromal expression

Parametric p-value	FDR	Hazard Ratio	SD of log intensities	Symbol	Name
0.016701	**0.499**	**40.565**	**0.213**	**IL1A**	**interleukin 1 alpha**
0.0594688	0.499	0.586	0.926	STAT1	signal transducer and activator of transcription 1
0.0733155	0.499	1.825	0.789	PTGS2	prostaglandinendoperoxide synthase 2
0.104058	0.499	1.672	0.698	ARG2	arginase 2
0.104263	0.499	9.968	0.184	PTGS1	prostaglandinendoperoxide synthase 1
0.13279	0.499	0.695	0.92	STAT1	signal transducer and activator of transcription 1
0.145289	0.499	3.366	0.3	IL1B	interleukin 1 beta
0.146316	0.499	0.377	0.35	IFNG	interferon gamma
0.154487	0.499	0.524	0.556	CASP1	caspase 1
0.161847	0.499	0.685	0.85	STAT1	signal transducer and activator of transcription 1
0.168951	0.499	0.497	0.47	CASP4	caspase 4
0.184746	0.499	0.148	0.184	NOS2	nitric oxide synthase 2
0.190927	0.499	1.684	0.564	PANX1	pannexin 1
0.201868	0.499	3.17	0.264	IFNB1	interferon beta 1
0.202424	0.499	0.434	0.388	STAT1	signal transducer and activator of transcription 1
0.24973	0.577	2.381	0.351	IL1B	interleukin 1 beta
0.329651	0.715	0.535	0.327	STAT1	signal transducer and activator of transcription 1
0.34783	0.715	2.026	0.256	ARG2	arginase 2
0.374337	0.729	0.588	0.387	IL18	interleukin 18

0.410049	0.759	1.56	0.419	ASL	argininosuccinate lyase
0.432597	0.762	0.681	0.56	CASP4	caspase 4
0.483879	0.814	0.778	0.594	PTGS1	prostaglandinendoperoxide synthase 1
0.535441	0.832	0.787	0.531	PTGS1	prostaglandinendoperoxide synthase 1
0.547111	0.832	1.462	0.414	GSDMD	gasdermin D
0.575291	0.832	0.63	0.348	STAT1	signal transducer and activator of transcription 1
0.584672	0.832	1.757	0.21	ARG1	arginase 1
0.611586	0.838	2.379	0.125	CASP5	caspase 5
0.67575	0.852	0.846	0.667	CASP1	caspase 1
0.677452	0.852	1.124	0.703	ASS1	argininosuccinate synthase 1
0.695389	0.852	0.491	0.148	IFNA1	interferon alpha 1
0.713871	0.852	0.624	0.235	IL1A	interleukin 1 alpha
0.765099	0.88	0.83	0.377	CASP1	caspase 1
0.784608	0.88	0.753	0.214	HMGB1	high mobility group box 1
0.81235	0.884	1.161	0.358	HMGB1	high mobility group box 1

Table 8.3: Survival in ER+ patients correlating to stromal expression

Parametric p-value	FDR	Hazard Ratio	SD of log intensities	Symbol	Name
0.0106608	**0.375**	**50.64**	**0.307**	**ARG2**	**arginase 2**
0.0202874	**0.375**	**2.974**	**0.603**	**CASP1**	**caspase 1**
0.0453502	**0.52**	**15.446**	**0.264**	**CASP1**	**caspase 1**
0.0601078	0.52	0.052	0.196	PTGS1	prostaglandinendoperoxide synthase 1
0.0702873	0.52	3.68	0.451	CASP1	caspase 1
0.142844	0.881	3.636	0.392	CASP1	caspase 1
0.209251	0.919	2.091	0.521	CASP4	caspase 4
0.220032	0.919	0.266	0.31	IFNB1	interferon beta 1
0.23125	0.919	0.148	0.228	IL1A	interleukin 1 alpha
0.334162	0.919	1.63	0.48	IL1B	interleukin 1 beta
0.432949	0.919	11.353	0.128	CASP5	caspase 5
0.43663	0.919	0.714	0.664	PTGS1	prostaglandinendoperoxide synthase 1
0.445034	0.919	3.789	0.155	IFNA1	interferon alpha 1
0.468113	0.919	0.192	0.139	ARG1	arginase 1
0.527062	0.919	0.849	1.151	PTGS2	prostaglandinendoperoxide synthase 2
0.55797	0.919	1.277	0.775	ASS1	argininosuccinate synthase 1
0.565125	0.919	0.783	0.665	PTGS1	prostaglandinendoperoxide synthase 1
0.639858	0.919	0.751	0.499	CASP4	caspase 4
0.736158	0.919	1.113	0.812	STAT1	signal transducer and activator of transcription 1
0.741625	0.919	0.567	0.179	IFNG	interferon gamma
0.74234	0.919	1.108	0.814	STAT1	signal transducer and activator of transcription 1

0.749627	0.919	1.477	0.217	STAT1	signal transducer and activator of transcription 1
0.754158	0.919	0.807	0.506	CASP1	caspase 1
0.758014	0.919	0.927	1.142	STAT1	signal transducer and activator of transcription 1
0.78996	0.919	1.249	0.311	ASL	argininosuccinate lyase
0.839528	0.919	1.163	0.376	HMGB1	high mobility group box 1
0.84385	0.919	0.778	0.225	ARG2	arginase 2
0.845876	0.919	0.853	0.329	STAT1	signal transducer and activator of transcription 1
0.847576	0.919	1.158	0.366	IL1B	interleukin 1 beta
0.852984	0.919	0.635	0.123	NOS2	nitric oxide synthase 2
0.870066	0.919	1.134	0.495	PANX1	pannexin 1
0.874548	0.919	1.227	0.202	HMGB1	high mobility group box 1
0.880916	0.919	0.784	0.177	IL1A	interleukin 1 alpha
0.883932	0.919	1.202	0.219	HMGB1	high mobility group box 1
0.892627	0.919	0.873	0.294	STAT1	signal transducer and activator of transcription 1
0.894175	0.919	0.898	0.338	IL18	interleukin 18